Domain Decomposition Approach for Deterministic/Stochastic EMC Time-Domain Numerical and Experimental Applications. Alleviating the Curse of Dimensionality

Imane Massaoudi

UNIVERSITÉ CLERMONT AUVERGNE
École Doctorale Sciences pour l'ingénieur
Institut Pascal - Département "Compatibilité ÉlectroMagnétique"

Year : 2023
Doctoral dissertation
in fulfillment of the requirements for the degree

DOCTOR OF CLERMONT AUVERGNE UNIVERSITY

Discipline : Electronics and Systems

Presented by
Imane Massaoudi

Domain Decomposition Approach for Deterministic/Stochastic EMC Time-Domain Numerical and Experimental Applications

Alleviating the Curse of Dimensionality

Defended on the 19^{th} of December 2023 and reviewed by the committee composed of:

M. Christian Vollaire	Professeur des Universités, Laboratoire Ampère, Lyon,	Président du jury
M. Alain Reineix	Directeur de Recherche CNRS, Xlim, Limoges,	Rapporteur
M. Mohammed Ramdani	Enseignant-chercheur HDR, ESEO, Angers,	Rapporteur
Mme. Elodie Richalot	Professeure des Universités, Univ. Gustave Eiffel, Paris,	Examinatrice
Mme. Isabelle Junqua	Ingénieure de Recherche, ONERA, Toulouse,	Examinatrice
M. Marc Olivas	Directeur de Recherche Technologique, WiN MS, Paris,	Examinateur
M. Pierre Bonnet	Professeur des Universités, IP, Clermont-Fd,	Directeur de thèse

Dedication

À mes très chers parents Mohammed et Naima,

À chaque chapitre de ma vie, votre amour inconditionnel, soutien inestimable et vos encouragements permanents ont été mes compagnons de route à chaque triomphe et à chaque épreuve. Cette thèse est un témoignage de votre dévouement sans fin et des valeurs de persévérance et de détermination que vous m'avez inculquées. Votre confiance en moi a nourri mes aspirations et m'a propulsé vers l'avant, et je vous en serai éternellement reconnaissante. Avec ma plus profonde gratitude et mon amour, je vous dédie ce travail, en hommage du rôle indispensable que vous avez joué dans l'élaboration de mon parcours et mes accomplissements.

Acknowledgments

This accomplishment would not have been possible without the guidance and support of colleagues, family, and close friends. To them, I extend my deepest appreciation and heartfelt thanks for their belief in me and their willingness to share their expertise. This work stands as a testament to the collective efforts and collaborative spirit of all those involved, and I am truly humbled by the privilege of having them by my side.

First and foremost, I owe my sincere gratitude to my thesis supervisor Professor **Pierre Bonnet** for providing guidance, support, and mentorship throughout this work. Your expertise, patience, and dedication have been invaluable in shaping both the direction and quality of my thesis. Your willingness to share your knowledge and insights, as well as your constructive feedback, have greatly contributed to my growth and development as a researcher. I am truly grateful for the time and effort you have invested in me, and I feel privileged to have had the opportunity to learn from you. Thank you for believing in my abilities and for providing me with the encouragement and resources needed to succeed. Your mentorship has not only enriched my academic experience but has also inspired me to strive for excellence in my future projects.

I am deeply grateful to the members of my thesis committee. Thank you Professor **Alain Reineix**, research director CNRS at Xlim, Limoges, and Professor **Mohammed Ramdani**, teacher-researcher HDR at ESEO, Angers, for accepting to be the reviewers of my thesis manuscript. Your insightful comments and constructive feedback significantly improved the quality of this work. I extend my sincere gratitude to the examiners Professor **Christian Vollaire**, professor of universities at Laboratoire Ampère, Lyon, Professor **Elodie Richalot**, professor of universities at University Gustave Eiffel, Paris, Professor **Isabelle Junqua**, research engineer at ONERA, Toulouse, and Professor **Marc Olivas**, technology research director at Win MS, Paris, who dedicated their time and expertise to critically evaluate this thesis. Their thorough examination, insightful comments, and constructive feedback have immensely contributed to the refinement of this work.

I extend my heartfelt gratitude for the pivotal role the ANR project **ECOCES** played in inspiring the initial idea for this research work. Their support and resources were indispensable in bringing this thesis to fruition. I am deeply grateful to the director of the project, Professor **Christian Vollaire**, for his unwavering belief in my abilities and for allowing me to be part of this research work. I extend my heartfelt appreciation to all the project's members for

their thoughtful comments, invaluable guidance, and unwavering support. Their expertise and dedication have been essential in overcoming challenges and achieving the goals of this thesis.

I want to thank Professor **Evelyne Gil**, the head of Institut Pascal, Vanessa Chaudron, Charlènes Fernandes and Pierre Servoir, the administrative secretaries. I would like to express my sincere appreciation to the entire CEM team for their invaluable support and collaboration throughout my thesis duration. Thank you Françoise, your willingness to take me in and mentorship have been an invaluable gift. I am deeply grateful for your support and encouragement. Thank you Christophe for trusting me with the responsibility of teaching and your support over these 3 past years. Thank you Sébastien for your help with the measurement set-up, Khalil for helping extend the scope and depth of a part of my research, Kofi for pushing me constantly to publish, and all the good memories I keep from my first conference. Thank you for all the scientific and nonscientific discussions we had and for maintaining the best cordial working environment for me.

Many thanks to the trainees, doctoral and postdoctoral students that I met in the CEM group, Ali, Fatima, Mincui, Liza, Lana, Hassan, Eric, Brahim and Veevek. Thanks for being real daily supporters. I wish you more success in your future career.

I want to take the opportunity to heartwarmingly thank all my friends, especially Mincui with whom not only did we have lunch and coffee/tea breaks together, but also helped me through the last stages of my thesis. I am forever grateful for your unconditional love and support during some of the difficult times of this thesis. Thank you for all the laughs we have shared, it will always be engraved in my memory. Thank you Fatima Ezzahra, for being the best friend I could ever ask for. You made my toughest moments easier with your kind and lovely words. Thank you for being a good listener and giving me valuable advice when I needed it the most. Thank you Lana, for all the laughs we had, for believing in me, and for pushing me to be as happy as I could be. Thank you Lisa for all the times we have shared, your friendship has undoubtedly made a positive difference in my life. Thank you Zineb for your support and kind words in times of doubt, for the funny talks we have frequently but also the tough ones, our friendship keeps growing and I am so appreciative of your presence in my life. Thank you Karim for being as supportive as you are. Our funny talks always made my days better. Thank you Nadir, Clovis and Abdivall for your support and encouragement. Thank you Ali for your help in times of need and kindness.

I am profoundly grateful to my family for their unwavering love, encouragement, and support

throughout the journey of completing this thesis. Their belief in me has been my strongest pillar, providing me with the motivation and determination to persevere through the challenges and uncertainties of academic pursuit. Words cannot fully express the depth of my gratitude for everything you have done for me. Your unwavering love, support, and sacrifices have been the cornerstone of my life's journey. I am forever grateful to my dearest father Mohammed, for his support and encouragement, and my lovely mother Naima for her love and prayers. Thank you both for everything you did for me, for providing me with the best education and helping me pursue my dreams. I would like also to thank my sisters, Nour el Houda and Asmae, for their unwavering support and understanding throughout the process of completing this thesis. Your love and kindness have kept me going through hard times along this journey. I thank also my brothers-in-law, Taha and Oussama, for their support and encouragement. And of course, thank you Soujoud (Swija), Lina (Layouna), Mohammed-Taha (m-taha), and the new baby boy, my lovely nieces and nephews for love, light, and the endless smiles they've brought to my days. And lastly, I want to thank my Lila, my everyday companion, my best pet friend, you've been a constant source of comfort, warmth, and companionship.

List of Contents

List of Acronyms

EMC	ElectroMagnetic Compatibility
EMI	ElectroMagnetic Interference
DD	Domain Decomposition
SC	Stochastic Collocation
CEM	Computational ElectroMagnetic
UQ	Uncertainty Quantification
SA	Sensitivity Analysis
RV	Random Variable
MC	Monte Carlo
PC	Polynomial Chaos
SR	Sample Rate
SC-DD	Stochastic Collocation Domain Decomposition

Abstract

This thesis introduces a novel domain decomposition (DD) method to solve linear stochastic electromagnetic problems in time domain. Temporal decomposition approaches are already widely used to manage models' complexity by performing computations at a local level, however, they often require the exchange of information and simulation results for each time iteration. The proposed technique consists of splitting a global linear system into non-overlapping sub-systems via one or several one-point exchange interfaces. It is based on the evaluation of impulse responses of each sub-system independently (partial solutions) and their linear combination through convolution products. As no sensitive or proprietary information of each sub-system is required for exchange, the confidentiality of the models is preserved. The method was extensively applied for several configurations of transmission line networks based on computational simulations and experimental set-ups to assess its performance and limitations. This comprehensive validation demonstrated the method's efficiency and potential for more complex linear EMC problems. However, another level of complexity, translated by the uncertainty dimension, adds to real-world problems. Although the efficiency of the DD technique is demonstrated for stochastic analysis by propagating the uncertainty in the sub-models, the computational cost grows exponentially with the increasing number of random variables in the system. To tackle this challenge, known as the curse of dimensionality, the stochastic collocation method was associated with the domain decomposition approach, based on an offline–online strategy motivated by the asynchronous nature of the DD technique allowing random variable separation. Numerical validations obtained for transmission line network applications highlight the interest of this original approach with the dramatic reduction of the evaluation cost of the model.

Keywords: domain decomposition, asynchronous, time-domain, linear, EMC, stochastic analysis, curse of dimensionality.

Résumé

Cette thèse introduit une nouvelle méthode de décomposition de domaine (DD) pour résoudre des problèmes électromagnétiques stochastiques linéaires dans le domaine temporel. Les approches de décomposition temporelles sont déjà largement utilisées pour gérer la complexité des modèles en effectuant des calculs à un niveau local, mais elles nécessitent souvent l'échange d'informations et de résultats de simulation pour chaque itération temporelle. La technique proposée consiste à diviser un système linéaire global en sous-systèmes qui ne se chevauchent pas via une ou plusieurs interfaces d'échange ponctuelles. Elle est basée sur l'évaluation des réponses impulsionnelles de chaque sous-système indépendamment (solutions partielles) et sur leur combinaison linéaire par le biais de produits de convolution. Comme aucune information sensible ou propriétaire de chaque sous-système n'est requise pour l'échange, la confidentialité des modèles est préservée. La méthode a été extensivement appliquée à plusieurs configurations de réseaux de lignes de transmission sur la base de simulations numériques et de set-ups expérimentaux afin d'évaluer ses performances et ses limites. Cette validation complète a démontré l'efficacité de la méthode et son potentiel pour des problèmes CEM linéaires plus complexes. Cependant, un autre niveau de complexité, traduit par la dimension d'incertitude, s'ajoute aux problèmes du monde réel. Bien que l'efficacité de la technique DD soit démontrée pour l'analyse stochastique en propageant l'incertitude dans les sous-modèles, le coût de calcul croît de manière exponentielle avec l'augmentation du nombre de variables aléatoires dans le système. Pour relever ce défi, connu sous le nom de malédiction de la dimensionnalité, la méthode de collocation stochastique a été associée à l'approche de décomposition de domaine, basée sur une stratégie hors ligne et en ligne motivée par la nature asynchrone de la technique DD permettant la séparation des variables aléatoires. Les validations numériques obtenues pour des applications de réseaux de lignes de transmission soulignent l'intérêt de cette approche originale avec la réduction spectaculaire du coût d'évaluation du modèle.

Mots clès: décomposition de domaine, asynchrone, domaine temporel, linéaire, CEM, analyse stochastique, malédiction de la dimensionnalité.

Résumé Etendu en Français

Introduction et contexte

AVEC l'intégration rapide de technologies avancées dans les véhicules de demain, la sécurité et la fiabilité constituent des véritables enjeux, tant pour la sécurité des passagers que pour le bon fonctionnement des équipements électriques/électroniques. Il est donc indispensable d'assurer la conformité aux normes limitant les émissions parasites du véhicule et respectant l'exposition des personnes aux champs électromagnétiques à l'intérieur du véhicule. La prise en compte de la Compatibilité ElectroMagnétique (CEM) dès le début de la phase de conception garantira la sécurité, la fiabilité, la fonctionnalité et la conformité.

L'utilisation de la simulation numérique pour l'analyse CEM des systèmes devient de plus en plus populaire, en raison de la difficulté et/ou non accessibilité aux mesures expérimentales, mais aussi grâce aux progrès des technologies informatiques et naissance de nouvelles techniques mathématiques. Malgré le progrès de ces méthodes numériques (efficacité à modéliser les phénomènes physiques, rapidité de convergence et modélisation de système de grande échelle), elles ne sont pas adaptées pour résoudre des problèmes intégrant plusieurs niveaux de complexité: *multi-échelles* et *multi-modèles*. Il est donc impératif d'échanger les différents modèles des sous-ensembles pour parvenir à une modélisation complète d'un système industriel. La confidentialité des modèles n'est donc pas respectée, et représente un réel défi dans le secteur industriel, où aucun des partenaires (assembleur ou intégrateur dans le contexte automobile) n'est disposé à échanger son modèle.

En plus de ces contraintes industrielles et techniques, l'évolution des technologies ajoute un nouveau niveau de complexité de *multi-incertitudes*. Ces incertitudes peuvent avoir de sérieux impact sur les performances CEM d'un système, et leur prise en compte est de plus en plus importante. Que l'on connaisse les multiples sources d'incertitudes existantes, liées à leur conception (propriétés géométriques et physiques), à leur environnement (paramètres externes ou systèmes voisins), ou non (pas de connaissance exacte sur les incertitudes du système), leurs quantifications requièrent l'utilisation de techniques adaptées, non-intrusives, pour prendre en compte la diversité et la multitude d'échelles et de méthodes.

Les méthodes de décomposition de domaine en général et d'hybridation dans le domaine temporel en particulier, ont été proposées pour résoudre ces problèmes complexes en découpant le

système global en plusieurs sous-systèmes plus simples. Généralement, la méthode numérique la plus appropriée est appliquée à chaque sous-domaine. Cependant, l'échange des modèles de chaque sous-système nécessite de partager des résultats et/ou données qui leur sont propres. Les techniques de co-simulation, connues aussi sous le nom de simulation coopérative, sont aussi des solutions alternatives à la simulation globale. Elles nécessitent néanmoins des échanges synchronisés entre les différents partenaires à chaque itération temporelle.

À ce jour, il n'existe pas de méthode permettant de résoudre un problème CEM complexe dans son intégralité (conduite et rayonnement) et dans sa diversité. Ces contraintes à la fois techniques et industrielles, rencontrées dans plusieurs domaines y compris l'automobile, ont inspiré le projet ANR **ECOCES** (Electromagnetic Compatibility Co-simulation Of Complex Electrical Systems), dans lequel s'inscrit les travaux de cette thèse. Le projet intègre trois sujets de thèse (Laboratoire Ampère de Lyon, Institut Pascal de Clermont-Ferrand et l'IETR d'Angers) et implique des partenaires académiques (GeePs) et industriels (Stellantis et Chiastek). Le défi pour tous les partenaires du projet est de développer une méthodologie de co-simulation pour évaluer les phénomènes CEM dans les systèmes complexes par le biais d'une simulation indépendante de tous les sous-systèmes. Dans cette approche, les différents modèles ne sont ni partagés entre les partenaires ni intégrés dans un outil unique, mais communiquent en temps réel via leurs interfaces.

Pour surmonter ces limitations, nous proposons au travers cette thèse, une méthode de décomposition de domaine pour résoudre des problèmes CEM linéaires dans le domaine temporel. L'objectif est de pouvoir modéliser les sous-systèmes de manière indépendante, sans échange itératif, tout en conservant la confidentialité des modèles de chaque sous-système. Différentes applications numériques et expérimentales ont été réalisées pour valider la méthode et prouver son efficacité. L'association de la technique proposée avec une approche stochastique, en l'occurrence la méthode de collocation stochastique, permet de prendre en compte les incertitudes dans des problèmes stochastiques complexes. Pour différentes configurations stochastiques, les multiples avantages de cette association sont mis en avant.

La Méthode de décomposition de domaine

Nous supposons que le système électrique linéaire global G, représenté dans la Figure (1a), a z terminaisons représentant soit des entrées (sources physiques injectées V_s), soit des sorties mesurées V_{out}.

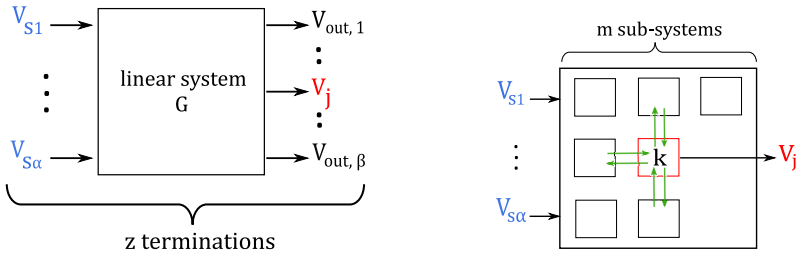

(a) (b)

Figure 1: *Représentations schématiques du système électrique linéaire global G de α entrées et β sorties (a), et de la subdivision du système électrique linéaire global G en m sous-systèmes disjoints (b).*

La méthode de décomposition de domaine (DD) proposée consiste à diviser le problème global G en m sous-problèmes disjoints via une ou plusieurs interfaces d'échange (Figure (1b)). La méthode est appliquée en tenant compte de deux hypothèses : 1) le système est divisé au niveau d'une interface ponctuelle (1D), 2) les propriétés électriques du système sont conservées au niveau de l'interface. Par conséquent, aucune réflexion de part et d'autre de l'interface (niveau de subdivision) n'est mesurée, et une parfaite adaptation au niveau de l'interface est assurée.

Parmi les sorties β du système G, nous nous intéressons à la sortie V_j mesurée à la terminaison j, localisée dans le sous-réseau k (n terminaison). La sortie V_j^k est obtenue en considérant la contribution directe de chaque source dans le sous réseau k, et les contributions indirectes de(s) autre(s) source(s) dispersée(s) dans les sous-système voisins, comme représenté sur la Figure (2a). Suivant le principe de la convolution, la sortie V_j^k est exprimée par

$$V_j^k = \sum_{\{i\}} h_{ij}^k * V_{si}^k + \sum_{\{l\}} h_{lj}^k * V_{\sim l}^k \tag{1}$$

Le premier terme du membre de droite de l'équation (1) traduit la contribution des p sources réelles $V^k_{s\{i\},\ \{i\}\subseteq\{1,\ldots,\alpha\}}$ avec $p < \alpha$, de l'ensemble initial des α sources. Tandis que le second terme donne la contribution des q sources équivalentes $V^k_{\sim\{l\},\ \{l\}\subseteq\{1,\ldots,n\}}$, pour $l \leqslant n$. Celles ci représentent explicitement l'effet des autres sources dispersées dans les sous-systèmes voisins, ramené aux interfaces d'échange (point de découpage).
Les termes h_{ij}^k, respectivement $h_{\sim l}^k$, sont les réponses impulsionnelles reliant les sources physiques injectées $V_{s\{i\}}^k$ à la sortie, respectivement les réponses impulsionnelles reliant les sources équivalentes $V_{\sim\{l\}}^k$ à la sortie mesurée au point j.

Les sources équivalentes $V_{\sim l}^k$ traduisent l'effet indirect des sources dispersées dans les sous-

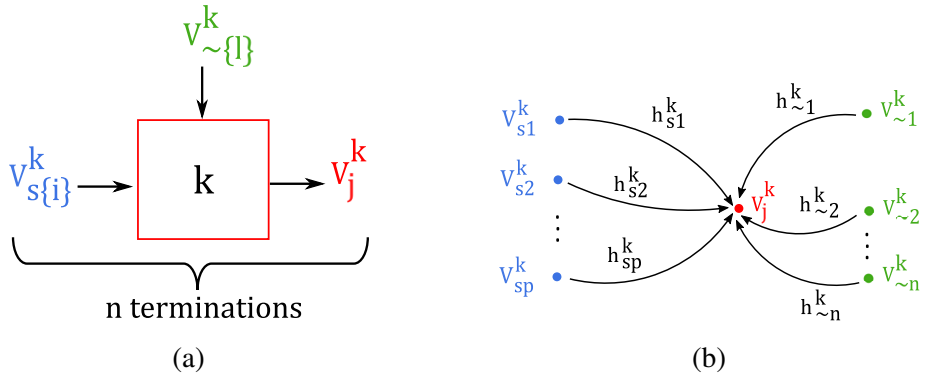

Figure 2: *Représentations schématiques du sous-système k de p sources physiques injectées* $V^k_{s\{i\}}$, *q sources équivalentes* $V^k_{\sim\{l\}}$ *et de la sortie* V^k_j *(a), et des réponses impulsionnelles* h^k_{si} *et* $h^k_{\sim l}$ *reliant les sources* $V^k_{s\{i\}}$, *respectivement,* $V^k_{\sim\{l\}}$ *à la sortie* V^k_j *(b).*

systèmes voisins au découpage. Chacune de ses sources représente la réponse du sous-système k (où l'observable est localisée) à l'onde incidente d'un sous-système voisin, mesurée à l'interface.

L'équation (1) considère uniquement la contribution de chaque système voisin au sous-système k à l'interface, or, pour retrouver le comportement physique du système global G comme s'il n'y avait pas eu de décomposition, il faut considérer les rétro-actions entre les différents sous-système. Cet effet est reconstitué à travers la ré-injection des sources équivalentes au niveau des interfaces l du sous-système k dans les m sous-systèmes voisins, à partir des nouvelles réponses impulsionnelles h^v_{ll}, $v \in \{1,..,m\}$. La formule finale permettant de retrouver les multiples réflexions des α sources entre les sous-systèmes pour un ordre q donné, est exprimée par

$$V^k_j = \sum_{\{i\}} h^k_{ij} * V^k_{si} + \sum_{\{l\}} h^k_{lj} * V^k_{\sim l,1} + \sum_{i=2}^{q} h^k_{lj} * \left(\prod_{\{v\}} h^v_{l_v l_v} * V^k_{\sim l,i}\right) \tag{2}$$

La source $V^k_{\sim l,i}$ est définie comme l'ordre i de la source équivalente, et est donnée par

$$V^k_{\sim l,i} = \prod_{\{v\}} h^v_{l_v l_v} * V^k_{\sim l,i-1} \tag{3}$$

Le terme $V^k_{\sim l,1}$ dans l'équation (2) fait référence au premier ordre de la source $V^k_{\sim l}$.

En pratique, cet ordre q n'est pas connu à l'avance et dépendra de la topologie du réseau (longueur, impédances caractéristiques et résistances de charge des lignes), de l'observable,

du choix de la décomposition ainsi que de l'intervalle de temps pour l'enregistrement de la sortie. Un critère d'arrêt, basé sur l'erreur calculée en incrémentant l'ordre q, peut être défini.

La méthodologie proposée présente l'avantage majeur de permettre la modélisation séparée et indépendante de chaque sous-système. Alors que d'autres approches dans le domaine temporel nécessitent un échange itératif pour chaque pas de temps, la méthode DD permet des simulations temporelles asynchrones basées sur l'évaluation des réponses impulsionnelles uniquement. Cet aspect particulier présente l'avantage supplémentaire de préserver la confidentialité de chaque modèle. Les informations sensibles ou propriétaires relatives à chaque sous-système restent inconnues car aucune autre information ou résultat ne sont requis pour l'échange. Cet avantage supplémentaire s'avère particulièrement important dans un contexte industriel, car il permet de conserver la propriété intellectuelle.

Validations numériques de la méthode de domaine de décomposition

La méthode DD proposée dans cette thèse est illustrée au travers des applications 1D de réseaux de lignes de transmission, sans pertes de généralité et à des fins d'illustration. Son aspect général permet d'étudier différentes configurations de réseaux de lignes indépendemment de la topologie du réseau, types de câbles et leurs caractéristiques mais aussi de l'observable. D'après le principe général de la DD décrit dans la section précédente, les propriétés physiques au niveau de l'interface de découpage doivent être conservées. Dans le cas des lignes de transmission, deux conditions sont à respecter: 1) la somme des longueurs des deux lignes résultantes au découpage doit être égale la longueur de la ligne initiale, 2) chacune de ses lignes doit être chargée par une résistance de valeur égale a l'impédance caractéristique de la ligne où le découpage a eu lieu pour assurer une continuité d'impédance.

L'illustration numérique de la méthode proposée est réalisée pour 3 cas:

1. **plusieurs interfaces**: afin de généraliser la méthode à plus d'une interface, une application de réseau de lignes pour laquelle la décomposition se produit à deux niveaux est étudiée. Le principe de l'approche est inchangé, mais sa formulation générale donnée par l'équation (2) est adaptée pour prendre en compte les sources équivalentes aux deux interfaces d'échange, ainsi que leurs réflexions dans les trois sous-réseaux.

2. **plusieurs outils**: la nature asynchrone de la méthode DD proposée permet de modéliser

chaque sous-système de manière entièrement indépendante. Par conséquent, différents outils numériques peuvent être utilisés pour caractériser chaque sous-réseau, i.e. évaluer ses réponses impulsionnelles. Dans ce contexte, la méthode de DD a été appliquée sur un réseau de ligne de transmission découpé en deux sous-réseaux, tel que le sous-réseau 1 est modélisé par la méthode numérique *différences finies* (FDTD: Finite Difference Time Domain en anglais), et le sous-réseau 2 par le logiciel commercial CST Cable Studio®. Étant donné que les deux outils emploient des pas de discrétisation temporels différents, une interpolation des réponses impulsionnelles est donc nécessaire avant leurs combinaison linéaire dans l'équation (2).

3. **plusieurs interfaces ponctuelles**: pour démontrer l'efficacité de la méthode à résoudre des réseaux de lignes plus complexes, nous proposons d'étudier un réseau multifilaire tel que chaque ligne est constituée de m conducteurs. Dans ce cas, l'interface de découpage est représentée par m interfaces ponctuelles. L'équation (2) est adaptée pour prendre en compte la contribution des sources équivalentes à chacune des m interfaces, et leurs multiples réflexions dans les sous-réseaux.

Pour les trois cas d'étude, la méthode de décomposition de domaine est comparée au résultat global. En général, le recourt à la méthode de DD est une alternative à la simulation globale à cause de sa difficulté et/ou non accessibilité. Nous considérons dans cette thèse que le résultat global est connu et servira comme référence pour valider notre approche. Les configurations des réseaux étudiés, la formulation adaptée de l'équation (2) selon l'observable, ainsi que le résultat de la DD comparé à la référence sont donnés dans la suite pour chacun des trois cas précédents. La source d'excitation pour toutes les configurations est un signal gaussien d'amplitude $1V$.

Cas 1: plusieurs interfaces

On propose d'étudier le réseau de lignes représenté sur la Figure (3a). On s'intéresse à la tension V_5 aux bornes de la résistance R_{L5} quand le réseau global est découpé au milieu de la ligne L_2 et L_6. Suivant le principe de la méthode de décomposition de domaine, l'observable est localisée dans le sous-réseau $k = 2$. Aucune source physique n'est injectée dans ce dernier, par conséquent, uniquement les contributions des sources équivalentes aux deux interfaces $l = 2$ et $l = 6$ sont évaluées. A partir de la formule générale donnée par l'équation (2), la tension V_5^2 est

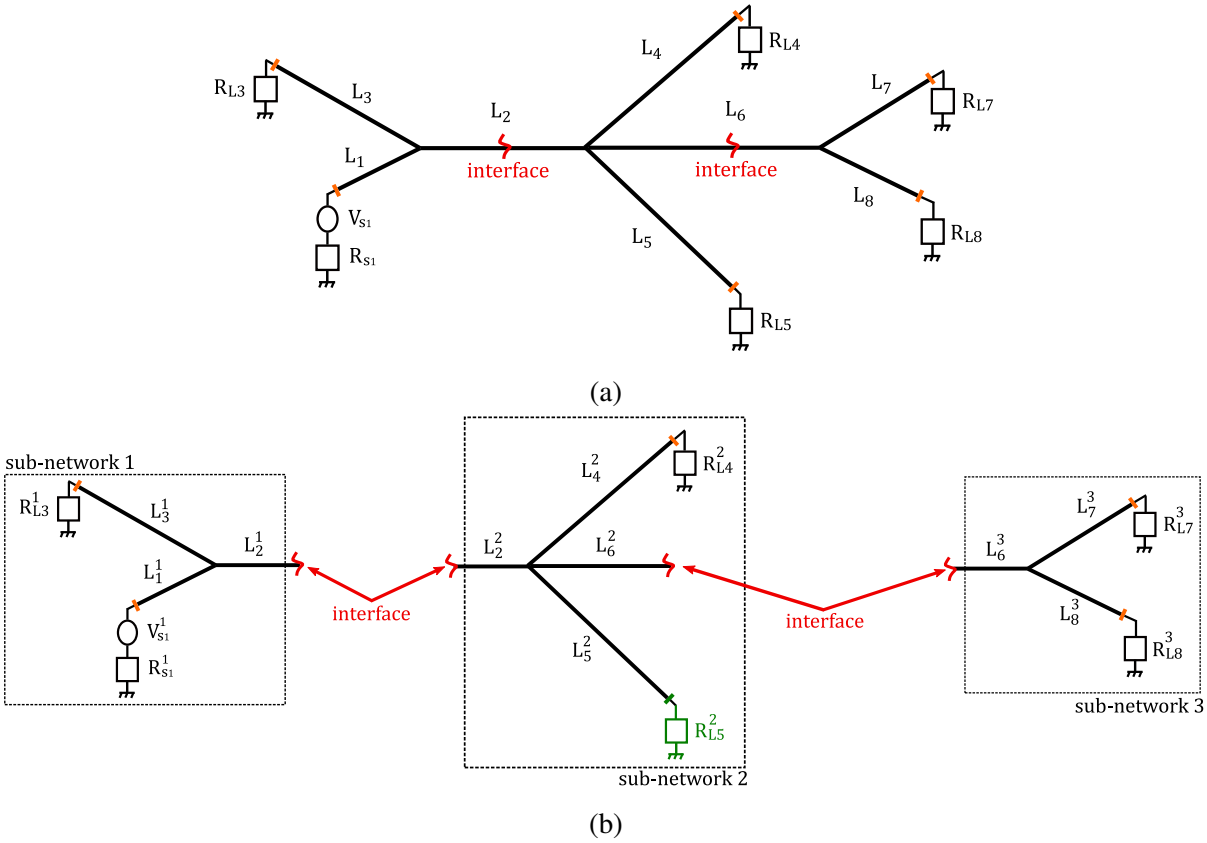

Figure 3: *Réseau global de lignes de transmission divisé au milieu des lignes L_2 et L_6 (a), sous-réseaux 1, 2 et 3 après la subdivision du réseau global (b).*

exprimée par

$$\begin{aligned} V_5^2 &= h_{25}^2 * V_{\sim 2}^2 + h_{65}^2 * V_{\sim 6}^2 + h_{25}^2 * V_{\sim 2,1}^2 + h_{65}^2 * V_{\sim 6,1}^2 \\ &+ \sum_{i=2}^{q} h_{25}^2 * \left(h_{22}^1 * (h_{22}^2 * V_{\sim 2,i}^2)\right) + \sum_{j=2}^{q} h_{25}^2 * \left(h_{66}^3 * (h_{66}^2 * V_{\sim 6,j}^2)\right) \\ &+ \sum_{k=2}^{q_3} h_{65}^2 * \left(h_{22}^1 * \left(h_{22}^2 * \left(h_{66}^3 * (h_{66}^2 * V_{\sim 2,k}^2)\right)\right)\right) \end{aligned} \tag{4}$$

avec $V_{\sim 2,i}^2$, respectivement $V_{\sim 6,j}^2$ sont définis comme le i-ème, respectivement le j-ème ordre de la source équivalente à l'interface $l = 2$, respectivement l'interface $l = 6$. Leurs expressions respectives sont données par

$$V_{\sim 2,i}^2 = h_{22}^1 * (h_{22}^2 * V_{\sim 2,i-1}^2) \tag{5}$$

$$V_{\sim 6,j}^2 = h_{66}^3 * (h_{66}^2 * V_{\sim 6,j-1}^2) \tag{6}$$

La source $V^2_{\sim 2,k}$ est quand à elle définie comme le k-ième ordre de la source équivalente $V^2_{\sim 6}$, et exprimée par

$$V^2_{\sim 2,k} = h^1_{22} * (h^2_{22} * V^2_{\sim 6,k-1}) \tag{7}$$

En évaluant la tension V^2_5 donnée par l'équation (4) pour les ordres $q_1 = 6$, $q_2 = 2$ et $q_3 = 1$, la méthode de décomposition permet de retrouver le résultat attendu, comme représenté sur la Figure (4).

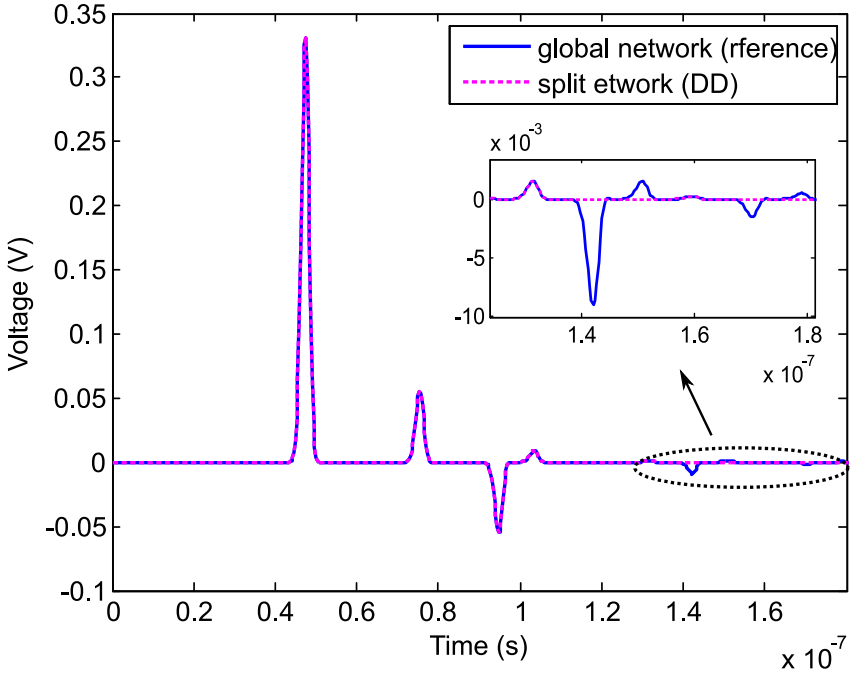

Figure 4: *Comparaison de la tension V_5 aux bornes de la résistance R_{L5} évaluée pour le réseau global (référence) et le réseau divisé (méthode DD).*

En synthèse, le principe de la méthode DD reste inchangé, mais la complexité de la formulation augmente avec le nombre d'interfaces considérées. Nous soulignons que l'ordre requis pour une bonne précision est relatif à la topologie du réseau, à la décomposition elle-même et à l'intervalle de temps pour l'enregistrement du signal. La formule finale peut être automatisée pour tenir compte des différentes décompositions et topologies du système étudié.

Cas 2: différents outils de simulation

On propose d'étudier le réseau de lignes représenté sur la Figure (5). On s'intéresse à la tension V_6 aux bornes de la résistance R_{L6} quand le réseau global est découpé au milieu de la ligne L_2 en deux sous-réseaux, comme représenté sur la Figure (5b).

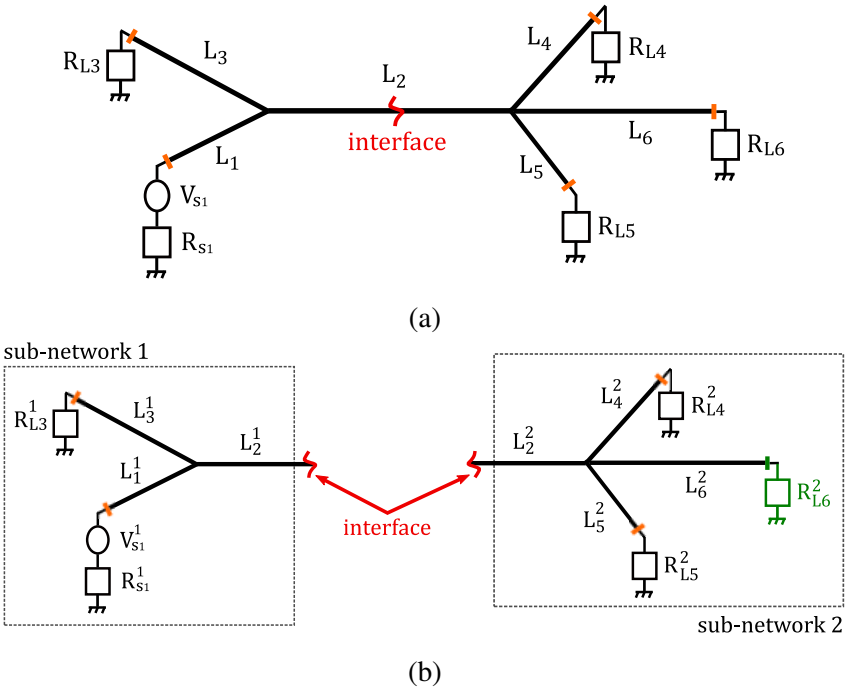

Figure 5: *Réseau global de lignes de transmission divisé au milieu de la ligne L_2, sous-réseaux 1 et 2 après la subdivision du réseau global (b).*

Le sous-réseau 1 est modélisé à l'aide du logiciel commercial CST Cable®, tandis que le sous-réseau 2 est évalué à l'aide de la méthode numérique des différences finies. Dans ce cas, le pas de discrétisation temporel utilisé dans CST Cable®, noté dt_1, est supérieur à dt_2, le pas de discrétisation temporel utilisé pour la simulation FDTD.
La tension V_6^2 déduite à partir de l'équation générale (2) est exprimée comme suit en utilisant la méthode de décomposition de domaine proposée:

$$V_6^2 = h_{26}^2 * (h_{12}^1 * V_{s1}^1) + h_{26}^2 * \Big(\underbrace{h_{22}^2 * \big(h_{22}^1 * (h_{12}^1 * V_{s1}^1)\big)}_{V_{\sim 2,1}^2} \Big) + \sum_{i=2}^{q} h_{26}^2 * \big(h_{22}^2 * (h_{22}^1 * V_{\sim 2,i}^2)\big) \quad (8)$$

avec $V_{\sim 2,i}^2$ est défini comme le i-ième ordre de la source équivalente au niveau de l'interface et

est donné par

$$V^2_{\sim 2,i} = h^2_{22} * (h^1_{22} * V^2_{\sim 2,i-1}) \tag{9}$$

Après l'interpolation des réponses impulsionnelles $h^2_{...}$ du sous-réseau 2 sur la base temporelle t_1 utilisée dans la modélisation du sous-réseau 1, la tension V^2_6 est évaluée pour l'ordre $q = 5$. Le résultat obtenu est présenté dans la Figure (6).

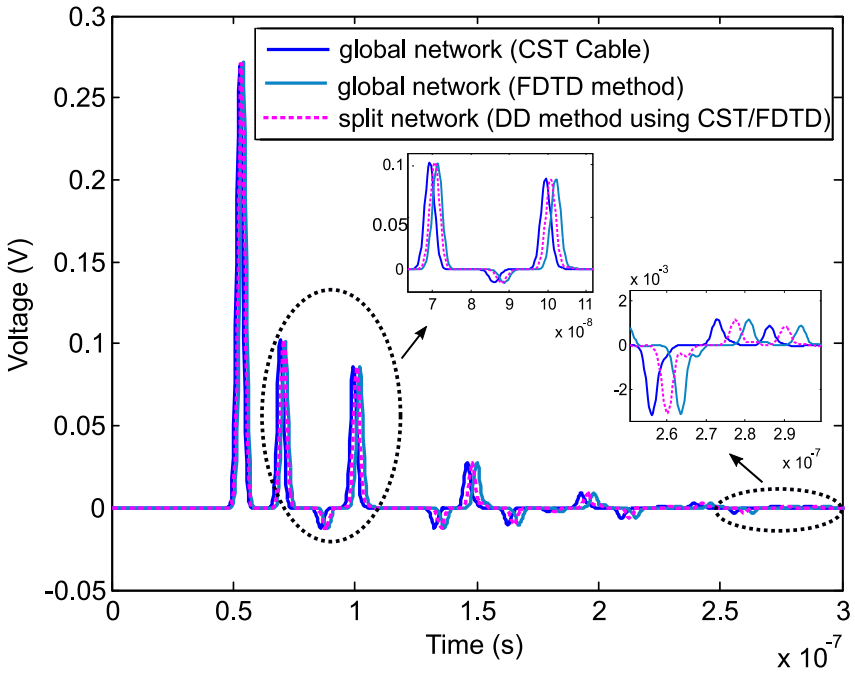

Figure 6: *Comparaison de la tension V_6 à travers la résistance R_{L6} évaluée pour le réseau global (référence) et le réseau divisé (application de la méthode DD pour deux outils numériques différents).*

Dans cette configuration, le résultat de la DD est comparé aux deux références, obtenue chacune en considérant une simulation globale en utilisant un seul outil numérique. Nous précisons encore que cette étape sert à valider note méthode, en pratique la référence n'est pas donnée. La méthode DD donne des résultats satisfaisants, et démontre son applicabilité avec des outils commerciaux d'une part, et son efficacité à approcher le résultat global de l'autre.

Cas 3: interfaces ponctuelles multiples

Nous étudions le réseau de lignes de transmission de la Figure (7a) composé de 5 multi-conducteurs (MTL) et de 2 jonctions. Chaque MTL se compose de trois câbles monofilaires importés directement de la bibliothèque CST Cable®: 'LIFY_0qmm5', 'LIF_0qmm8' et 'LIFY_0qmm10', correspondant respectivement aux lignes L_1, L_2 et L_3, dont les longueurs sont supposées égales. Pour cette configuration, nous proposons de diviser le réseau global au milieu de la ligne MTL_4 en 2 sous-réseaux comme représenté dans la Figure (7b).

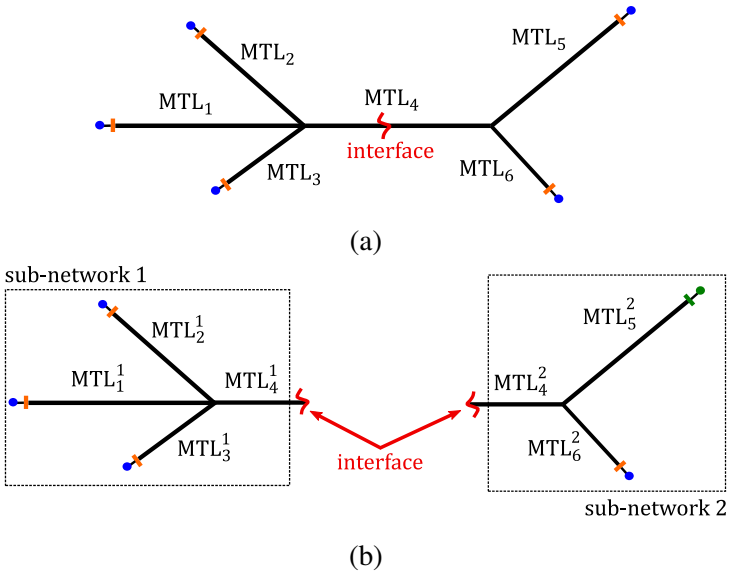

Figure 7: *Réseau multi-conducteur global divisé au milieu de la ligne MTL_4, sous-réseaux 1 et 2 après la subdivision du réseau global (b).*

La formulation finale permettant de retrouver la tension $V^2_{5,\,1}$ mesurée au niveau de la résistance de charge du conducteur 1 de la ligne multifilaire MTL_5 est donnée par

$$V^2_{5,\,1} = \sum_{m=1}^{3} \left(h^2_{45,m} * V^2_{\sim 4,m} + h^2_{45,m} * V^2_{\sim 4,m,1} + \sum_{i_m=2}^{q_m} h^2_{45,m} * \left(h^1_{44,m} * \left(h^2_{44,m} * V^2_{\sim 4,m,i_m} \right) \right) \right) \tag{10}$$

avec $V^2_{\sim 4,m,i_m}$ est défini comme le i-ème ordre des sources équivalentes à l'interface m de la ligne $L^2_{4,m}$. Leurs expressions sont déduites à partir de

$$V^2_{\sim 4,m,i_m} = h^1_{44,m} * \left(h^2_{44,m} * V^2_{\sim 4,m,i_m - 1} \right) \tag{11}$$

En évaluant l'équation (10) pour les ordres $i_1 = 5$, $i_2 = 1$ et $i_3 = 1$, le résultat obtenu est reporté sur la Figure (8).

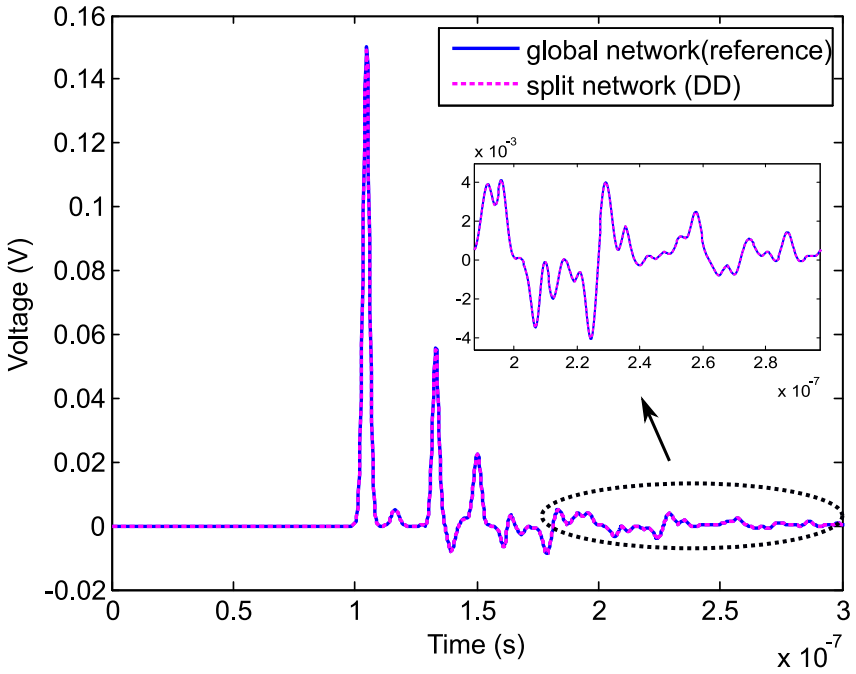

Figure 8: *Comparaison de la tension $V_{5,1}$ aux bornes de la résistance $R_{L5,1}$ évaluée pour le réseau global (référence) et le réseau divisé (application de la méthode DD pour deux outils numériques différents).*

Le résultat de la DD est en très bon accord avec la référence. La technique se généralise donc facilement à des cas avec plusieurs interfaces ponctuelles, indépendemment de la topologie du réseau, des types de câbles, du nombre de conducteurs dans la MTL, de la décomposition elle-même et de l'observable.

Validation expérimentale de la méthode de décomposition de domaine

La méthode DD proposée se distingue par sa caractéristique intrinsèque asynchrone permettant une modélisation indépendante de chaque sous-système. Cette indépendance est à la fois temporelle, puisqu'il n'y a pas d'échange itératif dans le temps, et spatiale, puisque le système est physiquement divisé. Sa transposition dans des expériences pratiques peut sembler du plus grand intérêt, compte tenu des difficultés à réaliser les mesures (limitations des ressources disponibles), d'une part, et de la multitude des partenaires impliqués dans les composants ou les parties du système étudié, d'autre part. Dans ce cas, la confidentialité des modèles est un véritable problème pour les différentes parties, et la méthode de décomposition proposée semble être une solution appropriée pour préserver la confidentialité des modèles.

A partir des résultats numériques démontrés dans la section précédente, la méthode de décomposition de domaine est générale et peut s'appliquer pour tout problème linéaire. Son principe reste inchangé pour les configurations expérimentales également, mais sa formulation, basée principalement sur l'évaluation des réponses impulsionnelles, n'est pas adaptée pour des applications pratiques en raison de limitations physiques. Une méthode alternative permettant d'extraire la réponse impulsionnelle d'un système linéaire à partir de n'importe quel signal temporel non nul réalisable expérimentalement est proposée. La transposition de la technique DD expérimentalement est étudiée pour deux réseaux de lignes de transmission. L'efficacité de la méthode à résoudre des applications dans un environnement réel est démontrée à partir des résultats obtenus.

Extraction expérimentale de la réponse impulsionnelle

La méthode DD est principalement basée sur l'évaluation des réponses impulsionnelles de chaque sous-système. En pratique, leurs extractions est un vrai défi étant donné la difficulté d'injection d'une impulsion de Dirac. Pour surmonter cette limitation physique, nous proposons une méthode alternative visant à retrouver la réponse impulsionnelle à partir de n'importe quel signal temporel et de sa réponse. L'approche a été initialement développée au sein de l'équipe CEM de l'Institut Pascal dans le cadre de la thèse d'Ali Al Ibrahim [128].

La réponse d'un système à un signal $\alpha(t)$ peut être obtenue soit directement en la mesurant, ou par l'intermédiaire du produit de convolution de la réponse impulsionnelle du système avec cette source, donnée par le produit $R(\alpha(t)) = h * \alpha(t)$. A partir de cette définition, une écriture

matricielle de ce produit de convolution peut être déduite, et réécrite de manière à faire apparaître une matrice P construite à partir de la source $\alpha(t)$. Cette matrice, appelée *matrice de passage*, permet de passer de la base canonique $\mathscr{B} = \{e_0, ..., e_m\}$ de l'espace vectoriel $\mathbb{R}^{m+1}$, à une nouvelle base $\mathscr{C} = \{\alpha(0), ..., \alpha(m)\}$, construite à partir du signal $\alpha(t)$. La réponse impulsionnelle h est donc évaluée en résolvant le nouveau système linéaire, telle que

$$h = (P^\top P + \varepsilon \, \mathrm{I_d})^{-1} P^\top R(\alpha) \tag{12}$$

où $\mathrm{I_d}$ est la matrice d'identité. Le paramètre de Tikhonov $\varepsilon > 0$ est choisi suffisamment petit pour ne pas fausser la solution, par exemple $\varepsilon = 1e-8$. Cette technique de régularisation [129] est utilisée pour s'affranchir de l'instabilité numérique du produit $P^\top P$ (qui est en général due au mauvais conditionnement).

Application de la méthode de décomposition expérimentale

La méthode DD permet de modéliser chaque sous-système de manière totalement indépendante. Comme indiqué précédemment, cette caractéristique est très importante pour les applications industrielles, où les partenaires ne partagent pas leurs systèmes (topologie, types de lignes, charges, etc.) pour des raisons de propriété et de confidentialité. Il est donc fort probable que les outils de mesure disponibles pour les différents partenaires ne soient pas les mêmes non plus. Les caractéristiques générales et asynchrones de la méthode DD permettent de s'affranchir de cette contrainte, les équipements utilisés pour l'injection et/ou l'acquisition sont totalement indépendants de la méthode.

Nous étudions le réseau de la Figure (9) composé de 7 câbles, tels que les lignes L_4^1 et L_4^2 sont interconnectées par un connecteur BNC-T. L'injection de la source se fait avec l'AWG (Arbitary

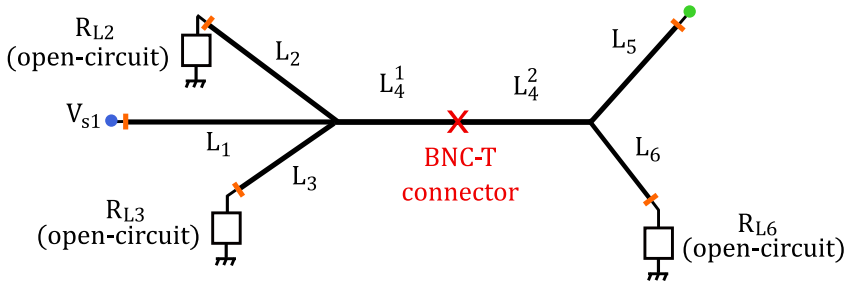

Figure 9: *Représentation schématique du réseau de lignes de transmission étudié.*

Wave Generator) à l'entrée de la ligne L_1 et l'acquisition de la tension V_5 est effectuée par les deux oscilloscopes (deux mesures globales sont réalisées), comme representé sur la Figure (10).

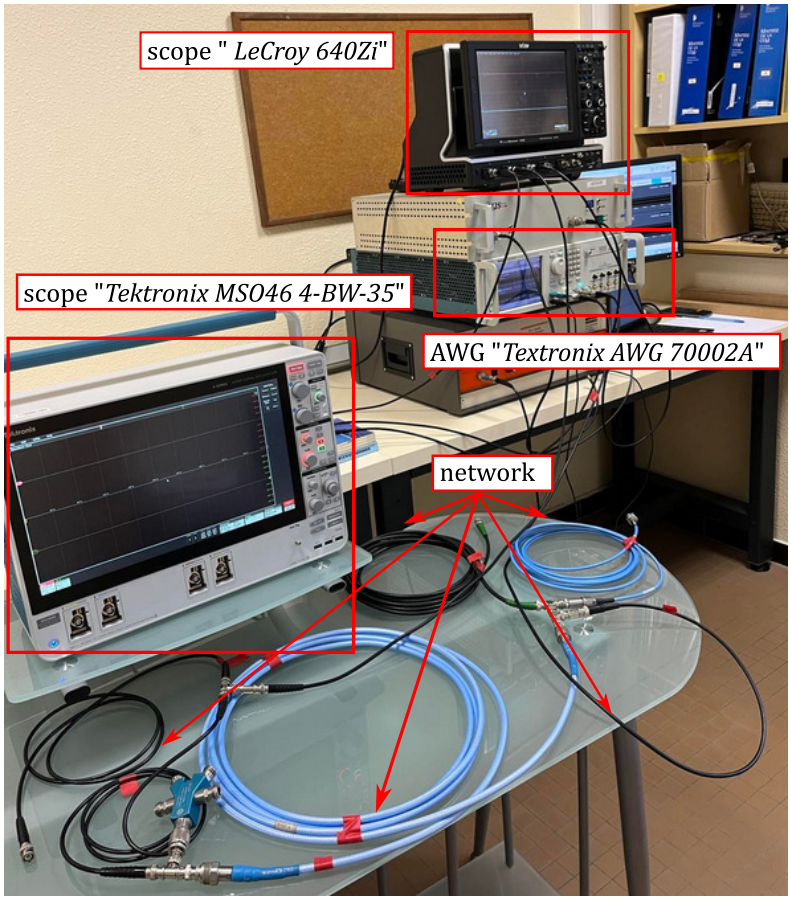

Figure 10: *Montage expérimental pour le réseau de câbles étudié, y compris les deux oscilloscopes utilisés pour l'application de la méthode DD.*

On s'intéresse à la tension V_5 mesurée à l'extrémité de la ligne L_5 par la méthode de DD en découpant le réseau global au niveau de l'interconnexion liant les lignes L_4^1 et L_4^2. L'observable est localisé dans le sous-réseau 2 ($k = 2$), son expression est déduite à partir de la formule (2), et exprimée par

$$V_5^2 = h_{45}^2 * V_{\sim 4,1}^2 + \sum_{i=2}^{q} h_{45}^2 * \left(h_{44}^1 * (h_{44}^2 * V_{\sim 4,i}^2)\right) \tag{13}$$

où $V_{\sim 4,1}^2$ est le premier ordre de la source équivalente au niveau de l'interface donné par le produit $(h_{14}^1 * V_{s1}^1)$. Le i-ième ordre de cette source est exprimé par

$$V_{\sim 4,i}^2 = h_{44}^1 * (h_{44}^2 * V_{\sim 4,i-1}^2) \tag{14}$$

Les réponses du sous-réseau 1 sont mesurées à l'aide de l'oscilloscope *Tektronix MSO46 4-BW-35* et d'un signal sinusoïdal pour $\alpha(t)$. Les réponses du sous-réseau 2 quant à elles sont

mesurées avec l'oscilloscope *LeCroy 640Zi* et une impulsion à double gaussienne pour $\alpha(t)$. Le dispositif expérimental pour l'extraction des réponses h_{14}^{1} et h_{45}^{2} est illustré dans les figures (11) et (12). L'évaluation des réponses h_{ll}^{k} au niveau de l'interface ($l = 4$) est similaire aux applications précédentes.

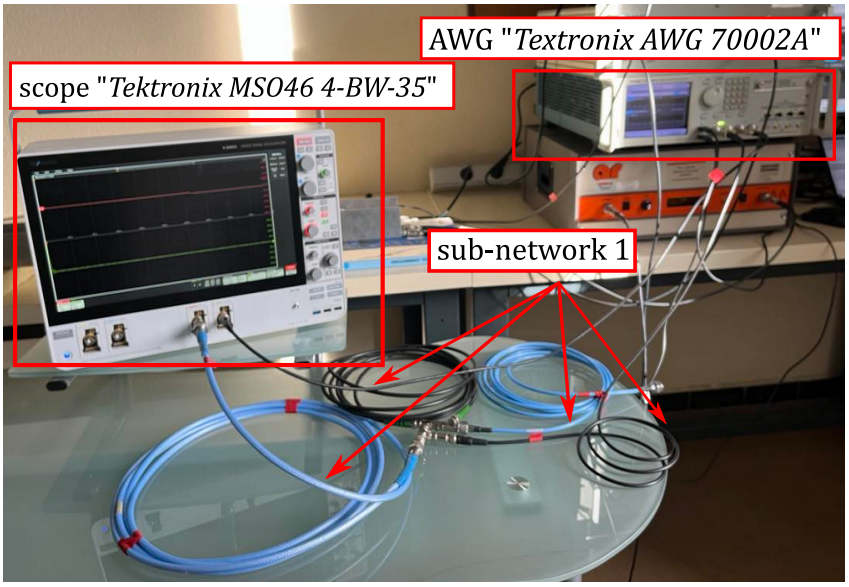

Figure 11: *Mesures expérimentales pour l'évaluation de la réponse h_{14}^{1} du sous-réseau 1.*

En utilisant la méthode alternative, proposée dans la section précédente, pour construire les réponses impulsionnelles de chaque sous-réseau et en suivant une technique d'interpolation de ces résultats, l'évaluation de l'équation (13) à l'ordre $q = 4$ donne le résultat reporté sur la Figure (13).
Les résultats mesurés avec les deux oscilloscopes pour le réseau global sont très proches, malgré leurs différences d'amplitude expliquées par le caractère aléatoire du bruit propre à chaque oscilloscope. La tension V_5 mesurée par la méthode DD est très proche de ces références. Les petites différences d'amplitude sont dues à des erreurs numériques dans l'interpolation des résultats ainsi que par le lissage des réponses mesurées $h_{...}^{k}$.

En synthèse, la méthode DD s'est avérée efficace dans les environnements de mesure. La technique a d'abord été adaptée pour la rendre expérimentalement réalisable, en proposant une méthode alternative d'extraction des réponses impulsionnelles qui surmonte les contraintes expérimentales. Conformément aux objectifs de la thèse, et pour mieux représenter une situation réelle dans laquelle la technique DD peut être utile, l'utilisation de différents oscilloscopes pour l'acquisition de données pour chaque sous-système a été étudiée. La caractéristique asyn-

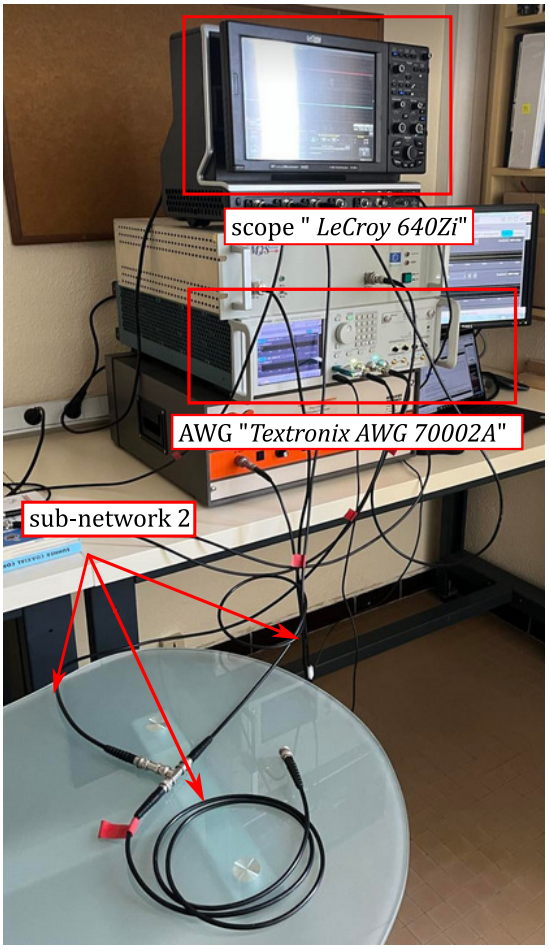

Figure 12: *Mesure expérimentale pour l'évaluation de la réponse h_{45}^2 du sous-réseau 2.*

chrone de la méthode permet de réaliser des études paramétriques, en ré-évaluant les sous-systèmes modifiés uniquement. Ce nouvel avantage semble prometteur pour les applications industrielles, où la plupart du temps, les expériences sont difficiles et coûteuses. Dans ce cadre, la méthode préserve la confidentialité du sous-système et n'échange aucune information sur sa topologie ou ses caractéristiques autres que ses réponses impulsionnelles.

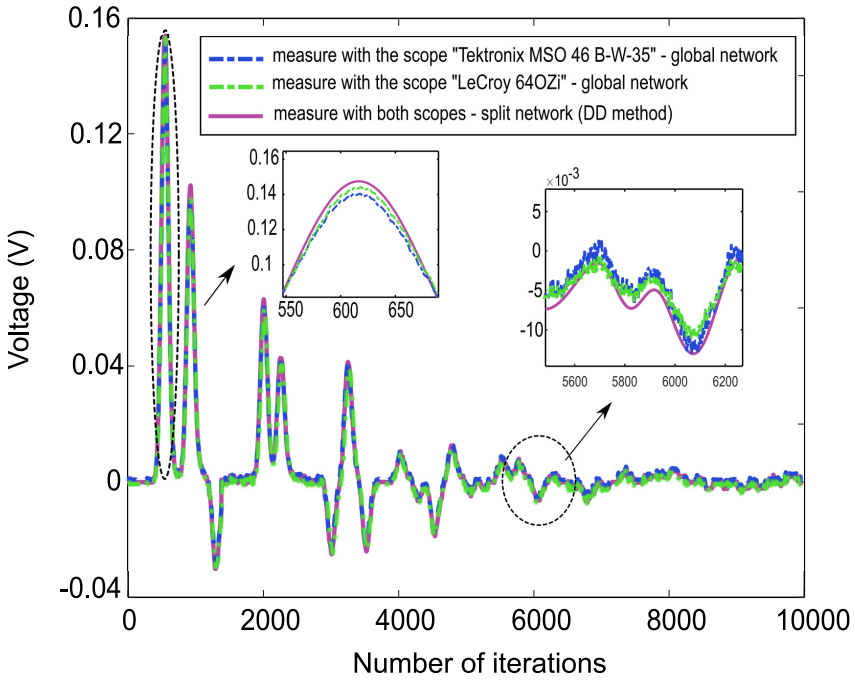

Figure 13: *Comparaison de la tension mesurée V_5 pour le réseau global (les deux références) et le résultat obtenu à l'aide de la méthode DD (réponses partielles mesurées) pour le réseau divisé.*

Association de la méthode de décomposition de domaine avec la technique de collocation stochastique

La nature asynchrone de la méthode DD présente un avantage majeur pour les études paramétriques. Que les réponses impulsionnelles soient calculées numériquement, à l'aide d'un code numérique ou d'un logiciel commercial, ou qu'elles soient mesurées expérimentalement, la modélisation des sous-systèmes modifiés offre des gains de temps et de ressources significatifs. Cette caractéristique particulière est encore plus marquée pour la dimension stochastique. Au cours des dernières années, la quantification de l'incertitude pour les problèmes de CEM a continué d'évoluer en fonction des progrès technologiques et des exigences industrielles. L'un des défis rencontrés réside dans la complexité des problèmes, reflétée par leur caractère multi-physique et multi-échelle. Un autre niveau de difficulté apparaît avec la dimension de l'incertitude. L'analyse stochastique devient difficile et coûteuse en termes de calcul, en particulier pour les systèmes à haute dimension. La méthode DD peut constituer une solution efficace à ces contraintes, car elle permet de passer de la résolution d'un système complexe global à des sous-systèmes plus simples ne se chevauchant pas et

d'une dimension stochastique inférieure.

La méthode DD est étendue aux applications CEM stochastiques linéaires dans le domaine temporel. Dans le cadre de ces travaux de thèse, la méthode de DD sera associée avec la technique de collocation stochastique, choisie pour ses multiples avantages (formulation simplifiée, caractère non-intrusif, et taux de convergence rapide). Le concept de la méthode DD stochastique est mis en pratique à travers des applications de réseaux de lignes de transmission. L'efficacité de la technique à propager les incertitudes entre les sous-systèmes est d'abord démontrée. Sa caractéristique asynchrone est ensuite mise en évidence avec différentes configurations d'intensités et de lois de distribution de variables aléatoires (VA). Étant donné qu'une analyse stochastique complète nécessite l'étude de toutes les combinaisons possibles, cela se traduit par un coût d'évaluation important du modèle. Ce coût est encore plus important lorsque le nombre de paramètres d'entrée stochastiques est élevé. Pour relever ce défi, appelé *la malédiction de la dimensionnalité*, une association offline-online de la méthode SC avec la stratégie DD est proposée.

Méthode de décomposition de domaine pour l'analyse stochastique

La méthode DD **déterministe**, telle que présentée jusqu'à présent, est basée sur l'évaluation des réponses impulsionnelles des sous-systèmes. La solution du système global est ensuite construite par une combinaison linéaire de ces solutions partielles, évaluées une seule fois et appelées **déterministes**. Dans le cas stochastique, les variations autour des valeurs nominales des VA dans un sous-système nécessitent une réévaluation des réponses impulsionnelles qui le caractérisent.

La formulation de la méthode DD stochastique est obtenue en projetant la sortie V_j^k de m entrées, donnée par

$$V_j^k(x_1,...,x_M) = \sum_{\{i\}} h_{ij}^k\big(x_1,...,x_M\big) * V_{si}^k\big(x_1,...,x_M\big) + \sum_{\{l\}} h_{lj}^k\big(x_1,...,x_M\big) * V_{\sim l}^k\big(x_1,...,x_M\big) \quad (15)$$

sur la base des polynômes de Lagarange, tel que

$$\begin{aligned} V_j^k(x_1,...,x_M) &\approx \sum_{t_1=0}^{n_1} ... \sum_{t_M=0}^{n_M} V_j^k\big({x_1}^{(t_1)},...,{x_M}^{(t_M)}\big)\big(L_{t_1}^1 \otimes ... \otimes L_{t_M}^M\big) \\ &\approx \sum_{t_1=0}^{n_1} ... \sum_{t_M=0}^{n_M} \Big[C_{Rs}^k\big({x_1}^{(t_1)},...,{x_M}^{(t_M)}\big) + C_{\sim s}^k\big({x_1}^{(t_1)},...,{x_M}^{(t_M)}\big)\Big]\big(L_{t_1}^1 \otimes ... \otimes L_{t_M}^M\big) \end{aligned} \quad (16)$$

avec $C_{Rs}^{k}\left(x_1,...,x_M\right)$, respectivement $C_{\sim s}^{k}\left(x_1,...,x_M\right)$, sont des termes décrivant la contribution des sources réelles, respectivement des sources équivalentes.
En se basant sur la propriété des polynômes de Lagrange (symbole de Kronecker) et sur les règles de quadrature, la moyenne et la variance de la sortie V_j^k sont exprimées par

$$\begin{aligned}\mathbb{E}\left[V_j^k(X_1,...,X_M)\right] &\approx \sum_{t_1=0}^{n_1}...\sum_{t_M=0}^{n_M}\omega_{t_1}...\omega_{t_M}V_j^k\left(x_1^{(t_1)},...,x_M^{(t_M)}\right)\\ &\approx \sum_{t_1=0}^{n_1}...\sum_{t_M=0}^{n_M}\omega_{t_1}...\omega_{t_M}\left[C_{Rs}^{k}\left({x_1}^{(t_1)},...,{x_M}^{(t_M)}\right)+C_{\sim s}^{k}\left({x_1}^{(t_1)},...,{x_M}^{(t_M)}\right)\right]\\ &\approx \sum_{t_1=0}^{n_1}...\sum_{t_M=0}^{n_M}\left[C_{Rs}^{k'}\left({x_1}^{(t_1)},...,{x_M}^{(t_M)}\right)+C_{\sim s}^{k'}\left({x_1}^{(t_1)},...,{x_M}^{(t_M)}\right)\right]\end{aligned} \tag{17}$$

avec

$$C_{Rs}^{k'}\left({x_1}^{(t_1)},...,{x_M}^{(t_M)}\right)=\omega_{t_1}...\omega_{t_M}C_{Rs}^{k}\left({x_1}^{(t_1)},...,{x_M}^{(t_M)}\right) \tag{18}$$

$$C_{\sim s}^{k'}\left({x_1}^{(t_1)},...,{x_M}^{(t_M)}\right)=\omega_{t_1}...\omega_{t_M}C_{\sim s}^{k}\left({x_1}^{(t_1)},...,{x_M}^{(t_M)}\right) \tag{19}$$

De même, la variance est exprimée comme suit

$$\begin{aligned}Var\left[V_j^k(X_1,...,X_M)\right] &= \sum_{t_1=0}^{n_1}...\sum_{t_M=0}^{n_M}\omega_{t_1}...\omega_{t_M}V_j^k\left(x_1^{(t_1)},...,x_M^{(t_M)}\right)^2-\mathbb{E}\left[V_j^k(X_1,...,X_M)\right]^2\\ &= \sum_{t_1=0}^{n_1}...\sum_{t_M=0}^{n_M}\left[C_{Rs}^{k"}\left({x_1}^{(t_1)},...,{x_M}^{(t_M)}\right)^2+C_{\sim s}^{k"}\left({x_1}^{(t_1)},...,{x_M}^{(t_M)}\right)^2\right]\\ &\quad-\mathbb{E}\left[V_j^k(X_1,...,X_M)\right]^2\end{aligned} \tag{20}$$

avec

$$C_{Rs}^{k"}\left({x_1}^{(t_1)},...,{x_M}^{(t_M)}\right)^2\approx\omega_{t_1}...\omega_{t_M}C_{Rs}^{k}\left({x_1}^{(t_1)},...,{x_M}^{(t_M)}\right)^2 \tag{21}$$

$$C_{\sim s}^{k"}\left({x_1}^{(t_1)},...,{x_M}^{(t_M)}\right)^2\approx\omega_{t_1}...\omega_{t_M}C_{\sim s}^{k}\left({x_1}^{(t_1)},...,{x_M}^{(t_M)}\right)^2 \tag{22}$$

Le calcul des indices de Sobol à l'aide de la méthode SC repose sur l'évaluation du modèle pour toutes les combinaisons possibles de VA. La variance conditionnelle pour une entrée donnée est obtenue en adaptant la formulation et en combinant le modèle déjà évalué pour l'entrée correspondante.

Les indices de sensibilité principaux et totaux de Sobol' sont donc récupérés selon leur définition

$$S_u = \frac{V_u}{V} \tag{23}$$

$$S_{T,u} = \sum_{u \subseteq v \subseteq \mathscr{U}} \frac{V_v}{V} \tag{24}$$

avec V_u est la variance partielle liée à la VA X_u évaluée à l'aide de la méthode DD, et donnée par

$$V_u = \sum_{i_1=1}^{n_1} ... \sum_{i_k=1}^{n_k} (V_j^k)_{u'} (x_{i_1}^1 ... x_{i_k}^k)^2 \omega^u - \sum_{w \subset u} V_w \tag{25}$$

La nouvelle sortie $(V_j^k)_{u'}$ fait référence au modèle évalué pour l'ensemble complémentaire u'. Son expression dépend des nouveaux termes $(C_{Rs}^k)_{u'}$ et $(C_{\sim s}^k)_{u'}$ traduisant respectivement la contribution des sources réelles et équivalentes dans le sous-système k pour l'ensemble complémentaire u'. Leurs expressions respectives sont données par

$$(C_{Rs}^k)_{u'}(x_1,...,x_k) = \sum_{\{i\}} (h_{ij}^k)_{u'}(x_1,...,x_k) * (V_{si}^k)_{u'}(x_1,...,x_k) \tag{26}$$

$$(C_{\sim s}^k)_{u'}(x_1,...,x_k) = \sum_{\{l\}} (h_{lj}^k)_{u'}(x_1,...,x_k) * (V_{\sim l}^k)_{u'}(x_1,...,x_k) \tag{27}$$

Application de la méthode de domaine de décomposition stochastique

Dans le cadre de l'analyse de fiabilité, l'analyse de la valeur seuil (threshold en anglais) peut être envisagée pour évaluer les risques potentiels les plus élevés de dysfonctionnement d'un système. La conséquence la plus critique des incertitudes des paramètres d'entrée peut concerner les valeurs de surtension et de surintensité de la sortie du système. Ces dernières peuvent causer de graves dommages aux équipements électriques et électroniques sensibles, entraînant la défaillance du système.

Dans ce contexte, nous étudions le réseau de lignes de transmission de la Figure (14) composé de 6 câbles coaxiaux RG-58 et de 2 jonctions et modélisé à l'aide du logiciel commercial CST Cable Studio®.
Sur la base de la méthode SC, on s'intéresse à la réponse stochastique (moyenne et variance) de la tension V_4 aux bornes de la résistance de charge R_{L4}, lorsque les longueurs L_3, L_5 et L_6 sont considérées comme des VA. Pour simplifier la notation dans la suite, ces VA L_3, L_5 et L_6 seront appelées R_1, R_2 et R_3 dans le même ordre. Chacun de ses paramètres suit une loi normal

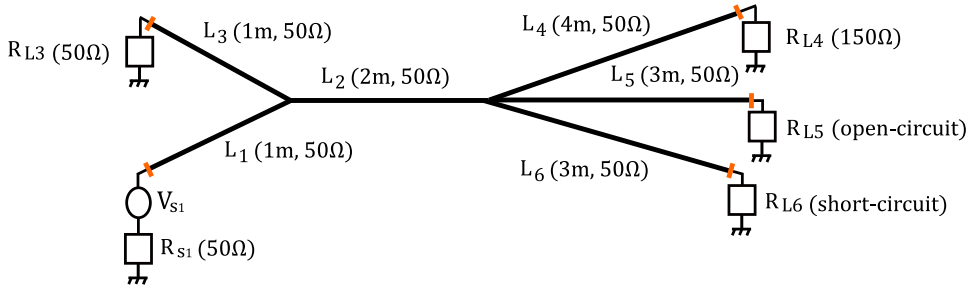

Figure 14: *Caractéristiques du réseau global étudié.*

$\sim \mathcal{N}(0,1)$, et varie avec des intensités 20%, 10% et 10%, dans le même ordre de leur définition.

Nous supposons que ce problème est maintenant résolu par la méthode DD, de sorte que le réseau est divisé au milieu de la ligne L_2 en deux sous-réseaux comme le montre la figure (5.16). En suivant le principe de la technique DD, la tension V_4^2, située au niveau du sous-réseau $k=2$, est exprimée comme suit

$$V_4^2 = h_{24}^2 * V_{\sim 2}^2 + h_{24}^2 * \underbrace{\left(h_{22}^2 * (h_{22}^1 * V_{\sim 2}^2)\right)}_{V_{\sim 2,1}^2} + \sum_{i=2}^{q} h_{24}^2 * \left(h_{22}^2 * (h_{22}^1 * V_{\sim 2,i}^2)\right) \tag{28}$$

où $V_{\sim 2}^2$ est la tension équivalente à l'interface d'échange donnée par le produit $(h_{12}^1 * V_{s1}^1)$, et $V_{\sim 2,i}^2$ est défini comme son i-ème ordre et exprimé comme suit

$$V_{\sim 2,i}^2 = h_{22}^2 * (h_{22}^1 * V_{\sim 2,i-1}^2) \tag{29}$$

Suite à la décomposition, la VA R_1 représentée par la longueur L_3 est située dans le sous-réseau 1, tandis que les deux VA R_2 et R_3 sont isolées dans le sous-réseau 2. La moyenne et l'écart-type de la tension stochastique V_4^2 sont respectivement donnés par

$$\begin{aligned}
\mathbb{E}\left[V_4^2(R_1,R_2,R_3)\right] &= \sum_{t_1=0}^{n}\sum_{t_2=0}^{n}\sum_{t_3=0}^{n} \omega_{t_1}\omega_{t_2}\omega_{t_3} * \left(h_{42}^2(r_2{}^{(t_2)}, r_3{}^{(t_3)}) * \left(h_{12}^1(r_1{}^{(t_1)}) * V_{s1}^1\right)\right) \\
Var\left[V_4^2(R_1,R_2,R_3)\right] &= \sum_{t_1=0}^{n}\sum_{t_2=0}^{n}\sum_{t_3=0}^{n} \omega_{t_1}\omega_{t_2}\omega_{t_3} * \left(h_{42}^2(r_2{}^{(t_2)}, r_3{}^{(t_3)}) * \left(h_{12}^1(r_1{}^{(t_1)}) * V_{s1}^1\right)\right)^2 \\
&\quad - \mathbb{E}\left[V_4^2(r_1,r_2,r_3)\right]^2
\end{aligned} \tag{30}$$

En évaluant la tension V_4^2 à l'ordre $q=4$, les valeurs de moyenne et d'écart-type sont en très bon accord avec la référence donnée par la simulation du réseau global. La technique DD prouve sa capacité à propager les incertitudes au sein du sous-réseau lorsque leurs deux paramètres ont été modifiés.

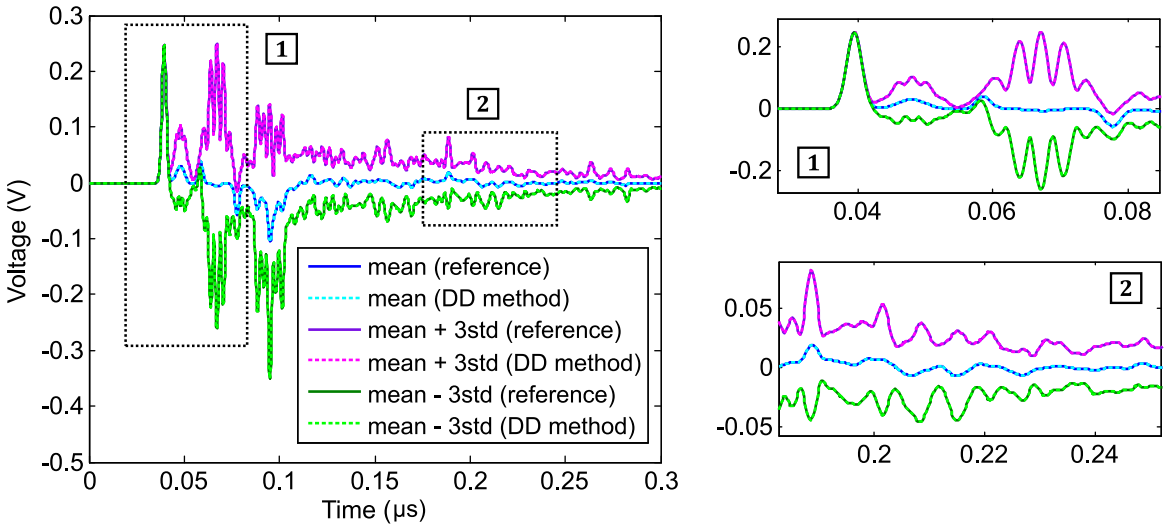

Figure 15: *Comparaison des valeurs moyennes et de l'écart-type de la tension V_3 pour les réseaux global (référence) et découpé (méthode DD pour $q = 4$).*

Conclusion et perspectives

Ces travaux de thèse sont principalement orientés vers le développement d'une approche de décomposition de domaine pour l'analyse CEM des systèmes linéaires complexes. L'évaluation de la réponse du système est garantie par les solutions partielles des sous-systèmes, modélisés indépendamment les uns des autres. La nécessité de développer de telles méthodes est principalement motivée par les limitations des approches existantes, l'hybridation des outils numériques temporels par exemple, pour 1) permettre des simulations totalement indépendantes des sous-systèmes, 2) préserver la confidentialité des modèles, et 3) dépasser la complexité d'adaptation de leur interface (pour la discrétisation temporelle et/ou spatiale) pour s'adapter à des applications générales concernant la géométrie et/ou les propriétés des matériaux des systèmes étudiés.

La méthode DD proposée est une technique facile à mettre en œuvre, basée sur une stratégie offline-online caractérisant des sous-systèmes moins complexes uniquement par leurs réponses impulsionnelles, à partir desquelles la solution globale est obtenue sur la base d'une combinaison linéaire. La technique offre trois avantages majeurs :

- la décomposition est **générale**, elle est indépendante du cas et peut être automatisée pour toute application linéaire,
- la formulation est **asynchrone**, ce qui signifie que les sous-systèmes sont modélisés in-

dépendamment au niveau hors ligne. Leurs réponses sont combinées dans la phase en ligne, afin de prendre en compte les propriétés physiques du problème initial et les couplages existants entre les sous-systèmes,

- la **confidentialité** des modèles est **préservée**, étant donné qu'aucune information propriétaire et/ou résultat n'est échangé.

Ces avantages ont été démontrés par des applications numériques pour différentes configurations (plusieurs interfaces, différents outils de modélisation, réseaux complexes à des interfaces ponctuelles multiples) de réseaux de lignes de transmission. La caractéristique asynchrone de la méthode DD est mise en évidence par les applications expérimentales, en particulier pour des équipements de mesure différents pour chaque sous-système. La configuration fournit non seulement une démonstration pratique de la véritable signification de la décomposition asynchrone, basée sur une caractérisation indépendante (à la fois temporelle et spatiale) à l'aide de différents instruments, mais elle s'approche également de situations réelles impliquant des fournisseurs et des assembleurs, dans le contexte automobile. Étant donné que les expériences ont tendance à être coûteuses (en termes de temps et de ressources humaines), la méthode DD permet des gains de coûts significatifs pour les études paramétriques.

Cet avantage supplémentaire présente un potentiel considérable pour des applications plus coûteuses : l'analyse stochastique. Les résultats obtenus ont démontré la capacité de l'approche de décomposition du domaine à propager les incertitudes au sein des sous-systèmes, tout en préservant la confidentialité des modèles stochastiques. En outre, la méthode DD stochastique atténue la malédiction de la dimensionnalité découlant des problèmes de dimension stochastique élevée. Elle réduit considérablement le nombre d'évaluations du modèle, généralement très coûteux à évaluer. Cette caractéristique est très prometteuse et maintient l'efficacité de techniques telles que SC et PC sans compromettre le coût de calcul.

Dans la continuité de cette thèse, nous proposons quelques perspectives pour des travaux futurs, concernant :

1. *l'aspect numérique*:

    - la technique de DD peut être intégrée dans une plate-forme de simulation impliquant plusieurs partenaires. Chaque partenaire modélise un sous-système m, et n'échange que deux informations: la réponse impulsionnelle de son système au niveau de l'interface et la tension d'onde entrante des sources physiques dans ce système au niveau de l'interface.

- la méthode de DD peut être appliquée aux problèmes de CEM en mode rayonné, ainsi qu'au couplage électromagnétique/électrique dans des cas particuliers (cavités électromagnétiques avec ouvertures).

2. *l'aspect expérimental* : la méthode DD peut être entièrement expérimentale, en commençant par l'évaluation des réponses impulsionnelles, en prenant en compte les ordres supérieurs, et en terminant par l'évaluation de la formulation finale. Cette nouvelle vision nécessite la mise en place d'un banc d'essai plus complexe, et le développement d'un système de contrôle des différents outils de génération et d'acquisition pour automatiser le processus de mesure.

3. *la dimension d'incertitude* : l'aspect d'incertitude peut être poussé plus loin en combinant la méthode DD avec différentes méthodes stochastiques, autres que SC et PCE, où le défi se pose avec des échantillons différents de part et d'autre de l'interface. La méthode devra donc être adaptée pour surmonter cette contrainte, mais l'idée et le principe de base restent les mêmes.

General Introduction and Context

Context

SAFETY standards in the automotive field are of paramount importance due to the inherent risks associated with transportation. In the ElectroMagnetic Compatibility (EMC) context, the rapid integration of advanced technologies into tomorrow's vehicles raises concerns about their safety and reliability. While these innovations offer numerous benefits, including improved efficiency and connectivity, they also introduce new complexities and potential vulnerabilities to electromagnetic interferences (EMI). It is therefore crucial to ensure compliance with standards limiting parasitic emissions from the car and respecting people's exposure to electromagnetic fields inside the vehicle while guaranteeing the proper operation of all equipments. Deploying new technologies requires therefore a thorough analysis of the electromagnetic performance of the complex vehicle systems. Considering electromagnetic compatibility in the early design phase will ensure safety, reliability, functionality, and compliance.

Nowadays, numerical simulation is an indispensable tool for automotive EMC modeling. It allows electric/electronic architecture validation in the early stage of design. These numerical computational methods have improved significantly over the past years. Their features (accurate modeling of the physical phenomena), speed (fast simulations) and size (large-scale problems) have evolved in response to advances in computer technologies and the emergence of new mathematical techniques. However, their use for full-system EMC simulations has not progressed proportionally due to both technical and industrial issues. Although assemblers and suppliers require a collaborative and interdependent exchange, neither of them is willing to provide their numerical model. Intellectual property protection is thus challenging, and alternative solutions should be proposed to preserve the confidentiality of models of all involved parts. The computation time and memory size for large system simulations are additional constraints to the established problem. Its complexity is reflected at different levels and requires an innovative approach compared with conventional strategies:

- *Multi-scale*: a single numerical method seems unable to cover the differences in scale (from system to component level). Despite the efficiency of hybridization methods (Finite Difference, Finite Volume), they still require to adapt their numerical time step and meshing parameters, making the conditions at the interfaces difficult to handle,

- *Multi-methods/models*: given the complexity of the configurations (geometries, materials, etc.), different specialized tools can be combined such that each sub-system is modeled with the most appropriate solver.

Up to this day, there is no software solution to solve a complex EMC problem in its entirety (conducted and radiated), and diversity. The challenge for all the ANR *ECOCES* project partners is to develop a co-simulation methodology for assessing EMC phenomena in complex systems through independent simulation of all sub-systems. In this approach, the various models are neither shared between partners nor integrated into a single tool, but communicate in real-time via their interfaces.

With the continuous evolvement of connected vehicles, their complexity goes beyond the established constraints with the uncertainty dimension, adding a *multi-uncertainties* level. EMC problems are growing needs for an accurate consideration of their randomnesses. Whether the multiple existing sources of uncertainties are known, related to their design (geometric and material properties), their environment (external parameters or neighboring systems), or unknown (no grip on system uncertainties), their quantification in co-simulation techniques requires the use of adapted techniques, intended to be *non-intrusive* to consider the diversity and multitude of scales and methods.

The aim of this thesis is to propose a domain decomposition approach to solve complex EMC problems in the time domain. Each sub-system is modeled independently from the others, and the exchange at the interface level should preserve the confidentiality of each model. Our work focuses on the quantification of uncertainties for EMC domain decomposition applications as well. The emphasis of the stochastic analysis is on the adaptability of the proposed methodology to take into account the uncertainties between the different sub-systems while acknowledging the diversity and complexity of the problem. The proposed technique should be general regarding the random variations in input data (intensities and distribution laws), the choice of stochastic methods, and the choice of observable parameters.

Academic and industrial partners

This thesis work was developed within the framework of the ANR[1] project *ECOCES* (Electromagnetic Compatibility Co-simulation Of Complex Electrical Systems) integrating three thesis subjects and involving academic and industrial partners. The project idea was

[1] `https://anr.fr/Projet-ANR-19-CE05-0016`

originally suggested by the automotive industrial partner **STELLANTIS**[2], according to the encountered problems.

Figure 16: *Academic and industrial partners.*

The first thesis was launched in October 2020, in the **Ampère laboratory**[3], whose research activities focus on the EMC of power systems, mainly extensive modeling of converters. The thesis work developed by Diallo Amadou Bayaghiou was devoted to setting up a co-simulation method for assessing the electromagnetic compatibility of power electronics systems. His thesis defense took place in Lyon on September 21st, 2023.

The second Ph.D. subject, whose work is presented in this manuscript, started in October 2020, in **Institute Pascal**[4] within the EMC team. Its main focus is put into deterministic and stochastic numerical models for solving electromagnetic problems (s.g. networks of multi-wire transmission lines, three-dimensional structures, etc.). These numerical simulations are complemented by experimental measurement using reverberant and anechoic chambers.

The third thesis is launched at **IETR**[5] and aims at proposing a co-simulation method at the

[2] `https://www.stellantis.com/fr`
[3] `http://www.ampere-lab.fr/`
[4] `http://www.institutpascal.uca.fr/`
[5] `https://www.ietr.fr/`

component level. The team's EMC research activities focus on innovative modeling strategies for the analysis of complex statistical systems, as well as statistical analysis.

The **GeePs**[6] laboratory is an active partner in the co-direction of A.-B. Diallo thesis. Its main areas of research are energy conversion systems and electromagnetic coupled problems. The laboratory combines a three-fold approach: theory, numerical modeling and experimental validation.

Chiastek[7], a co-simulation platform editor, provides high-value-added solutions for systems engineering based on complex product models in aerospace, automotive and other industries.

Thesis outline

The following thesis is composed of five chapters:

Chapter 1: This chapter starts with a non-exhaustive state-of-the-art of domain decomposition methods for computational electromagnetic applications, in both frequency and time domains. The thesis work developed in Ampère laboratory is briefly presented. Our work is positioned regarding the existing methods in the time domain while identifying the complementary our technique adds with respect to the ANR project specifications. The focus is later put on the stochastic analysis dimension and the motivations behind the necessity of considering the uncertainties in electromagnetic problems. The main used stochastic techniques for EMC applications for uncertainty quantification and sensitivity analysis are reviewed.

Chapter 2: This chapter presents the general principle of the Domain Decomposition (DD) method and its mathematical foundations to solve linear systems. After explaining its theory, the DD technique is illustrated by numerical applications in wiring networks. A different point-of-view of the DD method, regarding its implementation, is proposed for realistic real-world configurations. The new formulation of the technique is given, with numerical illustrations.

Chapter 3: This chapter proposes to extend the application of the DD method for different scenarios, and proves its efficiency for each of these configurations. The technique is generalized to more than one interface exchange to prove its efficiency for complex wire networks.

[6] `https://www.geeps.centralesupelec.fr/`
[7] `https://www.chiastek.com/`

For different simulation parameters of the numerical tool of each sub-system, the method still gives satisfactory results. Based on this, the robustness of the approach is demonstrated by using commercial software and numerical codes. Lastly, the DD methodology is applied to a multi-one-point interface decomposition problem. Its new formulation is detailed and implemented for a multi-wire network application.

Chapter 4: This chapter aims to validate the DD method experimentally to test its robustness in a measurement environment. The DD technique is first adapted to overcome some experimental constraints. It is then applied to different wiring network configurations. The DD technique is tested using different equipments for each sub-system. The demonstration, very close to reality, gives satisfactory results. Additional advantages of the DD technique are proved through parametric studies. The significant cost gain in terms of required measurement time is an additional advantage of the methodology.

Chapter 5: This chapter deals with the uncertainty dimension for electromagnetic problems solved using the proposed DD methods. After recalling some elements of probability, the focus is put on second-moment methods for the assessment of mean and variance, and global sensitivity analysis for the evaluation of Sobol' indices. The DD methodology's ability to propagate uncertainty between the sub-systems is demonstrated through two different EMC applications. The stochastic DD technique's aptitude in preserving the stochastic confidentiality of the models is later demonstrated. Finally, a discussion based on the dramatic reduction of the evaluation cost resulting in the association of the stochastic collocation method with the proposed DD methodology is carried out.

CHAPTER 1

Domain Decomposition Methods and Stochastic Analysis: State of the Art and Context

Contents

We begin this first chapter by reviewing the state-of-the-art of the different Domain Decomposition (DD) methods developed earlier for Computational ElectroMagnetic (CEM) problems. The adapted DD techniques for the ElectroMagnetic Compatibility (EMC) field, for frequency-domain analysis, are recalled. However, as this thesis focuses on the time domain, a literature review of the existing temporal DD methods, including the hybridization of numerical methods is presented. Both advantages and limitations of these proposed techniques will be discussed,with the aim of positioning our work within these existing techniques, regarding the specifications of the ANR project and the first thesis' objective. Within this framework, the research work developed in "Ampère laboratory" by Amadou Bayaghiou Diallo in his thesis focused on cooperative simulation methods referred to as *co-simulation* techniques. This new term will be defined in the following, along with the approach proposed by A.-B. Diallo. As the second thesis and initial main objective is to carry out a stochastic analysis for DD problems, the second section of this chapter starts by giving the motivation of stochastic studies for EMC problems. A non-exhaustive state-of-the-art of some of the most used stochastic techniques will be presented later.

1.1 Domain Decomposition methods

Domain Decomposition methods are powerful techniques used in the field of computational mathematics and scientific computing. The fundamental strategy of the DD methods is to decompose the entire computational domain into many subregions based on the local material properties and geometrical features. Subsequently, the most suitable numerical technique for each of the subregions is used. They address information exchange between subdomains in shared regions (field continuity, fluxes, etc.).

1.1.1 History of DD methods and their theoretical foundations

DD techniques were originally proposed by H. A. Schwarz who gave it its name [1], to determine the solution of a partial differential equation (equation of *Poisson*) on a domain of non-trivial form. Since analytical solutions could only be found for domains of a particular shape (disk and rectangle), he came up with the idea of decomposing the non-trivial domain into elementary domains to solve the equation separately (see Figure (1.1a)). The challenge, of course, is to link the solutions calculated on the sub-domains in order to reconstruct the solution on the whole domain. While assuming that g defined on $\partial\Omega$ is known, the aim is to retrieve the

Figure 1.1: Example of domain decomposition methods with overlap (a) and without overlap (b).

solution of the equation of *Poisson* on the domain Ω, such that

$$\begin{cases} -\Delta u &= 0 \text{ in } \Omega = \Omega_1 \cup \Omega_2 \\ u &= g \text{ in } \partial\Omega \end{cases}. \tag{1.1}$$

Shwarz proposes to alternately solve the problem in each of the sub-domains with transmission conditions based on the solution just computed in the neighboring subdomain. More precisely, Schwarz demonstrates that the *alternating Schwarz* algorithm initialized by u_2^0 and updated according to

$$\begin{aligned} -\Delta u_1^{n+1} &= 0 \text{ in } \Omega_1 \\ -u_1^{n+1} &= g \text{ in } \partial\Omega_1 \cap \partial\Omega \\ -u_1^{n+1} &= u_2^n \text{ in } \partial\Omega_1 \cap \overline{\Omega_2} \end{aligned} \tag{1.2}$$

$$\begin{aligned} -\Delta u_2^{n+1} &= 0 \text{ in } \Omega_2 \\ -u_2^{n+1} &= g \text{ in } \partial\Omega_2 \cap \partial\Omega \\ -u_2^{n+1} &= u_1^{n+1} \text{ in } \partial\Omega_2 \cap \overline{\Omega_1} \end{aligned} \tag{1.3}$$

converges to the solution of the *Poisson* problem (1.1) and therefore that this solution exists.

If the convergence is not achieved for a given ε, an additional iteration is performed. This way of iterating is known as the *multiplicative Schwarz* method. The convergence is controlled by the choice of overlap. The greater the overlap, the faster the algorithm will converge [2]. The *alternating Schwarz* method can be generalized to several subdomains. However, it is possible that some sub-domains are linked to several others, and care needs to be taken with the order in which the problems on the subdomains are solved. The disadvantage of the *alternating*

Schwarz method is its sequential nature since each sub-domain depends on the solution just obtained in the neighboring sub-domains via the boundary condition.

In order to overcome this limitation, P.-L. Lions has proposed a fully parallel version [3], which takes advantage of the power of the computer to increase computing speed. Instead of performing successive calculations at each iteration, each sub-domain is calculated in parallel. This translates simply into an index change in equations (1.2) and (1.3). The solutions u_1^n and u_2^n known at the iteration n are used in parallel to determine u_1^{n+1} and u_2^{n+1}. This new formulation is referred to as *additive Schwarz* method. The *parallel* version can also be generalized to more than two sub-domains. However, the convergence for multiple overlaps may be difficult to achieve (it requires finding the right sequence for applying boundary conditions in multiple overlaps). In addition, the number of elementary operations is doubled for these methods.

Various methods have been developed on the basis of the Schwarz method to extend this type of approach to a non-overlapping method and increase its algorithmic efficiency. In the follow-up work developed by Lions, a non-overlapping version of the Schwarz approaches was proposed in [4] (see Figure (1.1b)), based on *Robin* boundary conditions[1] [5].

In general, it is important to be able to handle domain decomposition methods without overlap, especially for heterogeneous problems. The non-overlapping domain decomposition techniques, also known as *substructuring methods*, overcome these constraints by new conditions (Schur's complement [6]) at the interfaces. They were initially introduced by Janusz Stanisław Przemieniecki in 1963 [7], and can be classified into two categories: the *Balancing Domain Decomposition* (BDD) [8], and the iterative *Finite Element Tearing and Interconnect* (FETI) [9].

In summary, DD methods can be categorized into two main families:

- *overlapping methods* also known as Schwarz methods, divide the global domain into overlapping regions. The local problems are solved on each sub-domain. The coupling between the solutions of the different sub-domains is ensured by the common overlapping region [1].
- *non-overlapping methods* or Schur's complement methods, separate the unknowns vari-

[1] For Ω a domain in which an equation is to be solved, and $\partial\Omega$ its edge, the *Robin* boundary condition is defined by $\alpha v + \beta \nabla v = g$.

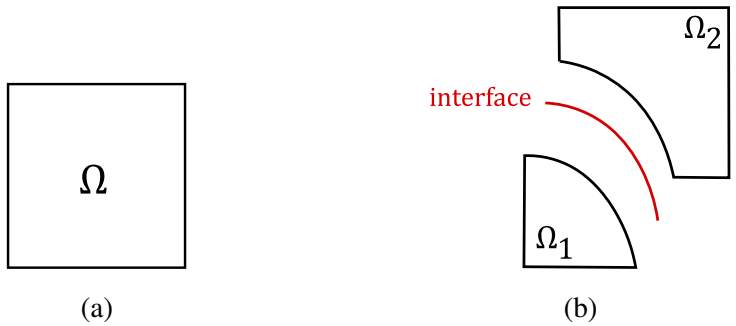

Figure 1.2: Example of Schur domain decomposition of the global domain Ω (a) into two subdomains Ω_1 and Ω_2 (b).

ables due to the decomposition into two subsets: one formed by the unknowns located on the interface and the other by the unknowns located inside the subdomains. Once the Schur complement has been formed with respect to the inner variables, a system involving the interface variables is solved first, the interior unknowns are later deduced [7].

1.1.2 Domain decomposition methods for electromagnetic applications

Throughout the years, the use of domain decomposition methods has been extended to many engineering fields, including computational electromagnetics. These methods aim to divide the computational domain into smaller subdomains to solve the electromagnetic equations efficiently. They allow for efficient parallelization and can handle large and complex geometries.

Domain decomposition techniques have been proposed for a wide array of applications. In [10], a non-overlapping DD method for electromagnetic radiation and scattering analysis of multi-target problems was presented. Lu and al. proposed in [11] an efficient algorithm based on a domain decomposition method and partial basic solution vectors technique for solving three-dimensional large-scale finite periodic electromagnetic problems. They introduced Robin-type conditions at interfaces between subdomains to enforce field continuity. Authors in [12] demonstrated the accuracy and flexibility of an embedded domain decomposition method in handling non-conformal geometries. Other researchers associated the DD method with other numerical tools. For instance, Diego M. Solís and al. [13] investigate the efficiency and accuracy of a surface integral equation domain decomposition approach for realistic electromagnetic compatibility engineering. The method provides an accurate and fast solution for real-life EMC/EMI studies. Other researchers have also been interested in combining

a domain decomposition approach with integral equations to solve electromagnetic wave scattering from non-penetrable objects. The method relieves the burden of mesh generation and is proved to be efficient and robust for solving multi-scale electromagnetic problems. In [14], the DD method was associated with a multi-solver for modeling multiple antennas conformally mounted on a large platform. The authors validated their association through numerical applications and measurements.

Broadly speaking, overlapping DD methods are known to be iterative techniques. They require local solvers at the transmission condition level to ensure convergence between the sub-models. In [15], the authors propose an iterative domain decomposition method (IDDM) for large-scale full-wave analysis of electromagnetic fields. This iterative solution may be computationally expensive, consequently, researchers focused on overcoming this cost by adapting the DD techniques to be independent from the iterations. In [16], the authors propose an iteration-free domain decomposition method, with Robin-type transmission conditions, for fast finite element analysis of electromagnetic problems. The approach does not suffer from the issue of convergence rate and avoids redundant computations. The use of a high-performance computing scheme and domain decomposition method, proposed by Wang and al. in [17], overcomes the convergence deficiency of conventional iterative solvers for large-scale electromagnetic problems.

Most of the existing DD methods are proposed for frequency-domain applications. However, few works in time-domain have emerged. A domain decomposition finite-difference time-domain (FDTD) technique has been proposed for solving large electromagnetic problems [18]. This method divides the computational domain into manageable subdomains with overlapping regions and uses perfectly matched layer (PML) layers to absorb outgoing waves. The tangential electric fields are stored on an interface plane to generate the field in the adjacent subdomain. The technique considers the effect of multiple reflections between the subdomains, allowing for accurate simulation of large electromagnetic problems that are difficult to handle using direct FDTD methods. Another dual-field time-domain finite-element domain-decomposition method for efficient computational electromagnetics was proposed by Lou and al. in [19]. The method divides the computation domain into non-overlapping subdomains and solves second-order vector wave equations to compute the electric and magnetic fields in each subdomain. The method requires minimum communication between subdomains, making it suitable for parallel computations.

One of the most widely used sub-categories of DD methods in the time domain are hy-

bridization of numerical tools [20–27]. Several works are based on the hybridization of the FDTD [28] method with other techniques. Q. Sun and al. [22] introduced a new hybrid method that combines the computational efficiency of finite-difference time-domain (FDTD) and the meshing flexibility of finite-element time-domain (FETD) for electromagnetic modeling with non-conformal meshes, to facilitate electromagnetic modeling by exploiting both the computational efficiency of FDTD and the meshing flexibility of FETD. The proposed hybrid method allows nonconformal meshing and overcomes late-time instability. The authors in [29] developed a 3-D hybrid implicit explicit single-field finite-difference time-domain (FDTD) method for the electromagnetic simulation of structures with fine details in one or two Cartesian directions. It requires the solution of tridiagonal matrices and explicit updates at each time step. The computational efficiency and accuracy of the method have been demonstrated through numerical examples and comparisons with other methods. Another hybrid time-domain technique that combines the finite element, finite difference, and method of moment techniques used to solve complex electromagnetic problems was proposed in [26]. This technique brings together the ability of the finite difference time domain (FDTD) scheme to handle arbitrary material properties, the versatility of the finite element time domain (FETD) to accurately model curved geometries, and the method of moments (MoM) to analyze thin-wire structures. It operates in the time domain, providing wide-band information from a single execution and simplifying the interfacing of different methods. In [27], the hybrid Finite Difference Time Domain (FDTD) - Partial Element Equivalent Circuit (PEEC) method is used to analyze the electromagnetic compatibility (EMC) of multilayer printed circuit boards (PCBs). This method combines the advantages of FDTD and PEEC techniques to reduce simulation times and improve computational efficiency. A similar EMC problem of PCBs and metallic antenna structures was solved through hybridization of the partial-element equivalent-circuit (PEEC) method and the method of moments (MoM) [23]. The PEEC technique is used to model the coupling from a homogeneous electric field into a system of conductors in the presence of a substrate, while the MoM is applied as a full-wave method for metallic scatterers such as antennas. This hybrid approach allows for a significant reduction in numerical complexity and computational effort while maintaining accuracy. Its validity has been demonstrated through numerical examples and measurements. In [25], L. Zhang and al. also studied the electromagnetic interference of PCBs. They proposed a modeling approach using an equivalent magnetic dipole array deduced from near-field scanning results obtained at a certain height over the PCB surface under test and the finite-difference time-domain (FDTD) algorithm.

Other researchers combined finite difference/finite volume methods, including P. Bonnet

and al. [30], who combined a finite-volume method with an unstructured conformal mesh to represent the scatterer and its immediate neighborhood, while using a classical finite-difference method with an efficient boundary condition, such as the PML formalism, for the remaining part of the computational domain. He and al. [31] proposed a new local time-step scheme that combines the finite difference and cell-centered finite volume methods and aims to improve the computational efficiency of the method. In [21], the authors propose a hybrid spectral finite-difference time-domain (FDTD) with the discrete-time time-domain vector fitting (TD-VFz) algorithm to analyze three-dimensional periodic structures excited by oblique incident plane waves over a wide frequency band.

Alternative hybridization methods to FDTD have also been proposed. In [32], the authors propose a fast time-domain finite element-boundary integral (FE-BI) method for electromagnetic analysis. The approach combines finite element and boundary integral field representations to achieve a sparse system matrix and solutions free of spurious modes. It utilizes higher-order vector basis functions and curvilinear tetrahedral elements to accurately model the geometry and represent the fields. To handle problems involving large electrical dimensions, a multilevel plane-wave time-domain (PWTD) algorithm is used to accelerate the evaluation of the boundary integrals. The proposed method demonstrates superior accuracy and efficiency in analyzing electromagnetic scattering phenomena in both two-dimensional (2-D) and three-dimensional (3-D) cases. An improved vector wave equation-based discontinuous Galerkin time-domain (IDGTD-WE) method has been proposed in [24] to efficiently solve electromagnetic problems. This method solves the electric field using the primal form of the discontinuous Galerkin time-domain (DGTD) technique based on vector wave equation, while the magnetic field is obtained using a weak form auxiliary equation related to the electric fields.

In summary, the growing interest in DD methods translates through the multitude of its applications for a wide panel of electromagnetic problems. Whether it concerns developing new approaches or improving existing techniques to overcome the new challenges that may arise with technological advances, the DD method's significance and relevance in current research and applications are demonstrated. This non-exhaustive state-of-the-art offers first insights into the existing DD approaches and helps position our work regarding the literature while meeting the ANR *ECOCES* project specifications. In this context, the main project idea is developing a *co-simulation* method for solving complex systems involving a multitude of system scales and physics. The term *co-simulation*, referring to cooperative simulation, may exhibit varying interpretations, and it necessitates a precise definition to avoid ambiguity. In the following section we distinguish between co-simulation in its real sense, and co-simulation as defined in the

context of this project. We further position the work developed by A.-B. Diallo, as one of the other theses of the project, regarding DD methods generally and our proposed DD technique specifically.

1.1.3 Co-simulation approaches

Co-simulation methods are simulation techniques that allow complex systems comprised of sub-systems to be easily simulated. These sub-systems behave conceptually like black boxes. They accept inputs, advance in time with a built-in solver routine up to the next communication point, and finally output some results. Co-simulation can be considered as the joint simulation of the already well-established tools. These co-simulation methods are different from other simulation techniques known as hybrid or parallel.

In his thesis [33], A.-B. Diallo defines the *co-simulation* as the interaction between two simulation tools. A detailed and comprehensive review of the co-simulation methods and their principles is presented. Broadly, the focus is put on three points:

1. *co-simulation methods*: the basic principle of the techniques as well as their classification depending on the coupling (generic or specific) are presented,

2. *concepts of interoperability*: the main causes of interoperability are definied. Other constraints such as model heterogeneity, the multiplicity and confidentiality of simulation tools are detailed,

3. *literature review of co-simulation methods*: the contributions in the automotive and electric power generation and distribution fields are reviewed.

After a thorough study of the difficulties encountered, and the limitations of existing solutions, regarding his thesis objectives, A. Diallo proposed an iterative co-simulation for strongly coupled, wide-frequency band sub-systems for the EMC study of electrical systems.

The approach is based on a Norton equivalent source and an iterative co-simulation algorithm based on the waveform relaxation method. The idea is to consider a high-level graphical partitioning, in which each sub-system studied is surrounded by simplified equivalent circuits representing adjacent sub-systems. The method has been proposed and tested on different applications modeled by electrical circuits (linear and non-linear), and extended to more complex EMC applications:

- for the evaluation of conducted electromagnetic disturbances (common mode and differential mode) in power electronics and validated by experimental measurements on physical prototypes,
- for the study of coupling between the sub-parts of a complex multiphysical system (induction power transfer system for electric vehicles) which is modeled on the one hand by electrical circuits and on the other by a 3D finite element model.

The proposed technique was also validated by experimental measurements and proved efficient in terms of intellectual property protection and computation time savings.

1.1.4 Kron's formalism and Diakoptics

Within the framework of circuit analysis, one of the first techniques in the literature is Kron's formalism. Initially, Gabrial Kron, an American engineer, developed a theory to apply tensor network analysis to the resolution of electrical circuits in the 1930s [34]. This method, mainly used to model electrical machines was nevertheless limited by the computing resources available at that time. Olivier Maurice was one of the first researchers who proposed using this tensor mathematical tool to solve complex EMC problems [35–37]. Kron's formalism extended to multiple EMC applications and several works have been proposed in the past years. In [38], Kron's method is applied to the study of electromagnetic interference in aerospace systems. The method involves using spacecraft and aircraft mock-ups to simulate the performance of Kron-based tools. These tools aim to evaluate the EM disturbances between antennas, electronic equipment, and portable electronic devices found in large systems. Authors in [39] proposed a Kron simulation of field-to-line coupling using both a meshed Taylor cell and a modified Taylor cell. Modified Kron's method has been applied to optimize the response of an LC filter and validate its use and benefits in [40]. Stojanovic and al. [41] proposed more recently a methodology for designing EMI filters based on the modified Kron's method for electromagnetic compatibility for filter attenuation calculation by considering magnetic couplings between components.

Broadly speaking, Kron's method is specifically focused on simplifying complex electrical circuits by dividing them into repetitive sub-circuits. A more general approach, known as *Diakoptics*, has been proposed by Kron in 1957 [42], and collected in his book "The piecewise solution of large scale system". The term *Diakoptics*, of Greek origin, (*dia*: systems, *kopto*: to cut) also known as the "Method of tearing", is a method that decomposes a system containing several variables into p sub-systems solved separately. The method uses the solutions of the i

sub-systems, $i \in \{1, \ldots, p\}$, to find the solution to the initial global problem [43, 44].

To introduce the Diakoptics method, Kron begins by explaining the different points of view from which a "system" can be described. In this case, for electrical systems, a network is made up of branches and impedances. On the one hand, according to Kron, the branches constitute meshes, representing the "graph" according to a combinatorial (algebraic) topology schematized by plane surfaces and lines; on the other hand, the representation of impedances follows a "point" topology described by equations. Physically, the network can only be realized in the presence of branches and impedances. Diakoptics is therefore based on a theory combining a graph and equations associated with a physical system.

In [45], F. Uriarte begins with a simplified explanation of the Diakoptics method. A linear system can be written in matrix form $AX = B$. The solution to the system X can be obtained by inverting the matrix A, but for systems with a large number of variables, calculating the inverse matrix can be very costly. By dividing the initial system into p sub-systems, the matrix A can be decomposed into p-block matrices, each describing the corresponding subsystem. Using algebraic calculations, F. Uriarte finds a formulation of the system solution based on the block matrices of the sub-systems, while respecting the physical conditions of the initial system (coupling between variables, boundary conditions, adaptation conditions). The new formulation of the solution shows the interest of the diakoptics method in the case where a sub-part of the global system varies, the solution of the problem only requires the calculation of the block matrix of this sub-system. The principle of the diakoptics method was taken up by A. Klos [46]. The author explains the matrix formulation of the diakoptics method. For an electrical network where voltages and currents can be expressed from Kirchhoff's laws, the equations at the network nodes and meshes are solved from the new matrix formulation using the diakoptics method.

The use of Diakoptics for electromagnetic problems gained prominence in the early 1990s [47–50]. A resurgence of interest in Diakoptics techniques for EMC applications occurred lately. In [51], the authors used a Diakoptics approach to a magnetic skin-effect problem. Another application of Diakoptics method using Volume Integral Equation (VIE) modeling of subsystems is proposed for 3D electromagnetic analysis in [52]. The technique combines the VIE and surface integral equation formulations, in conjunction with the method of moments (MoM). The authors in [53] used a discrete Green's function approach to couple disjoint domains in the FDTD grid based on the Diakoptics principle.

Overall, the principle of the Diakoptics technique seems very similar to the Domain Decomposition approaches. Although in the literature, many researchers consider the two approaches to be equivalent, there is a subtle difference between the two approaches. An early work proposed by C.-H. Lai in [54], discusses the common grounds between diakoptics and domain decomposition methods and their relation to parallel computing.

1.1.5 Electromagnetic topology

As part of the ongoing efforts to resolve complex electrical circuits and electromagnetic systems, the electromagnetic topology approach is a promising resolution method within the realm of electromagnetic inquiry. The approach was developed several years ago initially for aeronautics by C.-E. Baum in the USA [55], and was extended later for different electromagnetic applications. Its concept is to divide the space of interest into volumic zones to break down a total complex electromagnetic problem into a group of small problems independent of each other. The topological diagram is a helpful abstract vision of the geometry of a system, taking into account the electromagnetic interactions between the different volumes. With this diagram, an inventory of all the penetration paths into the previous volumes can be made and then an interaction graph is drawn. The formalism allows potential approximations to be introduced from graphs describing coupling situations and can lead to a singular simplification of the model to be simulated within the framework of computational structures.

Based on the decomposition into distinct but interconnected volumes, the topology approach was applied to the processing of cable harnesses. Through the thesis conducted by Jean-Philippe Parmantier [56], the first promising results have been obtained by applying this formalism and its experimental validation. As the method's potential arises for complex wiring systems, the research work carried out by J.-P Parmantier [56] and P. Besnier [57] has led to the development of numerical tools and has given birth to the software CRIPTE (referring to *Calcul sur Réseaux des Interactions Pertubatrices en Topologie Electromagnétique in French*) developed by the French Aerospace Lab **ONERA**. Several works based on the software were proposed for different electromagnetic applications. For instance, in [58] I. Junqua and al. discuss the analysis and evaluation of high-frequency electromagnetic wave penetration in complex oversized systems using the Power Balance approach and electromagnetic topology. In [59], the authors used the CRIPTE software to estimate the effect induced by loads on the conducted propagation of a spurious compromising signal that emanates from electronic devices.

The extension of the electromagnetic topology formalism for other EMC applications was demonstrated by various works, including shielding effectiveness estimation [60], dipole antenna design [61], intentional electromagnetic interference risk analysis [62] and reflectometry simulation for an aircraft harness [63].

Throughout this non-exhaustive state-of-the-art regarding electromagnetic topology formalism, we aimed to acknowledge the existence of the approach and its efficiency in resolving a wide range of electromagnetic complex problems. However, our methodology is distinguished by a different positioning, which will be presented in the section section.

1.1.6 Positioning of thesis work

Following the definition of DD methods generally, and hybridization of numerical tools especially, we can conclude on their different formulations regarding the method proposed by A.-B. Diallo. An upgraded non-overlapping iterative domain decomposition method with new boundary conditions may lead to similarities in formulation to A.-B. Diallo's thesis work. This aspect is out of the scope of our thesis.

The wide range of literature on DD methods proves how valuable tools they are for solving large-scale problems. However, they have some limitations, including

- *problem dependency*: the effectiveness of the DD method may depend on the studied problem (complex geometry, physical properties, strong coupling),
- *convergence and iteration*: overlapping DD methods require iterative solvers to achieve convergence.
- *preconditioning*: for iterative solvers, the choice of efficient preconditioners can be challenging.

This research field is active in addressing some of these limitations and making DD methods more accessible and efficient for a wider range of applications.

With the established state-of-the-art, we notice that the mainly existing DD methods are proposed for frequency domain applications. Their transposition to the time domain, however, is not straightforward. Despite few works proposed in the time domain, the majority of temporal DD techniques concern the hybridization of numerical methods. They proved their efficiency for different applications, however, they mainly depend on the numerical tools

themselves. A specific adaptation of the time step between sub-domains (FDTD methods), the spatial step (FVTD tools), or both in the case of hybridization of these two techniques, is required. The implementation of the hybrid method may be complex to achieve, as the numerical schemes need to be adapted or extended for the studied application while ensuring stability and consistency of the association of the different techniques.

In this thesis, we propose a domain decomposition technique in time domain for EMC linear applications that overcome most of these constraints. It is based on the evaluation of the impulse responses of the sub-systems, exchanged at the interface level(s). These partial solutions are associated through a linear combination (product of convolution) to retrieve the global solution. The main advantages of the technique are related to the following elements:

1. it is iteration-free: the method allows fully asynchronous simulations of the sub-systems,
2. it preserves the confidentiality of the models: no other information (data and/or result) other than the impulse responses of each sub-system is required for the exchange,
3. it is case-independent: the approach considered the studied systems as black boxes. It is general and may be applied with different numerical tools,
4. it is experimentally reproducible: its easy implementation can be also considered through measurement.

Moreover, within the framework of this thesis and its objectives, the proposed DD method is associated with a stochastic technique. It proved its efficiency for uncertainty propagation and allows significant computation cost gains.

1.2 Stochastic analysis: Uncertainty Quantification and Sensitivity Analysis

Probabilistic engineering aims at taking into account the uncertainties appearing in the modeling of physical systems and studying the impact of those uncertainties on the system response. This field combines the branches of physics on the one hand and applied mathematics on the other (e.g. statistics, probability theory and computer simulation). Ever since it emerged in electromagnetic engineering, various methods for introducing uncertainty analysis in models of physical systems have been proposed. In the framework of this thesis, we focus on uncertainty quantification and sensitivity analysis aspects for the stochastic study.

1.2.1 Introduction and motivations

Uncertainty quantification and its propagation are key elements for stochastic analysis in many engineering fields including EMC. They are crucial for understanding the reliability and limitations of models and simulations in the presence of uncertain inputs. Uncertainty Quantification (UQ) is the process of quantifying and analyzing the uncertainties in mathematical models, simulations, and data. The primary aim is to account for the effects of variability, randomness, and misspecification in models while helping with decision-making, risk assessment, and improvement of models' robustness.

With the increasing complexity of electromagnetic systems, computer models are required to design, simulate and predict their behavior since real experiments are, most of the time, nearly impossible to carry out. These numerical simulators feature a number of parameters characteristic of the physical phenomena under consideration. Due to a lack of knowledge or their intrinsic nature, the input parameters are subject to uncertainty. It is therefore essential to assess how these uncertainties affect the outputs of the calculation code, through uncertainty propagation studies and sensitivity analysis (SA). The interdisciplinary nature of UQ can be summarized in a few fundamental steps gathered in the "UQ methodology" framework [64, 65] represented in Figure (1.3).

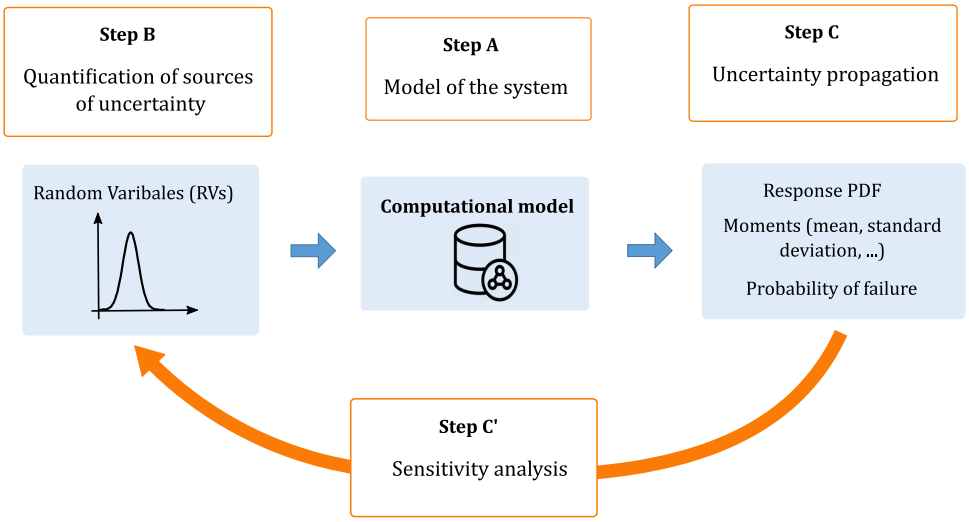

Figure 1.3: The uncertainty quantification (UQ) framework [64, 65].

The UQ methodology can be divided into four basic steps detailed below:

- Step A consists in *defining the model* that accurately represents the physical behavior of

the system. It can be either an analytical formula or a full multidisciplinary computational model. The modeling of the problem requires a clear definition of the input(s) and output(s) of the model.

- Step B consists in *quantifying the sources of uncertainty* affecting the input variables. They are usually classified as follows:
  - epistemic uncertainty: refers to uncertainty arising from a lack of knowledge or information. It is often associated with the limited understanding of a system or phenomenon,
  - aleatory uncertainty: arises from inherent variability or randomness in a system. It is gathered from observations/measurements showing a natural variability in the values of a given parameter.

  Several tools are available to model uncertain input variables depending on their nature. This step is beyond the scope of this thesis work, consequently, we consider that the input parameters follow a given distribution law and are modeled as random variables.

- Step C consists in *propagating the uncertainty* in the input parameters through the model. As a result, the response of the model is also random. Depending on the objectives of the stochastic analysis, different statistics of the output may be of interest: mean, standard deviation, other higher-order statistical moments, probability density function (PDF), etc.

- Step C' consists of carrying the *sensitivity analysis*, whose aim is to study how the input variables impact the variability of the output(s). The main SA methods will be outlined further.

1.2.2 Uncertainty Quantification in the EMC field

The interest of UQ in the EMC field, first and foremost, is enabling better control of electromagnetic compatibility margins by taking into account the random nature of the studied systems. For industrial needs, the probabilistic EMC analysis reinforces certain specifications upstream or relaxes others, depending on the level of safety required or any other constraints (financial, technical, ...). The stochastic analysis can also help determine the critical components of a piece of equipment, or the critical equipment within a system. In this case, reducing the uncertainties can be envisaged.

The first uncertainty propagation methods used in EMC focused on evaluating the statistical moments of the random response of systems [66]. The Monte Carlo (MC) method, for instance, is one of the most used approaches. It is based on the use of random processes to obtain numerical approximations, hence the name taken from the famous Monte Carlo casino, renowned for its games of chance. The method was invented and used during the World War II, for the nuclear weapon Manhattan Project. Its application then spreads to several engineering fields including EMC to model and analyze electromagnetic interference and compatibility. Researchers have used Monte Carlo methods to simulate electromagnetic wave propagation [67], scattering [68], and probabilistic risk analysis [69], making it an invaluable tool for predicting EMC performance. One of the many applications of the technique was the computation of the probabilistic-statistical model of a reverberation chamber [70], [71]. The technique was implemented for other applications, such as assessing the susceptibility of printed-circuit-board trace [72], designing antennas [73] or constructing electromagnetic field distribution for field-to-transmission line coupling in reverberation chamber [74].

To ensure good accuracy of the results, the MC method requires a relatively large number of realizations. Its slow convergence $(\frac{1}{\sqrt{N}})$, where N is the number of evaluations, often leads to prohibitive computation time. To overcome this limitation, several variants of the MC itself have been developed, commonly known as variance reduction methods such as the Quasi-Monte Carlo (QMC) [75]. Other alternative methods including the Kriging, polynomial chaos expansion and the stochastic collocation technique have been also proposed to reduce the number of evaluations of the model.

The Kriging technique, also known as Gaussian process regression, is a linear estimation method that guarantees minimum variance [76]. The main idea behind it is to generate a prediction or estimation of a variable of interest at a specific location based on a weighted average of nearby observed data points, taking into account the spatial relationships and correlations among the data points. The method was implemented for different applications in the EMC field [77]. For instance, authors in [78] proposed an algorithm based on the Kriging surrogate model to estimate extreme quantiles in electromagnetic compatibility risk analysis. In another application, the Kriging was combined with Monte Carlo simulation for efficient reliability analysis of radiated susceptibility in coaxial shielded cables [79].

The Stochastic Collocation (SC) method is a non-intrusive numerical approach used to solve stochastic differential equations (SDEs) or stochastic partial differential equations (PDEs) [80]. The technique projects the model's random response onto a base of Lagrange

polynomials. By using weighted sums, it is simple to approximate the statistical moments of the random quantity of interest. Its easy formulation increased its use by researchers in the EMC community. The method's versatility is proved by different applications, including the optimization of stochastic EMC/EMI experiments using resampling techniques [81], the probabilistic modeling evaluation of the reverberation chamber [82], and the stochastic modeling of the electrical parameters in the field of bio-electromagnetic compatibility [83]. Jointly implemented with the FDTD method, the SC technique is used to tackle complex stochastic problems for a dielectric resonator antenna [84].

Polynomial Chaos (PC) expansion is a probabilistic method that consists of developing a summable square function on a base of orthogonal polynomials (Hermite, Legendre, Laguerre, ...). Polynomial chaos theory was first introduced by Wiener in [85]. Its use in uncertainty propagation came along with the work of Roger Ghanem [86]. The general principle is to develop a physical system, described by the numerical model, on a basis called *polynomial chaos*. Over the years, it has been used in several EMC applications [87–91]. In [92], the authors used the polynomial chaos to model transmission lines in the time domain. The technique was employed in [93] to quantify uncertainty due to stochastic variation of material properties. Bdour and Reineix [94] considered the UQ of radiated susceptibility testing for randomized geometrical and electrical parameters of a printed circuit board (PCB).

The evaluation of the first and second statistical moments is essential for UQ, especially for variance-based sensitivity analysis. However, as previously mentioned UQ is not uniquely defined by mean trends, the assessment of PDF tail properties and high-level quantiles is required to compute the probability of failure for the studied system, in relation to a given failure criterion or set of criteria, e.g. threshold values. These methods are known as *reliability analysis* such as FORM/SORM techniques [95].

In the EMC field, *reliability analysis* are designed to take into account reliability or normative requirements imposed on systems potentially subject to EMI. In these cases, we are interested in the probability that an item of equipment or an electrical and/or electronic system will fail in relation to a given threshold values for currents, voltages or powers that must not be exceeded [95–97]. This approach aims to define the best compromise between the emission level of the electromagnetic environment and the immunity level of the system under study, either to satisfy requirements imposed by governmental or standards organizations or to define the best EMC sizing of equipment in terms of reliability and cost [98–100]. Within this context, the use of extreme values (quantiles) of an electromagnetic model subject to uncertainties was explored

in several works [101–103].

1.2.3 Sensitivity analysis methods

Broadly speaking, sensitivity analysis (SA) aims at quantifying the relative importance of each input parameter of a model. Methods of sensitivity analysis are usually classified into two categories [104]:

- *local sensitivity analysis* concentrates on the local impact of input parameters on the model [105]. It focuses on understanding the sensitivity of the model near a specific point in the parameter space. The simplest and most common way to study the sensitivity of inputs is to modify them one by one ("One-At-a-Time": OAT), while the others remain fixed at a nominal value,
- *global sensitivity analysis* looks at the variability of the model's output within its range of variation. It studies how the variability of the inputs affects the variability of the output, by determining how much of the variance of the output is due to a particular input or set of inputs [106–108].

In [109], Saltelli et al. (2000) gathered the global sensitivity analysis methods into two groups:

- *regression-based methods*: they involve fitting a linear regression to the model response on the input parameters. The standardized regression coefficients are then used as direct measures of sensitivity. The regression is required to be linear with respect to the data, otherwise, it is difficult to interpret the standardized coefficients [110],
- *variance-based methods*: these methods aim at decomposing the variance of the model response as the sum of the contribution of each input variable, as well as all possible combinations of interaction between them. They are also known as ANOVA techniques for "ANalysis Of VAriance" [111]. Several sensitivity indices have been created with this method including FAST (Fourier Amplitude Sensitivity Test) indices [112–115] and Sobol' indices [106, 110, 116]. In the work of our thesis, we base the SA on the Sobol' indices.

Other global sensitivity analysis techniques are available, including a qualitative type of global SA known as the screening methods [117]. Morris analysis is one of the most known screening methods. It is based on the "One At a Time" (OAT) design, where each input is varied while fixing the others. The approach allows to establish a hierarchy within the input variables

according to their influence on the variability of the response. However, this ranking is not quantifiable and doesn't consider the interactions between the input variables.

In the past few years, sensitivity analysis has become crucial for the assessment of stochastic analysis for many EMC problems. The SA identifies the factors that have the greatest influence on the electromagnetic performance of the studied system. This helps determine which design elements are most likely to cause electromagnetic interference (EMI) or susceptibility problems. By understanding which parameters have the greatest impact on the quantity of interest QoI, the optimization of the design will help minimizing electromagnetic interference, and consequently improving the overall EMC of the system. From an industrial point-of-view, the identification and quantification of potential influent input parameters in the design phase is of major interest in terms of the production cost.

For both classes, i.e. qualitative (screening methods) and quantitative (global SA approaches), SA has been applied to a wide range of EMC problems. For instance, authors in [95] addressed the safety assessment of transmission lines under uncertain radiated electromagnetic constraints, based on a global sensitivity analysis. Another application of SA for transmission lines was presented in [118] to analyze the risk of EMC failure in transmission lines. Several works evaluating the Sobol indices based on the polynomial chaos technique have been proposed, including antennas and electromagnetic structures modeling [119, 120] and investigating the stochastic response of a printed circuit board (PCB) due to an external plane wave excitation [94]. Other research works implemented Morris indices for the sensitivity analysis, including Yildiz and al. in [121] for EMC risk analysis of PCB, and Bdour and al. in [122] for electromagnetic risk assessment due to external electromagnetic waves in a coaxial shielded cable. The SA has also been implemented for bioEMC application in [123], where the authors examined how the variability in the brain morphology and the tissue properties affect the assessment of the homogeneous human brain exposed to high-frequency electromagnetic (EM) field.

Conclusion

Domain decomposition methods in computational electromagnetics play an important role in solving complex electromagnetic problems, especially in scenarios where traditional solvers may face limitations. These methods enable efficient parallel computations, accurate interface treatment, and the ability to tackle large-scale and intricate electromagnetic simulations. In this

chapter, we defined the fundamentals of DD techniques and discussed their main classifications in the first section. A non-exhaustive state-of-the-art of DD techniques for electromagnetic applications is given. It allowed to position our work, regarding the existing time-domain DD methods generally and the hybridization of numerical temporal tools particularly. As part of the ANR *ECOCES* project, we briefly highlighted the contribution of the research work of A.-B. Diallo, regarding co-simulation techniques. In the second section, we presented a comprehensive study of uncertainty quantification and sensitivity analysis in the context of EMC problems. In the next chapter, the formulation of the proposed DD technique will be given for a general linear electric system. Its implementation through numerical applications will enhance its understanding and practical implementation.

CHAPTER 2

Domain Decomposition Method for Linear Problems in Time-Domain

Contents

AFTER conducting a non-exhaustive analysis of the state-of-the-art regarding domain decomposition techniques generally, and in the time domain precisely, our proposed method is positioned within this framework to ensure its complementary to existing efforts while meeting the specifications of the ANR *ECOCES* project.

In this chapter, we present in detail the proposed Domain Decomposition (DD) method for solving linear electromagnetic problems in the time domain. In the first section, the theoretical basics of the approach are presented for general 1D electric systems with a one-point exchange interface. The method is illustrated with numerical 1D applications of transmission line networks, for which the subdivision occurs at the level of a transmission line. In practice, the decomposition must be carried out "naturally" while maintaining the physical meaningfulness of the initial problem. Consequently, the decomposition of a branched transmission lines network should happen at the junction level. In this context, the DD method is adapted for branched transmission line networks in the second section. The new formulation is illustrated with different configurations of networks. To conclude this chapter, both viewpoints of the proposed technique are compared to highlight their advantages, but also their limitations.

2.1 Decomposition domain method

In the upcoming section, we provide a thorough and detailed presentation of the proposed DD method. This will involve a comprehensive explanation of the underlying principles and the step-by-step procedure of the approach.

By definition, the output y of a linear system[1] of x inputs can be obtained based on its impulse response h. Based on the convolution product, defined by the operator (*), the output y is given by

$$y = h * x \tag{2.1}$$

The convolution is defined as a mathematical operation on two functions (f and g) that produces a third function ($f * g$) that expresses how the shape of one is modified by the other. It is expressed by

$$(f * g)(t) := \int_{-\infty}^{+\infty} f(\tau) g(t-\tau) d\tau \tag{2.2}$$

[1]The inputs x may be voltage/current sources or electric/magnetic fields, and the output y may be a voltage, current or an electromagnetic field.

and represents a fundamental concept in linear time-invariant systems theory and is used extensively to analyze and predict their behavior for different inputs [124].

We suppose that the global electric linear system G, represented in Figure (2.1a), has z terminations representing either inputs (physical injected sources V_s) or measured outputs V_{out}.

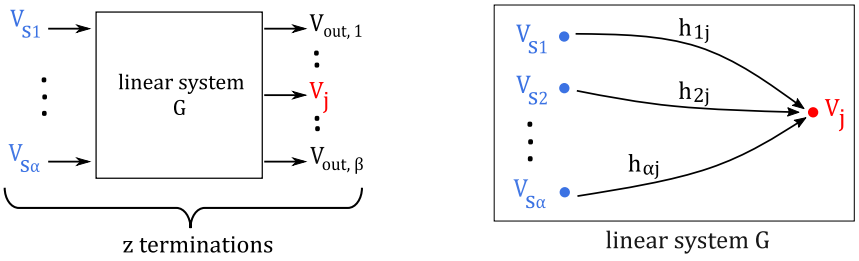

Figure 2.1: *Schematic representation of the global linear electric system G of α inputs and β outputs (a), and the impulse responses h_{ij} linking the sources $V_{si,\ i\in\{1,\dots,\alpha\}}$ to the output V_j.*

Among the β outputs of the system G, we are interested in the voltage V_j referring to the output voltage $V_{out,j}$ measured at the termination j. It is obtained by considering the inherent contribution of each source $V_{si,\ i\in\{1,\dots,\alpha\}}$, following the principle of the convolution in equation (2.1) such as

$$V_j = \sum_{i=1}^{\alpha} h_{ij} * V_{si} \tag{2.3}$$

where h_{ij} refers to the impulse response evaluated between the points i and j, as shown in Figure (2.1b).

For the other outputs, a similar equation to the expression (2.3) can be written.

2.1.1 Formulation of the DD method

The process of the method's application starts by dividing the global system G into m non-overlapping sub-systems. We focus on the sub-system k in which the variable of interest, i.e. the output V_j, is located, as shown in Figure (2.2a). It is important to mention that while other outputs may be featured in the sub-system k, our attention is directed towards one output only, which is the output V_j in our case.

The method is applied with careful consideration of two hypotheses: 1) the system is divided at a one-point interface (1D), 2) the electrical properties of the system are conserved at the interface level. Consequently, no reflections on both sides of the interface (subdivision level) are recorded, and a perfect matching at the interface level is ensured.
In the remainder of this manuscript, all upcoming variables denoted with a k exponent refer to the sub-system k. Consequently, the observable V_j will be denoted V_j^k when the DD method is applied.

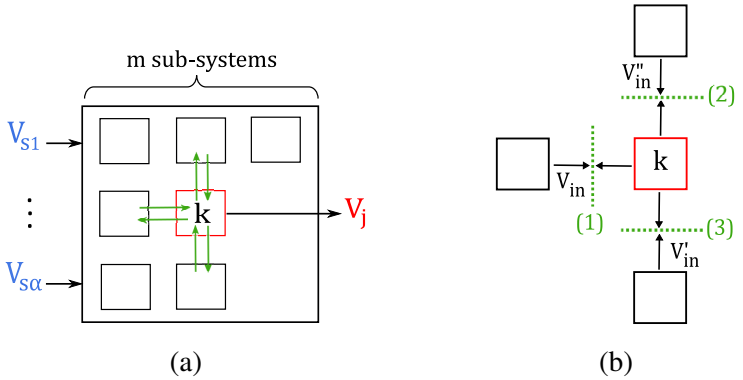

Figure 2.2: *Schematic representation of the subdivision of the global linear electric system G into m non-overlapping sub-systems using the DD method (a), and the incoming waves V_{in}, V'_{in} and V''_{in} from the neighboring sub-systems to the sub-system k (b).*

As a result of this decomposition, the physical injected sources $V_{si,\ i\in\{1,\dots,\alpha\}}$ are dispersed in different sub-systems. However, to maintain the physical behavior of the system, the contributions of each of these sources to the interface should be considered. At each one-point interface of the sub-system k, we define an equivalent source $V_\sim$ translating the contribution of the incoming waves from the neighboring sub-systems, as shown in Figure (2.2b). For instance, the equivalent source $V_\sim$ at the interface (1) refers to the response of the sub-system to the incoming wave V_{in}. Its expression is given on the basis of equation (2.1) as follows:

$$V_\sim = h * V_{in} \tag{2.4}$$

with h is the impulse response measured between the injection point of the input V_{in} and the interface.

Up to this point, we have only mentioned the contribution of each neighboring sub-system to the interface, whereas to recover the physical behavior of the global system as if no decomposition

has occurred, both retro-actions from each neighboring sub-system and the sub-system k must be considered. This exchange occurring at the interface level will be detailed later in this chapter. In the meantime, only the contributions of the neighboring sub-systems to the sub-system k are evaluated.

To establish the expression of the output V_j^k, we assume that the sub-system k featuring the observable V_j^k of n terminations includes p sources $V^k_{s\{i\},\ \{i\}\subseteq\{1,\ldots,\alpha\}}$ with $p<\alpha$, of the initial set of α sources as shown in Figure (2.3a). The contributions of the other sources (dispersed in the other sub-systems) are implicitly considered with the q equivalent sources $V^k_{\sim\{l\},\ \{l\}\subseteq\{1,\ldots,n\}}$, with $l \leqslant n$. Note that $\{i\}\subseteq\{1,\ldots,\alpha\}$, respectively, $\{l\}\subseteq\{1,\ldots,n\}$, are

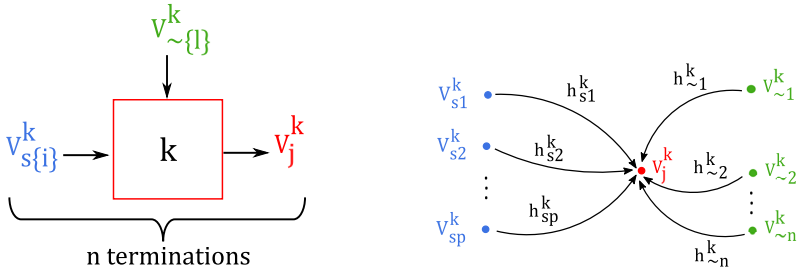

Figure 2.3: *Schematic representation of the sub-system k of p physical injected sources* $V^k_{s\{i\}}$*, q equivalent sources* $V^k_{\sim\{l\}}$ *and the output* V_j^k *(a), of the impulse responses* h^k_{si} *and* $h^k_{\sim l}$ *linking the sources* $V^k_{s\{i\}}$*, respectively,* $V^k_{\sim\{l\}}$ *to the output* V_j^k *(b).*

sub-sets of p sources indices, respectively, of q exchange interface indices. The first condition $p<\alpha$ ensures that at least one of the n terminations refers to the output j[2]. Whereas the condition $l=n$ translates the possibility of having equivalent sources only, with l referring to the index of termination in which the decomposition has occurred[3]. In addition, the number of terminations n of the sub-system k must be lower than the number of terminations z of the global system G.

Similarly to (2.3), the output V_j^k is assessed on the basis of the impulse responses h_{ij}^k of the sub-system k as follows:

$$V_j^k = \sum_{\{i\}} h_{ij}^k * V_{si}^k + \sum_{\{l\}} h_{lj}^k * V_{\sim l}^k \tag{2.5}$$

[2]If $i=n$, a physical voltage source is associated with each of the n terminations of the sub-system k. It means that the decomposition has not occurred.

[3]Depending on the network's topology and decomposition, the sub-network k may not feature any physical source. Its only contributions are retrieved from the equivalent sources at its interfaces.

with h^k_{ij}, respectively $h^k_{\sim l}$, are the impulse responses linking the physical injected sources $V^k_{s\{i\}}$ to the output, respectively, the impulse responses linking the equivalent sources $V^k_{\sim\{l\}}$ to the output.
To summarise, the proposed DD method retrieves the output V^k_j by considering the contributions of the physical sources and the equivalent ones at the exchange interfaces. The following algorithm recaps the key steps of the methodology.

Algorithm 1 Key steps to apply the DD method

1: Subdivide the global linear system G into m non-overlapping sub-systems.
2: Focus on the sub-system k in which the variable of interest V^k_j is located.
3: Evaluate the impulse responses $h^k_{\{i\}j}$ and $h^k_{\sim\{l\}}$ in equation (2.5).
4: Compute the output V^k_j through the convolution products of the evaluated impulse responses with the corresponding sources using equation (2.5).

The proposed methodology presents a major advantage of enabling the separate and independent modeling of each distinct sub-system. While other time-domain approaches require an iterative exchange for each time step, the DD method enables asynchronous temporal simulations based on the evaluation of impulse responses only. This particular attribute holds the additional benefit of preserving the confidentiality of each model. Sensitive or proprietary information pertaining to each sub-system remains unknown as no other information or result is required for exchange. This additional advantage proves especially significant within an industrial context ensuring that valuable intellectual property remains shielded.

2.1.2 Computational cost of the DD method

Generally speaking, DD techniques aim at reducing the overall computational cost for complex large-scale problems. It is therefore important to investigate whether our proposed DD method achieves a computational gain. In computer science, it is essential to differentiate between computational complexity and cost. The term *cost*, is used for precise measures as the actual amount of resources, primarily time and memory, that an algorithm uses. Whereas *complexity* is a mathematical measure usually described in terms of big O notation[4]. While they are related concepts, computational cost is more practical and specific, whereas computational complexity is more abstract and theoretical. Both are important for assessing

[4]Big O, also called Landau's symbol, is a symbolism used in complexity theory, computer science, and mathematics to describe the asymptotic behavior of functions [125].

and designing algorithms, however, it's possible to reduce the computational cost without reducing the computational complexity.

In our study, we define the computational cost as the summation of the cost of evaluation of the model, which is often the most expensive, and the computational complexity. In this thesis, we focus mainly on the cost of evaluation of the model itself and assume that the computational complexity is negligible.

We define the impulse responses as well as the sources in equation (2.5) as N-dimensional discrete vectors evaluated for each discrete time $t \in [0,(N-1)\Delta t]$, $(N \in \mathbb{N}^*)$, where Δt is the time step used for the simulation. The product of convolution in equation (2.5) becomes then a matrix product. The matrix form of the impulse responses $h^k_{\cdot\cdot}$, denoted $H^k_{\cdot\cdot}$, is built using only the impulse response to the unit impulse $\delta = [1,0,\ldots,0]_{N\times 1}$, delayed by one step of time for each column, and expressed as follows:

$$H^k_{\cdot\cdot} = \begin{pmatrix} h^k_{\cdot\cdot}(0) & 0 & \ldots & 0 \\ h^k_{\cdot\cdot}(1) & h^k_{\cdot\cdot}(0) & \ddots & \vdots \\ \vdots & h^k_{\cdot\cdot}(1) & \ddots & 0 \\ h^k_{\cdot\cdot}(N-1) & \vdots & \ddots & h^k_{\cdot\cdot}(0) \\ 0 & h^k_{\cdot\cdot}(N-1) & & h^k_{\cdot\cdot}(1) \\ \vdots & 0 & \ddots & \vdots \\ 0 & 0 & \ldots & h^k_{\cdot\cdot}(N-1) \end{pmatrix} \tag{2.6}$$

The computational complexity of the matrix product of the impulse response $H^k_{\cdot\cdot}$ with the source $V^k_{\cdot\cdot}$ is of the order $\sim O(N^2)$. For p sources featured in the sub-network k where the variable of interest is located, this product is evaluated $\sim O(p \times N^2)$. On the other hand, for q equivalent sources, the complexity cost is given by $\sim O(q \times N^2)$. However, as the equivalent sources $V^k_{\sim l}$ feature the other dispersed sources of the initial set of α sources in the neighboring sub-systems, its computational complexity should also be added. This aspect will be detailed later in this chapter.

Although the computational complexity seems high with the DD method, the evaluation of the output V^k_j through the impulse responses of smaller and less complex sub-systems is the real advantage[5]. Each sub-system v, $\{v\} \subseteq \{1,...,m\}$, is characterised by τ_v impulse responses.

[5]It may not be immediately obvious for 1D systems, but the DD approach allows important computational gain

This number is a constant parameter that depends only on the topology and subdivision of the system under study.

Throughout this manuscript, the proposed DD method is illustrated with transmission line network examples. It is therefore necessary to understand transmission line theory. The complete theory can be found in [126]. In the following, we recall the hypothesis on which transmission lines are based, as well as the Telegrapher's equations that underline them.

2.2 Transmission line theory fundamentals

The transmission line theory is based on the resolution of Maxwell's equations while considering a Transverse Electromagnetic (TEM) mode for the wave propagation along the line. More precisely, the electromagnetic fields are all restricted to directions normal to the direction of propagation. This assumption implies that the transverse dimensions of the line are small compared to the wavelength.

2.2.1 Transmission line model (*RLCG*) and Telegraph's equations

At high frequencies, a transmission line can be modeled by the cascading of quadrupoles of length dx, where dx is an infinitesimal length. Each of these quadrupoles is described by an RLCG model made up of the line's primary parameters: linear resistance (R in $\Omega.m^{-1}$), linear inductance (L in Hm^{-1}), linear capacitance (C in $F.m^{-1}$), and linear conductance (G in $S.m^{-1}$) as shown in Figure (2.4).

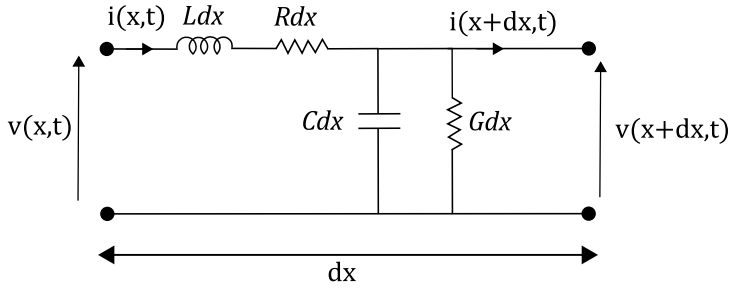

Figure 2.4: *Schematic representation of the elementary component of a transmission line (RLCG model).*

The propagation and coupling phenomena are represented by the distributed components: the inductance L and the capacitance C, whereas the losses phenomena are represented by the

for more complex structures (3D) and stochastic analysis, presented later in this manuscript.

resistance R and the conductance G.

For dx defined as an infinitesimal length, applying the Kirchhoff's equations to the circuit in Figure (2.4) gives the differential equations describing the instantaneous evolution of the voltage V and the current I in the transmission line.

$$\frac{\partial v(x,t)}{\partial x} = -Ri(x,t) - L\frac{\partial i(x,t)}{\partial t} \tag{2.7}$$

$$\frac{\partial i(x,t)}{\partial x} = -Gv(x,t) - C\frac{\partial v(x,t)}{\partial t} \tag{2.8}$$

These equations, known as the telegrapher's equations, predict the voltage and current distributions on a linear electrical transmission line. By successively deriving equations (2.7) and (2.8) with respect to x (space) and t (time), they can be combined to get two partial differential equations, each with only one dependent variable, either the voltage V or the current I, as follows:

$$\frac{\partial^2 v(x,t)}{\partial^2 x} = LC\frac{\partial^2 v(x,t)}{\partial t} + (RC+LG)\frac{\partial v(x,t)}{\partial t} + RGv(x,t) \tag{2.9}$$

$$\frac{\partial^2 i(x,t)}{\partial^2 x} = LC\frac{\partial^2 i(x,t)}{\partial t} + (RC+LG)\frac{\partial i(x,t)}{\partial t} + RGi(x,t) \tag{2.10}$$

Their resolution in the harmonic mode for a sine wave with pulsation $\omega = 2\pi f(rad/s^{-1})$, allows the voltage and current to be written as follows:

$$V(x,\omega) = V^{(+)}e^{-\gamma x} + V^{(-)}e^{\gamma x} \tag{2.11}$$

$$I(x,\omega) = I^{(+)}e^{-\gamma x} + I^{(-)}e^{\gamma x} \tag{2.12}$$

with $\gamma = \sqrt{(R+j\omega L)(G+j\omega C)}$ is the propagation constant.
The voltage $V(x,t)$ and current $I(x,t)$ waves, given respectively by equations (A.1.7) and (A.1.8), are linked by a characteristic impedance of the line Z_c line expressed by

$$Z_c = \sqrt{\frac{R+j\omega L}{G+j\omega C}} \tag{2.13}$$

Let's suppose that a transmission line of length L and characteristic impedance Z_c, is supplied at one end by a voltage generator V_s and loaded at the other end by an impedance Z_L, as shown in Figure (2.5).

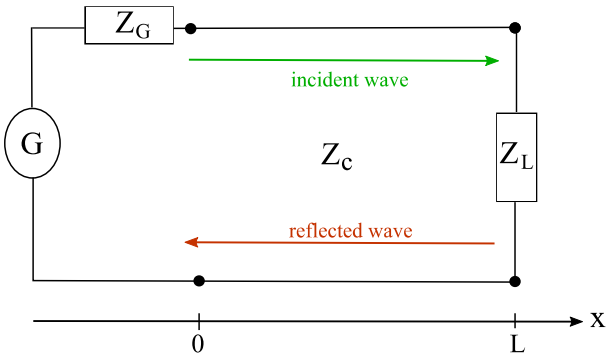

Figure 2.5: *Model of a transmission line of length L and characteristic impedance Z_c, excited by a voltage source g and loaded with an impedance Z_L.*

The voltage wave in equation (A.1.7) decomposes into a two-wave: an incident wave $V^{(+)}\, e^{-\gamma x}$ (represented by the green arrow in Figure 2.5) and a reflected wave $V^{(-)}\, e^{\gamma x}$ (represented by the red arrow in Figure 2.5). The ratio between these two components is called the reflection coefficient and translates the discontinuity of the impedance (impedance variation). Its expression, depending on the position on the line x, is given by

$$\Gamma_x = \frac{\text{reflected wave}}{\text{incident wave}} = \frac{V^{(-)}e^{\gamma x}}{V^{(+)}e^{-\gamma x}} = \frac{V^{(-)}}{V^{(+)}}e^{2\gamma x} \tag{2.14}$$

For sake of simplification, the reflection coefficient Γ_x can be expressed based on the impedance $Z(x)$ defined any point x on the line. The later links the voltage $V(x)$ to the current $I(x)$ at any given point x such as

$$Z(x,\omega) = \frac{V(x,\omega)}{I(x,\omega)} = Z_c\, \frac{V^{(+)}e^{-\gamma x} + V^{(-)}e^{\gamma x}}{V^{(+)}e^{-\gamma x} - V^{(-)}e^{\gamma x}} \tag{2.15}$$

Based on the definition of the reduced impedance $z(x,\omega)$ of $Z(x,\omega)$ given by

$$z(x,\omega) = \frac{Z(x,\omega)}{Z_c} \tag{2.16}$$

Its expression is deduced from equation (2.15) as follows:

$$z(x,\omega) = \frac{V^{(+)}e^{-\gamma x} + V^{(-)}e^{\gamma x}}{V^{(+)}e^{-\gamma x} - V^{(-)}e^{\gamma x}} = \frac{1 + \dfrac{V^{(-)}e^{\gamma x}}{V^{(+)}e^{-\gamma x}}}{1 - \dfrac{V^{(-)}e^{\gamma x}}{V^{(+)}e^{-\gamma x}}} = \frac{1 + \dfrac{V^{(-)}}{V^{(+)}}e^{2\gamma x}}{1 - \dfrac{V^{(-)}}{V^{(+)}}e^{2\gamma x}} \tag{2.17}$$

By replacing the reflection coefficient Γ_x given by the expression (2.14) in the previous equation (2.17), we obtain the relationship between the latter and the reduced impedance for any point x of the line, such that

$$z(x,\omega) = \frac{1+\Gamma_x}{1-\Gamma_x} \qquad ; \qquad \Gamma_x = \frac{z(x,\omega)-1}{z(x,\omega)+1} \tag{2.18}$$

At the load level $x = L$, the reflection coefficient Γ_L is expressed by

$$\Gamma_L = \frac{z(L)-1}{z(L)+1} = \frac{Z_L - Z_c}{Z_L + Z_c} \tag{2.19}$$

For the case of impedance matching, i.e. $Z_L = Z_c$, no reflections are measured at the injection point ($\Gamma_L = 0$). For the mismatch scenario, a part of the wave is reflected back to the injection point, while the other part of the wave continues to propagate in the transmission line. We define the transmission coefficient T_L as the ratio between the voltage wave transmitted to a load and the incident voltage wave, expressed as follows:

$$T_L = \frac{V(L,\omega)}{V^{(+)}e^{-\gamma L}} = \frac{V^{(+)}e^{-\gamma L} + V^{(-)}e^{\gamma L}}{V^{(+)}e^{-\gamma L}} = 1 + \Gamma_L \tag{2.20}$$

The transmission coefficient T_x can also be defined at any point x on the transmission line, based on its definition

$$T_x = \frac{V(x,\omega)}{V^{(+)}e^{-\gamma x}} \tag{2.21}$$

and the expression of the reflection coefficient Γ_x given by (2.18). Its final formulation is given by

$$T_x = 1 + \Gamma_x \tag{2.22}$$

2.2.2 Modeling of a branched transmission line network

As the basic principle of the transmission lines has been recalled for the case of a line with two uniform conductors, the focus is now put on branched networks. In this case, new conditions at the junction, allowing the interconnection between the multiple branches of the network, should be defined.

At the current node p, we can write Kirchhoff's laws such as

$$\sum_{m=1}^{M} i_m(p) = 0 \tag{2.23}$$

$$V_m(p) = V_{m'}(p), \qquad m' \in \{1, ..., m-1\} \tag{2.24}$$

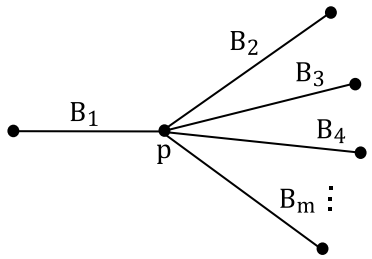

Figure 2.6: *Schematic representation of a network of m branches interconnected through a junction (node) p.*

with M is the number of branches arriving at the node p and m, m' two of these lines.

At the junction level, an impedance discontinuity occurs. As a consequence, reflections at the node appear. For instance, we suppose that a source is located at the input of the branch B_1 of the network in Figure (2.6). The signal propagating within the network observes an equivalent impedance Z_p. This latter is obtained by considering the parallel impedance of the characteristic impedances of the branches $B_{i,\ i\in\{2,..,m\}}$. This parallel impedance is considered as the load impedance Z_p of the branch B_1. Based on the definition of the reflection coefficient given by equation (2.14), its expression at the node (junction) is given by

$$\Gamma_1 = \frac{Z_p - Z_{c1}}{Z_p + Z_{c1}} \tag{2.25}$$

2.2.3 Modeling 1-D FDTD transmission lines

While numerous numerical methods exist to model transmission lines, we have chosen the Finite-Difference Time-Domain method (FDTD) to solve the Telegrapher's equations and illustrate the phenomenon of signal propagation in a wired network [127].

One-dimensional Finite Difference Time Domain (FDTD) scheme

The finite-difference principle is based on the approximation of differential operators. According to the "Leap-Frog" scheme, the currents I are placed in the middle of the segments and the voltages V at the ends, as shown in Figure (2.7).
For a given space step Δx and a time step Δt, we define the voltage $V|_p^n$ and current $I|_p^n$ as follows:

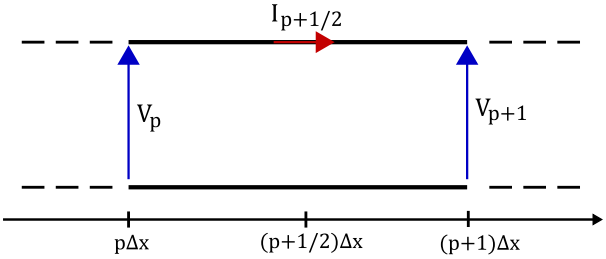

Figure 2.7: *Spatial discretization of transmission line equations.*

$$V|_p^n = v(p\Delta x,\, n\Delta t) \tag{2.26}$$

$$I|_p^n = i(p\Delta x,\, n\Delta t) \tag{2.27}$$

Assuming that the primary parameters of the transmission line (R, L, C and G) are constant along the line, the discretization of the telegraph equations (2.7) and (2.8) according to the FDTD scheme allows us to write the following system

$$V|_p^{n+1} = -\frac{2\Delta t}{(G\Delta t + 2C)\Delta x}\left(I|_{p+1/2}^{n+1/2} - I|_{p-1/2}^{n+1/2}\right) - \frac{G\Delta t - 2C}{G\Delta t + 2C}V|_p^n \tag{2.28}$$

$$I|_{p+1/2}^{n+1/2} = -\frac{2\Delta t}{(R\Delta t + 2L)\Delta x}\left(V|_{p+1}^n - V|_p^n\right) - \frac{R\Delta t - 2L}{R\Delta t + 2L}I|_{p+1/2}^{n-1/2} \tag{2.29}$$

These equations (2.28) and (2.29) are valid for all meshes (segments Δx) of the line, except for the first and last meshes, where boundary conditions are defined.

Based on Figure (2.8), the voltage V_1 at the first mesh is deduced from the voltage source V_s. This latter, representing a Thevenin source, is replaced by a Norton equivalent source.
The voltage V_1 is obtained based on Kirchhoff's laws and is expressed as follows:

$$V|_1^{n+1} = \left(\frac{\Delta x}{\Delta t}R_sC + 1\right)^{-1}\left\{\left(\frac{\Delta x}{\Delta t}R_sC - 1\right)V_1^n - 2R_sI_1^{n+1/2} + V_s^{n+1} + V_s^n\right\} \tag{2.30}$$

Similarly, the voltage V_{ndx+1} corresponding to the last mesh of the line (load-side) is given by

$$V|_{ndx+1}^{n+1} = \left(\frac{\Delta x}{\Delta t}R_LC + 1\right)^{-1}\left\{\left(\frac{\Delta x}{\Delta t}R_LC - 1\right)V_{ndx+1}^n + 2R_LI_{ndx}^{n+1/2} + V_L^{n+1} + V_L^n\right\} \tag{2.31}$$

The previous equations (2.30) and (2.31) are obtained considering that the transmission line is lossless ($R = 0$ and $G = 0$) for simplification purposes only. Their generalized expressions considering the presence of losses (R and G are non-null), as well as their demonstration can be found in the appendix *Tranmission lines theory*.

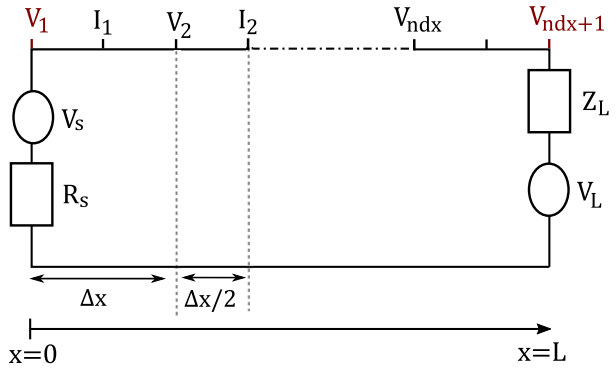

Figure 2.8: *Spatial and temporal discretization of voltages and currents along the transmission line.*

Branched transmission lines modeling using Finite Difference Time Domain (FDTD) Method

The FDTD method offers the possibility to model complex networks such as branched transmission lines interconnected through junction conditions in the time domain.
At the node level, the centered spatial discretization of the voltage equation can not be operated. Therefore, the half-spatial discretization (in left or right) is introduced.

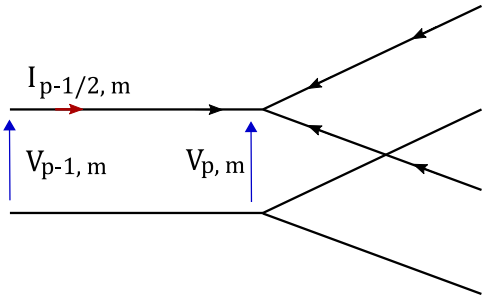

Figure 2.9: *Equivalent schematic for a three-branch current node.*

We extract the current $I|_{p,m}$ at the node p for each branch m as follows:

$$-I|_{p,m}^{n+1/2} = V|_{p,m}^{n+1}\left(\frac{G_m + 2C_m}{4}\right)\frac{\Delta x_m}{\Delta t} + V|_{p,m}^{n}\left(\frac{G_m - 2C_m}{4}\right)\frac{\Delta x_m}{\Delta t} - I|_{p-1/2,m}^{n+1/2} \tag{2.32}$$

Following equation (2.24), the voltages at the node p are equal for all the branches m. Based on equation (2.23) and by factoring $V|_{p,m}$, we obtain the equation at the node, expressed as follows:

$$V|_{p,m}^{n+1} \sum_{m=1}^{M} A_m = -V|_{p,m}^{n} \sum_{m=1}^{M} B_m + \sum_{m=1}^{M} I|_{p-1/2,m}^{n+1/2} \tag{2.33}$$

with:

$$A_m = \left(\frac{G_m \Delta t + 2C_m}{4} \right) \frac{\Delta x_m}{\Delta t} \quad , \quad B_m = \left(\frac{G_m \Delta t - 2C_m}{4} \right) \frac{\Delta x_m}{\Delta t} \tag{2.34}$$

defined for each branch m.

The detailed demonstration of equations (2.32) and (2.33) is reported in the appendix *Tranmission lines theory*.

Let's consider that the network shown in Figure (2.6) consists of 3 branches forming a Y transmission line network. We assume that an excitation source V_s is injected at the input of the line L_1 and that lines L_2 and L_3 are respectively loaded by impedances Z_{L2} and Z_{L3}, as shown in Figure (2.10).

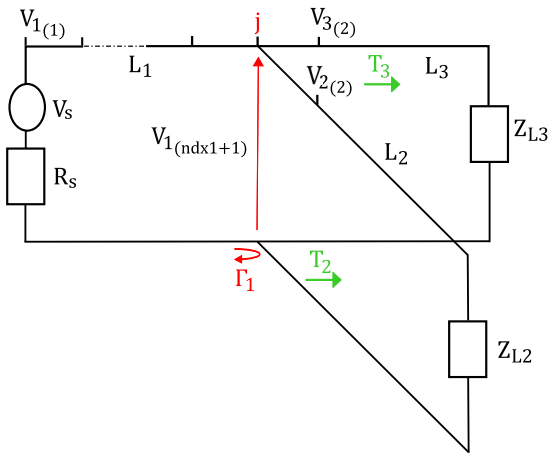

Figure 2.10: *Discretization of voltages at the junction level for a Y transmission line network.*

In this case, the node condition is translated through the following equation:

$$V_{1_{(ndx1+1)}} = V_{2_{(1)}} = V_{3_{(1)}} \tag{2.35}$$

The reflection coefficient at the junction Γ_1 is given based on equation (2.14), such as

$$\Gamma_1 = \frac{Z_{p,23} - Z_{c1}}{Z_{p,23} + Z_{c1}} \tag{2.36}$$

with $Z_{p,23}$ represents the equivalent parallel impedance of Z_{c2} and Z_{c3}.

The transmission coefficients T_2 and T_3 are deduced from equation (2.20) and equal $1+\Gamma_1$.

To synthesize, modeling a Y-network using the FDTD method consists of evaluating the voltages and currents along the branches using equations (2.28) and (2.29). At the junction level, new boundary conditions are implemented to ensure voltage equality through equation (2.33). The principle of the method can be easily generalized for complex networks with several branches and junctions.

Stability criterion

The stability criterion CFL (Courant–Friedrichs–Lewy) is a necessary condition for the stability of explicit time-stepping algorithms such as the FDTD method.
The condition expresses that a physical wave needs to propagate slower than the speed of the numerical dependency speed. The CFL condition is defined as the relation between the time and space steps given, for the 1D scheme, by

$$\Delta t \leq \frac{\Delta x}{c} \tag{2.37}$$

where c is the speed of the wave propagation in the considered medium.

2.2.4 Numerical illustrations

For numerical illustrations, we first propose to evaluate the propagation of a Gaussian signal along a uniform and lossless transmission line $(R = 0, G = 0)$, on the basis of equations (2.28), (2.29), (2.30) and (2.31). The Gaussian function, defined by equation (2.38), is implemented in the FDTD method.

$$G(t) = Ae^{\frac{-(t-t_c)^2}{(2\sigma^2)}} \tag{2.38}$$

with A and t_c are respectively the magnitude and the position of the center of the peak. Meanwhile σ controls the width of the Gaussian pulse.
The FDTD method is implemented considering a spatial discretization step $dx = 0.1m$ and a temporal discretization step $dt = 0.31\mu s$[6].

[6]The temporal discretization step dt is defined in compliance with the stability criterion CFL such as $dt = 0.95 \times \frac{dx}{c_0}$, with c_0 refers to the speed of light.

For a length $L = 1.5m$ and characteristic impedance $Z_c = 50\Omega$, three configurations of the load resistance R_L are considered: matched ($R_L = Z_c$), short-circuit and open circuit, as represented in Figure (2.11).

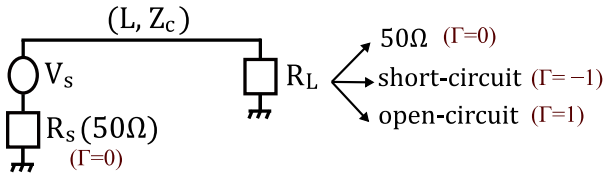

Figure 2.11: *A transmission line of length L and characteristic impedance Z_c, excited by a voltage source V_s and loaded with a resistance R_L.*

Considering that the source V_s is a Gaussian signal of magnitude $A = 2V$, $t_c = 0.12\mu s$ and $\sigma = 1.26ns$, the voltage at the entrance of the line is recorded for the three configurations of the load resistance R_L, as reported in Figure (2.12).

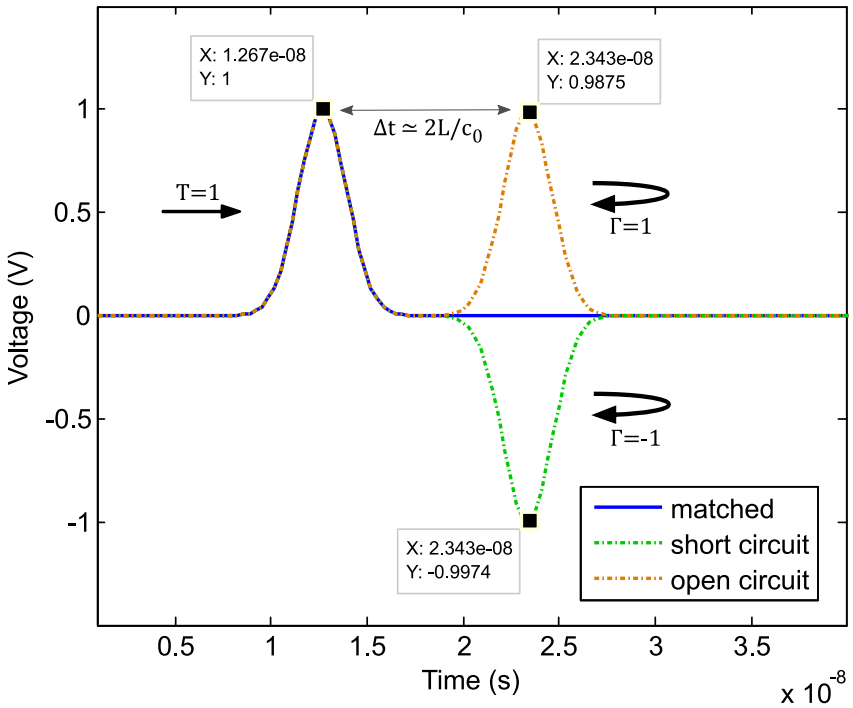

Figure 2.12: *Voltage at the entrance of the line evaluated for three load resistance configurations.*

The direct propagation of the Gaussian pulse is recorded for all three configurations with a total transmission (the line is matched on the generator side, $R_s = Z_c$). Their effects however are retrieved afterwards, through the reflection coefficients. In the matching case,

no reflection is measured. In the short-circuit and open-circuit cases, the wave is reflected with a negative sign ($\Gamma = -1$) and a positive sign ($\Gamma = 1$) respectively. Moreover, the measured time Δt between the two peaks (incident and reflected) corresponds to the required time to cross twice the length of the line, assuming a propagation speed equal to the speed of light c_0.

For the second application, we consider a Y transmission line network represented by three lossless and uniform lines as shown in Figure (2.13). The voltage V_s at the input of line L_1 is the Gaussian pulse defined with the same previous parameters.

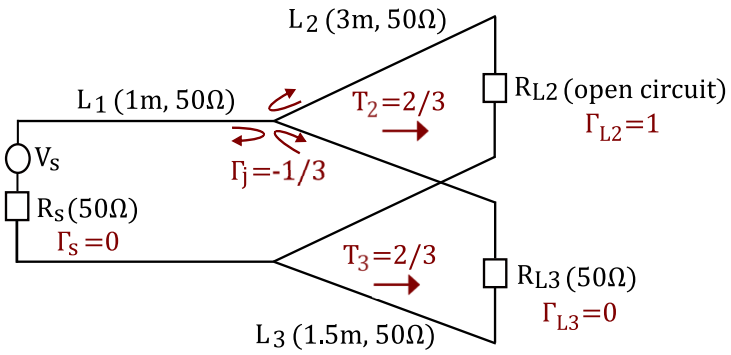

Figure 2.13: *Characteristic of the studied transmission line network.*

The voltage V_3 measured across the load resistance of line L_3, reported in nFigure (2.14), is obtained considering the direct propagation of the source V_s within lines L_1 and L_3 with a total transmission (matching at the generator level, $\Gamma_s = 0$). At the junction level, the impedance discontinuity is translated with the reflection coefficient Γ_j. In this case, as the characteristic impedances of the three lines are equal (50Ω), the reflection coefficients at the node for the three lines are equal ($\Gamma_j = -1/3$). Consequently, the Gaussian signal is transmitted to the other branches with a transmission coefficient $T = 1 + \Gamma_j = 2/3$. Due to the mismatch at the extremity of line L_2 (open circuit), a first reflection of the signal of positive sign ($\Gamma_{L2} = 1$) is retrieved at the observable level. The junction effect appears later with the second negative reflection ($\Gamma_j = -1/3$).

2.3 Numerical applications of the proposed DD method

Having established the general formulation of the DD method and recalled the fundamentals of the transmission lines theory, we can now proceed to apply the proposed DD technique for transmission line networks. By showcasing two applications, we will provide a step-by-step breakdown of the DD approach. This detailed walkthrough will offer a clear and tangible

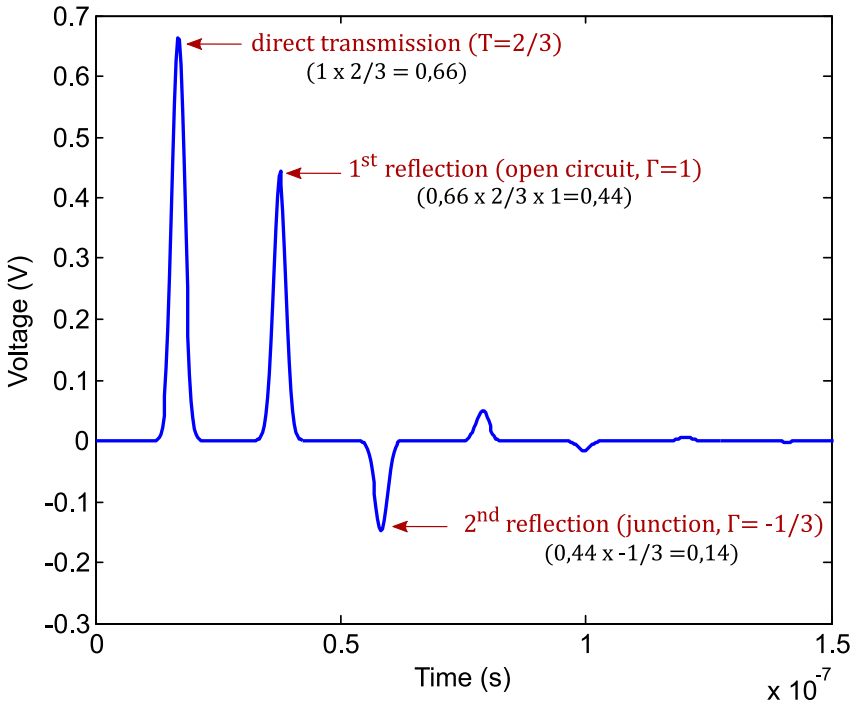

Figure 2.14: *Voltage V_3 across the load resistance R_{L3} of line L_3.*

understanding of how the method applies in practice, highlighting the key stages involved.

2.3.1 First case scenario: perfect matching at the interface level

First, we propose to study the transmission line network in Figure (2.15). The network consists of 5 uniform and lossless transmission lines of equal characteristic impedance $Z_{ci,\ i\in\{1,\ldots,5\}} = 50\Omega$. The two voltage sources V_{s1} and V_{s4} are Gaussian signals defined by equation (2.38) of parameters $A = 1V$, $\sigma = 1,26ns$ and $t_c = 7,91ns$.

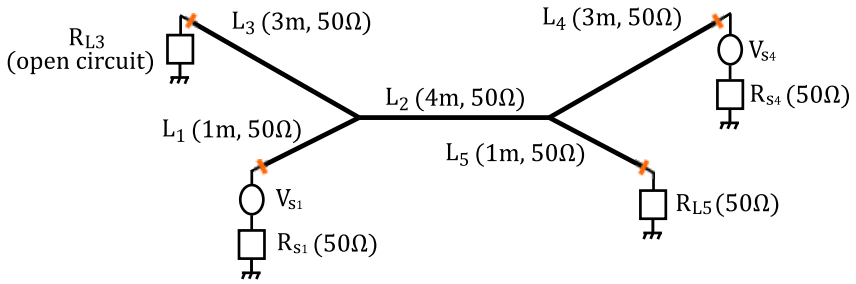

Figure 2.15: *Characteristic of the transmission line network.*

Based on equation (2.3), the voltage V_5 across the load resistance R_{L5} is retreived by considering

the inherent contribution of both sources V_{s1} and V_{s4}, such as

$$\begin{aligned} V_5 &= \sum_{i=1}^{\alpha=2} h_{i5} * V_{si} \\ &= h_{15} * V_{s1} + h_{45} * V_{s4} \end{aligned} \tag{2.39}$$

with h_{15}, respectively h_{45}, the impulse response linking the voltage V_{s1}, respectively, the voltage V_{s4} to the output V_5.

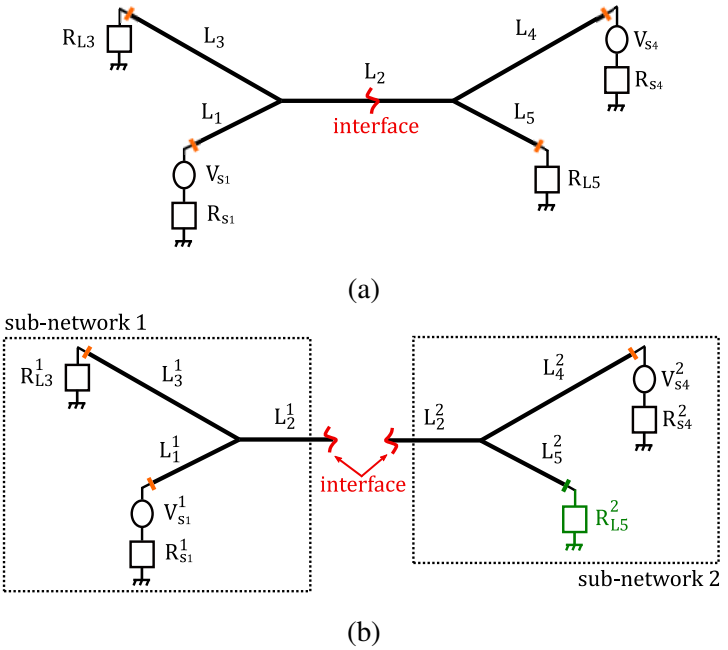

Figure 2.16: *Global transmission line network split at the middle of the line L_2 (a), sub-networks Y^1 and Y^2 after the subdivision of the global network (b).*

We aim to retrieve the voltage V_5, using the proposed DD method by splitting the global network at the middle of the line L_2 into two sub-networks Y^1 and Y^2, as shown in Figure (2.16). This decomposition results in the appearance of two lines L_2^1 and L_2^2, associated respectively to the sub-networks Y^1 and Y^2, whose length's sum is equal to the length of the initial line L_2 ($L_2^1 + L_2^2 = L_2$). In addition, since the subdivision occurs at the level of the line itself, the physical properties must be preserved. To maintain the impedance continuity of the intial line L_2, lines L_2^1, respectively L_2^2 are loaded with the resistances R_{L2}^1, respectively R_{L2}^2, both equal to the characteristic impedance Z_{c2} of the line L_2, as shown in Figure (2.17).
In the following, for each sub-network Y^k, $k \in \{1,2\}$, its characteristics (lengths, voltage sources and load resistance), are denoted with a k exponent. By identification, the lines L_1 and L_3 of the left-hand network are given by $L^1_{i,\ i\ \in\ \{1,3\}}$ ($k = 1$). On the other hand, the lines

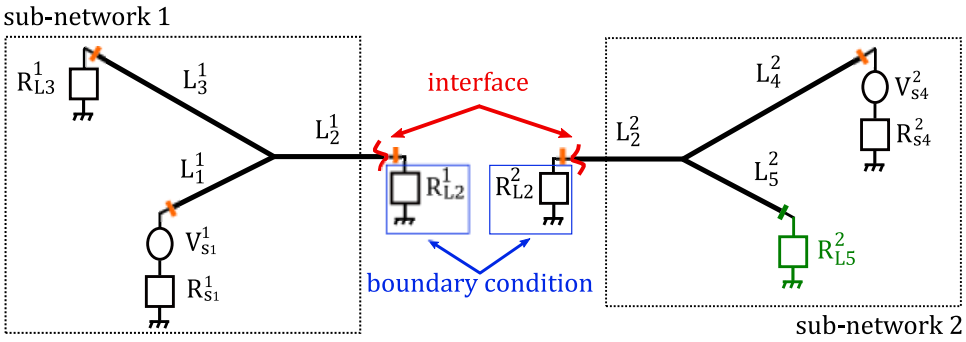

Figure 2.17: *Sub-networks Y^1 and Y^2 with load resistances R^1_{L2} and R^2_{L2} at the interface level of lines L^1_2 and L^2_2.*

L_4 and L_5 are expressed with the exponent $k = 2$ as a reference to sub-network Y^2. The output V_5 is denoted V_5^2 ($k = 2$), measured across the load resistance R^2_{L5}, when the DD method is applied.

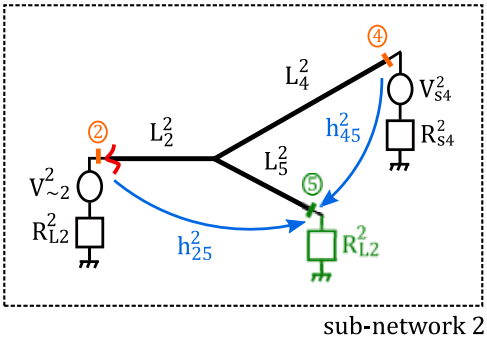

Figure 2.18: *Schematic representation of the contribution of the physical voltage source V^2_{s4} and the equivalent source at the interface level $V^2_{\sim 2}$ to the output through the corresponding impulse responses.*

Following the steps of the DD method given in the algorithm (1), the voltage V_5^2 of sub-network Y^2 ($k = 2$), recorded at the line L^2_5 ($j = 5$), is expressed on the basis of equation (2.5) as follows:

$$V_5^2 = h^2_{45} * V^2_{s4} + h^2_{25} * V^2_{\sim 2} \tag{2.40}$$

The first term of the right-hand member represents the contribution of the physical voltage source V^2_{s4} injected at the line L^2_4 ($i = 4$), whereas the right-hand term gives the contribution of the equivalent voltage source $V^2_{\sim 2}$ measured at the interface level ($l = 2$) at the line L^2_2 of sub-network Y^2. The latter represents the incoming wave from the sub-network Y^1 at the exchange interface as previously explained in section (2.1.1). Its explicit expression is given by

$$V^2_{\sim 2} = h^1_{12} * V^1_{s1} \tag{2.41}$$

where h_{12}^1 is the impulse response linking the voltage source V_{s1}^1 of sub-network Y^1 injected at line L_1^1 ($i = 1$), to the interface ($l = 2$).

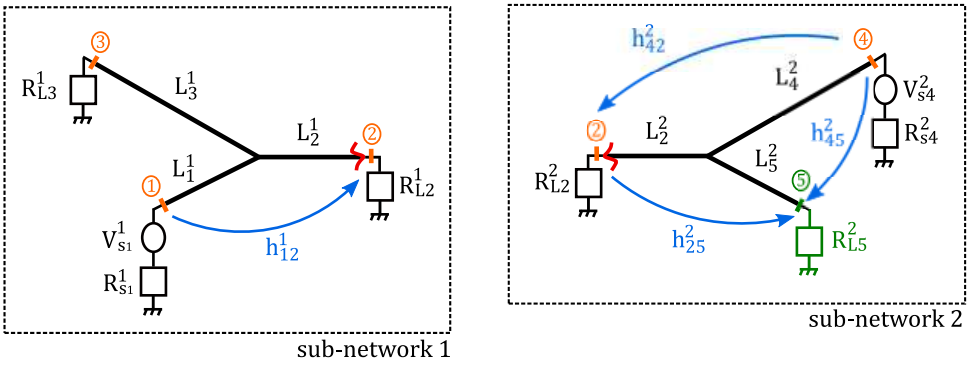

Figure 2.19: *Impulse responses h_{ij}^k for each sub-network Y^k, $k \in \{1,2\}$.*

Using the FDTD method, whose principle is recalled in (2.2.3), the voltage V_5^2 is computed and compared to the reference, given by the global network's result[7].

Remark 1 Note that the proposed DD method is interesting when the global result is either difficult to access or simply not given. Throughout this manuscript, the DD approach is compared to the global result, assumed given and serving as a reference, for validation purposes.

The obtained result using the DD technique, by computing equation (2.40), is compared to the reference in Figure (2.20). Only the first peak, translating the direct propagation of the source V_{s4}^2 within lines L_4^2 and L_5^2 with a magnitude equal $0.66V$ ($1 \times T = 2/3$), and the second peak reflecting the direct propagation of the source V_{s1}^1 translated by the right-hand term of equation (2.40), are recovered. The DD approach does not retrieve the expected result from the instant $t = 6.2.10^{-8}s$. In the upcoming section, a comprehensive investigation will be directed to understand the divergence of the obtained outcome.

Identification of the multiple orders in the DD's formulation

Upon the previous results, it is necessary to delve deeper into the method's formulation for a better understanding of the obtained outcome. In the initial formulation of the DD technique,

[7]The spatial and temporal discretization steps used for the FDTD method are respectively given by

$$dx = 0.1m$$
$$dt = 0.95 \times \frac{dx}{c_0} = 0.31ns$$

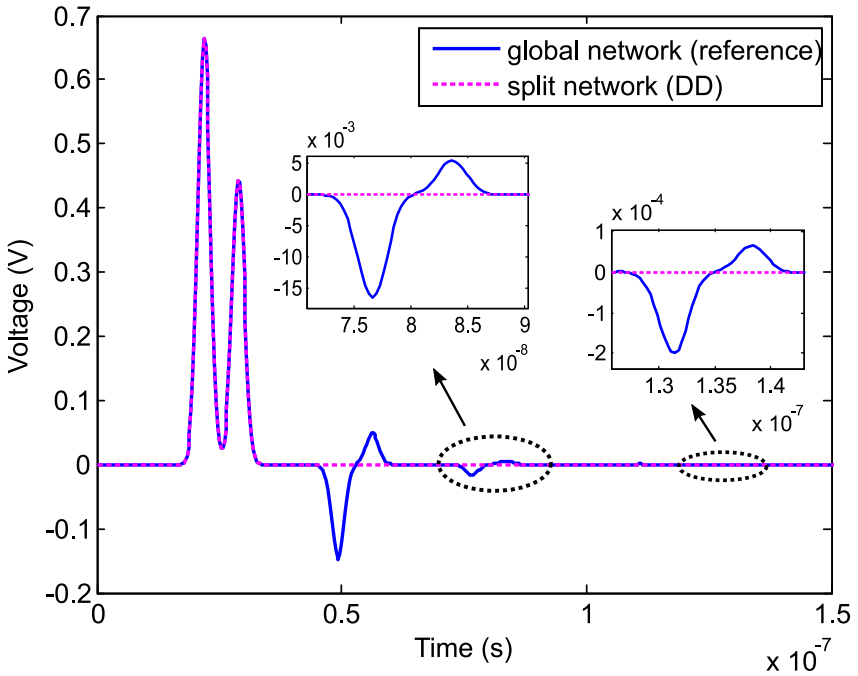

Figure 2.20: *Comparison of the voltage V_5 across the resistance R_{L5} evaluated for the global network (reference) and the split network (DD method).*

given by equation (2.40), only the direct propagation of the source V^2_{s4} within sub-network 2 is considered. Meanwhile, a part of this source is transmitted to the interface level.

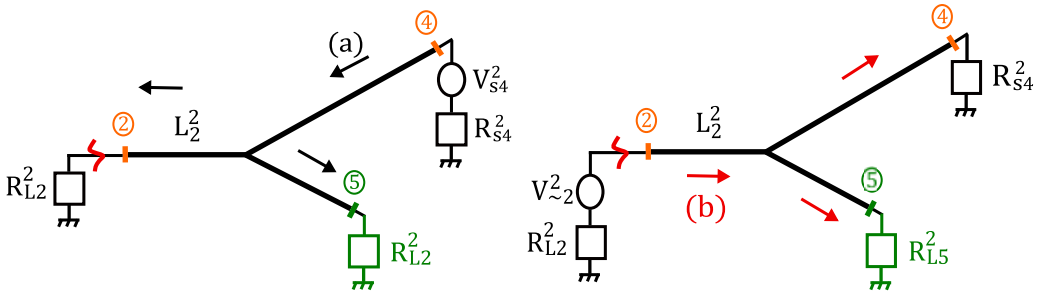

Figure 2.21: *Propagation path of the voltage source V^2_{s4} in the sub-network Y^2 in black and its re-injection in red (a), propagation path of the equivalent voltage $V^2_{\sim 2}$ within the sub-network Y^2 (b).*

This new incoming wave voltage, represented by the path (a) in Figure (2.21a) in black, is given by the product $(h^2_{42} * V^2_{s4})$. Its re-injection into the sub-network 2 on the other hand, represented by the path (b) in Figure (2.21b) in red, is given through the impulse response

h^2_{22}. The contribution of this new equivalent source at the interface is obtained based on the additional term A in equation (2.42).

Moreover, as previously mentioned in section (2.1.1), equation (2.40) considers only the retro-action of the sub-network Y^1 to the sub-network Y^2, through the incoming wave voltage $V^2_{\sim 2}$. In practice, the retro-actions between the two sub-networks should be evaluated. The retro-action of sub-network Y^2 to Y^1 is translated through the re-injection of the equivalent source, coming from sub-network Y^2 to the interface level, into sub-network Y^1.

$$V^2_5 = h^2_{45} * V^2_{s4} + h^2_{25} * (h^1_{12} * V^1_{s1}) + \underbrace{h^2_{25} * \left(h^1_{22} * (h^2_{42} * V^2_{s4})\right)}_{A} \tag{2.42}$$

From equation (2.42), the term A is based on a new impulse response h^1_{22}. This impulse response characterizes its corresponding sub-network when no physical voltage source is injected. For each sub-network $k \in \{1,2\}$, the impulse response h^k_{ll} is evaluated for the same injection and recording point, that is the interface level l.

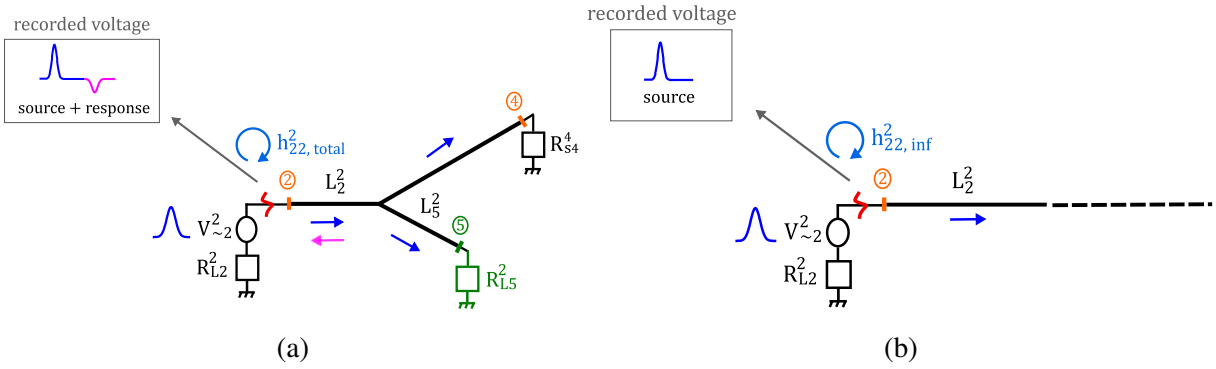

Figure 2.22: *Schematic representation of the evaluation of the impulse responses* $h^2_{22,\,total}$ *(a), and* $h^2_{22,\,inf}$ *(b) of sub-network* Y^2.

Note that the obtained impulse response contains actually the sum of the injected source and the sub-network's response. Therefore, an additional step is required to subtract the voltage source's transmission. For instance, for the sub-network Y^2, we first evaluate the impulse response denoted $h^2_{22,\,total}$ for which both the source and the response are recorded. Then, the line L^2_2 is supposed infinite (in practice very long), to ensure that no reflections are recorded. The evaluated impulse response $h^2_{22,\,inf}$, in this case, will retrieve only the transmission of the source. Subtracting both these impulse responses will give the impulse response h^2_{22} of the sub-network Y^2.

As time progresses the multiple reflections of both voltage sources V^1_{s1} and V^2_{s4} within the network appear. The following equation yields the multiple round-trips of these sources to the

$q-th$ order, such as

$$\begin{aligned} V_5^2 = h_{45}^2 * V_{s4}^2 + h_{25}^2 * (\underbrace{h_{12}^1 * V_{s1}^1}_{V_{\sim 2,1}^{2\ (1)}}) + h_{25}^2 * \left(h_{22}^1 * (\underbrace{h_{42}^2 * V_{s4}^2}_{V_{\sim 2,1}^{2\ (2)}})\right) \\ + \sum_{i=2}^{q_1} h_{25}^2 * \left(h_{22}^2 * \left(h_{22}^1 * V_{\sim 2,i}^{2\ (1)}\right)\right) + \sum_{j=2}^{q_2} h_{25}^2 * \left(h_{22}^2 * \left(h_{22}^1 * V_{\sim 2,j}^{2\ (2)}\right)\right) \end{aligned} \tag{2.43}$$

with $V_{\sim 2,\ i}^{2\ (1)}$, respectively $V_{\sim 2,\ j}^{2\ (2)}$ are defined as the i-th order, respectively the j-th order of the equivalent source at the interface level of sub-network Y^2 referring to the contribution of the voltage source V_{s1}^1, respectively V_{s4}^2 and expressed as follows:

$$V_{\sim 2,i}^{2\ (1)} = h_{22}^2 * (h_{22}^1 * V_{\sim 2,i-1}^{2\ (1)}) \tag{2.44}$$

$$V_{\sim 2,j}^{2\ (2)} = h_{22}^2 * (h_{22}^1 * V_{\sim 2,j-1}^{2\ (2)}) \tag{2.45}$$

The equivalent sources $V_{\sim 2}^{2\ (1)}$ and $V_{\sim 2}^{2\ (2)}$, of equation (2.43) refer to the first order of the multiple reflections of physical sources V_{s1}^1 and V_{s4}^2.

The voltage V_5^2 expressed by equation (2.43) is retrieved following two steps:

- The first step consists of evaluating the contribution of each of the real and equivalent sources in the sub-network of interest $k = 2$ (where the observable is located). The obtained result translates the direct propagation of each of the physical voltage source V_{s4}^2 within the sub-network 2 and the equivalent sources $V_{\sim 2}^{2\ (1)/(2)}$. The contribution of the latter, given by equation (2.42), is referred to as *first-order* since it translates the first retro-action of the neighboring sub-network 1 to the interface level.

- The second step evaluates the *higher-orders* of the equivalent sources obtained considering the recursive formulation given by the summation in equation (2.43). The additional terms translate the retro-actions of each sub-network on the other and retrieve the multiple reflections of the physical source V_{s4}^2 due to the mismatches of the network (junction and loads level).

Presenting the voltage V_5^2 in equation (2.43) by starting the summation of the recursive terms from $i = 2$ and $j = 2$ aligns with our philosophy of presentation, following the previous steps. The formulation can be however generalized such that the *first-order* term is integrated directly into the additional summation from $i = 1$ and $j = 1$, as follows:

$$V_5^2 = h_{45}^2 * V_{s4}^2 + \sum_{i=1}^{q_1} h_{25}^2 * \left(h_{22}^1 * h_{22}^2\right)^{(i-1)} * V_{\sim 2,1}^{2\,(1)} + \sum_{j=1}^{q_2} h_{25}^2 * \left(h_{22}^1 * h_{22}^2\right)^{(j-1)} * V_{\sim 2,1}^{2\,(2)} \quad (2.46)$$

Remark 2 Note that in the remainder of this manuscript, the formulation of the observable will be written considering the summation from order 2. This choice is justified, once again, by the philosophy based on which the proposed DD approach is presented. It allows the identification of the multiple retro-actions between the sub-networks at the interface level(s).

By computing the new equation (2.46) to the orders $q_1 = 4$ and $q_2 = 4$, the DD method recovers the multiple reflections of both voltage sources V_{s1}^1 and V_{s4}^2. The obtained result is reported in Figure (2.23) and superimposes perfectly the reference[8].

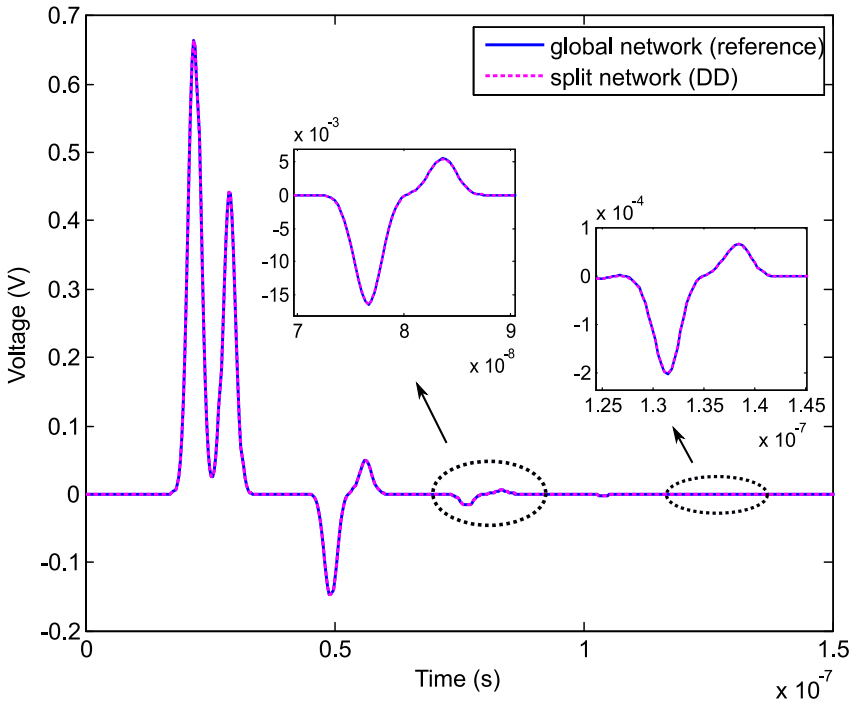

Figure 2.23: *Comparison of the voltage V_5 across the resistance R_{L5} evaluated for the global network (reference) and the split network (DD method applied for the orders $q_1 = 4$ and $q_2 = 4$).*

Based on this first result, we can already highlight the main advantages of the method: allowing fully asynchronous simulations for each sub-network, and preserving the confidentiality of the models by exchanging the impulse responses only.

[8]For this application, the orders q_1 and q_2 are equal. However, for other configurations, these orders may be different.

Application of the DD method for a specific case

To go even further on the validation of the DD technique, we propose a second application based on the same transmission line network in Figure (2.15). We consider that the only physical voltage source in the network is the voltage V_{s4}. Following the principle of the DD method, and by splitting the network at the middle of the line L_2, the voltage V_5^2 is retrieved on the basis of equation (2.5) such as

$$\begin{aligned} V_5^2 &= h_{45}^2 * V_{s4}^2 + h_{25}^2 * V_{\sim 2}^2 \\ &= h_{45}^2 * V_{s4}^2 + h_{25}^2 * \left(h_{22}^1 * (h_{42}^2 * V_{s4}^2)\right) \end{aligned} \tag{2.47}$$

Similarly to the previous case, the first term of the right-hand member of equation (2.47) translates the direct propagation of the voltage source V_{s4}^2 in sub-network Y^2. The equivalent voltage source at the interface on the other hand is expressed differently. In this case, no physical voltage source is injected in the sub-network Y^1, its contribution is thus only given through its impulse response h_{22}^1. Its product with the term $(h_{42}^2 * V_{s4}^2)$ gives the equivalent voltage $V_{\sim 2}^2$. Finally, the contribution of this latter to the output is recovered via its product of convolution with the impulse response h_{25}^2.
Equation (2.48) gives both contributions from each sub-network and their multiple round-trips for the q-th order.

$$V_5^2 = h_{45}^2 * V_{s4}^2 + h_{25}^2 * V_{\sim 2,1}^2 + \sum_{i=2}^{q} h_{25}^2 * \left(h_{22}^2 * (h_{22}^1 * V_{\sim 2,i}^2)\right) \tag{2.48}$$

with $V_{\sim 2,i}^2$ is defined as the i-th order of the equivalent source and is given by

$$V_{\sim 2,i}^2 = h_{22}^2 * (h_{22}^1 * V_{\sim 2,i-1}^2) \tag{2.49}$$

The voltage $V_{\sim 2,1}^2$ refers to the voltage $V_{\sim 2}^2$ in equation (2.47). This new notation designates the first order of the multiple round trips.

By applying equation (2.48) to the order $q = 3$, the voltage V_5^2 obtained with the DD method is in very good agreement with the reference as reported in Figure (2.24).
To summarize, for both applications, the essence of the method remains unchanged: evaluating the contributions of the physical and equivalent sources of the considered sub-network given by the general equation (2.5). The explicit formulation, however, depends on the studied case. The flow chart in Figure (2.25) gives the principle of the DD method for the two previously

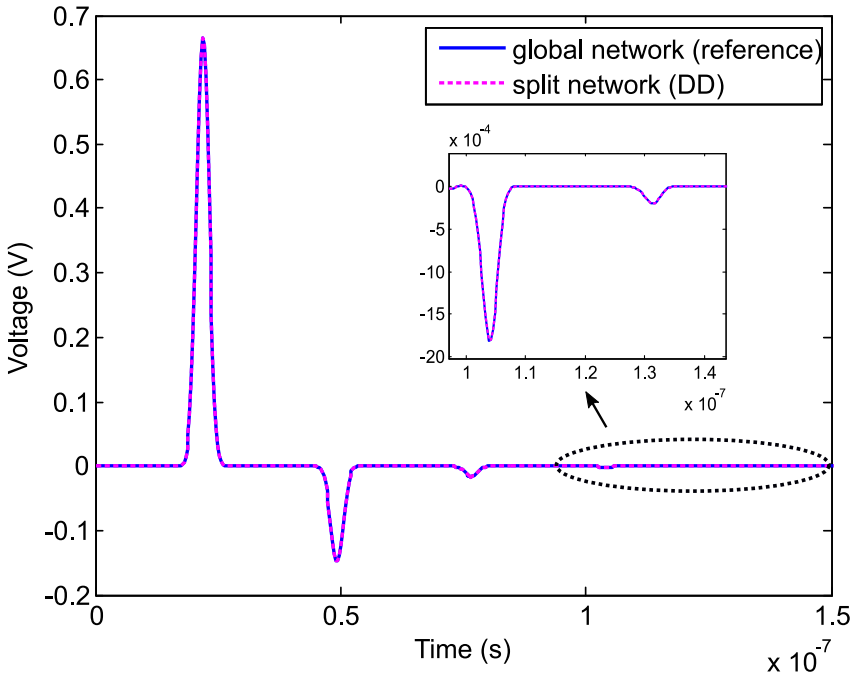

Figure 2.24: *Comparaison of the voltage V_5^2 across the resistance R_{L5}^2 for the global network (reference) and for the split network (DD method applied for the order $q = 3$).*

studied examples. Since the reference is not available in practice, a stopping criterion, based on the error calculated by incrementing the order q, can be defined.
Based on the previous results for both applications, the DD technique achieves the desired result for a given order q. In practice, this order q is not known in advance and will depend on the topology of the network (length, characteristic impedances and load resistances of the lines), the observable, the choice of the decomposition as well as the time interval for the output's recording.

To illustrate this statement, we consider the same network in Figure (2.15) with an open-circuit load at the line L_3^1 and only the voltage source V_{s4}^2, new reflections due to the mismatch ($\Gamma_{L3} = 1$) appears in the network. By applying equation (2.48) to the order $q = 2$, the DD method superimposes the reference result for the time interval $[0.0.1\mu s]$, as reported in Figure (2.26a). As time progresses, the method doesn't align with the reference, so a higher order ($q = 3$) is required to obtain the result reported in Figure (2.26b).

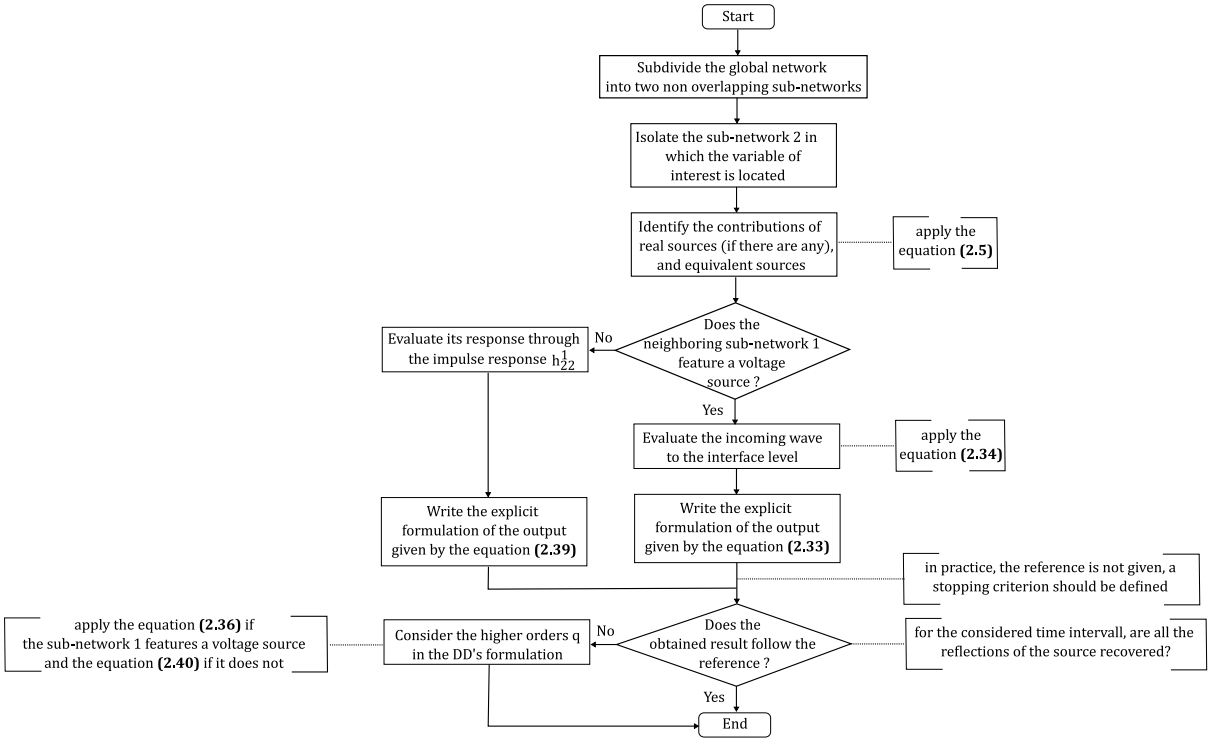

Figure 2.25: *Flow chart of the key steps of the DD method to evaluate the voltage V_5^2 across the load resistance R_{L5}^2 of the line L_5^2 in Figure (2.19) for two different configurations: the sub-network Y^1 features or does not feature a voltage source.*

2.3.2 Second case scenario: mismatch at the interface level

In general, each sub-network Y^k, $k \in \{1,2\}$, can be seen as a sub-system k for which an equivalent resistance R_{eq}^k appears at the exchange interface, as schematized in Figure (2.27). So far, these equivalent resistances were considered equal to the characteristic impedance of the line at which occurred the subdivision. Consequently, the hypothesis of preserving the electrical properties of the system at the interface level given in section (2.1.1) was verified.
If this assumption is not respected, the equivalent resistances R_{eq}^k are no longer equal. The coefficient of reflection Γ_k, for each sub-network k, thus appears at the interface level, which expression is based on equation (2.14) such as

$$\begin{cases} \Gamma_k = \dfrac{R_{eq}^s - R_{eq}^k}{R_{eq}^s + R_{eq}^k}, & \text{with } s \in \{1,2\} \text{ and } s \neq k \\ T_k = \Gamma_k + 1 \end{cases} \tag{2.50}$$

These reflection coefficients must be considered in the output's formulation.
We propose in the following to explore this configuration on the basis of the transmission line

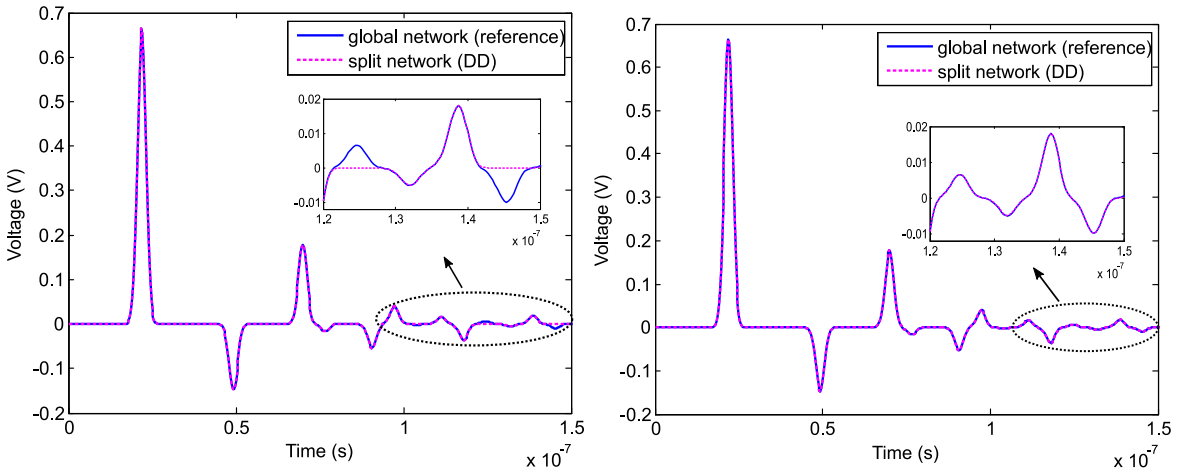

Figure 2.26: *Comparaison of the voltage V_5 across the resistance R_{L5} for the global network (reference) and the split network (DD method applied for the order $q = 2$ (a), for the order $q = 3$ (b)).*

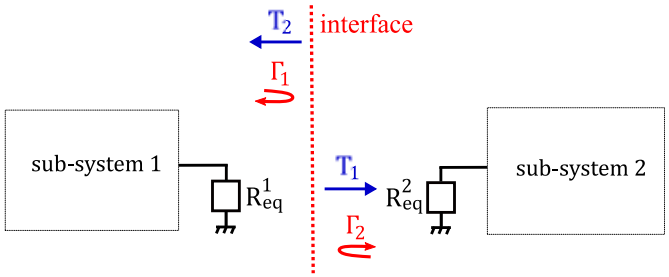

Figure 2.27: *Schematic representation of sub-systems 1 (sub-network Y^1) and 2 (sub-network Y^2) after splitting the global system (global network).*

network in Figure (2.28a). The latter consists of 6 uniform and lossless transmission lines and a voltage source V_{s4}. The latter is represented by the Gaussian signal in equation (2.38), such as $A = 1V$, $t_c = 7,91ns$ and $\sigma = 1,26ns$. We apply the DD method to the network at the node level connecting the lines L_2^1 and L_2^2, with the aim to evaluate the voltage V_5^2 across the load resistance R_{L5}^2. At the interface level appears the load resistances R_{L2}^k, $k \in \{1,2\}$, for each line L_2^k as shown in Figure (2.28b). Each of these resistances equals the characteristic impedance of the corresponding line ($R_{L2}^k = Z_{c2}^k$).

By identification, sub-systems 1 and 2 in Figure (2.27) are represented by sub-network 1 and 2 respectively. Due to the mismatch at the interconnection of lines L_2^1 and L_2^2 ($Z_{c2}^1 \neq Z_{c2}^2$), transmission T_k and reflection Γ_k coefficients at the interface level of each sub-network k, $k \in$

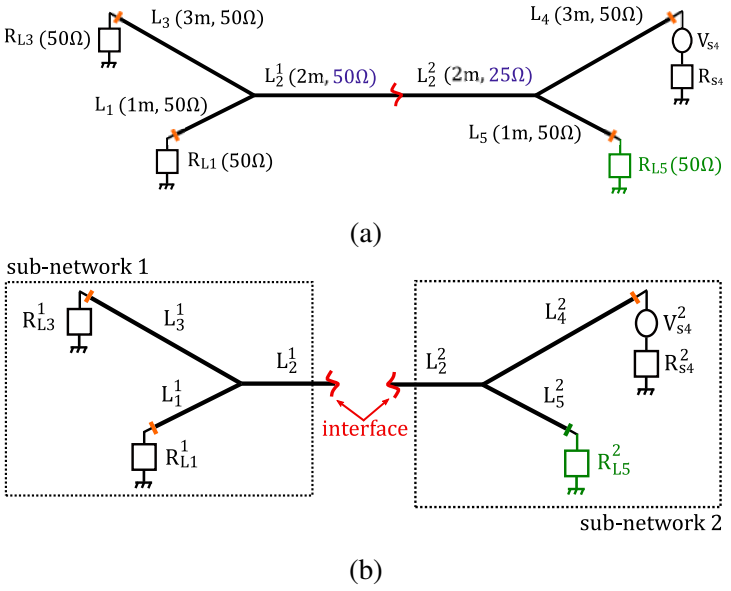

Figure 2.28: *Global transmission line network split at the node level connecting the lines L_2^1 and L_2^2 (a), sub-networks Y^1 and Y^2 after the subdivision of the global network (b).*

$\{1,2\}$, appear. Their respective expressions, deduced from equations (2.50), are given by

$$\Gamma_1 = \frac{R_{L2}^2 - R_{L2}^1}{R_{L2}^2 + R_{L2}^1} \quad , \quad T_1 = 1 + \Gamma_1 \tag{2.51}$$

$$\Gamma_2 = \frac{R_{L2}^1 - R_{L2}^2}{R_{L2}^1 + R_{L2}^2} \quad , \quad T_2 = 1 + \Gamma_2 \tag{2.52}$$

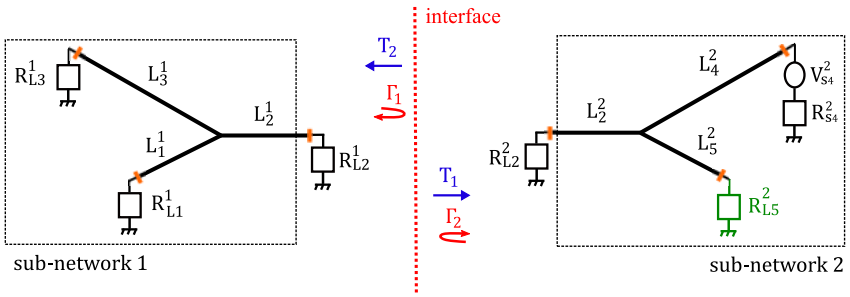

Figure 2.29: *Schematic representation of sub-networks 1 and 2 and their corresponding transmission and reflection coefficients at the interface level.*

Following the general principle of the DD method given by algorithm (1), we focus on the sub-network $k = 2$, where the observable V_5^2 is located. The latter is deduced from the general formulation given by equation (2.5), as follows:

$$V_5^2 = h_{45}^2 * V_{s4}^2 + h_{25}^2 * V_{\sim 2}^2 \tag{2.53}$$

where $V_{\sim 2}^2$, the equivalent source at the interface level of sub-network 2, is given by

$$V_{\sim 2}^2 = h_{22}^1 * (h_{42}^2 * V_{s4}^2) \tag{2.54}$$

The product $(h_{45}^2 * V_{s4}^2)$ in equation (2.53) gives the direct propagation of the voltage source V_{s4}^2 in the network, represented by the path (a) in Figure (2.30a). Whereas the product $(h_{42}^2 * V_{s4}^2)$ translates the retro-action of the neighboring sub-network 1 to the interface level $l = 2$, represented by the path (b) in Figure (2.30b).

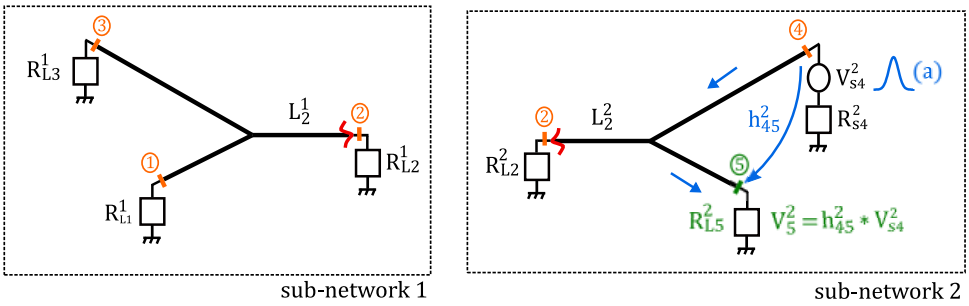

(a) *Schematic representation of the direct propagation of the voltage source V_{s4}^2 in the sub-network Y^2.*

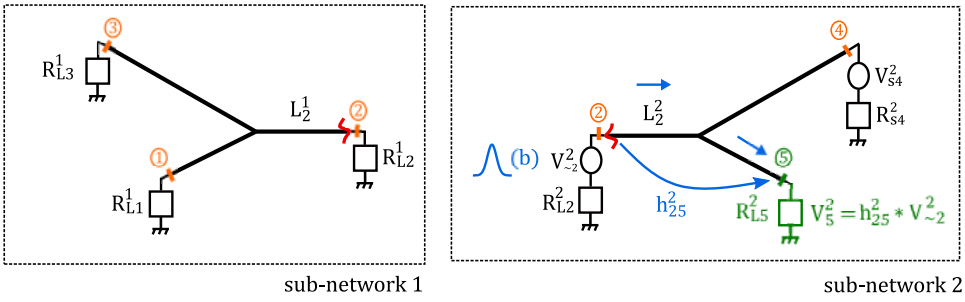

(b) *Schematic representation of the propagation of the equivalent source $V_{\sim 2}^2$ in the sub-network Y^2.*

Figure 2.30: *Schematic representation of the propagation paths of the voltage source V_{s4}^2 within the sub-network Y^2.*

The equivalent source $V_{\sim 2}^2$ is obtained at first by considering the transmission of the physical voltage source V_{s4}^2 to the interface level $l = 2$, through the product $(h_{42}^2 * V_{s4}^2)$. However, due to the mismatch at the interface, the transmission from sub-network 2 to sub-network 1 is made with the factor T_2. The contribution of sub-network 1 on the other hand is given through its impulse response h_{22}^1, since it has no physical source. Its product with the term $(h_{42}^2 * V_{s4}^2)$

gives the final contribution to the observable ($j = 5$, $k = 2$) is then retrieved through the product, with a transmission factor T_1 to physically consider the mismatch at the interconnection. The new expression of the voltage V_5^2, taking into account the impedance discontinuity at the interconnection level, is thus given by

$$V_5^2 = h_{45}^2 * V_{s4}^2 + T_1 * T_2 * \left(h_{25}^2 * \left(h_{22}^1 * (h_{42}^2 * V_{s4}^2) \right) \right) \tag{2.55}$$

By computing the previous equation, we observe the result reported in Figure (2.31), where the direct propagation of the source V_{s4}^2 (first gaussian peak of positive sign) and the first-order of the retro-action of sub-network 1 to 2 (first gaussian peak of negative sign) are retrieved. However, the obtained outcome doesn't yield the expected output, due to the incomplete evaluation of the voltage V_5^2 given by equation (2.55).

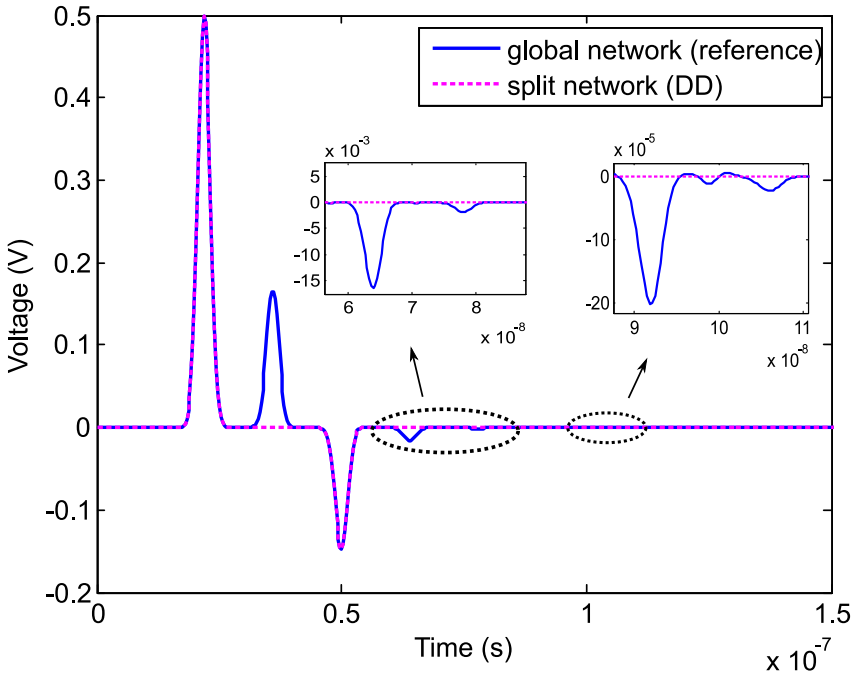

Figure 2.31: *Comparaison of the voltage V_5 across the resistance R_{L5} evaluated for the global network (reference) and the split network (DD method).*

Contrary to the general principle of the DD method where the decomposition occurs at a perfectly matched interface, the impedance discontinuity in this configuration causes a reflection of the incident wave $(h_{24}^2 * V_{s4}^2)$ with the factor Γ_2. Its contribution to the output is considered through the additional term in equation (2.56).

$$V_5^2 = h_{45}^2 * V_{s4}^2 + T_1 * T_2 * \left(h_{25}^2 * \left(h_{22}^1 * (h_{42}^2 * V_{s4}^2) \right) \right) + \Gamma_2 * \left(h_{25}^2 * (h_{42}^2 * V_{s4}^2) \right) \tag{2.56}$$

For a better understanding of the previous equations, we focus on the transmission and reflection phenomena at the interface level on both sides of sub-networks 1 and 2, as schematized in Figure (2.32).

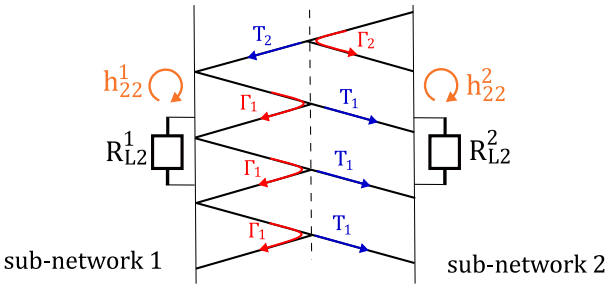

Figure 2.32: *Schematization of the transmission and reflection phenomena at the interface level* $l = 2$ *of each sub-network* k, $k \in \{1,2\}$.

Similarly to the previous examples, the retro-actions between both sub-network and the multiple reflections of the source V_{s4}^2 within the network should be considered with the additional term featuring the q-th order.

$$\begin{aligned} V_5^2 = h_{45}^2 * V_{s4}^2 + T_1 * T_2 * \left(h_{25}^2 * \left(h_{22}^1 * (h_{42}^2 * V_{s4}^2)\right)\right) + \Gamma_2 * \left(h_{25}^2 * (h_{42}^2 * V_{s4}^2)\right) \\ + \sum_{i=2}^{q} T_1 * \left(h_{25}^2 * \left(\Gamma_1 * h_{22}^2 * (h_{22}^1 * V_{\sim 2,i}^2)\right)\right) \end{aligned} \tag{2.57}$$

with $V_{\sim 2,i}^2$ is defined as the i-th order[9] of the equivalent source and is given by

$$V_{\sim 2,i}^2 = \Gamma_1 * \left(h_{22}^2 * (h_{22}^1 * V_{\sim 2,i-1}^2)\right) \tag{2.58}$$

By applying equation (2.57) to the order $q = 5$, the DD method retrieves the expected result as reported in Figure (2.33).
Although the formulation of the output is updated and requires consideration of the corresponding reflection and transmission coefficients, the core idea behind the DD method is unchanged and the obtained results are satisfying.

2.3.3 General explicit formulation of the DD method

Based on the previous numerical applications, and for different configurations, the initial general formula of the DD method given by equation (2.5) was insufficient to retrieve the

[9]The first order of the equivalent voltage source $V_{\sim 2,1}^2$ is given by: $\Gamma_1 * \left(h_{22}^1 * (h_{12}^2 * V_{s4}^2)\right)$.

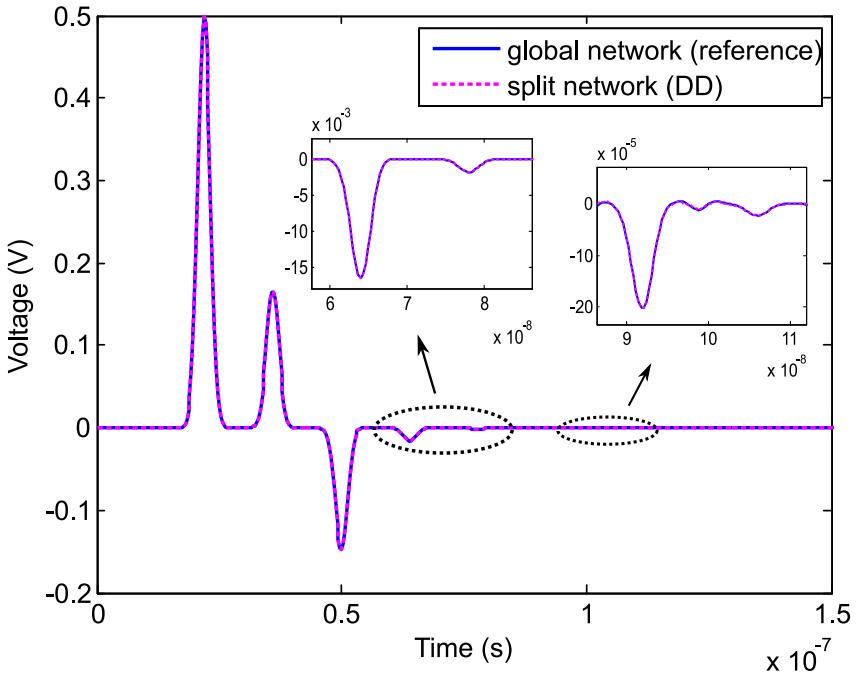

Figure 2.33: *Comparaison of the voltage V_5 across the resistance R_{L5} evaluated for the global network (reference) and the split network (DD method).*

expected result. Before giving the general explicit formulation of the DD technique, allowing to retrieve the multiple round trips of the physically injected sources into the network, we give the detailed expression of the equivalent sources $V^k_{\sim\{l\}}$. The latter reflects implicitly the effect of the dispersed sources in the $\{u\}$ neighboring sub-systems of k, where $\{u\} \subseteq \{1,...,m\}\backslash\{k\}$ is a subset of all the m sub-systems expect for the sub-system k. As demonstrated with the previous numerical applications, two configurations can be encountered: 1) the neighboring sub-system(s) may not feature any physical source, 2) the neighboring sub-system(s) features one or more physical sources. We give in the following the possible combinations arising from these configurations:

1. 1^{st} case: if the $\{u\}$ neighboring sub-systems feature a physical source V^u_{si}:

$$V^k_{\sim l_u} = h^u_{il_u} * V^u_{si} \tag{2.59}$$

2. 2^{nd} case: if the $\{u\}$ neighboring sub-systems does not feature a physical source:

$$V^k_{\sim l_u} = \prod_{\{u\}} h^u_{l_u l_u} * (h^k_{ij} * V^k_{si}) \tag{2.60}$$

where l_u is the index of termination in which the decomposition has occurred between the sub-networks k and u.

The final formula of the voltage V_j^k given for the order q, is written as follows:

$$V_j^k = \sum_{\{i\}} h_{ij}^k * V_{si}^k + \sum_{\{l\}} h_{lj}^k * V_{\sim l,1}^k + \sum_{i=2}^{q} h_{lj}^k * \left(\prod_{\{v\}} h_{l_v l_v}^v * V_{\sim l,i}^k\right) \tag{2.61}$$

where $\{v\} \subseteq \{1,...,m\}$ is a subset of all the m sub-systems, and $V_{\sim l,i}^k$ is defined as the i-th order of the equivalent source such as

$$V_{\sim l,i}^k = \prod_{\{v\}} h_{l_v l_v}^v * V_{\sim l,i-1}^k \tag{2.62}$$

The term $V_{\sim l,1}^k$ refers to the first order of the source $V_{\sim l}^k$.

We specify that the given expressions (2.59) and (2.60) translate the incoming wave from the neighboring sub-systems to the interface level of the sub-system of interest k. In other configurations (see the application in (2.3.1)), a new equivalent source from the physical source itself in the sub-system k appears at the exchange interface. Equation (2.60) is given with the assumption that the sub-network k features a physical source V_{si}^k.

With the explicit expression of the equivalent sources, their computational complexity, whose principle was established earlier in (2.1.2), is evaluated in detail in Table (2.1).

Case	Computational complexity
1^{st} case	$\sim O(card(u) \times N^2)$
2^{nd} case	$\sim O(card(u) \times N^3 + N^2)$

Table 2.1: Computational complexity of the evaluation of the equivalent sources for both cases.

The quantity $card(u)$ refers to the number of elements in the subset $\{u\}$.

The total computational complexity of the output V_j^k of equation (2.5) can be deduced for both cases. It is of the order of $\sim O(p \times N^2 + q \times card(u) \times N^3)$ for the first case, and the order $\sim O(p \times N^2 + q \times card(u) \times N^4 + q \times N^3)$ for the second.

The computational complexity is given for information purposes for a complete assessment of our approach. However, as mentioned in the section (2.1.2), we are more interested in the

potential gain of the evaluation cost, of the model itself, with our technique.

For illustration purposes and a better understanding of how the previous expressions can be practically implemented, we apply these generated equations for the two configurations mentioned above.

- 1^{st} case: we suppose that the global linear system G in Figure (2.34a) has $z = 7$ terminations, of $\alpha = 3$ physical sources and $\beta = 4$ outputs, among these we are interested in the output at the termination $j = 6$. Using the DD method, the network is split at two levels into $m = 3$ non-overlapping sub-systems. Consequently, new terminations $l = 4$ and $l = 7$ appear at the decomposition levels as shown in Figure (2.34b). Following this decomposition, each source is located in a given sub-system, whereas the output is located in the sub-system 2 ($k = 2$) as represented in Figure (2.34c).

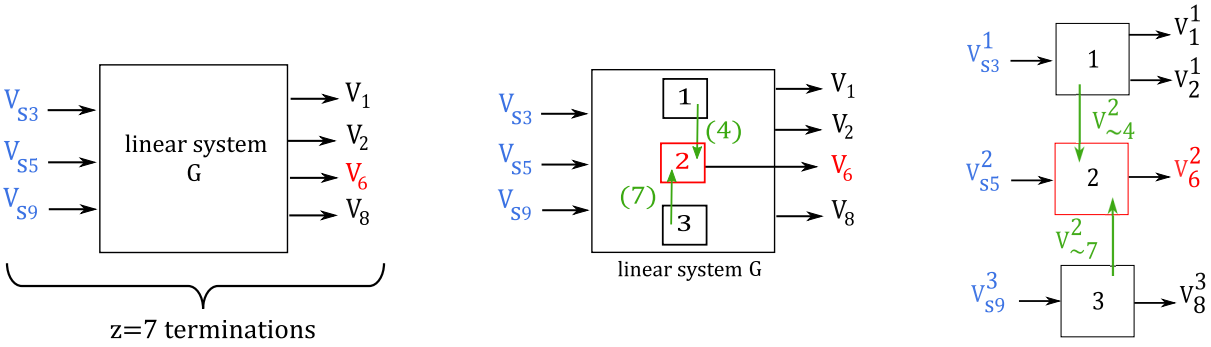

Figure 2.34: *Schematic representation of the studied system (a), its decomposition (b), and dispersion of physical sources and isolation of the output (c) for the first configuration.*

In this configuration, both $\{u\} \in \{1,3\}$ neighboring sub-systems feature a physical source (V^1_{s3} and V^3_{s9}). The equivalent sources at the interface levels of the sub-system 2, $l = 4$ and $l = 7$, are deduced from equation (2.59) as follows:

$$V^2_{\sim 4} = h^1_{34} * V^1_{s3} \tag{2.63}$$

$$V^2_{\sim 7} = h^3_{97} * V^3_{s9} \tag{2.64}$$

The voltage V^2_6 is thus evaluated based on the general DD formula given by equation (2.61) and the above explicit expressions of the equivalent sources at the two in-

terfaces.

$$\begin{aligned} V_6^2 &= h_{56}^2 * V_{s5}^2 + h_{46}^2 * V_{\sim 4}^2 + h_{76}^2 * V_{\sim 7}^2 \\ &= h_{56}^2 * V_{s5}^2 + h_{46}^2 * (h_{34}^1 * V_{s3}^1) + h_{76}^2 * (h_{97}^3 * V_{s9}^3) \end{aligned} \tag{2.65}$$

- 2^{nd} case: we consider the global linear system G in Figure (2.35a), of $z = 8$ terminations ($\alpha = 1$ and $\beta = 7$). The decomposition occurs at 2 levels $l = 4$ and $l = 7$, and the output, i.e. the voltage V_6, is located in sub-system 2 as schematized in Figure (2.35b). Contrary to the previous case, none of the neighboring sub-systems u, $\{u\} \in \{1,3\}$, feature a physical source and thus they exchange only their inherent impulse response $h_{l_u l_u}^u$ as shown in Figure (2.35c).

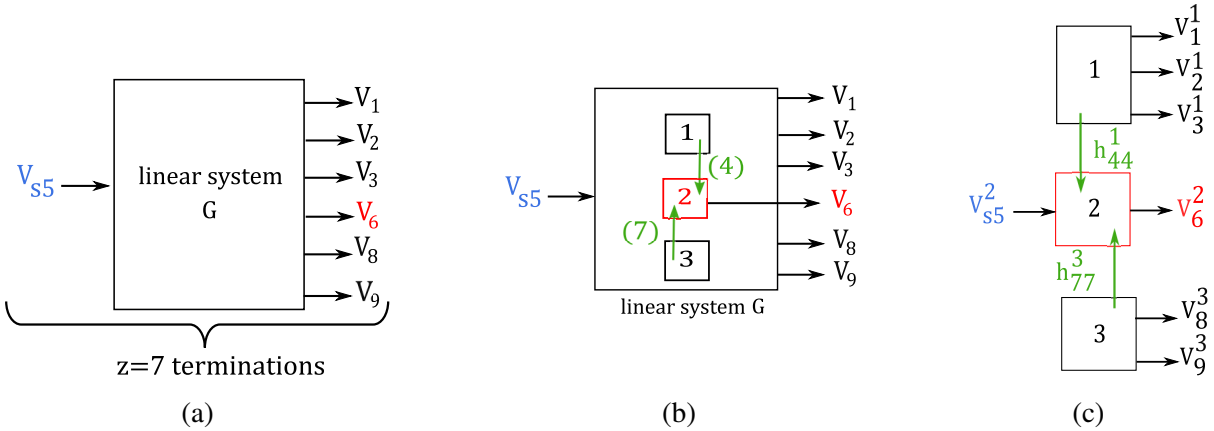

Figure 2.35: *Schematic representation of the studied system (a), its decomposition (b), and dispersion of physical sources and isolation of the output (c) for the second configuration.*

The equivalent sources at the exchange levels, deduced from equations (2.60), are expressed by

$$\begin{aligned} V_6^2 &= h_{56}^2 * V_{s5}^2 + h_{46}^2 * V_{\sim 4}^2 + h_{76}^2 * V_{\sim 7}^2 \\ &= h_{56}^2 * V_{s5}^2 + h_{46}^2 * \left(h_{44}^1 * \left(h_{54}^2 * V_{s5}^2\right)\right) + h_{76}^2 * \left(h_{77}^3 * \left(h_{57}^2 * V_{s5}^2\right)\right) \end{aligned} \tag{2.66}$$

An additional combination can be encountered, where sub-system 1 features a source V_{s3}^1 and sub-system 3 doesn't. In this case, the equivalent source translating the contribution of sub-system 2 is given by equation (2.63), whereas the contribution of sub-system 3 is retrieved through its impulse response h_{77}^3. The output V_6^2 is thus given by

$$\begin{aligned} V_6^2 &= h_{56}^2 * V_{s5}^2 + h_{46}^2 * V_{\sim 4}^2 + h_{76}^2 * V_{\sim 7}^2 \\ &= h_{56}^2 * V_{s5}^2 + h_{46}^2 * \left(h_{34}^1 * V_{s3}^1\right) + h_{76}^2 * \left(h_{77}^3 * \left(h_{57}^2 * V_{s5}^2\right)\right) \end{aligned} \tag{2.67}$$

The general nature of the proposed decomposition method enables its automation for: 1) the evaluation of multiple outputs for different configurations (terminations, distribution of α inputs and β outputs, and the decomposition itself), 2) the realization of domain decomposition in industrial context without loss of models' confidentiality. Typically, a graphical user interface (GUI) can be developed such that each sub-system v is characterized by a block in the GUI. They each exchange both their inherent impulse response h_{ll}^v and the equivalent source, whose expressions were detailed earlier. The exchange of the incoming wave from one sub-system to the interface, reveals neither the source of excitation in this sub-system, nor its topology. This is an additional advantage of the DD method and is easier to implement, especially for a third-party user of the interface.

2.4 Adapting the DD method for practical applications

So far, the DD method is based on the decomposition of the network at the transmission line itself. The method has been validated through the first numerical applications. However, the subdivision at the cable itself is a rather special case. In practice, the decomposition will take place at an interconnection, which is, in the case of lines, a junction. The last application of the DD method in the previous section (2.3.2) introduces a new take on the DD method for more practical and realistic applications. In this section, we progressively demonstrate the principle of the DD method when the decomposition takes place at the level of the junction itself.

2.4.1 Formulation for two interconnected systems

To reiterate the method's formulation, we consider the linear electric system for which the subdivision occurs at the node level in Figure (2.27). Let's suppose that this system under study is represented by two transmission lines, uniform and lossless, as schematized in Figure (2.36). At the entrance of the line L_1^1 is injected the source V_{s1}^1, represented by the Gaussian signal of equation (2.38) with $A = 1V$, $t_c = 8ns$ and $\sigma = 1.26ns$. The two lines are interconnected by a node at which the subdivision occurs. The modeling of the network is implemented using the FDTD technique, with a time step $dt = 0.31ns$ chosen in compliance with the stability criterion of the numerical tool.

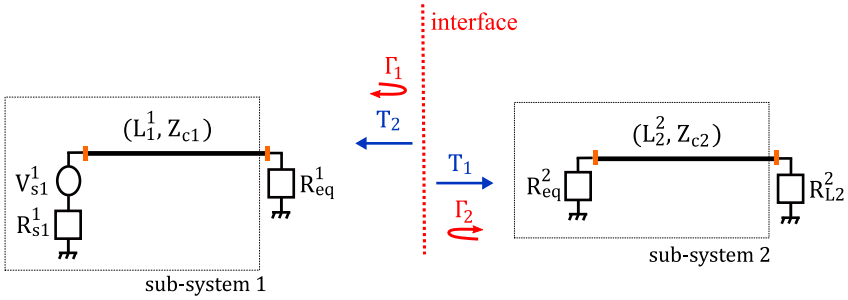

Figure 2.36: *Schematic representation of sub-systems 1 and 2, represented each by a transmission line, after splitting the global system.*

This decomposition separates the two transmission lines into two distinct and non-overlapping sub-networks. At the interface level appears an equivalent resistance R^k_{eq}, for each line L^k_k, equal to its characteristic impedance Z_{ck}.

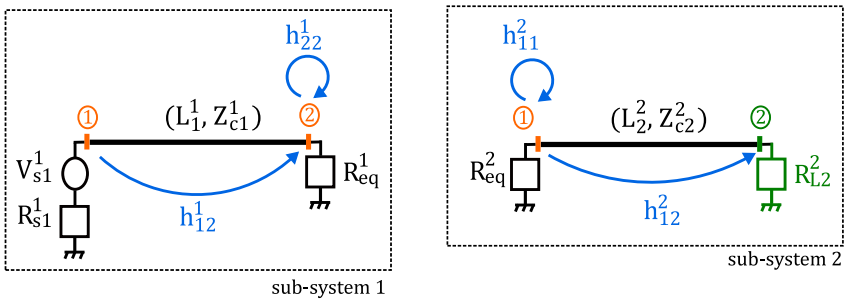

Figure 2.37: *Impulse responses $h^k_{\cdot\cdot}$ for each sub-system k, $k \in \{1,2\}$.*

The voltage V^2_2 across the resistance R^2_{L2} of the line L^2_2 of sub-system 2 is retrieved based on the general principle of the DD method given by equation (2.5), such as

$$V^2_2 = h^2_{12} * V^2_{\sim 1} \tag{2.68}$$

The sub-network 2 has no physical voltage source, consequently, only the right-hand term of equation (2.5), translating the contribution of the neighboring sub-network 1 to the interface, is considered. As previously detailed in the section (2.1.1), the incoming wave voltage to the interface $V^2_{\sim 1}$ is expressed by

$$V^2_{\sim 1} = h^1_{12} * V^1_{s1} \tag{2.69}$$

As the system's decomposition occurred at the node, its physical property (impedance continuity) must be considered in the formulation of the DD. In contrast to line-level decomposition previously presented where the impulse responses contain the network characteristics and take

into account its mismatches, the decomposition at the node level does not. In this new configuration, each line is loaded by a load resistance equal to its characteristic line, at the decomposition level a perfect match is then recorded. Consequently, the physical behavior of the junction is not included. On this basis, we consider the coefficient of transmission T_1 on a second step at the linear combination of the partial solutions (i.e. the impulse responses), to translate the propagation of the incoming wave (the equivalent source $V^1_{\sim 1}$) from the neighboring sub-system 1 to the interface level. The voltage V^2_2 is thus given by

$$\begin{aligned} V^2_2 &= h^2_{12} * V^2_{\sim 1} \\ &= h^2_{12} * \left(T_1 * (h^1_{12} * V^1_{s1}) \right) \end{aligned} \tag{2.70}$$

Let's consider that the lines $L_1(1m)$ and $L_2(2m)$ have respectively a characteristic impedance equal to 50Ω and 100Ω. The voltage across the resistance $R_{L2} = 50\Omega$, retrieved based on equation (2.70) with $T_1 = \frac{4}{3}$, is reported on Figure (2.38).

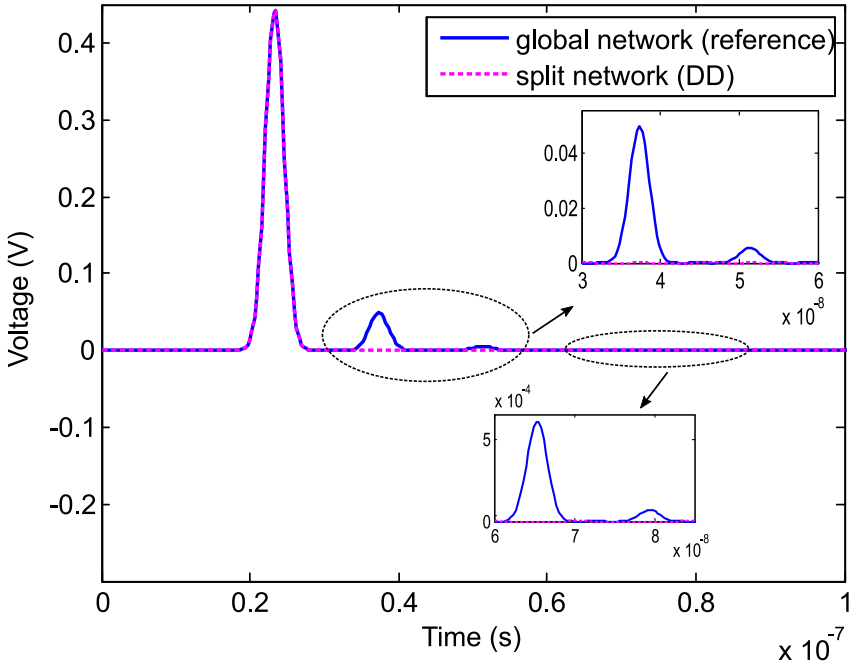

Figure 2.38: *Comparaison of the voltage V_2 across the resistance R_{L2} evaluated for the global network (reference) and the split network (DD method).*

We observe the excellent agreement of the DD method's result with the reference for the first direct propagation of the Gaussian pulse within the system. However, from the instant $t = 3.23.10^{-}8s$, the approach is unable to recover the desired result. In fact, its formulation given

by equation (2.70), considers only the transmission of the injected source to the measuring point. Its reflection, due to the mismatch at the node, should be considered through the impulse response h^2_{11} of sub-network 2 multiplied by the reflection coefficient $\Gamma_2 = \frac{-1}{3}$. Its contribution to the output is thus retrieved by the additional term in equation (2.71) such as

$$V^2_2 = h^2_{12} * \left(T_1 * (h^1_{12} * V^1_{s1})\right) + h^2_{12} * \left(\Gamma_2 * \left(h^2_{11} * T_1 * (h^1_{12} * V^1_{s1})\right)\right) \tag{2.71}$$

As previously outlined, the multiple reflections of the injected voltage source within the network must be considered through the impulse responses h^k_{ll} of each sub-network k. The final formulation retrieving the multiple round-trips of the voltage source to the q-th order is given by

$$\begin{aligned} V^2_2 = h^2_{12} * \left(T_1 * (h^1_{12} * V^1_{s1})\right) + h^2_{12} * \underbrace{\left(\Gamma_2 * \left(h^2_{11} * T_1 * (h^1_{12} * V^1_{s1})\right)\right)}_{V^2_{\sim 1,1}} \\ + \sum_{i=2}^{q} h^2_{12} * \left(\Gamma_2 * \left(h^2_{11} * T_1 * (h^1_{22} * V^2_{\sim 1,i})\right)\right) \end{aligned} \tag{2.72}$$

with $V^2_{\sim 1,i}$ is defined as the i-th order of the equivalent source and is given by

$$V^2_{\sim 1,i} = \Gamma_2 * \left(h^2_{11} * T_1 * (h^1_{22} * V^2_{\sim 1,i-1})\right) \tag{2.73}$$

and $V^2_{\sim 1,1}$ refers to the first order of the equivalent source at the interface.

By applying equation (2.72) for the order $q = 3$, the desired result is yielded as reported in Figure (2.39).
In summary, the principle of the DD method remains unchanged, but the discontinuity effects at the junction must be taken into account. The transmission coefficient allows us to take into account the direct propagation of the contribution of the neighboring network at the observable level, while the reflection coefficients are needed to recover the higher orders that reflect the multiple reflections.

2.4.2 Formulation for a branched transmission line network

Now that we have established the principle of the method and detailed its formulation for two interconnected transmission lines, we extend its application to a branched transmission line network. In this case, the decomposition at the interconnection level (junction) makes

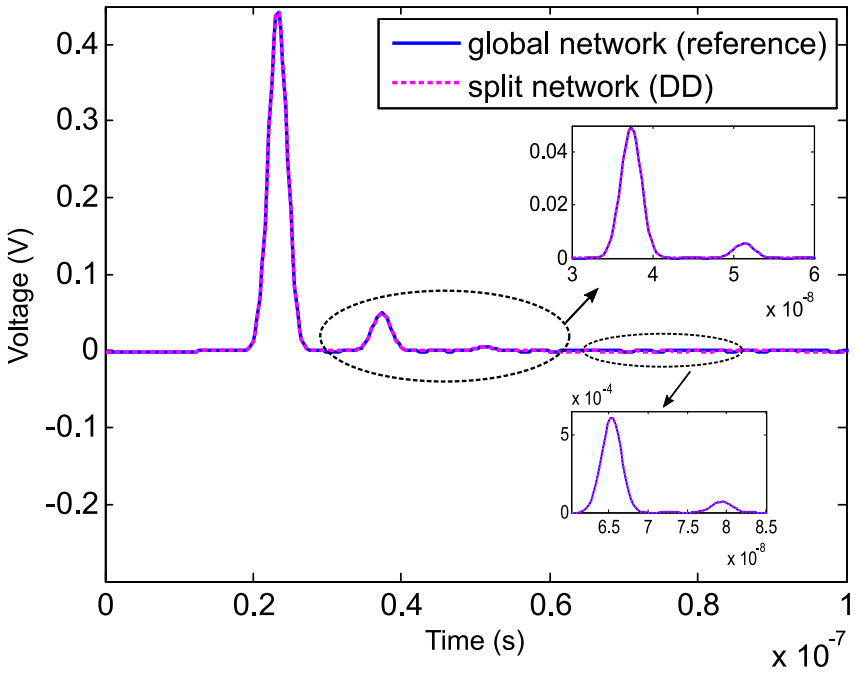

Figure 2.39: *Comparaison of the voltage V_2 across the resistance R_{L2} evaluated for the global network (reference) and the split network (DD method).*

even more sense and represents more realistic cases. In this section, we consider a Y transmission line network consisting of three uniform and lossless transmission lines, as shown in Figure (2.40a). Following this decomposition appears the equivalent load resistance R^k_{eq}, equal to the characteristic impedance of the line L^k_k, $k \in \{1,2,3\}$, at the interface level of each subsystem as shown in Figure (2.40b). We assume that all three lines have equal characteristic impedance $Z_{ck} = 50\Omega$, $k \in \{1,2,3\}$. The reflection coefficient at the junction level is thus equal for three lines[10]. In the following, we propose to study three configurations according to which the loads of the lines and the observable will be modified. This study aims to demonstrate the applicability of the technique for different cases. For all the cases, the source V_{s1} injected at the entrance of the network at line L_1 is a Gaussian signal of equation (2.38) (with $A = 1V$, $t_c = 1.2ns$ and $\sigma = 1.26ns$), and the results are obtained with the FDTD method implemented for $dt = 0.31ns$.

[10]The reflection coefficient Γ_i at the junction level of the line $L_{k,\ \{1,2,3\}}$ is evaluated on the basis of equation (2.25) such as

$$\Gamma_k = \frac{Z_p - Z_{ck}}{Z_p + Z_{ck}}$$

with Z_p is the equivalent impedance of parrallel characteristic impedances $Z_{cs,\ s\neq k}$.

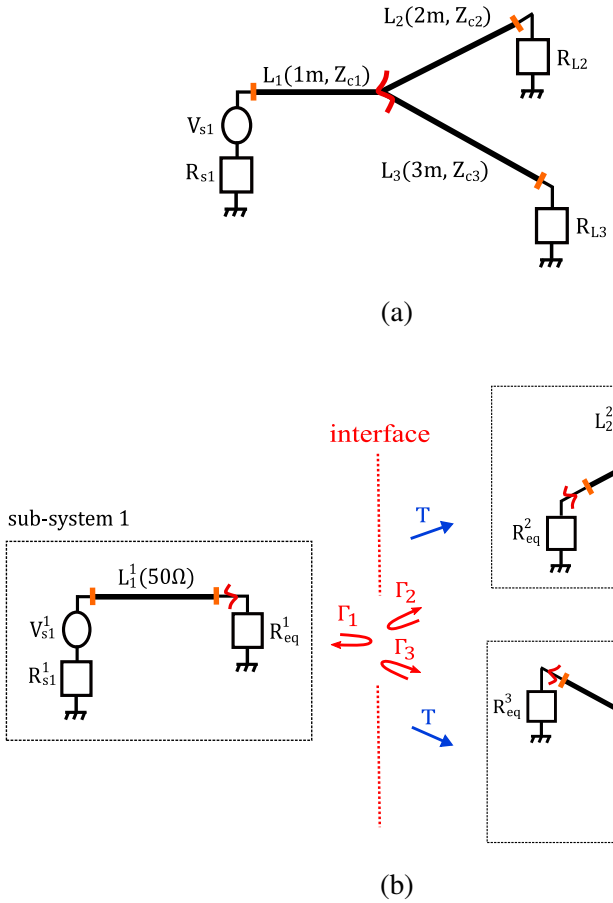

Figure 2.40: *Global Y transmission line network and its characteristics (a), isolation of each line in a distinct sub-system after the subdivision at the junction level (b).*

First case study

To begin with, we evaluate the voltage V_3^3 across the load resistance R_{L3}^3 for the network in Figure (2.41). In this case, the contribution of sub-network 1 to the interface is given by the product $(h_{12}^1 * V_{s1}^1)$, denoted $V_{\sim 1}^3$, whereas sub-network 2 is characterized by its inherent impulse response h_{11}^2 since no physical voltage source is featured.
Following the principle of the DD technique, the voltage V_3^3 is expressed by

$$\begin{aligned} V_3^3 = {} & T * (h_{13}^3 * V_{\sim 1}^3) + T * \Big(h_{13}^3 * \big(T * (h_{11}^2 * V_{\sim 1}^3)\big)\Big) \\ & + T * \Big(h_{13}^3 * \big(\underbrace{\Gamma * h_{11}^2 * T * (h_{11}^2 * V_{\sim 1}^3)}_{V_{\sim 1,1}^3}\big)\Big) + \sum_{i=2}^{q} T * \Big(h_{13}^3 * \big(\Gamma * h_{11}^2 * T * (h_{11}^2 * V_{\sim 1,i}^3)\big)\Big) \end{aligned} \tag{2.74}$$

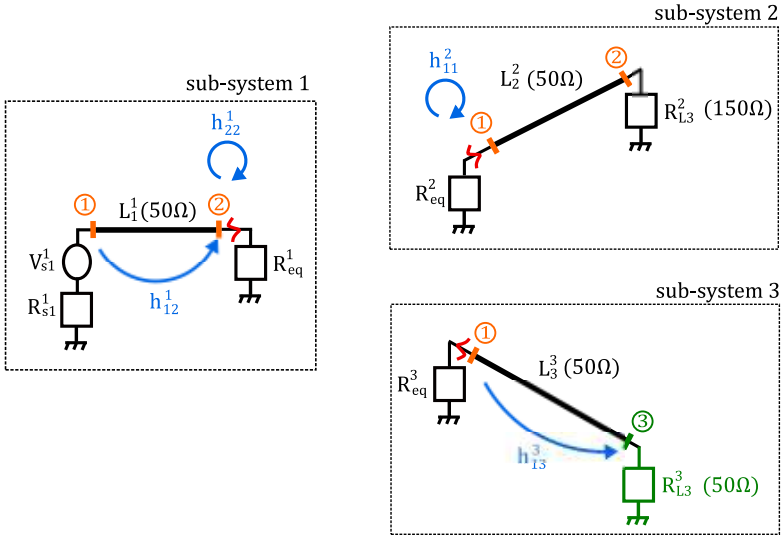

Figure 2.41: *Schematic representation of the impulse responses of each sub-network after the subdivision of the global network at the junction level - first case study.*

with $V^3_{\sim 1,i}$ is defined as the i-th order of the equivalent source at the interface level and is given by

$$V^3_{\sim 1,i} = \Gamma * (h^2_{11} * V^3_{\sim 1,i-1}) \tag{2.75}$$

The first term of the right-hand member of equation (2.74) gives the direct transmission of the equivalent voltage at the interface $V^3_{\sim 1}$ to the output. The second term translates the propagation of the source V^1_{s1} within lines L^1_1 and L^2_2 before their transmission to sub-network 3. The third term considers the reflection at the junction level through the re-injection of the equivalent source in sub-network 2. Finally, the right-hand term yields the multiple reflections of the voltage source V^1_{s1} to the q-th order.

By applying equation (2.74) for the order $q = 2$, the DD method retrieves the multiple reflections of the voltage source V^1_{s1} as reported in Figure (2.42).

Second case study

We focus now on the voltage V^2_2 across the load resistance R^2_{L2} in Figure (2.43). The evaluation of the voltage V^2_2 is very similar to the previous case[11]. The equivalent source to the

[11]Configurations 2 and 3 are symmetrical. The aim is to demonstrate that the method is valid regardless of the observable. The values of the load resistances of the lines at which the observable is located are chosen so as to ensure reflection, so the impulse response h^p_{ll} of the corresponding sub-network p, $p \in \{2,3\}$, can be evaluated.

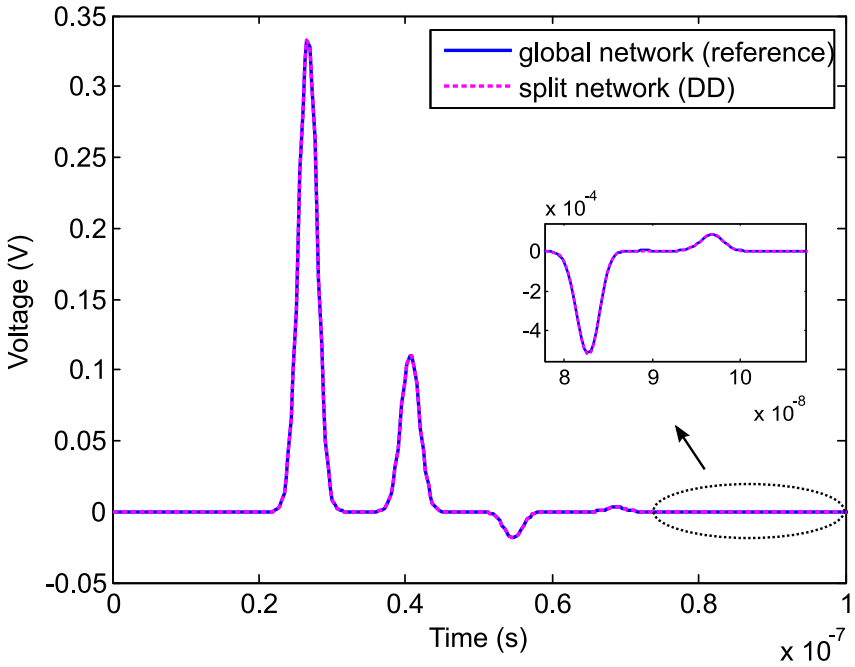

Figure 2.42: *Comparaison of the voltage V_2 across the resistance R_{L2} evaluated for the global network (reference) and the split network (DD method).*

interface, denoted $V^2_{\sim 1}$, is unchanged and is given by the product $(h^1_{12} * V^1_{s1})$.

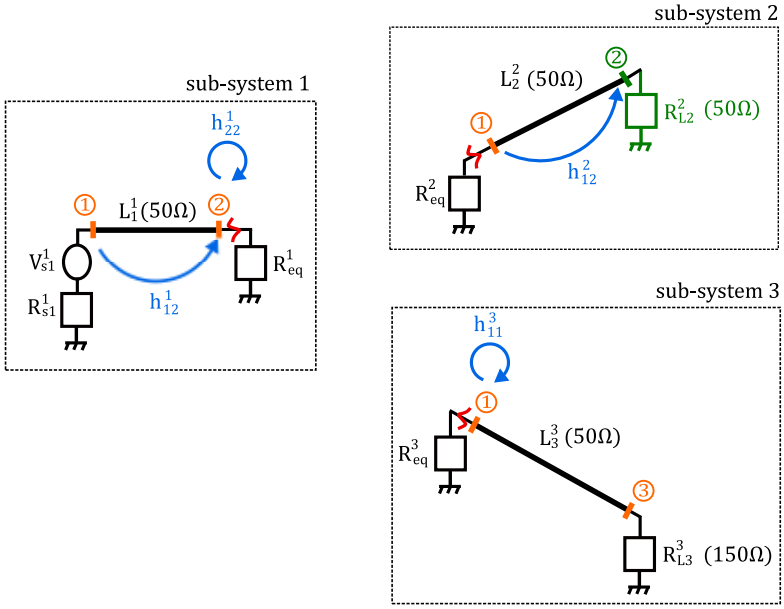

Figure 2.43: *Schematic representation of the impulse responses of each sub-network after the subdivision of the global network at the junction level- second case study.*

The final expression of the voltage V_2^2 is inspired from equation (2.74) and expressed as follows:

$$V_2^2 = T * (h_{12}^2 * V_{\sim 1}^2) + T * h_{12}^2 * \left(T * h_{11}^3 * V_{\sim 1}^2\right) + T * \Big(h_{12}^2 * \big(\underbrace{\Gamma * h_{11}^3 * T * h_{11}^3 * V_{\sim 1}^2}_{V_{\sim 1,1}^2}\big)\Big) + \sum_{i=2}^{q} T * \left(h_{12}^2 * \Gamma * h_{11}^3 * T * h_{11}^3 * V_{\sim 1,i}^2\right) \tag{2.76}$$

with $V_{\sim 1,i}^2$ is defined as the i-th order of the equivalent source at the interface level and is given by

$$V_{\sim 1,i}^2 = \Gamma * (h_{11}^3 * V_{\sim 1,i-1}^2) \tag{2.77}$$

Following the same reasoning as above, each term translates the contribution of a sub-network to the output. The result obtained with the DD method for the order $q = 2$ superimposes perfectly the reference as reported in Figure (2.44).

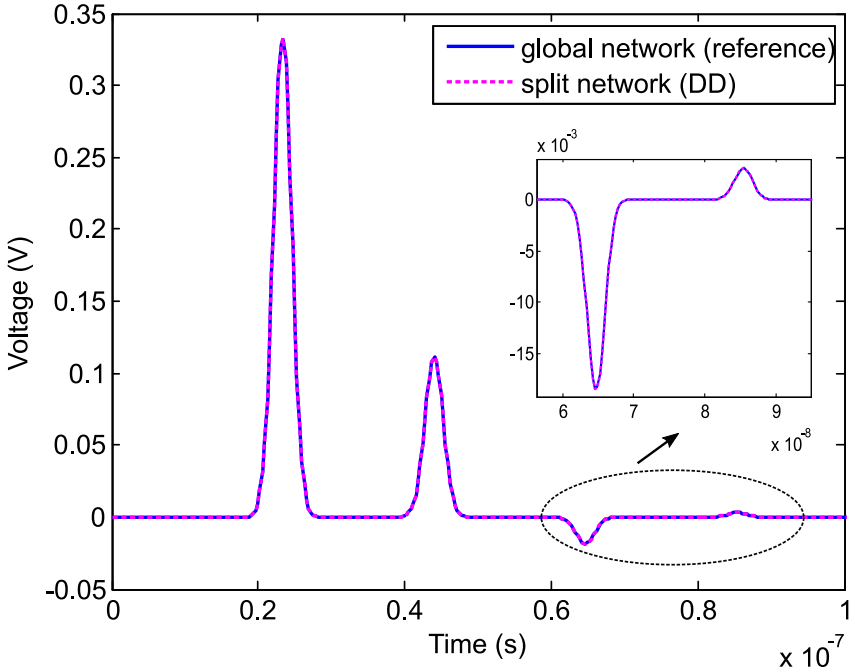

Figure 2.44: *Comparaison of the voltage V_2 across the resistance R_{L2} evaluated for the global network (reference) and the split network (DD method).*

Third case study

For the third configuration, represented in Figure (2.45), the impulse response h_{11}^2 of the

sub-network 2 is added to the voltage formulation V_2^2.

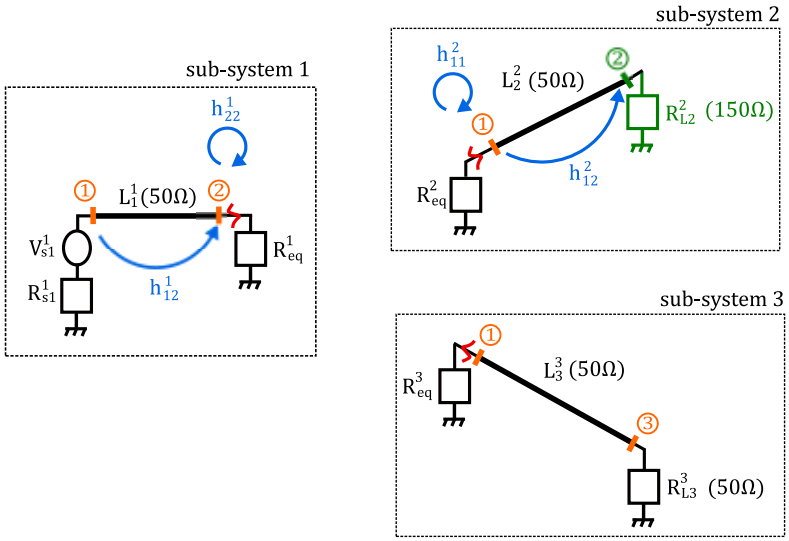

Figure 2.45: *Schematic representation of the impulse responses of each sub-network after the subdivision of the global network at the junction level - third case study.*

In fact, as the line L_2^2 is unmatched at its end ($R_{L2}^2 \neq Z_{c2}^2$)[12], its reflection must thus be considered through the impulse response h_{11}^2. The new formulation of the voltage V_2^2 is expressed as follows:

$$V_2^2 = T * (h_{12}^2 * V_{\sim 1}^2) + T * \left(h_{12}^2 * \underbrace{(\Gamma * h_{11}^2 * V_{\sim 1}^2)}_{V_{\sim 1,1}^2} \right) + \sum_{i=2}^{q} T * \left(h_{12}^2 * (\Gamma * h_{11}^2 * V_{\sim 1,i}^2) \right) \quad (2.78)$$

with $V_{\sim 1,i}^2$ is defined as the i-th order of the equivalent source at the interface level and is given by

$$V_{\sim 1,i}^2 = \Gamma * (h_{11}^2 * V_{\sim 1,i-1}^2) \quad (2.79)$$

By applying this equation to the order $q = 4$, the DD method gives the result reported in Figure (2.46), for which the direct transmission of the signal V_{s1}^1 as well as its multiple reflections are recovered.

To summarize, for both applications (matched or unmatched lines at their ends), the core idea of the method remains unchanged. Depending on the configuration, the inherent impulse re-

[12]This confugration can be considered as generalisation of the 2nd confiuration. To generalize, the formula of the output can be written by integrating the responses h_{ll}^p, if no reflections are measured these are thus null.

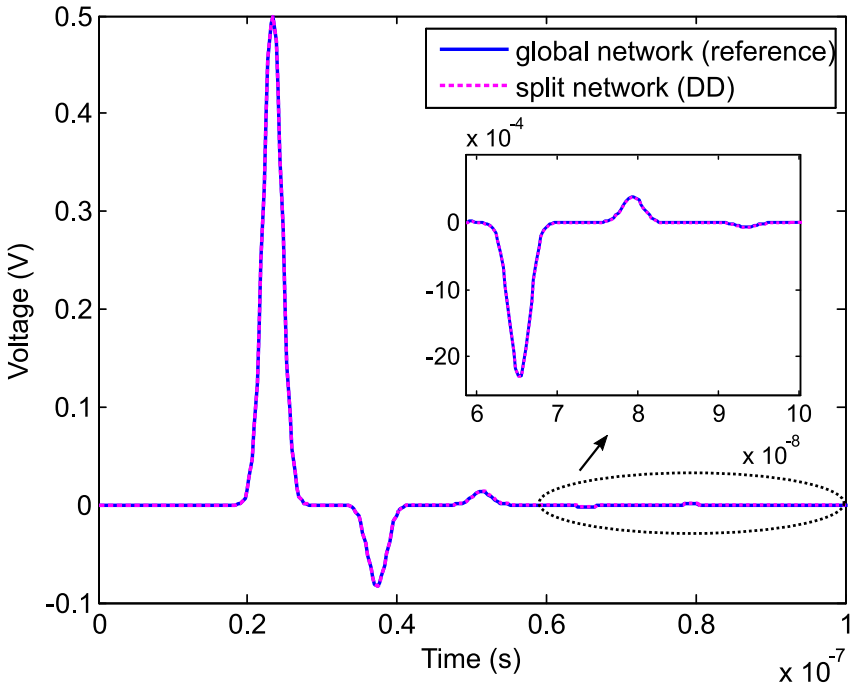

Figure 2.46: *Comparison of the voltage V_2 across the resistance R_{L2} obtained for the reference (global system) and the DD method (split system).*

sponses h^i_{11}, $i \in \{1,2,3\}$, may be required in the explicit formulation. The key steps for evaluating the observable using the new decomposition method (junction-level subdivision), for the Y transmission lines network in Figure (2.40a), are given in the flow chart in Figure (2.47).
For the studied cases, the proposed technique retrieves the desired result by integrating the coefficients of reflection and transmission (due to the mismatch at the junction) in its formulation. The method is independent of the configuration studied (topology, line characteristics, and observable), its formulation can thus be generalized and automatized.

2.5 Synthesis and Discussion

Throughout the various applications, we bring together the key findings from the proposed DD method for 1D linear applications. We discuss whether the method answers the objectives related to the research project. By highlighting the strengths of this approach and acknowledging its inherent limitations, we aim to provide a well-rounded evaluation.
Firstly, the DD technique meets the ANR *ECOCES* project's specifications and thus the first objective of the thesis:

1. The DD method allows fully asynchronous temporal simulations: it bypasses the iterative

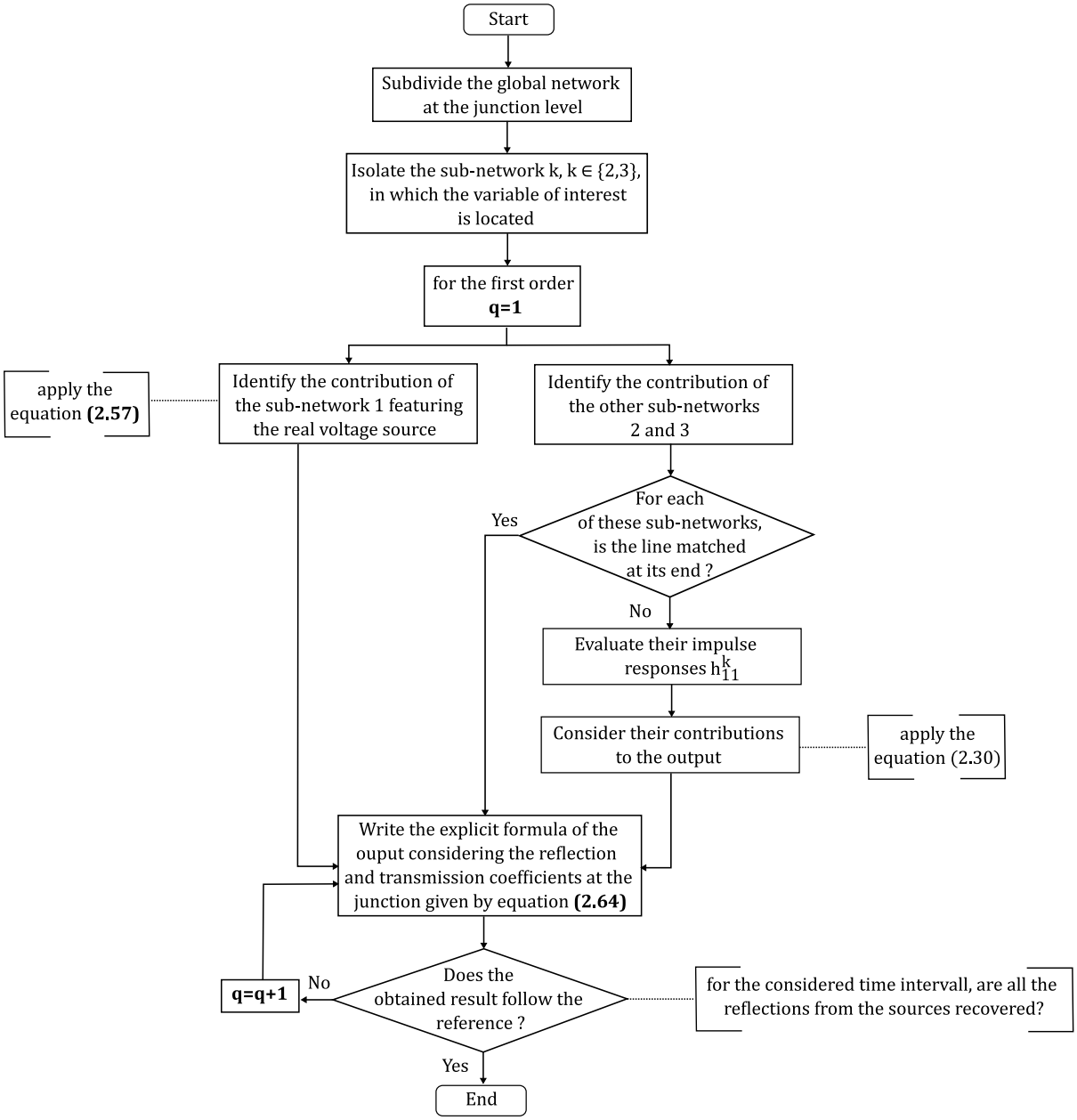

Figure 2.47: *Flow chart of the DD method's steps to evaluate the voltage V_k^k across the load resistance R_{Lk}^k for two different configurations when the subdivision occurs at the junction level for a Y-network only.*

exchanges at each time step required for the existing co-simulation methods, or numerical temporal hybridization methods,

2. The confidentiality of the models is preserved: the exchange of the impulse response at

the interface level is sufficient to retrieve the output through a specific linear combination, without revealing the sub-system's topology or characteristics.

Without loss of generality, the method is mainly illustrated for transmission line networks but its general formulation and easy-to-implement nature allow different linear applications. These main advantages enable further use of the DD technique for different applications whose focus is put in the next chapter. A new point-of-view of the DD method is presented in the second section for which the decomposition occurs at the interconnection. This new subdivision choice, aligning with the requirements of real-world applications, calls for adapting the general formula of the DD technique.

The core of both approaches remains unchanged, but their points of view differ. A comparative analysis of these methodologies is thus valuable to ascertain the suited applications for each.
In this comparison, both approaches have their own strengths and limitations. The DD method based on the decomposition of the network at the junction is more practical, making it suitable for real-world scenarios. However, any mismatches at the junction are considered in a later stage. Depending on the studied configuration, the output expression can be tricky to recover, especially with higher orders. In addition to exchanging impulse responses, reflection and transmission coefficients are also essential to the exchange. This additional information can therefore undermine one of the primary advantages of the DD method: preserving the confidentiality of the models.
The initial formulation of the DD method based on the subdivision at the line itself, on the other hand, is exempt from this constraint, as the junction's mismatches are implicitly taken into account within the evaluated impulse responses of the sub-networks.
For both standpoints of the DD methodology, no convergence criterion is defined upstream. In other words, the higher orders considered to obtain the reference are not known in advance. The latter is increased until the desired result is found, which is also only assumed to be given. In practice, no reference is available and convergence criteria should be defined.

Conclusion

In this chapter, the general principle of the proposed domain decomposition method is given for 1D linear electric systems. Its detailed formulation is given for transmission line network applications using the FDTD numerical tool. The approach is detailed when the global network is subdivided at one of its lines. The obtained results validate the technique as the higher orders (multiple round-trips of the physical voltage sources) are considered in the final

formulation. The general nature of the method allows a generalized expression of the output, for which different configurations can be studied. As part of our analysis, the complexity cost of the DD technique was established for a rounded analysis. Despite the method's ability to achieve the desired outcome (compared to the reference given by the global result), the application under consideration demonstrates the method's feasibility for academic cases. Its subdivision choice remains less realistic, given the choice of subdividing the system at the level of the line itself.

To overcome this limitation, we propose a different point-of-view of the proposed method, in which the subdivision takes place at a natural interconnection level, the junction in the case of a branched transmission lines network. This new choice of decomposition represents more realistic cases, especially in the industrial context. Although the subdivision principle has been modified, the essence of the decomposition method itself remains unchanged. Isolating the sub-network in which the observable is located first and then identifying the different contributions from the neighboring sub-networks are still the key steps to evaluate the output. With the new approach, the impact of the junction should be considered through the reflection and transmission coefficients in the final formulation. The new formulation of the DD technique is illustrated with different configurations of a Y-transmission lines network. The results obtained, considering the q-th order, are very satisfying. In conclusion, both viewpoints of the DD method produced very good results. For each, we discussed the advantages and limitations for an accurate portrayal of our proposed approach. In the remainder of this manuscript, for the sake of simplicity, we base our analysis on the DD method when the decomposition happens at the line itself.

CHAPTER 3

DD Method and Numerical Applications

Contents

WITH general formulation and simple mathematical foundations, the DD method is highly promising for more complex cases. To this end, we aim to demonstrate throughout this chapter, the robustness of the decomposition method proposed in the section (2.1.1) for new numerical study cases. In the first section, we consider that a global transmission line network is divided along two interfaces. The new formulation of the DD approach is explicitly given for this configuration. We then later utilize one of its major advantages, which is its asynchronous aspect, to model each sub-system with a different numerical tool. To begin with, the same method FDTD is used for each sub-system but implemented with different discretization time steps. The principle as well as the numerical results are presented in section 2. In section 3, two different numerical tools (numerical code based on the method FDTD and the commercial software CST Cable®) are considered for modeling each sub-system. Finally, the approach is generalized for a 3-one-point interface for a multiconductor transmission line network. The numerical application and the obtained result are presented in section 4.

3.1 Domain decomposition through two interfaces or more

The proposed DD method is based on the evaluation of the impulse responses of each sub-network asynchronously, from which their linear combination yields the desired result. The method is indeed general, but its final formulation depends on the network's topology, subdivision and observables. In this section, we aim at retrieving the observable when the global network is divided into 3 sub-networks. The core of the DD technique is unchanged, but its formulation must consider the contributions of the equivalent sources at both interfaces.

3.1.1 Problem statement

Let's consider the global transmission line network in Figure (3.1) consisting of 8 uniform and lossless transmission lines and three junctions. The system is excited by the voltage source V_{s1}, injected at the entrance of the line L_1. This excitation source is the Gaussian pulse expressed by equation (2.38) whose parameters are: $A = 1V$, $t_c = 12ns$ and $\sigma = 0,95ns$. The problem is modeled using the FDTD method, with careful attention to the choice of the time step to respect the CFL criterion ($dt = 0.3ns$).
We aim to retrieve the voltage V_5 across the load resistance R_{L5} when the global network is subdivided simultaneously at the middle of the lines L_2 and L_6, as shown in Figure (3.2a).
As a result, three sub-networks, whose properties (lengths L, characteristic impedances Z_c and load resistances R_L) are denoted with the exponent $k \in \{1,2,3\}$, are distinguished as shown in Figure (3.2b). The impedance continuity at both interfaces is ensured by adapting the ends of

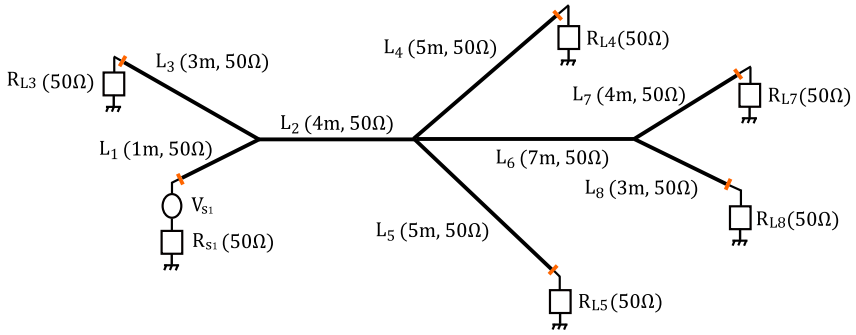

Figure 3.1: *Characteristic of the transmission line network.*

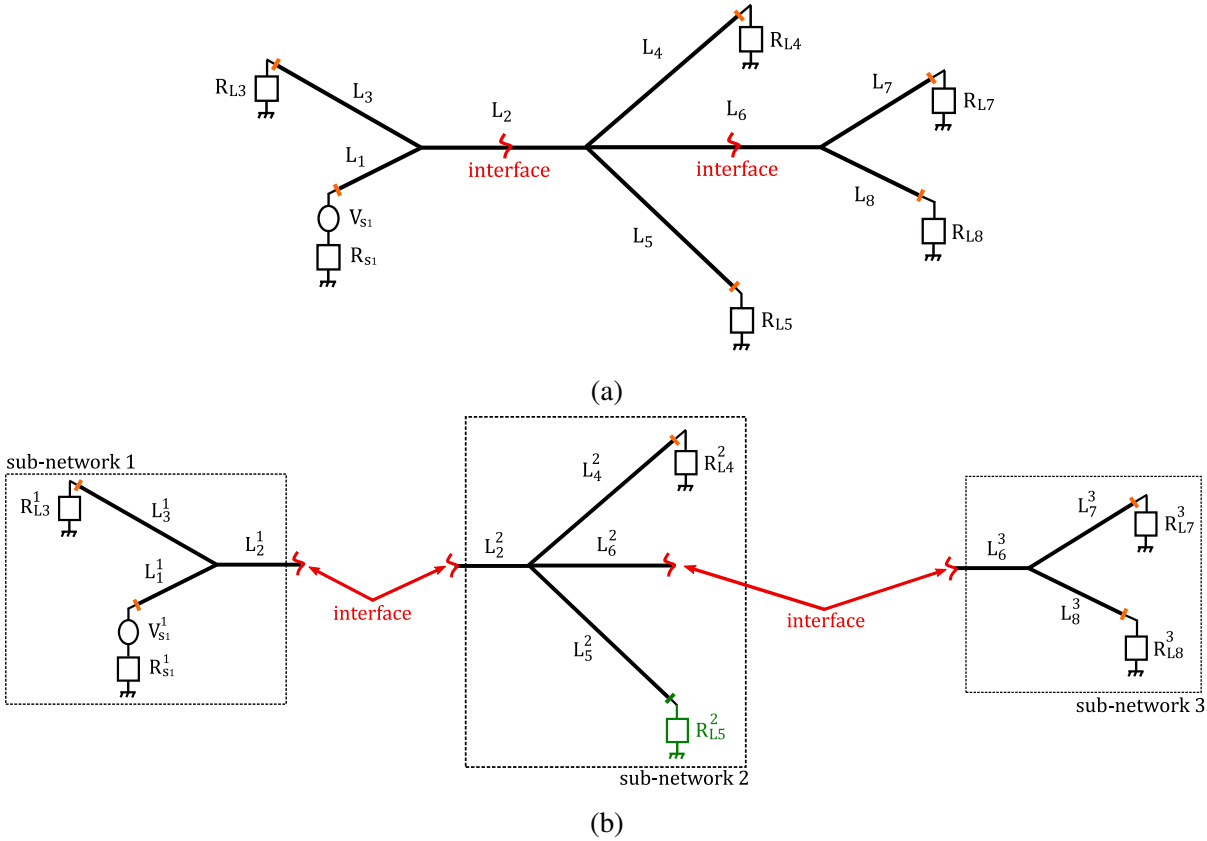

Figure 3.2: *Global transmission line network split at the middle of lines L_2 and L_5 (a), sub-networks 1, 2 and 3 after the subdivision of the global network (b).*

the lines L_2 and L_6, such as lines L_2^1 and L_2^2 (resp. lines L_6^2 and L_6^3) are loaded with resistances equal to the characteristic impedance Z_{c2} (resp. Z_{c6}) of the line L_2 (resp. L_6).

3.1.2 DD method application and results

To evaluate the voltage V_5^2 across the load resistance R_{L5}^2, the focus is put on the sub-network 2 ($k = 2$), where the observable is located.

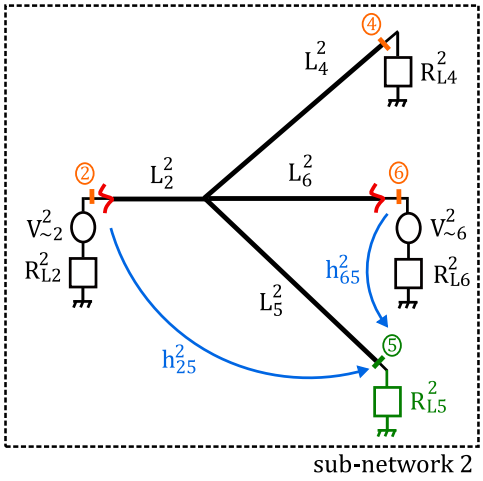

Figure 3.3: *Schematic representation of the equivalent voltage sources $V_{\sim 2}^2$ at the line L_2^2 and $V_{\sim 6}^2$ at the line L_6^2.*

Based on the general principle of the DD approach given by equation (2.5), the voltage V_5^2 reads

$$\begin{aligned} V_5^2 &= \sum_{\{l\}} h_{l5}^2 * V_{\sim l}^2 \\ &= h_{25}^2 * V_{\sim 2}^2 + h_{65}^2 * V_{\sim 6}^2 \end{aligned} \tag{3.1}$$

where $\{l\} \in \{2, 6\}$.

As no physical voltage source is injected into sub-network 2, only the contributions of the equivalent voltage sources at each interface given by $V_{\sim 2}^2$, respectively, $V_{\sim 6}^2$ are considered through the left-hand term, respectively the right-hand term of equation (3.1).

The next step is to retrieve these equivalent voltage sources $V_{\sim 2}^2$ and $V_{\sim 6}^2$. As explained in the section (2.1.1), these voltages are the incoming waves from the neighboring sub-networks to the exchange interfaces[1]. This configuration is a particular case of the 2^{nd} scenario in sec-

[1]In our study, these sources are explicitly given for academic studies. In practice, these quantities are supplied by sub-system integrators. Either a global external "master" or one of the involved partners collects and assembles the data.

tion (2.3.3), for which the sub-network of interest ($k = 2$) doesn't feature a physical source. The voltage $V^2_{\sim 2}$ is the incoming voltage wave from sub-network 1 to the first interface ($l = 2$) and is expressed as follows:

$$V^2_{\sim 2} = h^1_{12} * V^1_{s1} \tag{3.2}$$

Its product with the impulse response h^2_{25} translates the direct propagation of the physical voltage source V^1_{s1} within lines L^2_1, L^1_2, L^2_2 and L^2_5, while considering the effect of the mismatch at the junctions of both sub-networks 1 and 2.

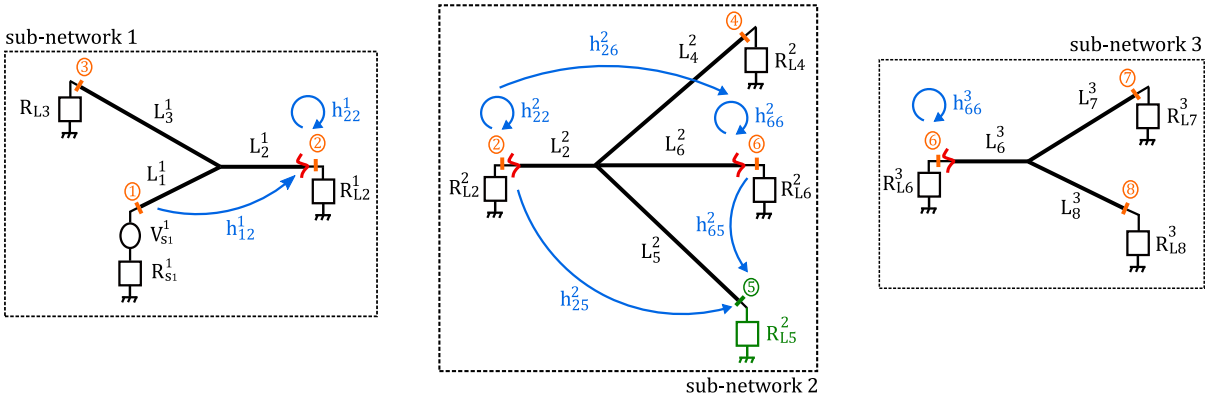

Figure 3.4: *Impulse responses $h^k_{..}$ characterizing each sub-network k, $k \in \{1,2,3\}$.*

On the other hand, the second equivalent source $V^2_{\sim 6}$ is obtained by considering the contribution from the sub-network 3 and the "secondary " propagation of the voltage source V^1_{s1} within the sub-network 2[2]. The final expression of the incoming voltage wave to the second interface is given by

$$V^2_{\sim 6} = h^3_{66} * (h^2_{26} * V^2_{\sim 2}) \tag{3.3}$$

The impulse response h^3_{66} characterizes the sub-network 3 as the latter has no physical voltage source.

Equation (3.1) can only recover the direct propagation of the Gaussian source in the network. New additional terms are evaluated in equation (3.4) to recover the multiple round-trips of the voltage source V^1_{s1}.

[2]In this configuration, second-order effects may appear before first-order. This depends on the reflections in the network, the decomposition and the observable.

$$V_5^2 = h_{25}^2 * V_{\sim 2}^2 + h_{65}^2 * V_{\sim 6}^2 + h_{25}^2 * \underbrace{\left(h_{22}^1 * h_{22}^2 * V_{\sim 2}^2\right)}_{V_{\sim 2,1}^1} + h_{65}^2 * \underbrace{\left(h_{66}^3 * h_{66}^2 * V_{\sim 6}^2\right)}_{V_{\sim 6,1}^2} + \underbrace{\sum_{i=2}^{q_1} h_{25}^2 * \left(h_{22}^1 * h_{22}^2 * V_{\sim 2,i}^2\right)}_{A} + \underbrace{\sum_{j=2}^{q_2} h_{65}^2 * \left(h_{66}^3 * h_{66}^2 * V_{\sim 6,j}^2\right)}_{B} \tag{3.4}$$

with $V_{\sim 2,i}^2$, respectively $V_{\sim 6,j}^2$ are defined as the i-th, respectively the j-th order of the equivalent source at the first interface level ($l = 2$), respectively the second interface level ($l = 6$) of the sub-network 2. Their respective expressions are given by

$$V_{\sim 2,i}^2 = h_{22}^1 * (h_{22}^2 * V_{\sim 2,i-1}^2) \tag{3.5}$$

$$V_{\sim 6,j}^2 = h_{66}^3 * (h_{66}^2 * V_{\sim 6,j-1}^2) \tag{3.6}$$

The equivalent voltage $V_{\sim 2}^2$ at the first interface at the line L_2^2 is re-injected within sub-networks 1 and 2. Their contributions to the output are thus considered through their inner impulse responses h_{22}^1 and h_{22}^2. The multiple reflections are retrieved to the order q_1 by evaluating the term A in equation (3.4). Similarly, the voltage $V_{\sim 6}^2$ at the second interface at the line L_6^2 is re-injected within sub-networks 2 and 3, characterized each by their inner impulse responses h_{66}^2 and h_{66}^3. The additional term B in equation (3.4) allows retrieving the multiple round-trips of the equivalent source $V_{\sim 6}^2$ to the q_2-th order.

By computing equation (3.4) to the orders $q_1 = 6$ and $q_2 = 2$, the DD method retrieves the direct propagation of the source V_{s1}^1 within lines sub-networks 1 and 2 (translated by the first gaussian peak), as well as some of its reflections (due to the mismatch at the junctions) within the three sub-networks, as reported in Figure (3.5).

This difference in results is due to the incompleteness of equation (3.4). In fact, the latter considers the retro-actions between sub-networks 1 and 2 (through the term A), and the retro-actions between sub-networks 2 and 3 (through the term B). The retro-actions between sub-networks 1 and 3 however are missing[3]. The complete formulation considering all the retro-actions between the three sub-networks is expressed by

[3]In this configuration, the retro-actions between sub-networks 1 and 3 are necessary, it may not be the case in other applications depending of the studied network (lengths, loads and characteristic impedances of the lines), the observable and the considered time interval. Due to the attenuation of the signal, these retro-actions may be negligible and thus not necessary.

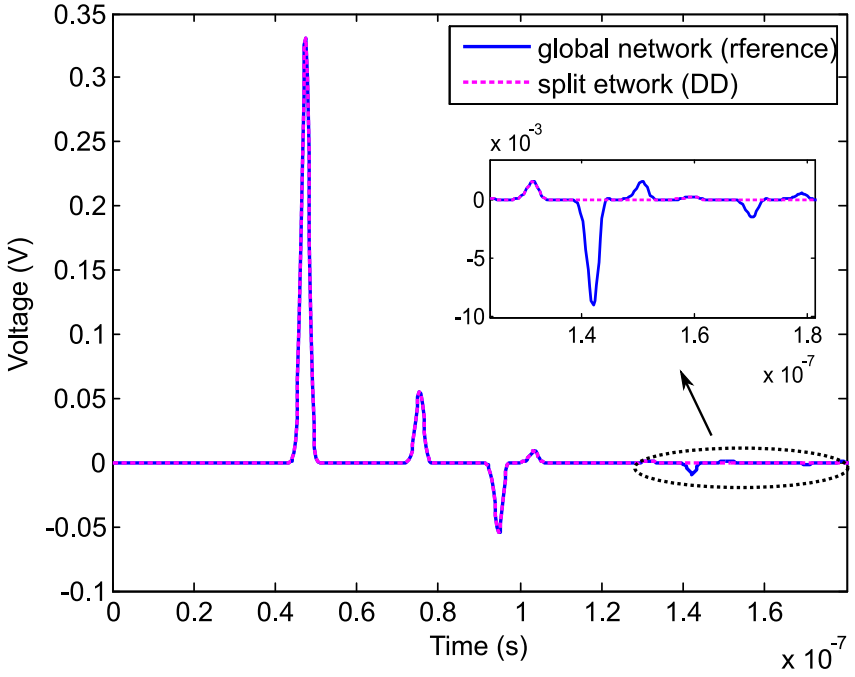

Figure 3.5: *Comparison of the voltage V_5 across the resistance R_{L5} evaluated for the global network (reference) and the split network (DD method).*

$$
\begin{aligned}
V_5^2 = {} & h_{25}^2 * V_{\sim 2}^2 + h_{65}^2 * V_{\sim 6}^2 + h_{25}^2 * V_{\sim 2,1}^2 + h_{65}^2 * V_{\sim 6,1}^2 \\
& + \sum_{i=2}^{q} h_{25}^2 * \left(h_{22}^1 * h_{22}^2 * V_{\sim 2,i}^2 \right) + \sum_{j=2}^{q} h_{25}^2 * \left(h_{66}^3 * h_{66}^2 * V_{\sim 6,j}^2 \right) \\
& + \sum_{k=2}^{q_3} h_{65}^2 * \left(h_{22}^1 * h_{22}^2 * h_{66}^3 * h_{66}^2 * V_{\sim 2,k}^2 \right)
\end{aligned}
\tag{3.7}
$$

with $V_{\sim 2,k}^2$ is defined as the k-th order of the equivalent source $V_{\sim 6}^2$, and expressed by

$$
V_{\sim 2,k}^2 = h_{22}^1 * (h_{22}^2 * V_{\sim 6,k-1}^2) \tag{3.8}
$$

By re-evaluating the voltage V_5^2 for $q_1 = 6$, $q_2 = 2$ and $q_3 = 1$, the DD method yields the excepted result as reported in Figure (3.6).

In synthesis, the principle of the DD method remains unchanged, however, the complexity of the formulation increases with the number of interfaces considered. We again emphasize that the required order for good accuracy is relative to the network's topology, the decomposition itself and the time interval for signal recording. It is also important to mention that there is

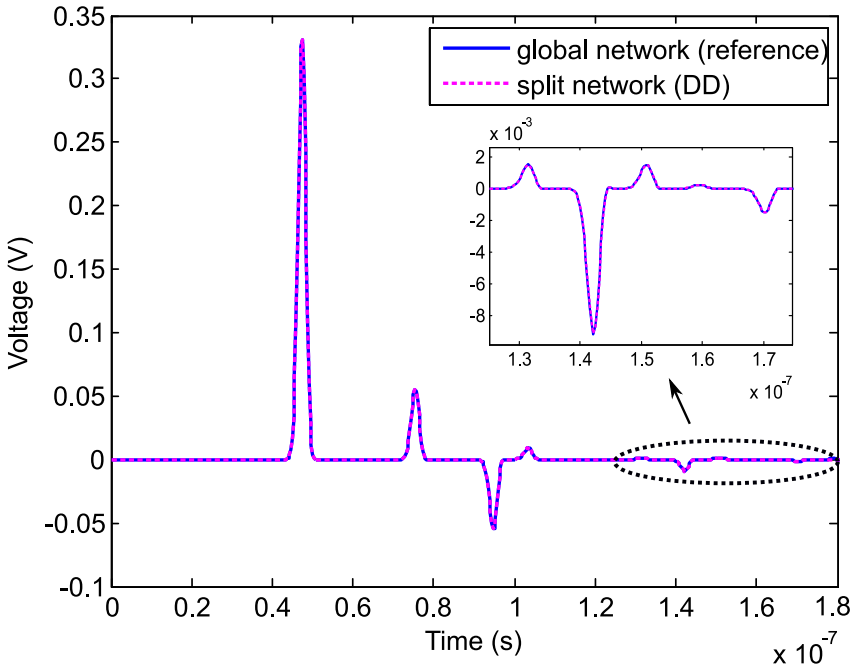

Figure 3.6: *Comparison of the voltage V_5 across the resistance R_{L5} evaluated for the global network (reference) and the split network (DD method applied for the orders $q_1 = 6$, $q_2 = 2$ and $q_3 = 1$).*

no order to follow when evaluating the final output. In other words, some reflections of the signal may appear earlier than the complete direct propagation of the injected signal (for the considered time interval). In this configuration, the higher orders should be considered from the early stages of the computation of the output. The final formula can be automatized to take into account the different decompositions and topologies of the system under study.

3.2 Decomposition domain application for different time steps

For all the previously studied examples, and without loss of generality, the same numerical method was used to model each sub-network. The latter is only a "tool" for evaluating impulse responses and is not related to the decomposition method itself. In this section, we propose a new application for which different discretization time steps will be considered for each sub-network.

3.2.1 Problem statement

We propose to study the following transmission line network represented in Figure (3.7), of 5 transmission lines supposed uniform and lossless.

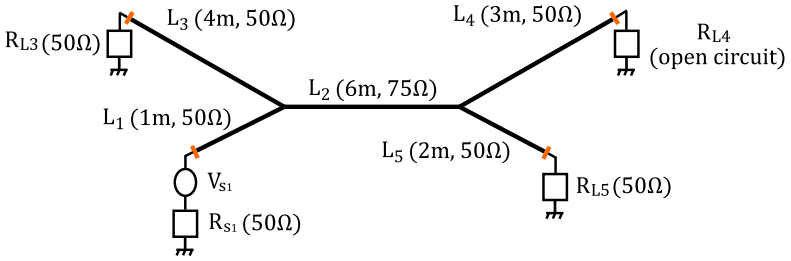

Figure 3.7: *Characteristic of the transmission line network.*

The voltage source V_{s1}^1, injected at the entrance of the network at the line L_1, is a Gaussian pulse given by equation (2.38) of parameters $1V$, $t_c = 15ns$ and $\sigma = 1,3ns$.
We suppose that the global network is subdivided at the middle of the line L_2 into two sub-network Y^k, $k \in \{1,2\}$. To maintain the physical condition at the interface, both lines L_2^k are loaded with a resistance R_{L2}^k equal to the characteristic impedance Z_{c2} of the line L_2.

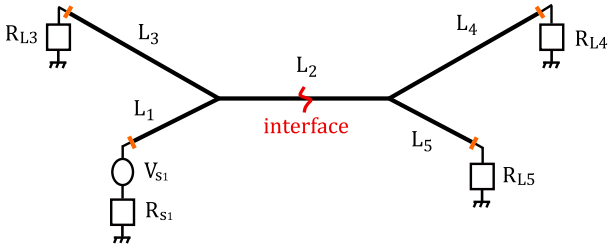

(a)

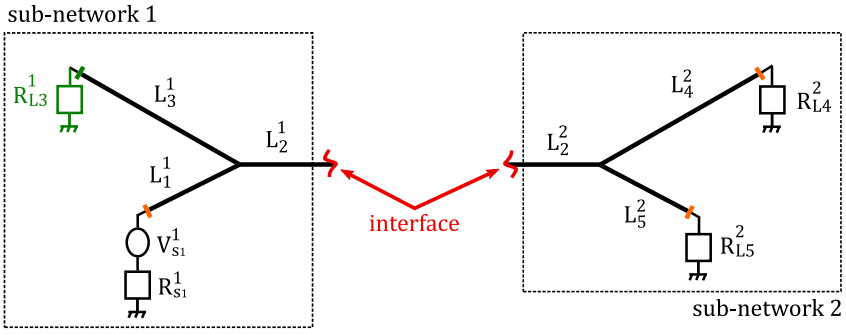

(b)

Figure 3.8: *Global transmission line network split at the middle of the line L_2 (a), sub-networks 1 and 2 after the subdivision of the global network (b).*

3.2.2 DD method application and results

Following the principle of the DD method given in the algorithm (1), the focus is put on the sub-network Y^1 where the variable of interest, i.e. the voltage V_3^1 across the load resistance R_{L3}^1, is located.

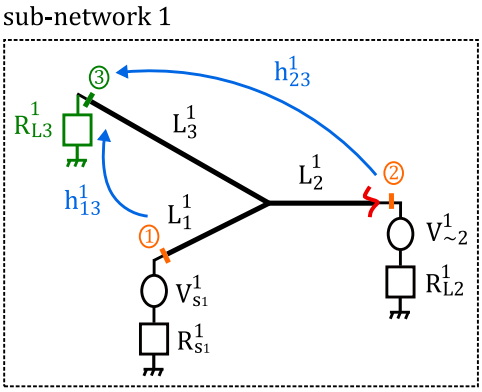

Figure 3.9: *Schematic representation of the contribution of the physical voltage source V_{s1}^1 and the equivalent source at the interface level $V_{\sim 2}^1$ to the output through the corresponding impulse responses.*

Based on equation (2.5), the voltage V_3^1 reads as follows:

$$\begin{aligned} V_3^1 &= h_{13}^1 * V_{s1}^1 + h_{23}^1 * V_{\sim 2}^1 \\ &= h_{13}^1 * V_{s1}^1 + h_{23}^1 * \left(h_{22}^2 * (h_{12}^1 * V_{s1}^1)\right) \end{aligned} \tag{3.9}$$

We identify the contribution of the voltage source V_{s1}^1 to the output given by the left-hand term. The right-hand term, on the other hand, gives the contribution of the equivalent source $V_{\sim 2}^1$ at the interface. The latter is obtained by considering the propagation of the voltage source V_{s1}^1 to the interface level, expressed by the product $(h_{12} * V_{s1}^1)$, first, then its multiplication with the inner impulse response h_{22}^2 of the sub-network Y^2.
The final formula of the voltage V_3^1 is retrieved by considering both the retro-action of the sub-network Y^1 on sub-network Y^2 and the multiple round-trips of the source V_{s1}^1 within the network. The re-injection of the equivalent source $V_{\sim 2}^1$ within the sub-network Y^1 first, and the sub-network Y^2 second, allows recovering the reflections of the signal V_{s1}^1 due to the mismatch at both junctions and the open-circuit at the end of the line L_4^2.

$$V_3^1 = h_{13}^1 * V_{s1}^1 + h_{23}^1 * \underbrace{\left(h_{22}^2 * (h_{12}^1 * V_{s1}^1)\right)}_{V_{\sim 2,1}^1} + \sum_{i=2}^{q} h_{23}^1 * \left(h_{22}^2 * (h_{22}^1 * V_{\sim 2,i}^1)\right) \tag{3.10}$$

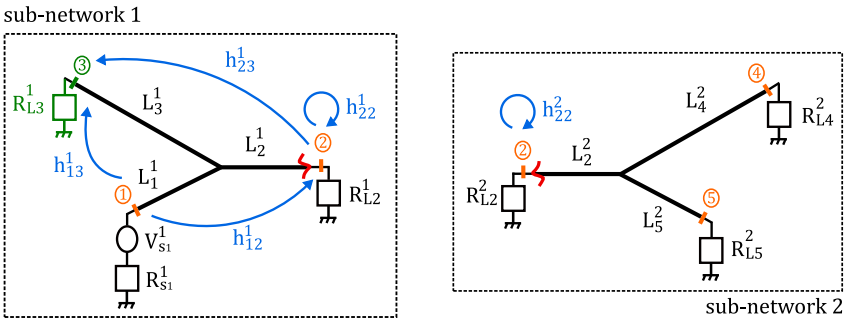

Figure 3.10: *Impulse responses $h^k_{\cdot\cdot}$ characterizing each sub-network k, $k \in \{1,2\}$.*

with $V^1_{\sim 2,i-1}$ is defined as the i-th order of the equivalent source at the interface level and is given by

$$V^1_{\sim 2,i} = h^2_{22} * (h^1_{22} * V^1_{\sim 2,i-1}) \tag{3.11}$$

As we've mentioned earlier, each sub-network will be modeled based on a discretization time step for the FDTD numerical method. In other words, the impulse responses $h^k_{\cdot\cdot}$, $k \in \{1,2\}$ of the sub-network k will be evaluated considering a time step dt_i, $i \in \{1,2\}$. Both these temporal discretization steps are defined in compliance with the FDTD method's stability criterion, such as:

$$dt_1 = 0,90 \times \frac{dx}{v} \tag{3.12}$$

$$dt_2 = 0,99 \times \frac{dx}{v} \tag{3.13}$$

with $dx(0,1m)$, respectively v, are the spatial discretization step, respectively the speed of propagation, assuming to be equal to the speed of light $c_0 = 3 \times 10^8 m.s^{-1}$ in this case.
The output will be then obtained after a post-processing interpolation of the responses of one sub-network with respect to the time step of the other.
Nevertheless, as the result obtained with the DD method is verified using the global simulation (as a reference), the choice of temporal discretization step is an issue that emerges. In practice, the decomposition method is relevant when the global result is not available, either because it is difficult or impossible to access, or for confidentiality reasons of the models. In the context of this thesis, we consider that the global result is given for both time steps, as reported in Figure (3.11). While both results follow the same pattern, the difference in their time step discretization reveals subtle variations, more precisely a time shift.
Initially, we consider that both sub-networks are evaluated with the same temporal discretization step dt_1, then dt_2 for validation purposes. The results obtained by applying equation (3.10)

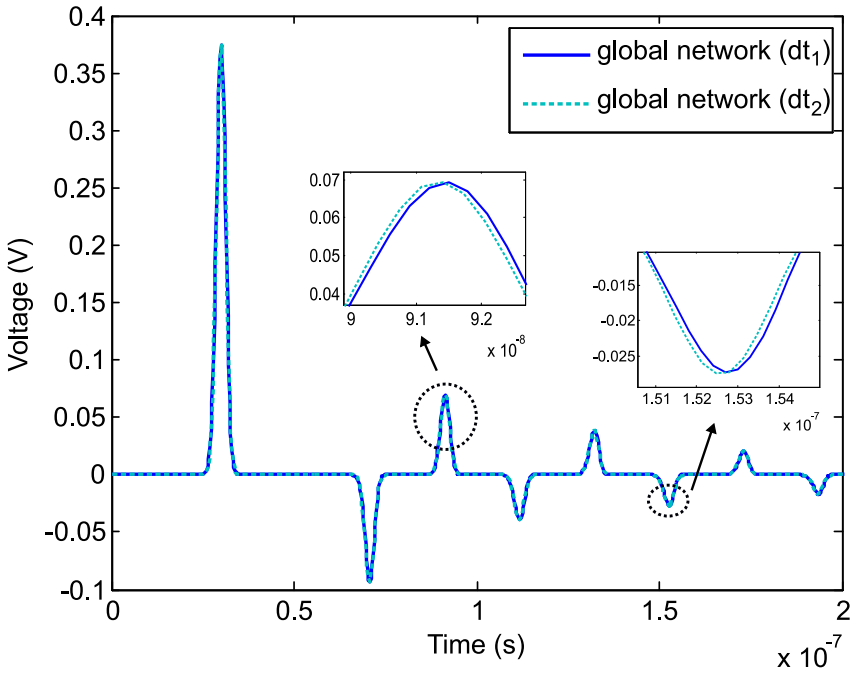

Figure 3.11: *Voltage V_3 across the resistance R_{L3} evaluated for the global network for both temporal discretization steps.*

for $q = 3$, reported in Figure (3.12), validates the DD method as they retrieve the expected result.

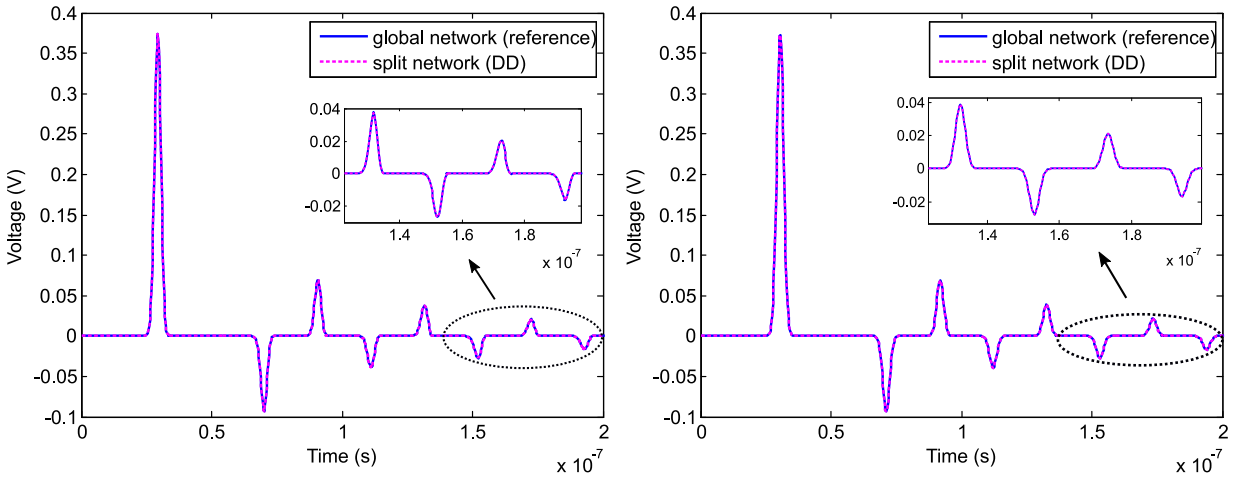

(a) (b)

Figure 3.12: *Comparison of the voltage V_3 across the resistance R_{L3} for the global network (reference) and the split network (using the DD method with the temporal discretization step dt_1 (a), with the temporal discretization step dt_2 (b)).*

In the following, we suppose that the impulse responses of the sub-network Y^1 are evaluated considering the temporal discretization step dt_1. Whereas, the sub-network Y^2 is modeled with the temporal discretization step dt_2.

In the post-processing stage, we interpolate the impulse responses of the sub-network Y^1 on the basis of the time for which the impulse responses of sub-network Y^2 are evaluated. In other words, the interpolation of the signals (impulse responses $h^2_{..}$) with the larger time step (dt_2) to match the time instances of the signals (impulse responses $h^1_{..}$) with the smaller time step (dt_1) is required to ensure that the resulting combined output is synchronized.

By evaluating equation (3.10) for the order $q = 3$, and based on a linear interpolation method, the obtained result with the DD approach is compared to the references, evaluated for both steps dt_1 and dt_2, as shown in Figure (3.13).

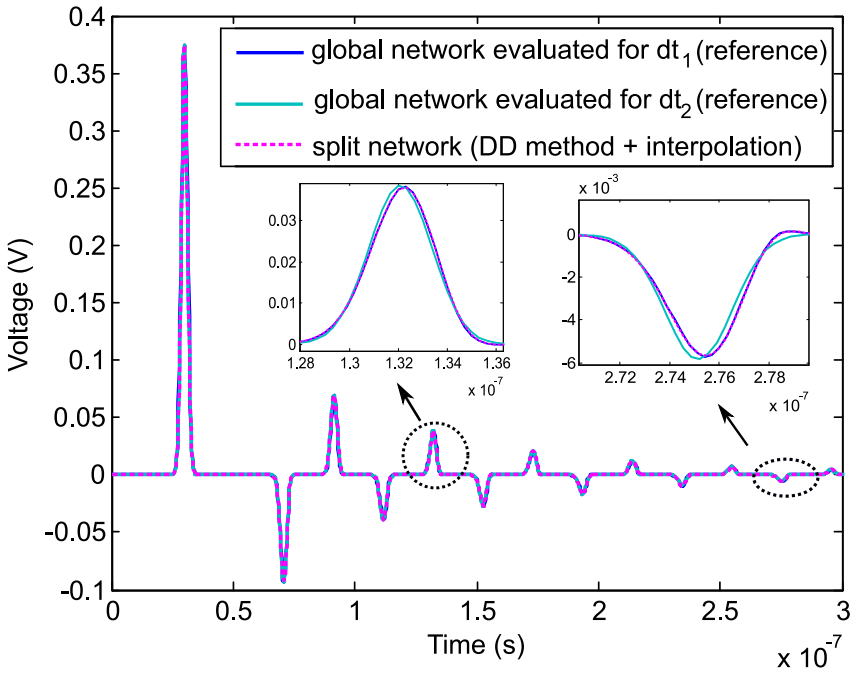

Figure 3.13: *Comparison of the voltage V_3 across the resistance R_{L3} evaluated for the global network for both temporal discretization steps and the split network (using the DD method with interpolation of the impulse responses of each sub-network).*

The obtained result resembles the expected outcome. However, we observe slight differences between the reference and the DD method result. First, achieving a precise comparison comparable to the reference is challenging, since we have two references slightly different. In addition, the interpolation introduces a certain degree of approximation, and may thus introduce errors. These small differences do not undermine the use of different solvers.

3.3 Domain decomposition application to different numerical softwares

As demonstrated earlier, the DD method provides very good results with different temporal discretization steps of the FDTD method for each sub-network. These results are promising and introduce new possibilities for the use of two different numerical tools. This specific aspect of the DD technique will be a major advantage, especially in the industrial context where the deployed tools are not necessarily the same.

3.3.1 Problem statement

In this section, we study a new transmission line network whose topology and characteristics are represented in Figure (3.14). The excitation source V_{s1}, injected at the entrance of the network at the line L_1, is the same Gaussian pulse used in the previous application. We are interested in the voltage V_6 across the load resistance R_{L6} when the global network is split at the middle of the line L_2, as shown in Figure (3.15a).

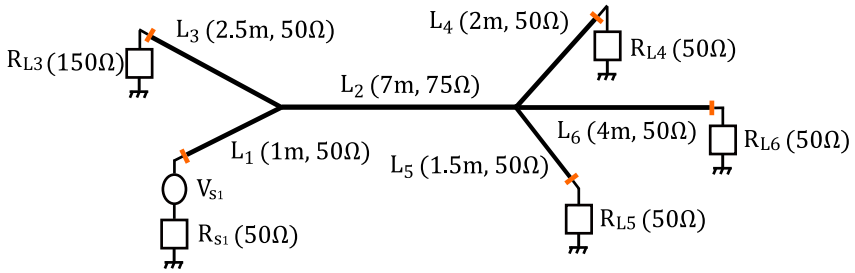

Figure 3.14: *Characteristic of the transmission line network.*

The line L_2^1 referring to the sub-network 1, (resp. L_2^2 referring to the sub-network 2) is loaded with a resistance R_{L2}^1 (resp. R_{L2}^2) equal to the characteristic impedance Z_{c2} of the line L_2 to ensure the impedance continuity at the subdivision level.

3.3.2 DD method application and results

The voltage V_6 is now denoted V_6^2 as a reference to the sub-network 2 ($k = 2$). In this case, only the contribution of the incoming wave voltage from the sub-network 1 to the interface level given by the product $(h_{12}^1 * V_{s1}^1)$, is considered since no physical voltage source is featured in the sub-network 2. The explicit voltage V_6^2 is evaluated on the basis of equation (2.5) and reads

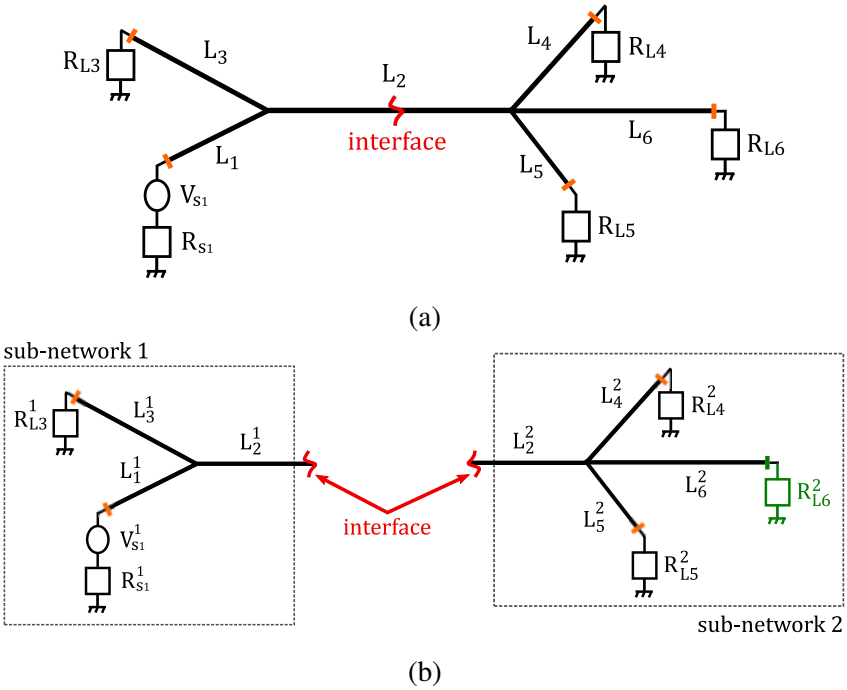

Figure 3.15: *Global transmission line network split at the middle of the line L_2, sub-networks 1 and 2 after the subdivision of the global network (b).*

$$\begin{aligned} V_6^2 &= h_{26}^2 * V_{\sim 2}^2 \\ &= h_{26}^2 * (h_{12}^1 * V_{s1}^1) \end{aligned} \tag{3.14}$$

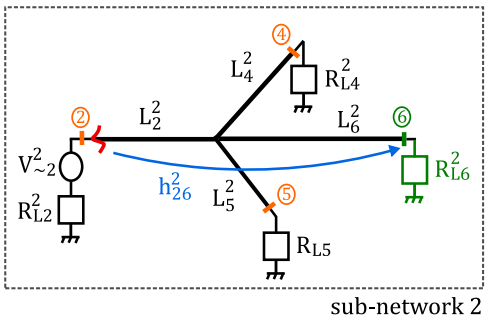

Figure 3.16: *Schematic representation of the contribution of the equivalent source at the interface level $V_{\sim 2}^2$ to the output through the corresponding impulse response.*

The higher q-th orders of the multiple reflections of the source V_{s1}^1 within the network are retrieved by re-injecting the equivalent source $V_{\sim 2}^2$ at the sub-network 1 (through its impulse

response h^1_{22}) and then the sub-network 2 (through its impulse response h^2_{22}).

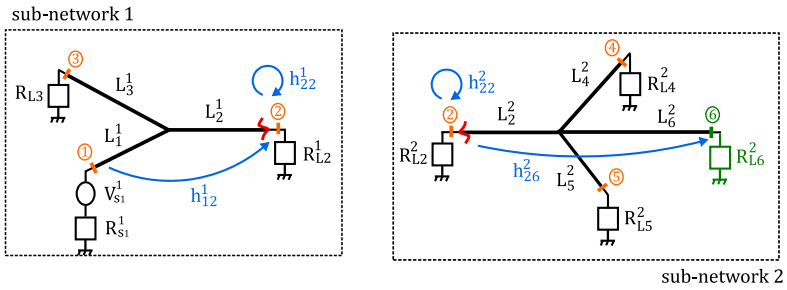

Figure 3.17: Impulse responses $h^k_{..}$ characterizing each sub-network k, $k \in \{1,2\}$.

The following expression yields the direct propagation of the voltage V^1_{s1} as well as its multiple reflections (due to the mismatch at the junctions and the load R^1_{L3} at the end of the line L^1_3):

$$V^2_6 = h^2_{26} * (h^1_{12} * V^1_{s1}) + h^2_{26} * \Big(\underbrace{h^2_{22} * (h^1_{22} * (h^1_{12} * V^1_{s1}))}_{V^2_{\sim 2,1}} \Big) + \sum_{i=2}^{q} h^2_{26} * \big(h^2_{22} * (h^1_{22} * V^2_{\sim 2,i}) \big) \quad (3.15)$$

with $V^2_{\sim 2,i}$ is defined as the i-th order of the equivalent source at the interface level and is given by

$$V^2_{\sim 2,i} = h^2_{22} * (h^1_{22} * V^2_{\sim 2,i-1}) \quad (3.16)$$

In the following, the DD method will be evaluated using two numerical tools: the finite-difference method (FDTD code) and the commercial software CST Cable®.

CST Cable Studio®

CST Cable Studio® is an electromagnetic simulation tool designed for real-world cables in complex electromagnetic problems. The software combines transmission lines theory, electric/electronic circuits and 3D full-wave simulations for fast and accurate analysis.
The software offers the possibility to model a variety of types of cables (single wires, twisted cables, ribbon cables and coaxial cables with different shieldings) stored in a pre-defined library. More complex cable harnesses can also be built with the help of the 3D components.
CST Cable Studio® generates equivalent circuits from the cable harness based on classical transmission line theory. It automatically meshes the cable harness along its length and calculates the transmission line parameters on these segments.

The schematic model enables the circuit simulation of the whole system in time and frequency domains while maintaining a tight interface with the 3D transient solvers to easily exchange impressed currents and voltages.
The software enables two types of transmission line modeling: lumped and modal. The lumped modeling approach approximates a transmission line by a series of discrete (or lumped) R, L, C and G devices. Each RLCG combination models a short section of the transmission line. The valid frequency range for the whole model is therefore limited by the length of this unit because the length of the section must be considerably smaller than the shortest wavelength of the propagating signal. The modal approach on the other hand describes a transmission line by its secondary characteristics (wave impedance Z and propagation delay v). Throughout this manuscript, the software is used with the lumped modeling approach.
For this application, we will consider the ideal model of transmission lines pre-defined in the schematic tab of the software. This choice is to approach in the best way the numerical code (FDTD) which is also given for RLCG uniform and lossless transmission lines.
The modeling of the network of Figure (3.14) using the CST Cable® ideal transmission line model is represented in Figure (3.18).

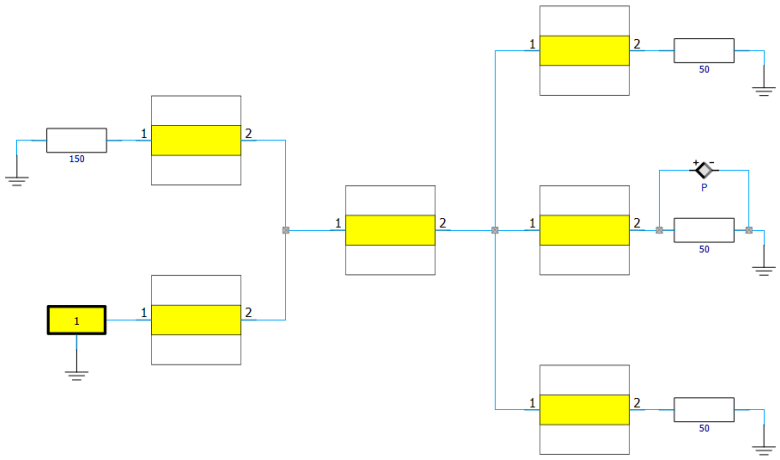

Figure 3.18: *Schematic modeling of the global transmission line network using the CST Cable® software.*

The left-hand block (1) represents an external port serving to define the simulation type (Transient, AC, S-parameters...). In our case, we consider a transient analysis for time-domain simulation, its parameters are:

- simulation time duration = $0.3\mu s$,

- total frequency = $300MHz$.

We first compare the result of the global network using both numerical tools: the FDTD method and the software CST Cable®.
From the results represented in Figure (3.19), we can notice very similar patterns for the two methods. Peak magnitudes are very close as they only depend on the characteristic impedances of the lines and load resistances. The temporal shift on the other hand is due to the different time steps considered in the two modeling methods. In fact, the time step in the FDTD method is defined according to the stability criterion and therefore depends on the spatial discretization step.

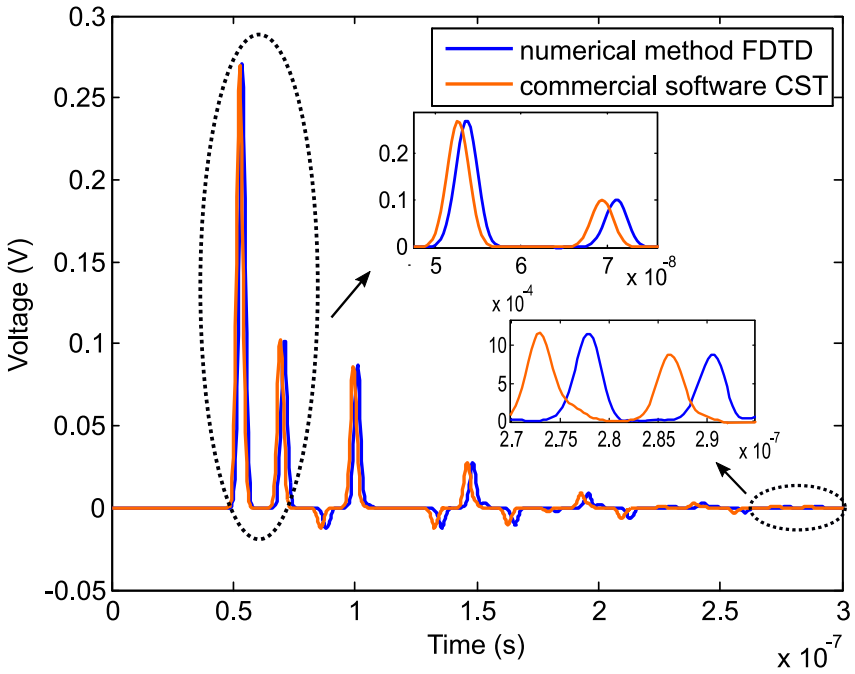

Figure 3.19: *Comparison of the voltage V_6 across the resistance R_{L6} evaluated for the global network using two different numerical tools: the FDTD method and the software CST Cable®.*

Initially, the DD method will be evaluated using the CST Cable® software, i.e both sub-networks are modeled with the software. The goal is to demonstrate the robustness of the method and its applicability with commercial software. We model the sub-networks 1 and 2 with respect to the decomposition at the middle of the line L_2 as represented in Figure (3.20). After evaluating the required impulse responses $h^k_{\cdot\cdot}$ for each sub-network k, $k \in \{1,2\}$ (schematized in Figure 3.17), the voltage V_6^2 in equation (3.15) is assessed. Based on the obtained result for $q = 5$, reported in Figure (3.21), the DD method yields the expected output.

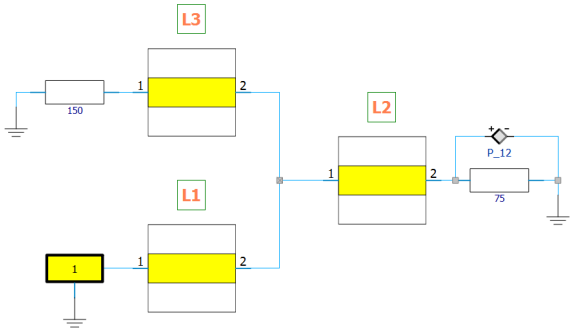

(a)

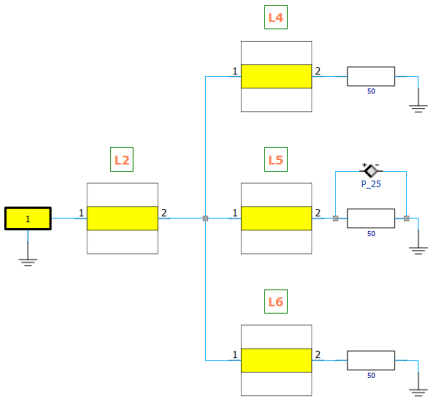

(b)

Figure 3.20: *Schematic modeling of the sub-network 1 (a) and the sub-network 2 (b) using the CST Cable ® software after splitting the global network at the middle of the line L_2.*

The DD method is, therefore, valid and can be applied with other commercial tools[4].
In the following, each sub-network will be modeled by a different numerical tool. An after-processing based on data interpolation is required to retrieve the output. Let's consider that sub-network 1 is modeled with the commercial software CST Cable®, whereas sub-network 2 is evaluated using the numerical finite difference method. In this case, the temporal discretization step used in CST Cable® denoted dt_1, is greater than dt_2, the temporal discretization step employed for the FDTD simulation.
After interpolating the impulse responses $h^2_{..}$ of sub-network 2 on the time basis t_1 employed in the modeling of the sub-network 1, the voltage V^2_6 is evaluated. The obtained result is reported

[4]Commercial software often do not share their numerical models.

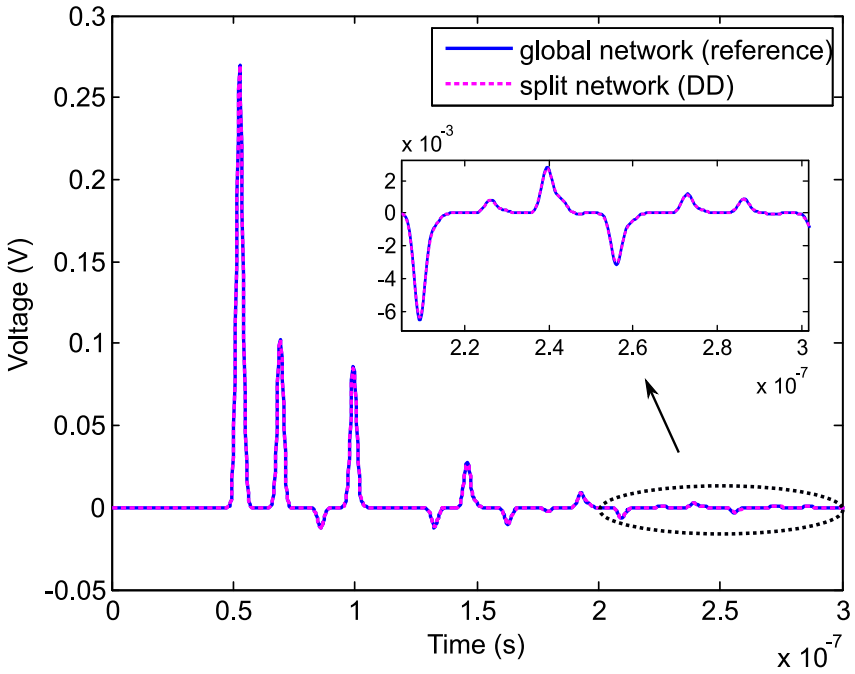

Figure 3.21: *Comparison of the voltage V_6 across the resistance R_{L6} evaluated for the global network (reference) and the split network (DD method) using the commercial software CST Cable®.*

in Figure (3.22).

The DD method yields satisfactory results; however, once again, the comparison lacks precision, since we have two references.

3.4 Domain decomposition application to a multiconductor transmission line network

With the validation of the DD method using the commercial software CST Cable®, we utilize its modeling of real cables to study multiconductor transmission lines. In this case, the DD technique is applied for m one-point interfaces, with m the number of conductors in one multiconductor bundle. In this section, we implement the DD technique for 3 one-point interfaces ($m = 3$ conductors). The new output formulation and the obtained results will be presented.

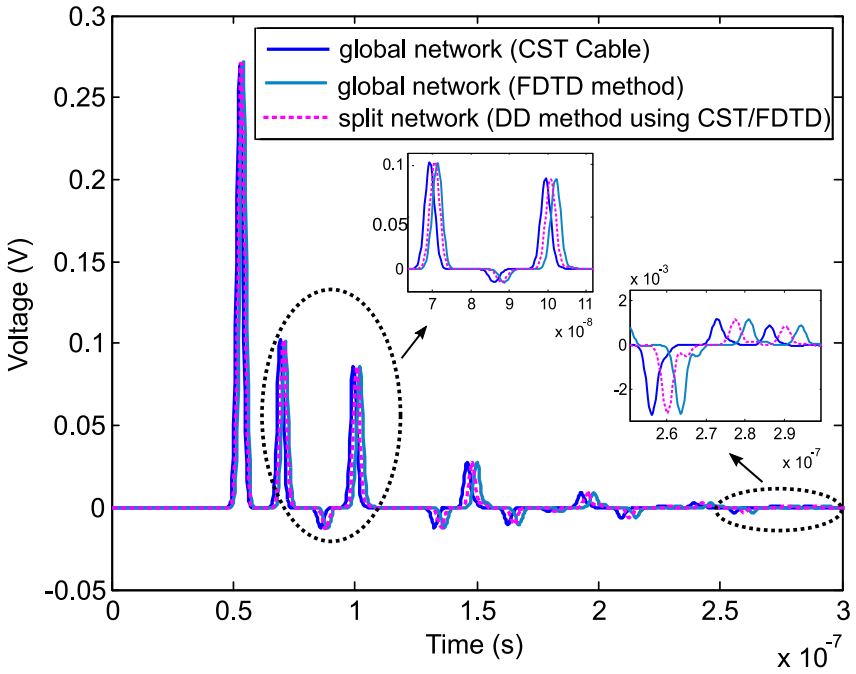

Figure 3.22: *Comparison of the voltage V_6 across the resistance R_{L6} evaluated for the global network (reference) and the split network (DD method application for two different numerical tools).*

3.4.1 Problem statement

Let's consider the transmission line network in Figure (3.23) consisting of 5 multiconductors (MTL) and 2 junctions.

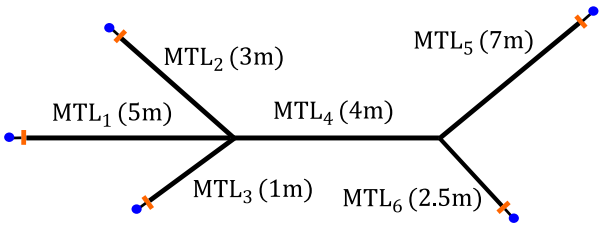

Figure 3.23: *Characteristic of the transmission line network.*

Each MTL consists of three single-wire cables imported directly from the CST Cable® library: 'LIFY_0qmm5', 'LIF_0qmm8' and 'LIFY_0qmm10', corresponding respectively to the lines L_1, L_2 and L_3, whose lengths are supposed equal.
For improved identification, we give the following notation to facilitate comprehension for readers:

- the MTL is denoted with a n indice: MTL_n with $n \in \{1,2,3,4,5,6\}$,
- the lines constituting the MTL_n, are denoted $L_{n,m}$ with $m \in \{1,2,3\}$,
- the load resistance of a line $L_{t,m}$ is denoted $R_{Lt,m}$, with $t = n \setminus \{4\}$.

In Figure (3.24a), we present a close-up view of each MTL[5]. At the MTL_1 level, we suppose that an excitation voltage source $V_{s1,1}$ is injected at the entrance of the line $L_{1,1}$. The other two conductors, i.e lines $L_{1,2}$ and $L_{1,3}$ are loaded with the resistance $R_{L1,2}$, respectively $R_{L1,3}$.
The load resistance values are summarized in Table (3.1).

		$t=1$	$t=2$	$t=3$	$t=5$	$t=6$
MTL_t	L_1	$R_{s1,1}=37\Omega$	$R_{L2,1}=35\Omega$	$R_{L3,1}=37\Omega$	$R_{L5,1}=35\Omega$	$R_{L6,1}=35\Omega$
	L_2	$R_{L1,2}=35\Omega$	$R_{L2,2}=42\Omega$	$R_{L3,2}=37\Omega$	$R_{L5,2}=35\Omega$	$R_{L6,2}=35\Omega$
	L_3	$R_{L1,3}=42\Omega$	$R_{L2,3}=35\Omega$	$R_{L3,3}=37\Omega$	$R_{L5,3}=35\Omega$	$R_{L6,3}=35\Omega$

Table 3.1: *Values of the load resistances $R_{Lt,m}$ for each line L_m for the MTL_t.*

Based on the cross-section of one MTL of the network, represented in Figure (3.24b), we identify the three conductors, the isolator (in blue) and the screen (in green) to ensure the ground connection.
For this configuration, we propose to split the global network at the middle of the MTL_4 into 2 sub-networks as represented in Figure (3.25a). To ensure this impedance continuity at the subdivision level, each line $L^k_{4,m}$ of the sub-network $k \in \{1,2\}$ is loaded with a resistance equal to the characteristic impedance of the corresponding line of the initial MTL_4, such as $R^k_{L4,m} = Z_{c4,m}$.

3.4.2 DD method application and results

We aim to evaluate the voltage $V^2_{5,1}$ measured across the load resistance $R^2_{L5,1}$ of conductor 1 of the MTL^2_5. In this case, the interface is represented by 3 one-point interfaces. Consequently, the voltage $V^2_{5,1}$ is retrieved on the basis of the general formulation of the DD method, given by equation (2.5), updated for three interfaces.

$$\begin{aligned} V^2_{5,1} &= \sum_{m=1}^{3} h^2_{45,m} * V^2_{\sim 4,m} \\ &= h^2_{45,1} * V^2_{\sim 4,1} + h^2_{45,2} * V^2_{\sim 4,2} + h^2_{45,3} * V^2_{\sim 4,3} \end{aligned} \tag{3.17}$$

[5]In the schematic representation in Figure (3.24a), the exponent p refers to the MTL 2 or 3, whereas the exponent q refers to the MTL 5 or 6.

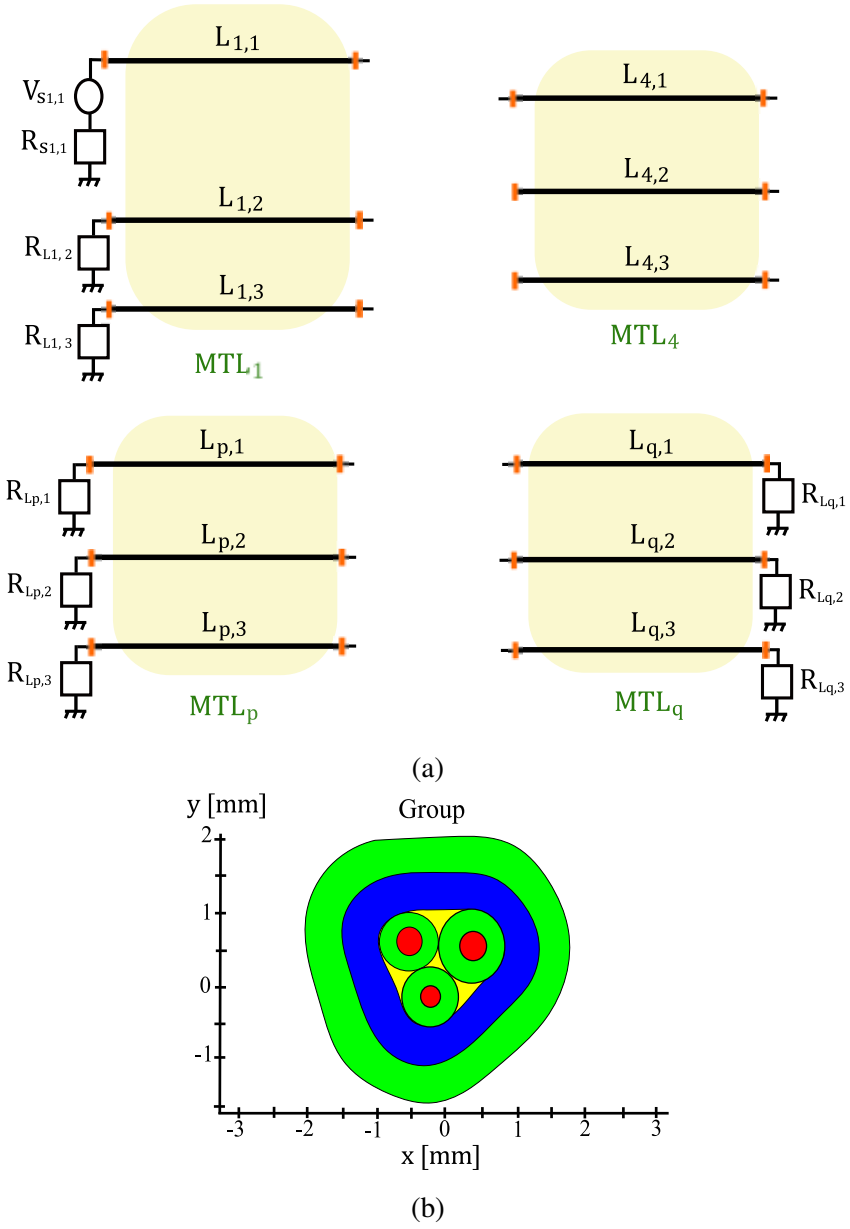

Figure 3.24: *Conductors $L_{n,t}$ and their load resistance for each MTL_t (a), the cross-section of the cable group used for the multiconductor lines of the studied network (b).*

At each one-point interface, at the line $m \in \{1,2,3\}$ of the MTL_4^2, appears an equivalent source $V^2_{\sim 4,m}$. Each one of these sources represents the incoming voltage wave from the sub-network 1 to each interface of the line $L^1_{4,m}$. Their explicit expression is given by

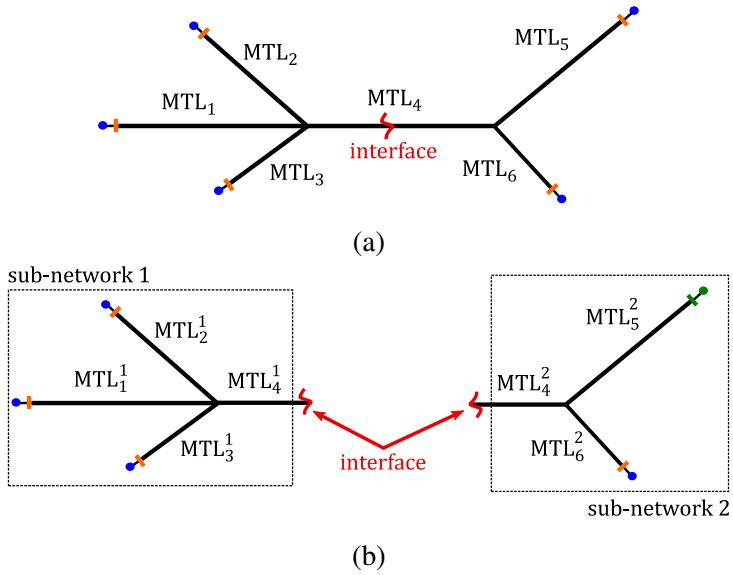

Figure 3.25: *Global multiconductor network split at the middle of the line MTL_4, sub-networks 1 and 2 after the subdivision of the global network (b).*

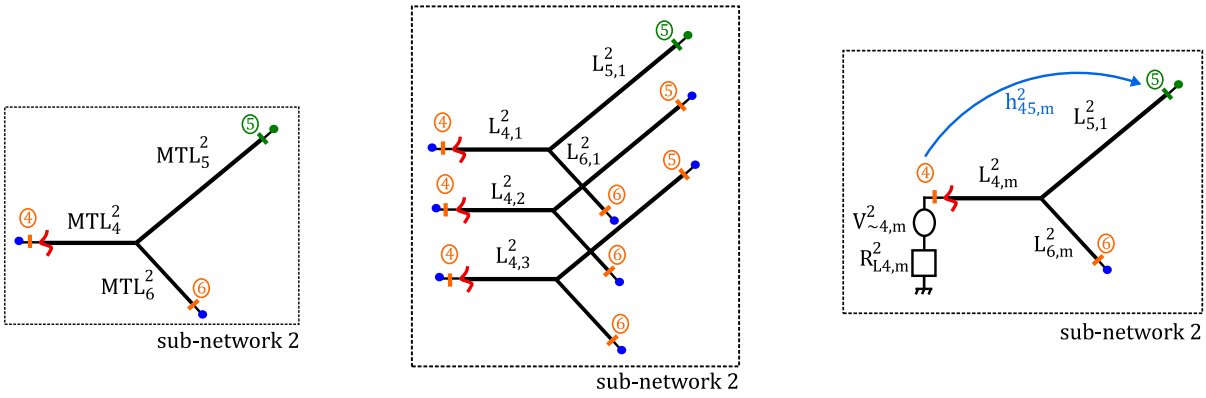

Figure 3.26: *Schematic representation of the contribution of the equivalent sources $V^2_{\sim 4,m}$ at the m interface to the output through the corresponding impulse response.*

$$V^2_{\sim 4,1} = h^1_{14,1} * V^1_{s1,1} \tag{3.18}$$
$$V^2_{\sim 4,2} = h^1_{14,2} * V^1_{s1,1} \tag{3.19}$$
$$V^2_{\sim 4,3} = h^1_{14,3} * V^1_{s1,1} \tag{3.20}$$

with $h^1_{14,m}$ is the impulse response measured between the termination $i = 1$ (source) and $l = 4$ (interface) for each line $L^2_{4,m}$.
Equation (3.17) gives the contribution of each equivalent source $V^2_{\sim 4,m}$ to the output, through

the impulse response $h^2_{45,m}$.

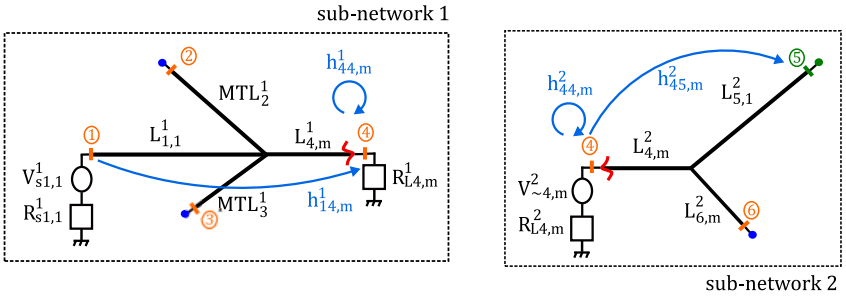

Figure 3.27: *Impulse responses $h^k_{ij,m}$ for each sub-network Y^k, $k \in \{1,2\}$.*

However, the formulation is incomplete as multiple reflections of the voltage $V^1_{s1,\,1}$ within the network aren't considered yet. At each interface m, the equivalent source $V^2_{\sim 4,m}$ is re-injected at the sub-network Y^1 first and the sub-network Y^2 second through the corresponding impulse responses $h^1_{44,m}$ and $h^2_{44,m}$. The first order of reflection of these equivalent sources, denoted $V^2_{\sim 4,m,1}$, is expressed as follows:

$$\begin{aligned} V^2_{\sim 4,m,1} &= h^1_{44,m} * (h^2_{44,m} * V^2_{\sim 4,m}) \\ &= h^1_{44,m} * \left(h^2_{44,m} * (h^1_{14,m} * V^1_{s1,1})\right) \end{aligned} \tag{3.21}$$

Their contributions to the output ($j = 5$, $m = 1$ and $k = 2$) are given by the product of convolution of each of these sources with the corresponding impulse response $h^2_{45,m}$.
The final formulation allowing to retrieve the multiple round-trips of the source to the orders q_1, q_2 and q_3 is expressed as follows:

$$V^2_{5,\,1} = \sum_{m=1}^{3} \left(h^2_{45,m} * V^2_{\sim 4,m} + h^2_{45,m} * V^2_{\sim 4,m,1} + \sum_{i_m=2}^{q_m} h^2_{45,m} * \left(h^1_{44,m} * (h^2_{44,m} * V^2_{\sim 4,m,i_m})\right) \right) \tag{3.22}$$

with $V^2_{\sim 4,m,i_m}$ is defined as the i-th order of the equivalent sources at the interface m of the line $L^2_{4,m}$. Their respective expressions are given by

$$V^2_{\sim 4,m,i_m} = h^1_{44,m} * (h^2_{44,m} * V^2_{\sim 4,m,i_m-1}) \tag{3.23}$$

By evaluating equation (3.22) for the orders $i_1 = 5$, $i_2 = 1$ and $i_3 = 1$, the obtained result is reported in Figure (3.28).
The first Gaussian pulse represents the direct propagation of the source $V^1_{s1,\,1}$ within the first conductors (L_1) of the multiconductors 1,2 and 5. Starting from the instant $t = 1.45e-7s$,

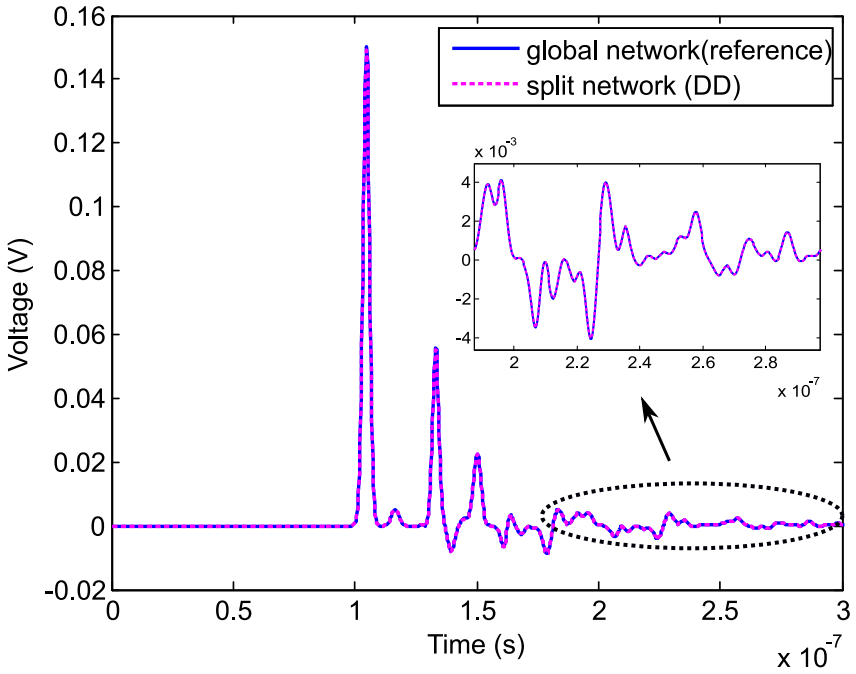

Figure 3.28: *Comparison of the voltage $V_{5,\,1}$ across the resistance $R_{L5,1}$ evaluated for the global network (reference) and the split network (DD method application for two different numerical tools).*

the crosstalk effect appears due to the closeness of the conductors. In fact, the terms in equation (3.22) referring to conductor 1 (line L_1) for the corresponding MTL translate the direct transmission of the source to the output, meanwhile the terms referring to the other two conductors (lines L_2 and L_3) give the crosstalk effect. Although the different interactions between the interfaces themselves are not considered in the formulation, the DD result approaches very well the reference. Their effect is small and may be negligible, however in different configurations depending on the topology of the network, types of cables, number of conductors in the MTL, the decomposition itself and the observable, their effect may be required to retrieve the expected output.

Conclusion

In this chapter, the proposed DD method was applied to a diverse range of cases to ascertain its effectiveness and versatility. The obtained results underscored the method's robustness and its potential to address a wide spectrum of real-world EMC applications. In the first section, the DD technique was applied for two exchange interfaces. Although the formulation

of the output is more challenging and requires the evaluation of more impulse responses, the method demonstrated its applicability for more than one exchange interface. In the second and third sections, the aim was to utilize the asynchronous nature of the method allowing independent simulations for the use of different numerical tools for the characterization of the sub-systems. In addition to showcasing its applicability with commercial software, the DD approach provided meaningful results and promises a wide array of potential future applications. In the last section, another dimension of the method is analyzed, for which the exchange interface is represented by multiple one-point interfaces. The new formulation of the DD method achieved the intended objectives and affirms its efficacy for more complex applications.

For different configurations, the method remains effective. Its underlying theoretical principle allows easy implementation for different study cases. The obtained results emphasize the practical utility it offers for future work.

CHAPTER 4

Experimental Validation of the DD Method

Contents

THE proposed DD method stands out through its asynchronous intrinsic feature allowing independent modeling of each sub-system. This independence is both temporal, as no iterative exchange in time is involved, and spatial since the system is physically split up. Different configurations of the applicability of the DD method can be envisaged, but its transposition into practical experiments may seem of the biggest interest. In real-world applications, experimental realizations may be difficult to achieve given the available resources on one hand, and the multitude of involved partners for either component(s) or part(s) of the system under study on the other. The confidentiality of the models in this case is a real issue of the different parties, referred to as *equipment manufacturer* (component level) and *assembler* (system level) in the industrial field. The proposed decomposition method appears to be a suitable solution as it meets the requirements: preserving the confidentiality of the models.

From the previous chapters, we concluded on the general aspect of the DD approach for different numerical configurations. Its core remains unchanged for experimental configurations too, however, it is not ready for practical applications yet due to physical limitations. The aim of this chapter is to put the DD method into practice after upgrading its principle to satisfy the encountered physical limitations. In the first section, a proposed method for extracting impulse responses experimentally is presented. The transposition of the DD technique onto practical application is later detailed. Different configurations of wiring networks, using the experimental DD technique are studied to demonstrate its efficiency in the second section.

4.1 Experimental DD method

Within the scope of this thesis and in line with its objectives, the experimental realization is intended to validate the DD method when the impulse responses are measured experimentally. The combination of the latter through the general equation (2.61) is post-processed later numerically. We therefore refer to the experimental realization as the characterization of the sub-systems through their impulse responses. However, we can also consider the whole process (characterization of impulse responses and their association) in a totally experimental setting. This approach will be discussed further in this chapter.

4.1.1 Experimental impulse response extraction

The DD method is mainly based on the evaluation of impulse responses of each subsystem. In practice, their extraction is challenging given the difficulty of injection of a Dirac pulse. To overcome this physical limitation, we propose an alternative method aimed at

recovering the impulse response from any temporal signal and its response. The approach was initially developed within the EMC team of Institute Pascal as part of the thesis of Ali al Ibrahim [128].

By definition, the excitation of a linear system by the Dirac impulse $\delta(t)$ gives its impulse response $h(t)$.

$$\begin{cases} V_{in} = \delta(t) \rightarrow V_{out} = h(t) \\ V_{in} = \alpha(t) \rightarrow V_{out} = R(\alpha(t)) \end{cases} \tag{4.1}$$

where V_{in} is the excitation source.
The response V_{out} of this linear system to any time signal $\alpha(t) \neq 0$, denoted $R(\alpha(t))$, can also be retrieved from the product of convolution of the impulse response h with the signal $\alpha(t)$, expressed by

$$R(\alpha(t)) = h(t) * \alpha(t) \tag{4.2}$$

or

$$\begin{pmatrix} R(0) \\ R(1) \\ \vdots \\ \vdots \\ R(m) \end{pmatrix} = \begin{pmatrix} h(0) & 0 & \dots & \dots & 0 \\ h(1) & h(0) & \ddots & & \vdots \\ \vdots & h(1) & \ddots & \ddots & \vdots \\ \vdots & \vdots & \ddots & \ddots & \vdots \\ h(m) & h(m-1) & \dots & h(1) & h(0) \end{pmatrix} \begin{pmatrix} \alpha(0) \\ \alpha(1) \\ \vdots \\ \vdots \\ \alpha(m) \end{pmatrix}. \tag{4.3}$$

based on the matrix form of the impulse response.
From this expression, the linear system is deduced

$$\begin{cases} R(\alpha(0)) &= h(0)\alpha(0) \\ R(\alpha(1)) &= h(0)\alpha(1) + h(1)\alpha(0) \\ \quad \dots & \\ R(\alpha(m)) &= h(0)\alpha(m) + \dots + h(m)\alpha(0). \end{cases} \tag{4.4}$$

This system is re-arranged differently where a new matrix P, constructed uniquely from the signal $\alpha(t)$, is revealed.

$$\underbrace{\begin{pmatrix} R(0) \\ R(1) \\ \vdots \\ \vdots \\ R(m) \end{pmatrix}}_{R(\alpha)} = \underbrace{\begin{pmatrix} \alpha(0) & 0 & \dots & \dots & 0 \\ \alpha(1) & \alpha(0) & \ddots & & \vdots \\ \vdots & \alpha(1) & \ddots & \ddots & \vdots \\ \vdots & \vdots & \ddots & \ddots & \vdots \\ \alpha(m) & \alpha(m-1) & \dots & \alpha(1) & \alpha(0) \end{pmatrix}}_{P} \underbrace{\begin{pmatrix} h(0) \\ h(1) \\ \vdots \\ \vdots \\ h(m) \end{pmatrix}}_{h} \tag{4.5}$$

We define $\mathscr{B} = \{e_0, ..., e_m\}$ as the canonical basis of the vector space $\mathbb{R}^{m+1}$. By supposing that $\mathscr{C} = \{\alpha(0), ..., \alpha(m)\}$ also forms a basis for $\mathbb{R}^{m+1}$, the matrix P is then inversible and is called the transition matrix of $\mathscr{C}$ à $\mathscr{B}$.
The impulse response h is the solution of the linear system (4.5)

$$h = P^{-1}\, R(\alpha) \tag{4.6}$$

However, depending on the signal $\alpha(t)$, the matrix P may be non-square, so its inverse matrix P^{-1} may be not be assessable. To overcome this problem, the two terms of equation (4.5) are multiplied by $P^{\top}$, the transpose of P

$$P^{\top}\, R(\alpha) = P^{\top}\, P\, h \tag{4.7}$$

However, the poor conditioning in general of the $P^{\top}P$ matrix makes its inversion numerically unstable. Tikhonov's regularization technique [129] is then used. The system becomes

$$P^{\top}\, R(\alpha) = (P^{\top}\, P + \varepsilon\ \mathrm{I_d})h \tag{4.8}$$

where $\mathrm{I_d}$ is the identity matrix. The Tikhonov parameter $\varepsilon > 0$ is chosen small enough not to distort the solution, e.g. $\varepsilon = 1e-8$.

Finally, the impulse response h is given by

$$h = (P^{\top}\, P + \varepsilon\ \mathrm{I_d})^{-1} P^{\top}\, R(\alpha) \tag{4.9}$$

This new alternative method for impulse response extracting will be practically illustrated through a cable network later in this chapter.

4.1.2 Transposition of the DD method experimentally

The DD method is once again interesting when the global result is difficult if not impossible to retrieve. This constraint is more accentuated for the experimental measurements, due to the required resources they involve (equipment, time and operators). Similarly to the numerical validation of the DD method in Chapters 2 and 3, the global result will be assumed known for validation purposes of the proposed method.

The essence of the DD method remains unchanged, the exact same steps in algorithm (1) are followed. In other words, after locating the sub-system featuring the variable of interest V_j^k, the contributions of both real and equivalent sources within this sub-system should be

assessed. The transposition of the DD method experimentally therefore consists of extracting the impulse responses in equation (2.61), using the alternative method proposed in section (4.1.1) first, and combining these partial experimental solutions in a post-processing step through the convolution product in equation (2.61).

The evaluation of the impulse responses h_{ij}^k in equation (2.61), starts by measuring the response of the system k at the termination j to the excitation source, that is the signal α, injected at the termination i. This measured response R_{ij}^k is thus associated with the matrix P build using the signal α to retrieve the impulse response h_{ij}^k, following equation (4.9). Similarly, the impulse response h_{lj}^k is extracted based on the measured response R_{lj}^k of the system when the source α is injected at the interface level l, and the matrix P. We will further demonstrate that different signals α can be used to extract the impulse responses.
In summary, the following algorithm details the key steps for experimental realization of the DD method:

Algorithm 2 Key steps to apply the experimental DD method

1: Subdivide the global linear system G into m non-overlapping sub-systems.
2: Focus on the sub-system k in which the variable of interest V_j^k is located.
3: **Measure** the response R_{ij}^k and R_{lj}^k of the sub-system k to the signal α (non-null signal and experimentally achievable).
4: Extract the impulse responses $h_{\{i\}j}^k$ and $h_{\sim\{l\}}^k$ in equation (2.61) based on the alternative method proposed in section (4.1.1).
5: **Compute** the output V_j^k through the convolution products of the **measured** impulse responses with the corresponding sources using equation (2.61).

4.2 Experimental DD method in wiring networks

As part of our experimental validation, the DD experimental technique is put into practice for transmission line networks. The topology of the studied network and the type of cables (length, characteristic impedances and loads) is irrelevant to the approach. Its general feature enables its independence from the type of studied network while ensuring the one and only hypothesis that is linearity.

4.2.1 Experimental setup

The experimental DD method's set-up requires an Arbitrary Wave Generator (AWG), a

scope and the wire network consisting of different types of cables (including coaxial cables RG58, RG59) connected using BNC-T connectors to create the junctions.

The *AWG70002A Tektronix* generator allows the generation of arbitrary signals with an amplitude of 250mVp-p. To ensure that generation starts after the first trigger, the "trigged and continuous" mode on the AWG is selected. The trigger signal used is reported in Figure (4.1).

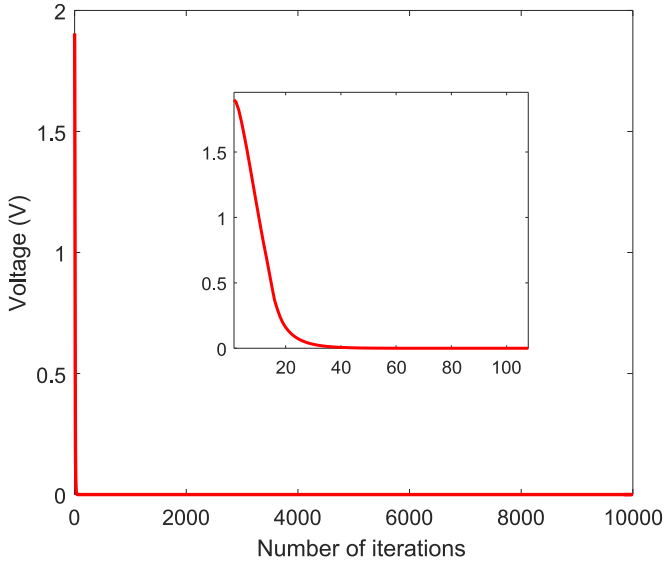

Figure 4.1: *Trigger signal used with the AWG.*

The measurements are acquired using the scopes *LeCroy 640Zi* and/or *Tektronix MSO46 4-BW-35*[1]. while ensuring synchronization with the generation (one channel is used for triggering, and another one for the acquisition of the measurement). To avoid sampling problems, the measuring sampling frequency must be greater than or equal to the sampling frequency of the waveform generated by the AWG. This sample rate (SR) refers to the rate at which the scope samples the input signal. It is typically measured in samples per second (S/s). A higher sample rate allows the oscilloscope to capture and display fast-changing signals with more detail.

4.2.2 Extraction of the impulse responses experimentally

The idea behind the experimental DD method is to evaluate by measurement the partial solutions (impulse responses) required to yield the global solution. Therefore, we first start by putting into practice the alternative method proposed in section (4.1.1) to extract the impulse

[1]Thanks to the ANR *ECOCES* funding in acquiring this equipment.

response of a system when the latter is excited by a non-null signal $\alpha(t)$. We propose to study the Y-transmission line network in Figure (4.2), consisting of three RG-58 coaxial cables of different lengths. The injection takes place at the entrance of the network at line L_1 (blue point) using the AWG, while the response $R(\alpha(t))$ is recorded at the end of line L_2 (green point) using the scope *Tektronix MSO46 4-BW-35*.

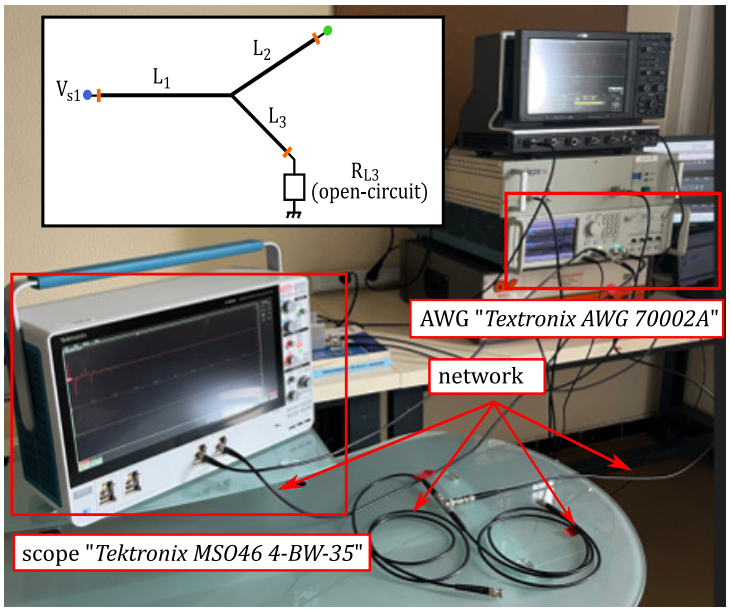

Figure 4.2: *Experimental bench of the studied line network for the extraction of the impulse response.*

Let's consider that the excitation source $\alpha(t)$ is the sine-wave signal in Figure (4.3a). The network's response to this system is reported in Figure (4.3b). Based on these two signals, α and $R(\alpha)$, the impulse response h_{12} measured between the injection ($i = 1$) and recording ($j = 2$) points, is retrieved based on equation (4.9). By definition, the impulse response of a linear system links whatever input signal to its output. The response of the studied network to the Gaussian pulse in Figure (4.4a), is given by the product of convolution of the impulse response h_{12} with this source, following equation (2.1), such as

$$R_G = V_2 = h_{12} * G(t) \tag{4.10}$$

The perfect agreement of the response R_G and the response V_2 retrieved based on the impulse response, reported in Figure (4.4b), demonstrated that the latter is evaluated correctly. The proposed alternative method is therefore capable of constructing the impulse response from any signal and its response, based on a change of base. The convolution product, however, is

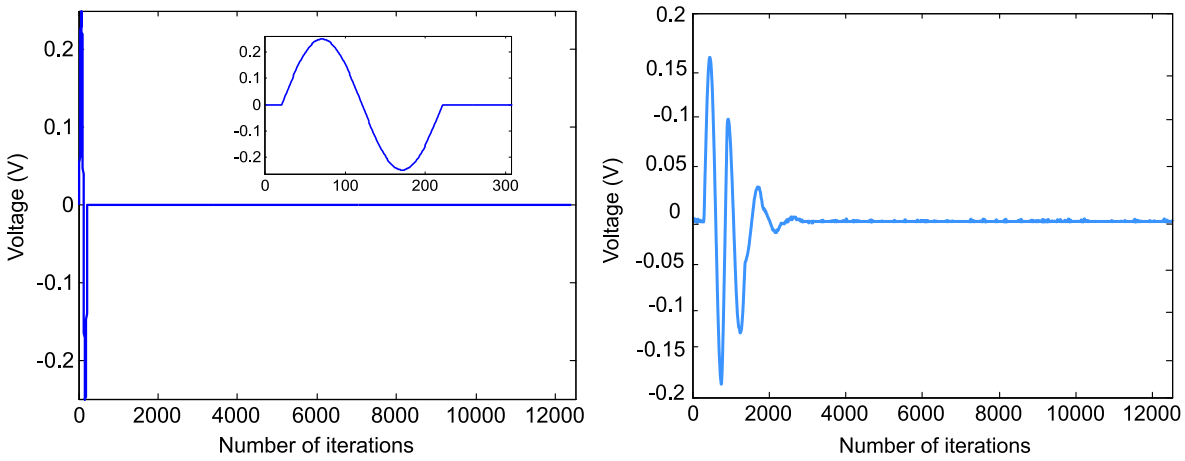

Figure 4.3: *Excitation source (sin-wave signal) (a) and its response (b).*

verified using a signal with a narrower bandwidth than that of the signal used to construct the impulse response.

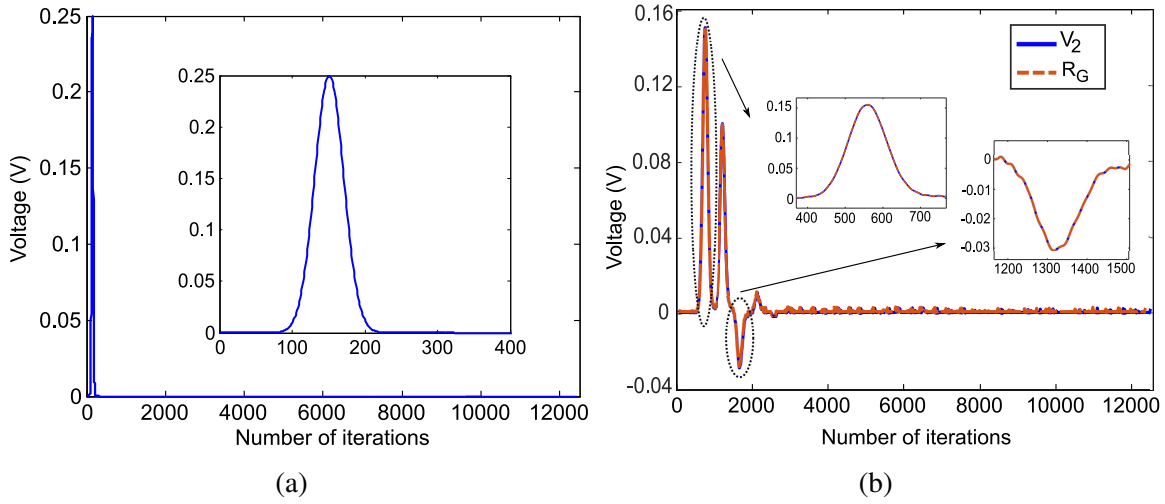

Figure 4.4: *Excitation source (Gaussian pulse) (a), the comparison of the response R_G with the result of convolution of equation (2.1).*

We base the extraction of the impulse responses in the following results on this approach. The asynchronous feature of the DD technique will allow an additional advantage, as it enables different excitation signals for each sub-system. This aspect will be highlighted in a further application.

4.3 Experimental applications of the DD method

With the theoretical foundations of the DD method in place and its upgrading for practical applications, different configurations of wiring networks will be presented in this section. The aim is to demonstrate the applicability of the method in a real-world environment, and its efficiency with additional experimental constraints.

4.3.1 First scenario: measurement with a single scope

We study the network in Figure (4.5), consisting of 6 cables of different types and lengths. The two lines L_2^1 and L_2^2 are interconnected through a BNC-T connector, at which the decomposition will occur later. This configuration is more realistic and closer to reality, as the subdivision will naturally take place at the level of an interconnection.

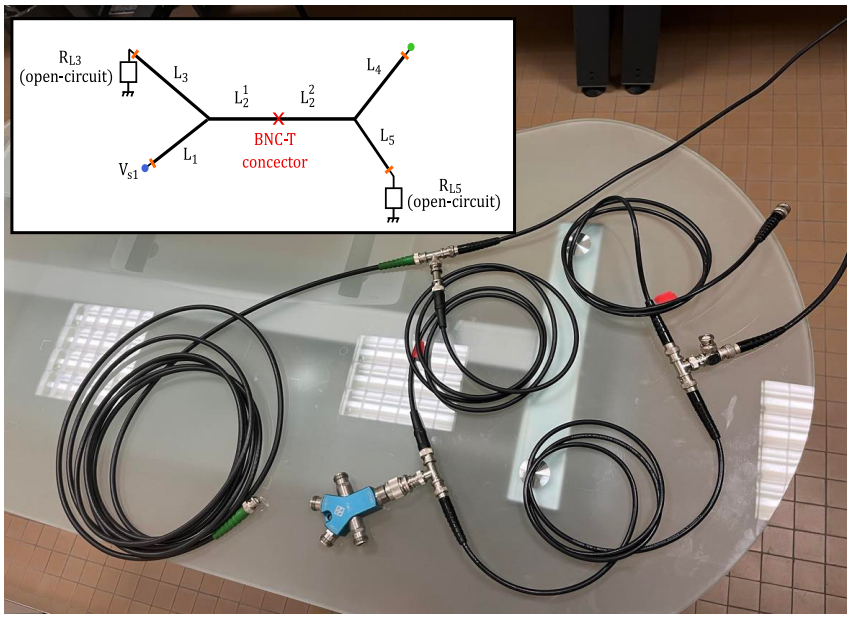

Figure 4.5: *The studied transmission line network.*

The injection of the excitation source using the AWG happens at the input of line L_1, whereas the scope measures the voltage at line L_4, as shown in the set-up in Figure (4.6).
For a Gaussian excitation pulse of magnitude $0.25V$ (limited by the AWG), the voltage V_4 of the global network is measured with a SR of $10GS/s$, as reported in Figure (4.7)
We can identify the direct propagation of the Gaussian pulse through lines L_1, L_2^1, L_2^2 and L_4 of the network through the first recorded peak. The impact of the mismatches in the network is recorded with a positive sign for the open-circuit loads and a negative sign for the mismatch at

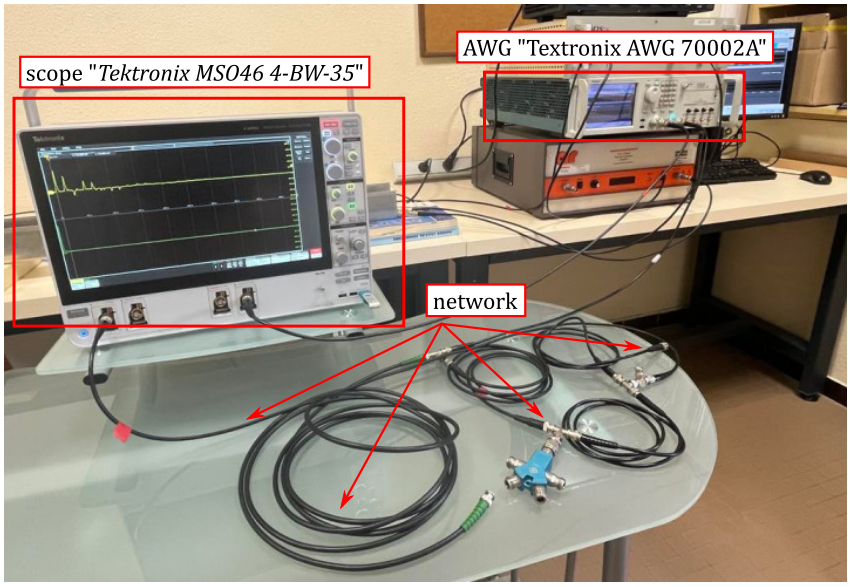

Figure 4.6: *Experimental bench of the studied line network.*

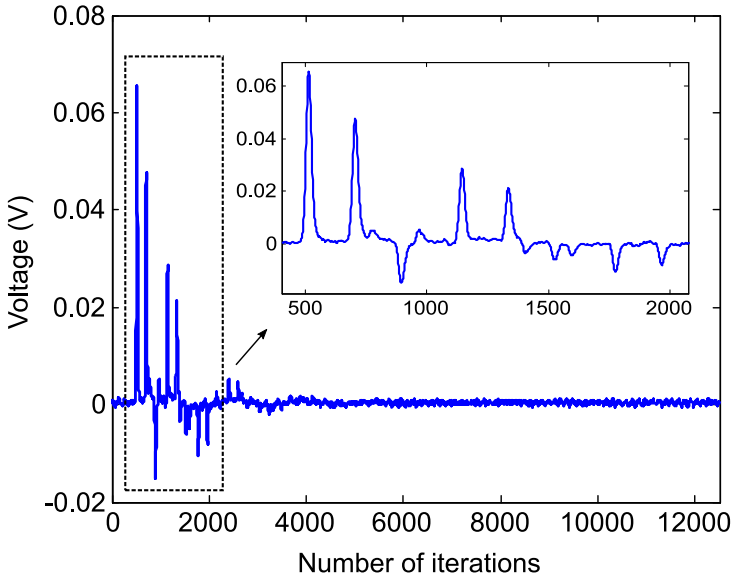

Figure 4.7: *Voltage V_4 measured at the termination of line L_4 for the global network, using the scope in Figure (4.6).*

the junction.

We aim to retrieve this result by decomposing the global network into two networks at the level of the interconnection (through the BNC-T connector). The voltage V_4^2, located at the sub-network $k = 2$, is expressed following equation (2.61) as follows:

$$V_4^2 = h_{24}^2 * \underbrace{(h_{12}^1 * V_{s1}^1)}_{V_{\sim 2,1}^2} + \sum_{i=2}^{q} h_{24}^2 * \left(h_{22}^2 * h_{22}^1 * V_{\sim 2,i}^2\right) \tag{4.11}$$

where $V_{\sim 2,i}^2$ is defined as the i-th order of the equivalent source at the interface and expressed by

$$V_{\sim 2,i}^2 = h_{22}^2 * \left(h_{22}^1 * V_{\sim 2,i-1}^2\right) \tag{4.12}$$

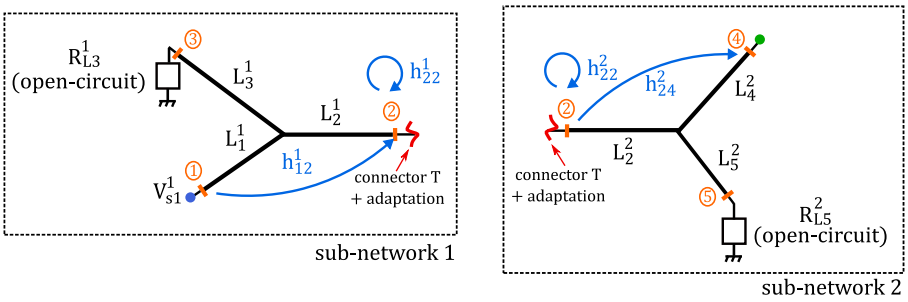

Figure 4.8: *Impulse responses h_{ij}^k for each sub-network Y^k, $k \in \{1,2\}$.*

For this configuration, the only physical injected source is located in sub-network 1, consequently the contribution of the equivalent source at the interface to the output should considered.

First, we evaluate the response R_{12}^1 based on which the impulse response h_{12}^1 will be constructed later. From the experimental set-up in Figure (4.9), the injection happens at the input of line L_1 ($i = 1$), and the line L_2^1 is connected to the scope for recording ($l = 2$). Similarly, the response R_{24}^2 for sub-network 2 is measured at the termination $j = 4$ when line L_2^2 is connected to the AWG for injection, as shown in the set-up in Figure (4.10). Both responses, in addition to the source, are used to construct the corresponding impulse responses following the method in section (4.1.1).

The exact evaluation of the voltage V_4^2 with the DD method requires considering the multiple-round trips of the injected signal between the two sub-networks to a given order q. This involves introducing new impulse responses h_{22}^1 and h_{22}^2 characterizing each of the corresponding sub-networks, when no physical source is injected. The procedure of their evaluation, detailed in section (2.3.1), requires two steps. The first one measures the impulse response, denoted $h_{22,total}^k$, containing both the excitation and the response, represented schematically in Figure (2.22a). Experimentally, this measure is realized using a BNC-T connector, connected to

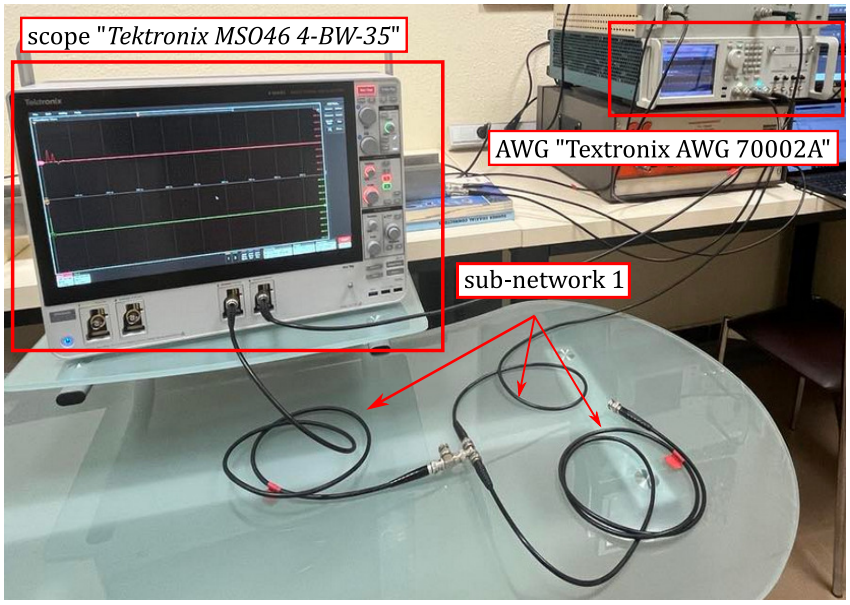

Figure 4.9: *Experimental bench of sub-network 1.*

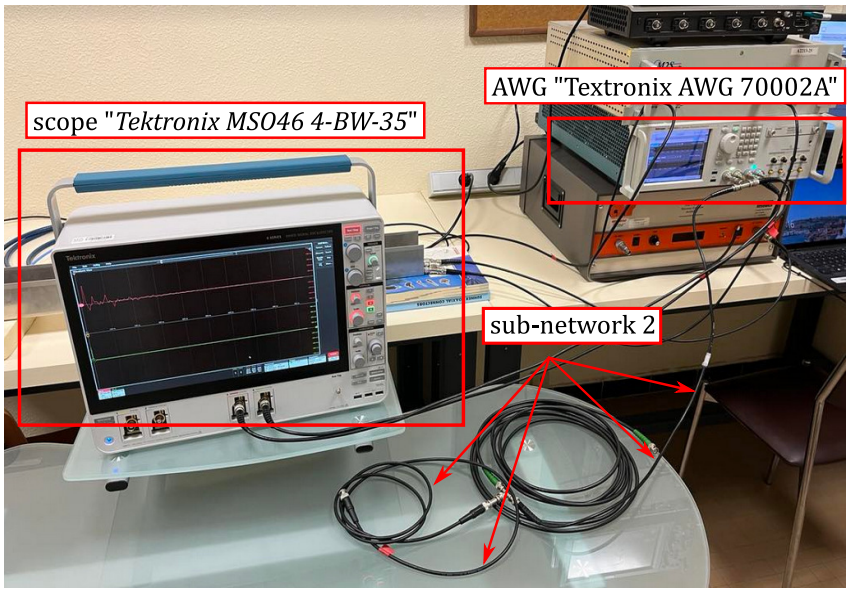

Figure 4.10: *Experimental bench of sub-network 2.*

the AWG, the cable at which the decomposition has occurred (L_2^k), and the scope for measurement, as shown in Figure (4.11). The second step, represented in Figure (2.22b), evaluates the impulse response $h_{22,inf}^k$ when the line L_2^k is supposed infinite so that no reflections are recorded. It translates experimentally either by considering a very long cable or ensuring perfect matching. In our case, a 50Ω-match is loaded to both lines L_1^2 and L_2^2 given their characteristic

impedance is of 50Ω (coaxial cables).

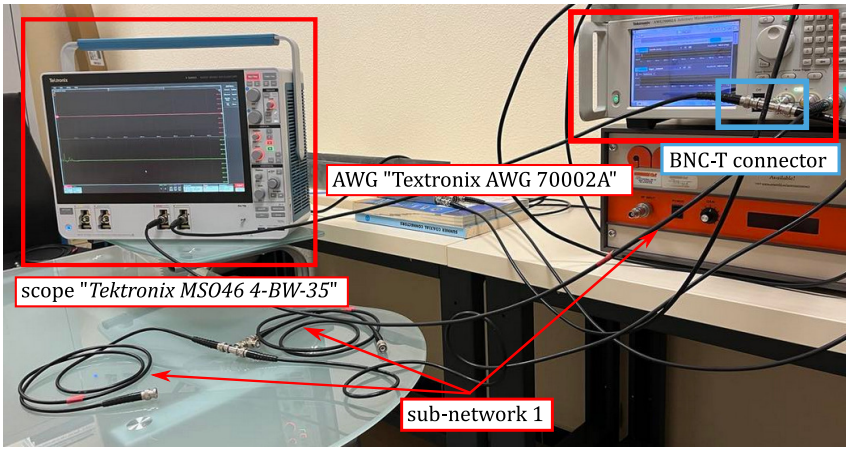

Figure 4.11: *Experimental set-up for the measurement of the response* $R^1_{22,total}$ *of sub-network 1.*

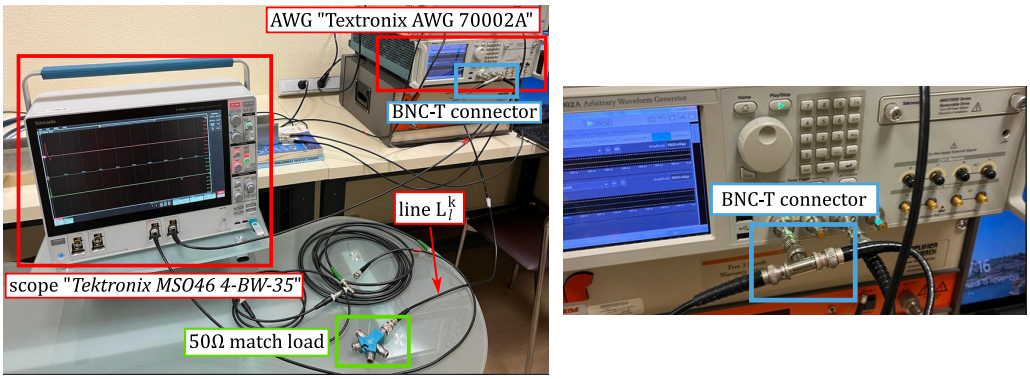

Figure 4.12: *Experimental set-up for the measurement of the response* $R^k_{22,inf}$ *of sub-network k, and the zoom at the BNC-T connector level.*

By computing the equation (4.11), to the order $q = 4$, the DD method retrieves the expected output. First, we notice that the global result (reference) is noisy, whereas the one obtained with our method is smoother. In fact, due to the inherent noise of the scope (and its random nature), the evaluation of the global response is also impacted. To overcome this experimental constraint, two steps are considered: 1) we calculate the average of the measured responses $R^k_{..}$ for 1k acquisition using the scope [2], 2) we smooth the data (in a software post-processing step)

[2]This feature is proposed by the mathematical mode of the scope. For our measurements, the noise is reduced by a factor $1e3$ with this averaging technique.

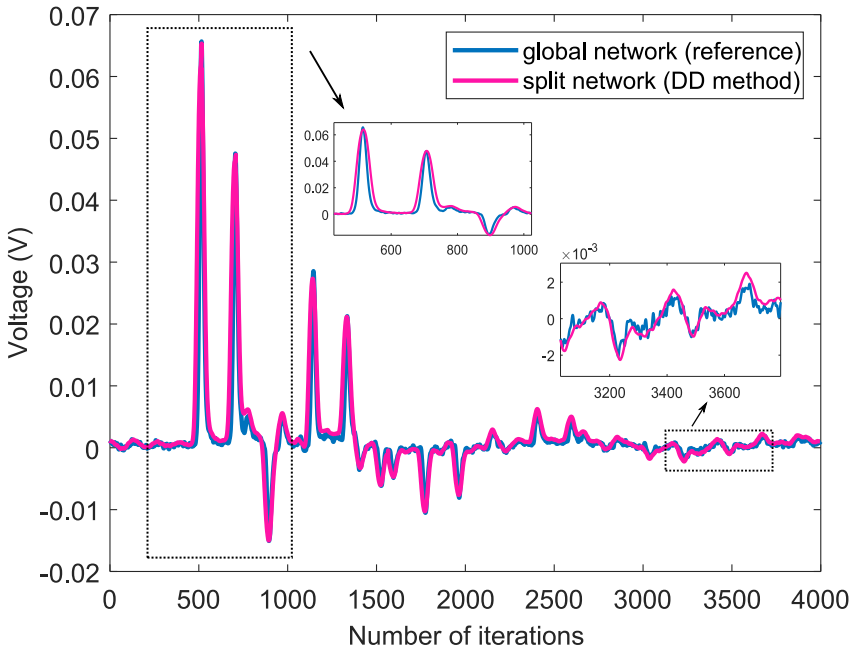

Figure 4.13: *Comparison of the measured voltage V_4 for the global network and the obtained result using the DD method (measured partial responses) for the split network.*

before evaluating the impulse responses. The same steps will be considered for the upcoming applications.

4.3.2 Second scenario: measurement with different scopes

With the previous results, the DD method proves its efficiency in recovering the global solution through measured partial solutions. As mentioned earlier, this feature is very important for industrial applications, where partners won't share their systems (topology, types of lines, loads, etc.) for property and confidentiality reasons. It is therefore highly probable that the measurement tools available for the different partners are not the same either. The general and asynchronous features of the DD method overcome this constraint, the equipment used for injection and/or acquisition is totally independent of the method. Within this context, we propose to study new configurations where the partial responses of each sub-network will be measured using a different scope.

4.3.2.1 Acquisition with the same SR

We consider the transmission line network in Figure (4.14), where lines L_2^1 and L_2^2 are interconnected with the BNC-T connector (decomposition level). For this configuration, the

injection at the entrance of line L_1 is carried out with the AWG, while the voltage V_3 will be measured using both scopes with an equal SR ($25MS/S$). In general, the SR is an inherent parameter to the scope pre-defined by the constructor, the chosen SR in our study is the common one to both used scopes.

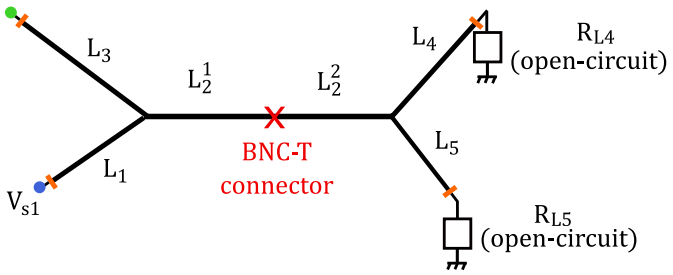

Figure 4.14: *Schematic representation of the studied transmission line network.*

As mentioned previously through this manuscript, we suppose that the reference (global result) is given for validation purposes. However, the use of two different scopes requires comparing our technique with two references, each measured with one scope. Following the decomposition, at the interconnection level of lines L_2^1 and L_2^2, two sub-networks can be identified. The voltage V_3^1 located in sub-network 1 is expressed based on equation (2.61) as follows:

$$V_3^1 = h_{13}^1 * V_{s1}^1 + h_{23}^1 * \underbrace{\left(h_{22}^2 * (h_{12}^1 * V_{s1}^1)\right)}_{V_{\sim 2,1}^1} + \sum_{i=2}^{q} h_{23}^1 * \left(h_{22}^2 * (h_{22}^1 * V_{\sim 2,i}^1)\right) \tag{4.13}$$

where $V_{\sim 2,i}^1$ is the i-th order of the equivalent source at the interface level, expressed by

$$V_{\sim 2,i}^1 = h_{22}^2 * (h_{22}^1 * V_{\sim 2,i-1}^1) \tag{4.14}$$

We suppose that all the responses $R_{\cdot\cdot}^1$ of sub-network 1 are measured using the scope *Textronix AWG 70002*, as shown in Figure (4.17).
The response R_{22}^2 of sub-network 2, on the other hand, is measured using the scope *LeCroy 640Zi* as shown in Figure (4.18).
The process requires two measurements, the first one measures the total response $R_{22,total}^2$ as shown in Figure (4.18), and the second one measures the response of the sub-network 2 considering a perfectly adapted line L_2^2. The difference of both acquisitions gives the response R_{22}^2.
The same procedure is followed to measure the response R_{22}^1, at the interface level, when no equivalent source is injected. The corresponding set-up is shown in Figure (4.19).
The corresponding impulse responses of both sub-networks are extracted upstream through the proposed method in section (4.1.1), considering that the signal $\alpha(t)$ is a double-gaussian pulse.

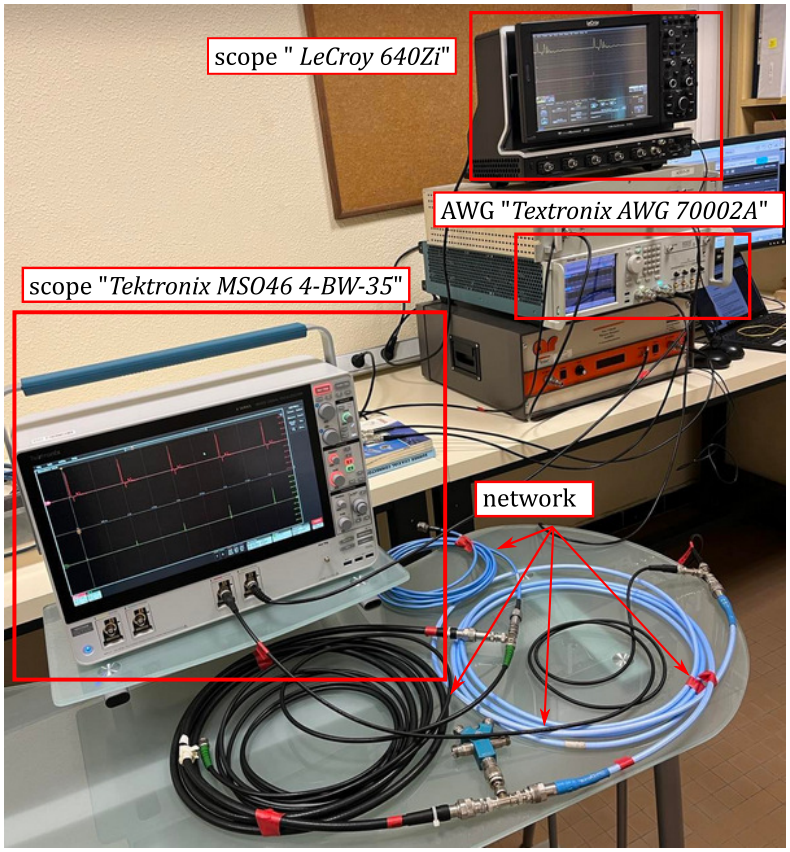

Figure 4.15: *Experimental set-up for the studied wire network including both scopes used of the experimental DD method.*

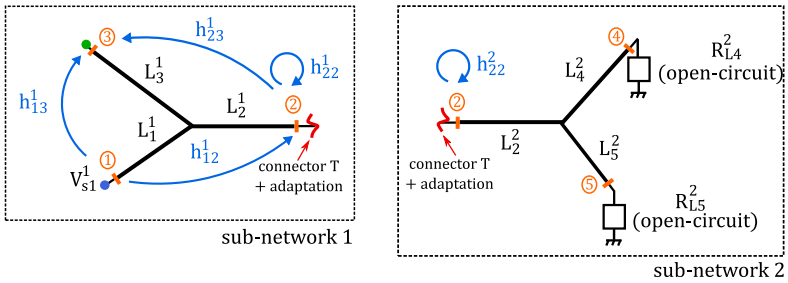

Figure 4.16: *Impulse responses h_{ij}^k for each sub-network Y^k, $k \in \{1,2\}$.*

In this configuration, sub-network should be characterized through 4 impulse responses. This is a special case and does not diminish the advantage of the method demonstrated throughout this chapter.

The obtained result for computing equation (4.13) to the order $q = 2$ is reported in Figure (4.20).

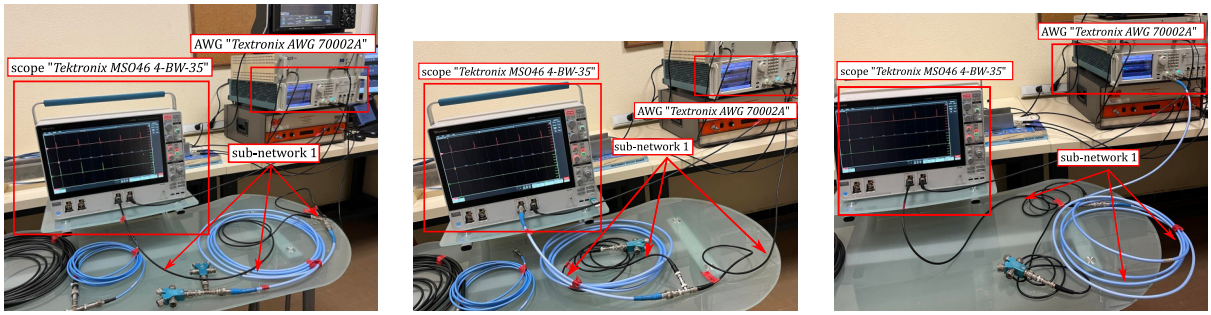

(a) *Response* R^1_{13} (b) *Response* R^1_{12} (c) *Response* R^1_{23}

Figure 4.17: *Experimental measurement for the evaluation of the responses* $R^k_{\cdot\cdot}$ *of both sub-networks* $k \in \{1,2\}$.

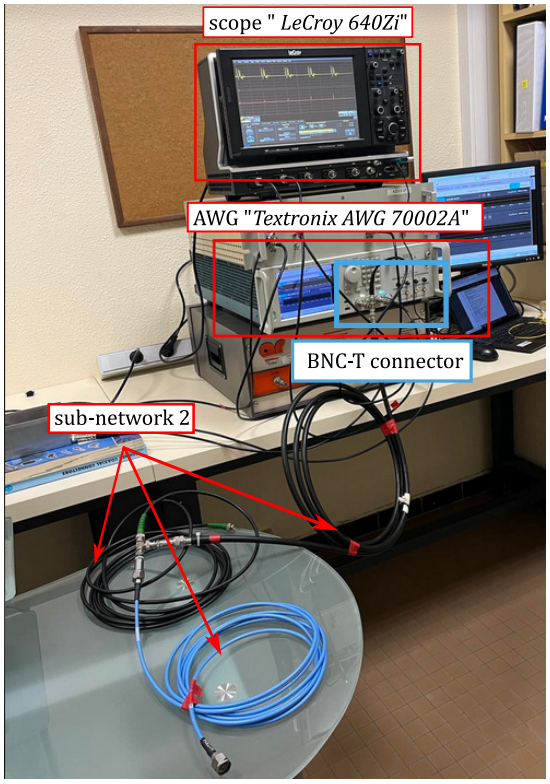

Figure 4.18: *Experimental measurement for the evaluation of the responses* R^2_{22} *of sub-network 2.*

The DD method's result follows the overall pattern of both references, however, in some instances, the differences are more accentuated. In fact, the measured results lack precision due to the lower SR chosen[3]. In the next section, we consider two different sampling rates for each

[3]A low SR can lead to unprecise measures. Timing errors, interpolation artifacts, and missed transient effects

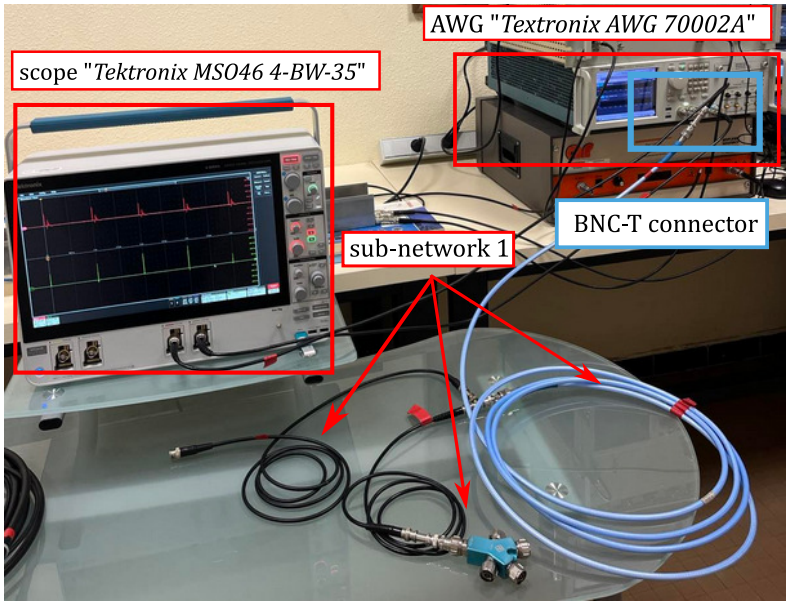

Figure 4.19: *Experimental measurement for the evaluation of the responses R^1_{22} of sub-network 1.*

scope, with respect to the frequency spectrum of the measured signals for a better acquisition.

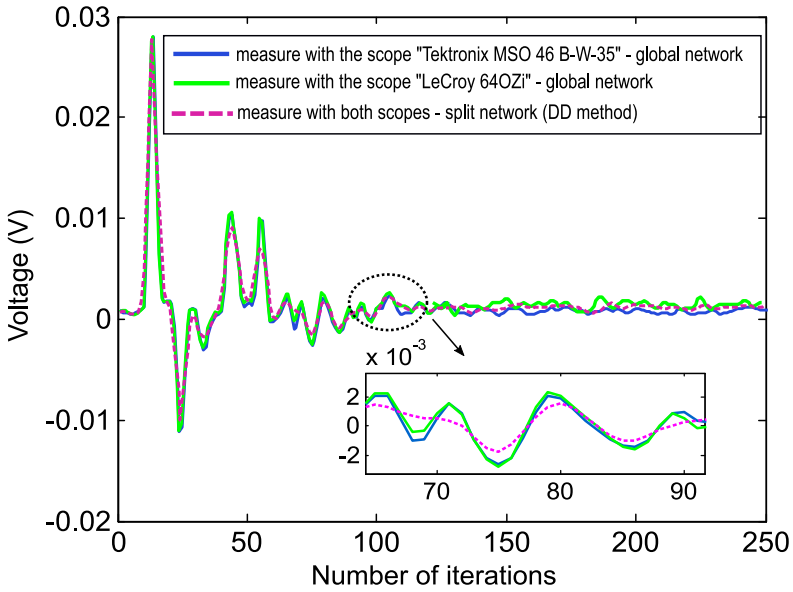

Figure 4.20: *Comparison of the measured voltage V_3 for the global network (both references) and the obtained result using the DD method (measured partial responses) for the split network.*

can affect measurements, especially high-frequency signals.

4.3.2.2 Acquisition with different SR

We utilize for the upcoming application the DD method's main advantage (asynchronous feature) to construct the matrices $P_{\cdot\cdot}^{k}$, in equation (4.5), using different signals $\alpha(t)$ for each sub-network k.

We study the network in Figure (4.22) consisting of 7 cables, such that lines L_4^1 and L_4^2 are interconnected with a BNC-T connector. The injection with the AWG of the source is at the entrance of line L_1 and the acquisition of the voltage V_5 is carried by both scopes.

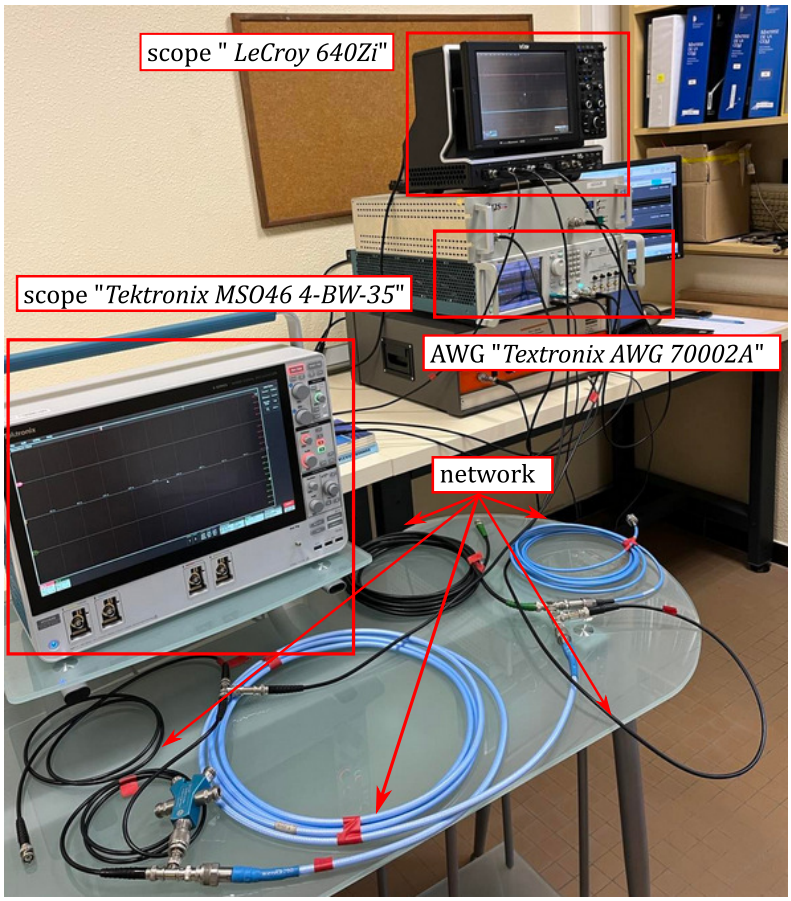

Figure 4.21: *Experimental set-up for the studied wire network including both scopes used of the experimental DD method.*

The responses $R_{\cdot\cdot}^1$ of sub-network 1 are measured using the scope *Tektronix MSO46 4-BW-35* ($SR = 10GS/s$) and a sine-wave signal for $\alpha(t)$. The responses $R_{\cdot\cdot}^2$ of sub-network 2 on the other hand, are measured with the scope *LeCroy 640Zi* ($SR = 25GS/s$) and a double-gaussian pulse for $\alpha(t)$. The experimental set-up for the extraction of responses R_{14}^1 and R_{45}^2 are shown

in Figures (4.24) and (4.25). The evaluation of the responses R_{ll}^{k} at the interface level ($l = 4$) is similar to the previous applications.

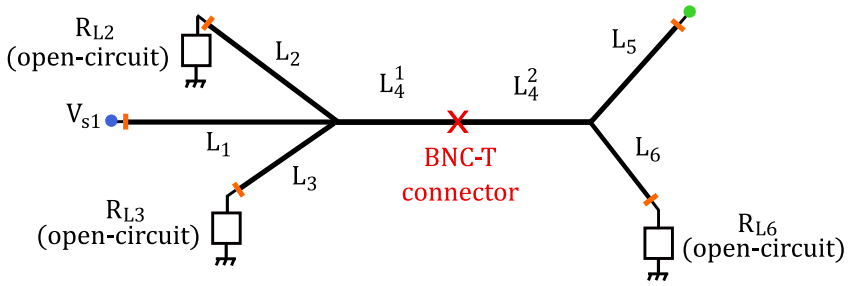

Figure 4.22: *Schematic representation of the studied transmission line network.*

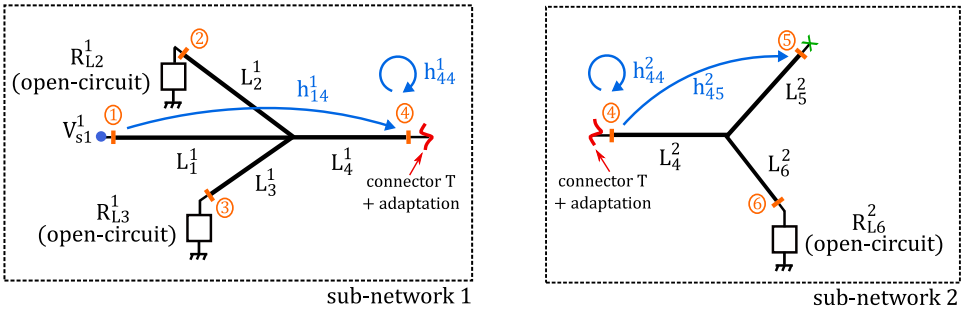

Figure 4.23: *Impulse responses $h_{ij,m}^{k}$ for each sub-network Y^{k}, $k \in \{1,2\}$.*

The voltage V_5^2, measured at the termination $j = 5$, is deduced from equation (2.5) and is expressed by

$$V_5^2 = h_{45}^2 * V_{\sim 4,1}^2 + \sum_{i=2}^{q} h_{45}^2 * \left(h_{44}^1 * (h_{44}^2 * V_{\sim 4,i}^2)\right) \tag{4.15}$$

where $V_{\sim 4,1}^2$ is the first order of the equivalent source at the exchange level given by the product $(h_{14}^1 * V_{s1}^1)$. The i-th order of this source is expressed by

$$V_{\sim 4,i}^2 = h_{44}^1 * (h_{44}^2 * V_{\sim 4,i-1}^2) \tag{4.16}$$

Using the proposed alternative method to construct the impulse responses of each sub-network and following an interpolation technique of these results, the computation of equation (4.15) to the order $q = 4$ gives the result reported in Figure (4.26).

The new choice of SR allows better precision and gives better results. We can see that the results measured with the two scopes for the global network are very close. The small differences in amplitude can be explained by the random nature of the noise specific to each scope. The

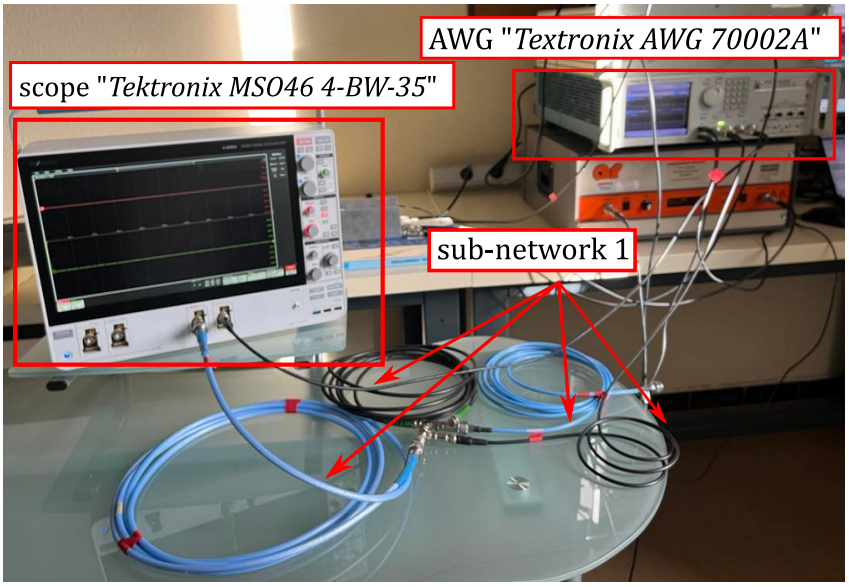

Figure 4.24: *Experimental measurement for the evaluation of the response* R^1_{14} *of sub-network 1.*

retrieved voltage V_5 using the DD method is very close to these references. The small differences in amplitude can be explained by numerical errors in interpolating the results as well as the smoothing of the measured responses $R^k_{\cdot\cdot}$.

4.3.3 Parametric study using experimental DD method

Throughout this chapter, we demonstrate the DD method's efficiency for practical applications. Its asynchronous formulation allows characterizing each sub-system independently. Consequently, modifications in one of them will only require the re-evaluation of its impulse responses. Experimentally, this aspect enables important gains of cost, due to the difficulty of measurements and resources they require, mainly time.

We propose to study a new configuration of a cable network in Figure (4.27), for which the variable of interest is the voltage V_3. The decomposition occurs at the interconnection level of lines L^1_2 and L^2_2, and resembles the application in section (4.3.2.1). The voltage V^2_3 is thus retrieved based on equation (4.13). The latter is recorded using the scope *LeCroy 640Z* for a sample rate of $10GS/s$. In this configuration, the responses of both sub-networks are measured using the same scope.
By evaluating equation (4.15) to the order $q = 3$, the DD method gives a satisfactory result, as reported in Figure (4.28a).

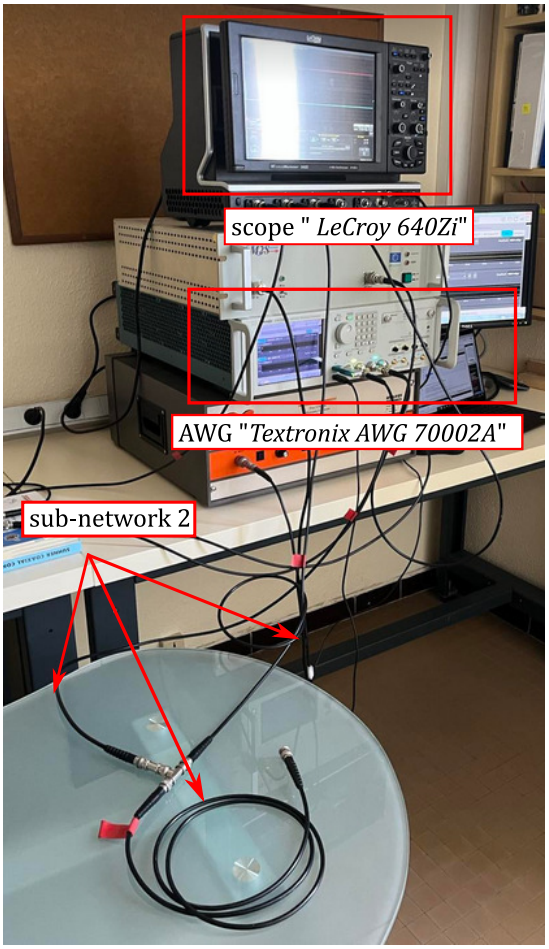

Figure 4.25: *Experimental measurement for the evaluation of the response R^2_{45} of sub-network 2.*

We now exploit the asynchronous nature of the DD method for a parametric study by modifying a parameter of sub-network 1, in this case, the cable representing the line L^1_2 is replaced by another cable of different length and characteristic impedance. This modification requires the re-evaluation of the impulse responses $h^1_{\cdot\cdot}$ of sub-network 1, however, the response h^2_{22} of sub-network 2 is not re-evaluated as the corresponding sub-network is intact. The obtained result with the new measured impulse response, reported in Figure (4.28b), follows the overall pattern of the reference. Around 2000 iterations, the impact of the modifications is recorded as different reflections of different magnitudes appear due to the different characteristic impedances of the used cables. The DD method enables parametric experimental studies with a lower cost, as only the modified sub-systems are measured for the new configuration.

The significant gain cost that offers the DD for experimental applications for parametric studies

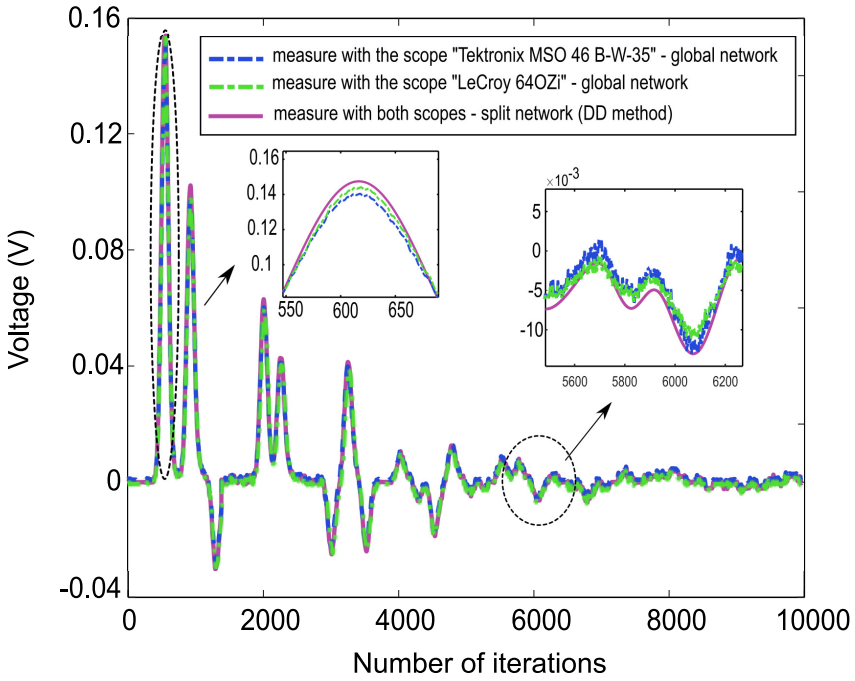

Figure 4.26: *Comparison of the measured voltage V_5 for the global network (both references) and the obtained result using the DD method (measured partial responses) for the split network.*

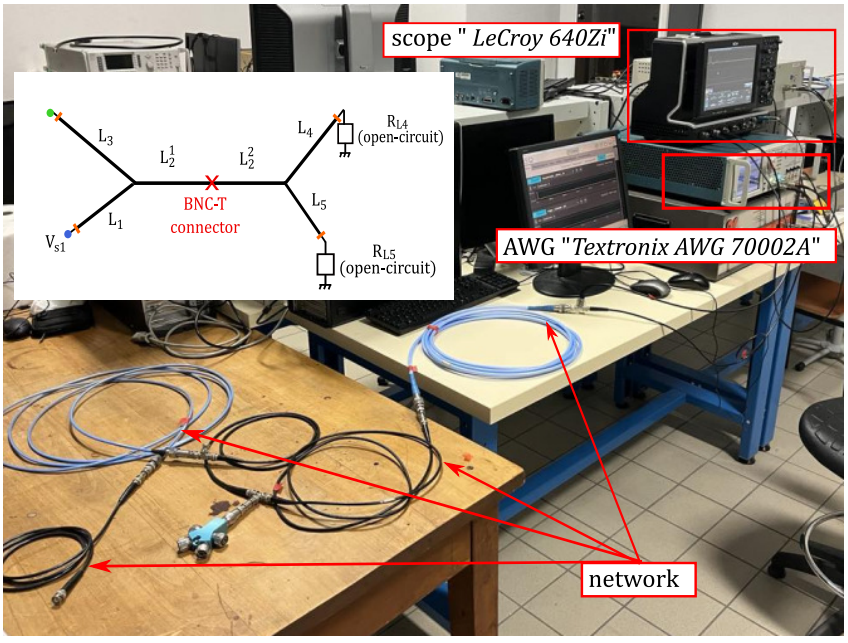

Figure 4.27: *Experimental set-up for the studied wire network for parametric analysis.*

offers other possibilities of combining measurements with numerical simulations. This alter-

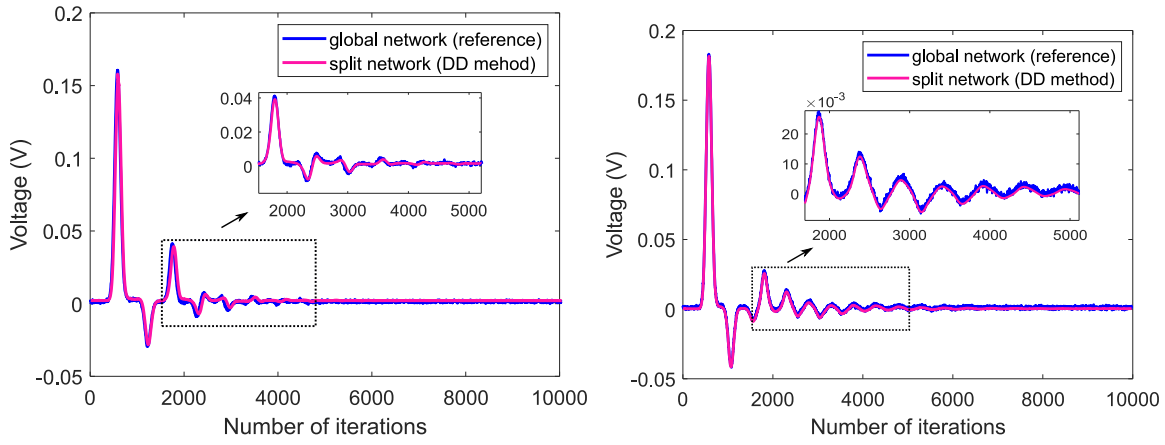

(a) *Initial configuration* (b) *Modified configuration*

Figure 4.28: *Comparison of the measured voltage V_3 for the global network (both references) and the obtained result using the DD method (measured partial responses) for the split network.*

native also has the advantage of enabling parametric studies to be carried out upstream of the measurement, allowing the most influential parameters in the configuration studied to be identified in advance, for stochastic study.

Conclusion

Throughout this chapter, the DD method proved to be efficient in measuring environments. The technique was first adapted to make it experimentally feasible, by proposing an alternative method for impulse responses' extracting that overcomes experimental constraints. Then, experimental tests were conducted in wiring networks to demonstrate the applicability of the technique when the impulse responses were measured. In line with the thesis objectives, and to better represent a real-life situation where the DD technique can be useful, additional experiments were carried out with the use of different scopes for data acquisition for each sub-system. From the obtained results, we conclude that the choice of the sampling rate is very crucial for the precision of the result. The DD method may be unable to retrieve the expected output when a low SR is chosen, as important data isn't acquired. In the last section, we utilize the asynchronous feature of the method for parametric study. We highlighted the significant gain cost the technique offers as only modified sub-systems are re-measured. This new advantage seems to be promising for industrial applications, where most of the time, the experiments are difficult and costly. Within this framework, the method preserves the confidentiality of the subsystem and doesn't exchange any information about its topology or characteristics other than

its impulse responses. As a perspective, the DD method can be fully experimental. In other words, not only the impulse responses are measured, the injection of the equivalent source to the sub-system of interest is carried out experimentally. To consider the final formula for the q-order, the experiment will require re-injection of the equivalent source at the interface level between the sub-networks. Experimentally, additional equipment will be required with an automatization of the injection and acquisition of the data.

CHAPTER 5

DD Method for Stochastic EMC Applications

Contents

WITH the asynchronous nature of the DD method comes a major advantage for parametric studies. Whether the impulse responses are computed numerically, through a numerical code or commercial software or measured experimentally with the proposed benchmark, re-modeling the modified sub-systems only offers significant time and resource gains. This particular feature is more emphasized for the stochastic dimension. For the past years, uncertainty quantification for EMC problems has continued to evolve in line with technological advances and industrial requirements. One of the encountered challenges lies in the complexity of the problems, reflected by their multi-physics and multi-scale. Another layer of difficulty arises with the uncertainty dimension. Stochastic analysis becomes challenging and computationally expensive, especially for high-dimensional systems. The DD method can be an effective solution to these constraints, as it goes from solving a global complex system to simpler non-overlapping sub-systems of a lower stochastic dimension.

The aim of this chapter is to extend the DD approach to stochastic linear time-domain EMC applications. Before diving into the association of a stochastic method and the proposed DD technique, it is essential to outline the framework of the stochastic study. The Uncertainty Quantification principle (UQ) is presented in section 1 while recalling the main theoretical basis for probabilistic analysis. The mathematical foundation of Monte Carlo (MC), Stochastic Collocation (SC) and Polynomial Chaos (PC) approaches is described with a focus on mean and variance assessment. Following the uncertainty quantification, we proceed to define the Sobol' indices for global sensitivity analysis. With a solid theoretical foundation in place for both UQ and SA, the stochastic DD method based on the association of the SC technique and the deterministic DD approach is formulated in section 2. Its concept is put into practice through applications of transmission line networks in section 3. Through the different applications, the stochastic DD method's ability to propagate uncertainties between the sub-systems is demonstrated first, then its asynchronous feature is highlighted when different configurations of intensities and distribution laws of RVs are studied. Given that a complete stochastic analysis will require the study of all possible combinations, it translates into an important evaluation cost of the model. This cost is even more important when the number of stochastic input parameters is high. To tackle this challenge, referred to as *the curse of dimensionality*, an offline–online association of the SC method with the DD strategy is proposed. Its advantages, based on RV separation, are discussed in the last section. Through a theoretical gain for an optimal configuration of decomposition, the stochastic DD method proves significant evaluation cost reduction.

5.1 Elements of probability theory and stochastic modeling

Physical systems are often represented by mathematical models, ranging from simple analytical formulas to sets of partial differential equations. The latter may be solved using specific numerical schemes such as finite difference [130] or finite element methods [131], implemented as simulation computer codes (step A in Figure (1.3)). The mathematical formulation of this model can be given by the function

$$M: \begin{array}{c} \mathscr{D}_x \subseteq \mathbb{R}^M \to \mathscr{D}_y \subseteq \mathbb{R}^n \\ x \mapsto y \end{array} \tag{5.1}$$

where $x = (x_1, ..., x_M)^T$ is a set of M input variables and y the response of the model[1]. In general, the mapping $M(.)$ can be either defined using an analytical formula or a high-fidelity computational model. As this model may intricate a chain of multi-physics resulting in multiple sources of complexity, this computer model can be known only point-by-point. In this sense, the mapping M can be referred to as a $black-box$ model. It is known only through pointwise evaluations for each input variable for which the computer program is run.

In the case where uncertainties are associated with the input parameters, the latter are modeled as random variables. Consequently, the model's output becomes a random variable (RV) denoted Y, such as

$$M: \begin{array}{c} \mathscr{D}_x \subseteq \mathbb{R}^M \to \mathscr{D}_y \subseteq \mathbb{R}^n \\ X \mapsto Y \end{array} \tag{5.2}$$

where $X = (X_1, ..., X_M)^T$ is a M-dimensional vector of RVs.

For a proper definition, we consider the probability space $(\Omega, \mathscr{A}, \mathbb{P})$ where Ω is the sample space, $\mathscr{A}$ is a sigma-algebra (whose elements are called events) and $\mathbb{P}$ is a probability on $\mathscr{A}$. All the random quantities (random variables) considered in this thesis will be assumed as continuous variables and are defined in this probability space.
A random variable X defined on $(\Omega, \mathscr{A}, \mathbb{P})$, with values in $\mathbb{R}$, is an application of Ω in $\mathbb{R}$, measurable from $(\Omega, \mathscr{A})$ into $(\mathbb{R}, \mathscr{B}_\mathbb{R})$, where $\mathscr{B}_\mathbb{R}$ is a basis in $\mathbb{R}$. For each element $\omega \in \Omega$, $X(\omega) \in \mathbb{R}$ is called an ω-realization, or more simply a realization of X denoted x. In the following, random variables will be denoted by capital letters, and deterministic variables (and

[1]The input parameters generally include geometric parameters of the studied structure and/or its physical properties (electric/magnetic). It can also refer to parameters associated with the excitation source(s). In our study, we consider that the output y is real ($\in \mathbb{R}^n$), but it may be complex ($\in \mathbb{C}$) for other configurations.

in particular realizations of random variables) by lower-case letters.

The distribution of a random vector X can be described using two tools:

- its joint cumulative distribution function (CDF) $F_X : \mathbb{R}^M \to [0,1]$ which assigns a probability to the event $\{X \leq x\}$, such as $F_X(x) = F_{X_1,...,X_M}(x_1,...,x_M) = \mathbb{P}\{X \leq x\} = \mathbb{P}\{X_1 \leq x_1,...,X_M \leq x_M\}$,
- its joint probability density function (PDF) (assuming it exists, in the continuous case) $F_X : \mathbb{R}^M \to \mathbb{R}_+$ defined such that $f_X(x) = f_{X_1,...,X_M}(x_1,...,x_M) = \frac{\partial^M F_X(x)}{\partial x_1 ... \partial x_M}$. The PDF function verifies the following property $\int_{\mathbb{R}} f_X(x)dx = 1$.

The full probabilistic content of the response Y is contained in its probability density function. In practice, it is not directly computable except in simple academic cases. Consequently, methods for uncertainty propagation have to be devised. These methods may be broadly classified into three categories, according to the specific information on the random response that is sought:

1. *second-moment methods* deal with computing the mean value and variance of the model response. They merely give some information on the central part of the response PDF,
2. *structural reliability methods* essentially investigate the tails of the response PDF by computing the probability of exceeding a prescribed threshold (probability of failure),
3. *spectral methods* represent the complete randomness of the response in an intrinsic way by using suitable tools of functional analysis. They allow the analyst to solve problems by a straightforward post-processing of their basic output, namely expansion coefficients on a suitable basis of functions.

5.1.1 Assessement of mean and standard deviation

In this thesis, we base our UQ on second-moment methods to evaluate the mean and variance of the response Y. The mean μ_X refers to the first moment and provides the average or expected value of a random variable. It gives an idea of the "typical" value we might expect to observe. By calculating the mean, we can identify the most likely outcome and use it as a point of reference for decision-making. The standard deviation σ_X, on the other hand, defined as the second moment, measures the degree of dispersion or spread of values around the mean. A higher standard deviation indicates significant variability in outcomes, while a lower standard deviation suggests more consistency. The respective expressions of mean and standard

deviation are given by

$$\mu_X = \mathbb{E}[M(X)] = \int_{\mathscr{D}_x} M(x) f_X(x)\,\mathrm{d}x \tag{5.3}$$

$$\sigma_X^2 = Var[M(X)] = \mathbb{E}\Big[\big(M(X)-\mu_X\big)^2\Big] = \int_{\mathscr{D}_x} \big(M(x)-\mu_X\big)^2 f_X(x)\,\mathrm{d}x \tag{5.4}$$

with $\sigma_X = \sqrt{Var[M(X)]}$ is the standard deviation (std).
From the two first moments, we define the coefficient of variation (CV) as the ratio of the standard deviation to the mean, expressed as a percentage[2]. It provides insight into the relative variability of a dataset. Its expression is given by

$$\delta X = \frac{\sigma_X}{|\mu_X|}, \tag{5.5}$$

with $\mu_X \neq 0$.
The centered moment of order r of X, $r \in \mathbb{R}^*$, can be expressed by the quantity

$$\mu_X^r = \mathbb{E}\Big[\big(M(X)-\mu_X\big)^r\Big] = \int_{\mathscr{D}_x} \big(M(x)-\mu_X\big)^r f_X(x)\,\mathrm{d}x \tag{5.6}$$

While fully acknowledging the numerous existing stochastic methods, we focus within the framework of this thesis on three methods: Monte Carlo, stochastic collocation and polynomial chaos.

Monte Carlo method

The Monte Carlo method uses the law of large numbers to evaluate a deterministic quantity, usually an integral representing the mathematical expectation of a certain random variable X [132]. MC is regarded as the reference for its simple implementation and its robustness (its convergence is independent of the dimension of the problem being addressed).
The first and second stochastic moments of the response Y of the model M reads as follows:

$$\mathbb{E}[Y] = \mathbb{E}[M(X)] = \frac{1}{N}\sum_{i=1}^{N} M(x^{(i)}) \tag{5.7}$$

$$Var[Y] = Var[M(X)] = \frac{1}{N}\sum_{i=1}^{N} \Big(M\big(x^{(i)}\big) - \mathbb{E}[M(X)]\Big)^2 \tag{5.8}$$

where $(x^{(i)})_{i=1\ldots N}$ is a N-realization sample of the random variable X.

[2]The CV can be useful to evaluate before conducting a sensitivity analysis, this step is not carried out in our context.

Stochastic collocation method

The stochastic collocation method is based on the projection of the model's response onto a basis of Lagrange polynomials of order n, such as

$$\mathscr{M}(x) \approx \sum_{i=0}^{n} M(x^{(i)}) L_i(x) \tag{5.9}$$

with $L_i(x) = \prod_{k=0,\ k\neq i} \frac{x-x_k}{x_i-x_k}$ are Lagrange polynomials chosen due to their property $L_i(x_j) = \delta_{ij}$ (δ_{ij} is the Kronecker symbol[3]).

The collocation points x_i correspond to the points in the Gauss quadrature rule attached to the probability distribution of random inputs (e.g., Legendre polynomials for a uniform distribution and Hermite polynomials for a Gaussian distribution). The choice of an adapted quadrature rule gives

$$\int_{-\infty}^{+\infty} g(u)p(u)du \approx \sum_{j=0}^{n} \omega_j g(x_j) \tag{5.10}$$

where p is the probability density of random variable X, and g a function with a sufficient regularity. The collocation weights ω_j are chosen in a way to ensure an exact quadrature rule for polynomials with a degree lower or equal to $2n+1$.

From the polynomial projection of the response Y, it becomes easy to approximate its statistical moments considering Lagrange polynomials and the quadrature rules [133]. The expectation (mean), is expressed as follows:

$$\begin{aligned} \mathbb{E}[\mathscr{M}(X)] &= \int_{\mathscr{D}_x} \mathscr{M}(x) f_X(x) dx \\ &\approx \int_{\mathscr{D}_x} \sum_{i=0}^{n} M(x^{(i)}) L_i(x) f_X(x) dx \\ &\approx \sum_{i=0}^{n} \omega_i M(x^{(i)}) \end{aligned} \tag{5.11}$$

The same approach is used to evaluate the variance $Var[\mathscr{M}(X)]$, such as

[3]The kronecker symbol δ_{ij} equals 1 if $i = j$, and 0 otherwise.

$$
\begin{aligned}
Var[\mathscr{M}(X)] &= \int_{\mathscr{D}_x} \mathscr{M}(x)^2 f_X(x)dx - \mathbb{E}[\mathscr{M}(X)]^2 \\
&\approx \int_{\mathscr{D}_x} \Big(\sum_{i=0}^{n} M(x^{(i)})L_i(x)\Big)\Big(\sum_{j=0}^{n} M(x^{(j)})L_j(x)\Big) f_X(x)dx - \mathbb{E}[\mathscr{M}(X)]^2 \\
&\approx \sum_{k=0}^{n} \omega_k M(x^{(k)})^2 - \mathbb{E}[\mathscr{M}(X)]^2
\end{aligned}
\tag{5.12}
$$

In general, the number n referring to the collocation points, is low. The rapid convergence rate of the SC technique is one of its main advantages. Numerical results of a practical application will compare the convergence of the SC technique and the MC reference method in the upcoming sections.

For the multivariate case of M input parameters, mean and variance are obtained by generalizing the principle of the stochastic collocation method, by the projection of the multivariate model $M(x_1,...,x_M)$ on the Lagrange polynomial basis. The multi-dimensional expansion of the SC method is formed as a weighted tensor product ($\otimes$) of the one-dimensional Lagrange polynomial L_i, such as

$$
\mathscr{M}(x) = \sum_{i_1=1}^{n_1} ... \sum_{i_M=1}^{n_M} M\big(x_{i_1}^1,...,x_{i_M}^M\big)\big(L_{i_1}^1 \otimes ... \otimes L_{i_M}^M\big) \tag{5.13}
$$

where L_{is}^s, $s \in \{1,..,M\}$, previously defined in (5.1.1), is expressed by

$$
L_i^s(x^s) = \prod_{k=0,\ k\neq i} \frac{x^s - x_k^s}{x_i^s - x_k^s} \tag{5.14}
$$

We can demonstrate that the first two moments are respectively given by

$$
\mathbb{E}[\mathscr{M}(X)] \approx \sum_{p=0}^{n_1} ... \sum_{q=0}^{n_i} ... \sum_{k=0}^{n_M} \omega_p ... \omega_q ... \omega_k M(x_1^{(p)},...,x_i^{(q)},...,x_M^{(k)}) \tag{5.15}
$$

$$
\begin{aligned}
Var[\mathscr{M}(X)] \approx &\sum_{p=0}^{n_1} ... \sum_{q=0}^{n_i} ... \sum_{k=0}^{n_M} \omega_p ... \omega_q ... \omega_k M(x_1^{(p)},...,x_i^{(q)},...,x_M^{(k)})^2 \\
&- \mathbb{E}[\mathscr{M}(x_1^{(p)},...,x_i^{(q)},...,x_M^{(k)})]^2
\end{aligned}
\tag{5.16}
$$

Polynomial chaos method

The Polynomial chaos (PC) method, also called polynomial chaos expansion (PCE), represents a random variable in terms of a polynomial function of random variables.

PC methods can be classified as intrusive or non-intrusive [134]. An intrusive approach, known as the stochastic Galerkin method (SGM), introduces the calculation of PC coefficients directly into the numerical model [135]. This has the advantage of determining the coefficients in a single run of the numerical model but may be very delicate to implement. In contrast, the non-intrusive approach does not require the numerical model itself but considers it as a black box [136]. In the following, we focus on the formulation of the PC basis and its coefficients for the non-intrusive methods.

We consider the model in equation (5.2) of M uncertain parameters represented by independent random variables $\{X_1, ...X_M\}^T$. Assuming that its response $Y = M(X)$ has finite variance, it belongs to the so-called Hilbert space of second-order random variables, which allows for the following representation

$$Y = M(X) = \sum_{\alpha \in \mathbb{N}^M} y_\alpha \Psi_\alpha(X) \tag{5.17}$$

The random variable Y is therefore cast as an infinite series, in which $\{\Psi_\alpha\}$ is a numerable set of random variables (which form a basis of the Hilbert space), and $\{y_\alpha\}$ are coefficients, also referred to as *coordinates* of Y in this basis. The polynomials Ψ_α satisfy the orthogonality property defined by

$$< \Psi_i, \Psi_j > = \int_{\mathbb{R}^M} \Psi_i(x)\Psi_j(x) f_X(x)\, dx = \|\Psi_i\|^2 \delta_{ij} \tag{5.18}$$

where δ_{ij} is the Kronecker symbol and $f_X(x) = \prod_{i=1}^{M} f_{X_i}(x_i)$ is the density function joined to X. The normalizing factor $\|\Psi_i\|^2$ is expressed by

$$\|\Psi_i\|^2 = \int_{\mathbb{R}^M} \Psi_i^2(x) f_X(x)\, dx \tag{5.19}$$

For standard distributions, the associated families of orthogonal polynomials are given by the Askey scheme [137].

For each random variable X_i, we associate the family of orthonormal polynomials $\{\pi_k^{(i)},\ k \in \mathbb{N}\}$ with regard to $f_{X_i}(x_i)$. While assuming that the degree of $\{\pi_k^{(i)}\}$ is k for $k > 0$ and $\pi_0^{(i)} \equiv 1 (1 \leq i \leq M)$, a multivariate polynomial basis $\{\Psi_\alpha,\ \alpha \in \mathbb{N}^M\}$ is built by tensorizing the M families of unidimensional polynomials, such as

$$\Psi_\alpha \stackrel{\text{def}}{=} \prod_{i=1}^{M} \pi_{\alpha i}^{(i)}(x_i) \tag{5.20}$$

where α_i is the degree of the univariate polynomial $\pi(\alpha_i)$ in the direction of x_i for $1 \leq i \leq M$.

The representation of the random response in equation (5.17) is exact when the infinite series is considered. However, in practice, only a finite number of terms may be computed. For this purpose, a truncation scheme has to be adopted. Since the polynomial chaos basis is made of polynomials, it is natural to consider a polynomial truncated series up to a certain degree. We define the total degree of a multivariate polynomial Ψ_α by

$$\alpha \stackrel{\text{def}}{=} \sum_{i=1}^{M} \alpha_i \tag{5.21}$$

The truncation method consists of selecting polynomials in the chaos basis of a degree less than or equal to a maximum given degree p, such as

$$\mathscr{A}^{M,p} = \{\alpha \in \mathbb{N}^M : \alpha \leq p\} \tag{5.22}$$

The truncated series, with P terms, is thus expressed as follows:

$$Y = M(X) \equiv \sum_{|\alpha| \leq p} y_\alpha \Psi_\alpha(X) \tag{5.23}$$

with P referring to the number of polynomials in the basis [86]. Its expression is given by

$$P = card\,\mathscr{A}^{M,p} = \binom{M+p}{M} = \frac{(M+p)!}{M!p!} \tag{5.24}$$

The computation of the polynomial coefficients will depend on the nature of the PC method: intrusive or non-intrusive [86]. We focus on the projection method for the evaluation of the coefficients for the non-intrusive approach.

The projection method relies on the orthonormality of the PC basis [138]. Each coefficient y_α is the orthogonal projection of the random response Y onto the corresponding basis function $\Psi_\alpha(X)$, such as

$$y_\alpha = \mathbb{E}[M(X), \Psi_\alpha(X)] = \int_{\mathscr{D}_x} M(x)\Psi_\alpha(X) f_X(x)\, dx \tag{5.25}$$

In practice, the expression below is estimated using numerical integration techniques (quadrature rules), which aim at approximating the multidimensional integral by a weighted sum as follows:

$$y_\alpha \approx \sum_{i=1}^{N} \omega^{(i)} M(x^{(i)}) \Psi_\alpha(x^{(i)}) \tag{5.26}$$

where $x^{(i)} = \left\{x_1^{(i)}, ..., x_M^{(i)}\right\}$ and $\omega^{(i)} = \left\{\omega_1^{(i)}, ..., \omega_M^{(i)}\right\}$ are the quadratures points and the corresponding weights.

The projection of the response of a model $Y = M$ on an orthonormal polynomial basis allows the computation of the statistics of the model response from the coefficients polynomial coefficients. The first moments, i.e. the expectation and the variance, are calculated from the approximation of the system response and the orthogonality property of the polynomials of the chaos basis. The expectation and variance of the output Y are given by

$$\mathbb{E}[Y] = \hat{y}_0 \tag{5.27}$$

$$var[Y] = \sum_{\alpha=1}^{P-1} \hat{y}_i^2 \tag{5.28}$$

For the multivariable case, the polynomial basis is constructed so as to keep only the polynomials of degree less than or equal to the order q chosen, using the corresponding polynomials to each RV chosen according to the distribution law.

5.1.2 Global sensitivity analysis: Sobol' indices

Let's consider the output Y of the deterministic model M of a M-dimensionnal set of random inputs $X = (X_1, ..., X_M)^T$. This function can be decomposed in the following form [111, 139]

$$Y = \sum_{u \subseteq \mathscr{U}} M_u(X_u) = \mathscr{M}_0 + \sum_{i=1}^{M} M_i(X_i) + \sum_{1 \leq i < j \leq M} M_{ij}(X_i, X_j) + ... + M_{12...M}(X) \tag{5.29}$$

where $\mathscr{U} = \{1, 2, ..., M\}$. The summation of the constant M_0, the univariate functions $\{M_i(x_i), 1 \leq i \leq M\}$, bivariate functions $\{M_{ij}(x_i, x_j), 1 \leq i \leq j \leq M\}$, etc. is called ANOVA (ANalysis Of VAriance) decomposition, if

$$\int M_u(x_u) dx_u = \mathbb{E}[M_u] = 0 \tag{5.30}$$

is fulfilled for all $u \subseteq \mathscr{U} \setminus \emptyset$. In this case, the functions M_0 to $M_{1..M}$ can be written as conditional expectations as follows:

$$
\begin{aligned}
M_0 &= \mathbb{E}[M(X)] \\
M_i(x_i) &= \mathbb{E}[M(X)|X_i = x_i] - \mathscr{M}_0 \\
M_{ij}(x_i,x_j) &= \mathbb{E}[M(X)|X_i,X_j = x_i,x_j] - M_i(x_i) - M_j(x_j) - M_0 \\
&\dots \\
M_{1\dots M}(x_1,\dots,x_M) &= \mathbb{E}[M(X_1,\dots,X_M)|X_1,\dots,X_M = x_1,\dots,x_m] - \sum_{w\subset\mathscr{U}} M_w
\end{aligned}
\tag{5.31}
$$

The conditional expectation $\mathbb{E}[M(X)|X_i]$ is the average of Y where only the values of the i-th input quantity X_i considered are conditioned (fixed). Similarly for the expectation $\mathbb{E}[M(X)|X_i,X_j]$ where only the values of the input quantities X_i and X_j considered are conditioned. They translate their contributions to the variance of the output not considered in the first-order indices S_i and S_j.

It may be shown that the summands, except $\mathscr{M}_0$, are mutually orthogonal in order to have the uniqueness of this decomposition and consequently to ensure the decomposition of the *total* variance into a sum of *partial* variances [106, 140]

$$
V \overset{\text{def}}{=} Var[Y] = \sum_{i=1}^{M} V_i + \sum_{1\le i<j\le M} V_{ij} + \dots + V_{12\dots M} \tag{5.32}
$$

By dividing all the terms in eq. (5.32) by the variance V of the model's output, the following expression is obtained

$$
1 = \sum_{i=1}^{M} \frac{V_i}{V(Y)} + \sum_{1\le i<j\le M} \frac{V_{ij}}{V(Y)} + \dots + \frac{V_{12\dots M}}{V(Y)} \tag{5.33}
$$

Therefore, Sobol relies on this decomposition to define all first and higher-order sensitivity indices of all input quantities X_i, such as

$$
1 = \sum_{i=1}^{M} S_i + \sum_{1\le i<j\le M} S_{ij} + \dots + S_{12\dots M} \tag{5.34}
$$

This formulation allows retrieving the Sobol' index of order 1 measuring the main effect for a given input quantity X_i as follows:

$$
S_i = \frac{V_i}{V} \tag{5.35}
$$

The second-order sensitivity index of the random variables X_i and X_j represents the interaction between the two variables. The Sobol' index is given by

$$S_{ij} = \frac{V_{ij}}{V} \tag{5.36}$$

The Sobol' indices are then defined as the ratio of the partial variances to the total variance so that the sum of these indices is equal to one.

For M input random variables, the total number of indices is equal to $2^M - 1$. In general, we are only interested in the indices of order 1, 2 and the total indices noted S_{Ti}. The latter are defined as the sum of all the Sobol' indices containing the index i and expressed by

$$S_{Ti} = 1 - S_{\sim i} \tag{5.37}$$

where $S_{\sim i}$ is the sum of all the Sobol' indices that do not include the index i.

The Monte Carlo method was one of the first techniques used to compute Sobol' indices [109]. However, their computation requires the evaluation of the model for a new set of RVs, introducing additional computational costs. Alternatively, accelerating methods, as introduced earlier, overcome not only the expensive computational cost of stochastic moments but also the Sobol' indices computation. In the literature, the most commonly used approach to evaluate these indices is the PC technique. They are deduced directly from the polynomial expansion coefficients, thanks to their decomposition into sums of orthogonal functions [141].

For any subset variables $u = \{i_1, ..., i_s\} \subset \{1, ..., M\}$, one defines the set of multivariate polynomials Ψ_α which depends only on u, such as

$$\mathscr{A}_u = \{\alpha \in \mathscr{A} : \alpha_k \neq 0 \text{ if and only if } k \in u\} \tag{5.38}$$

where $\mathscr{A}_u$ forms a partition of $\mathscr{A}$.

Note that $\mathscr{A}_i$ corresponds to the polynomials depending only on parameter x_i. Using this notation, the terms in equation (5.23) may be gathered according to the parameters they depend on

$$M(X) = M_0 + \sum_{u \subset \{1,...,m\}} M_u(X_u) \tag{5.39}$$

where

$$M_u(X_u) = \sum_{\alpha \in \mathscr{A}_u} y_\alpha \Psi_\alpha(X) \tag{5.40}$$

Consequently, due to the orthonormality of the PC basis, the partial variance reads

$$Var[M_u(X_u)] = \sum_{\alpha \in \mathscr{A}_u} y_\alpha^2 \tag{5.41}$$

The Sobol' indices at any order may thus be computed by a mere combination of the squares of the coefficients. The first-order PC-based Sobol' indices are defined as follows:

$$S_i = \frac{\sum\limits_{\alpha \in \mathscr{A}_i} y_\alpha^2}{\sum\limits_{\alpha \in \mathscr{A},\ \alpha \neq 0} y_\alpha^2} \ ; \ \mathscr{A}_i = \{\alpha \in \mathscr{A} : \alpha_i > 0\ , \alpha_{j \neq i} = 0\} \tag{5.42}$$

whereas the total PC-based Sobol' indices are given by

$$S_i^T = \frac{\sum\limits_{\alpha \in \mathscr{A}_i^T} y_\alpha^2}{\sum\limits_{\alpha \in \mathscr{A},\ \alpha \neq 0} y_\alpha^2} \ ; \ \mathscr{A}_i^T = \{\alpha \in \mathscr{A} : \alpha_i > 0\} \tag{5.43}$$

In this thesis, we propose to evaluate Sobol' indices using the stochastic collocation method. This choice is justified by its simple mathematical foundation, non-intrusive nature and rapid convergence rate. This work has been developed over the last few years within the EMC team at the Institute Pascal [142]. In the literature, a few researchers elaborated the global sensitivity analysis on the SC based on Gary's initial work in [143]. However, as these applications were mainly dedicated to structural dynamics applications, our contribution to the EMC field is further emphasized.

The computation of Sobol' indices using the SC method is driven by its evaluation of the model for all the possible combinations of RVs. The conditional variance for a given input is obtained by adapting the formulation and combining the already evaluated model for the corresponding input. Based on equation (5.31), the conditional variance V_u of the subset variables u is given by

$$\begin{aligned} V_u &= Var[\mathscr{M}_u(X_u)] = \mathbb{E}[\mathscr{M}_u^2(X_u)] \\ &= \mathbb{E}\Big[\Big(\mathbb{E}\big[\mathscr{M}_u(X_u)\big] - \sum_{w \subset u} \mathscr{M}_w\Big)^2\Big] \\ &= \mathbb{E}\Big[\Big(\mathbb{E}\big[\mathscr{M}_u(X_u)\big]\Big)^2\Big] - \mathbb{E}\Big[\sum_{w \subset u} \mathscr{M}_w^2\Big] \\ &= \mathbb{E}\Big[\mathbb{E}\big[\mathscr{M}_u(X_u)\big]\Big]^2 - \sum_{w \subset u} V_w \end{aligned} \tag{5.44}$$

We begin by evaluating the conditional expectation $\mathbb{E}\big[\mathscr{M}_u(X_u)\big]$, expressed in its integral form by

$$\mathbb{E}\big[\mathscr{M}_u(X_u)\big] = \int \mathscr{M}_u(X_u) dX_{u'} \tag{5.45}$$

where u' is the complement set of u.

By replacing the multi-dimensional expansion of the model M in the Lagrange polynomial basis given by equation (5.13), in the previous equation, we obtain the following expression

$$\int \mathscr{M}(X_u) dx_{u'} = \int \sum_{i_1=1}^{n_1} \dots \sum_{i_M=1}^{n_M} M\big(x_{i_1}^1, \dots, x_{i_M}^M\big) \big(L_{i_1}^1 \otimes \dots \otimes L_{i_M}^M\big) dx_{u'} \tag{5.46}$$

We re-arrange the equation (5.46) by separating the Lagrange polynomials that depend on x_u (i.e. L^u) and those depending on $x_{u'}$ (i.e. $L^{u'}$). Subsequently, the integration over $x_{u'}$ is conducted, whereby $\int \Big(L^{u'} \otimes L^u\Big) dx_{u'} = \omega^{u'} \otimes l^u$.

$$\begin{aligned} \int \mathscr{M}(X_u) dx_{u'} &= \sum_{i_1=1}^{n_1} \dots \sum_{i_M=1}^{n_M} M\big(x_{i_1}^1, \dots, x_{i_M}^M\big) \int \Big(L^{u'} \otimes L^u\Big) dx_{u'} \\ &\approx \sum_{i_1=1}^{n_1} \dots \sum_{i_M=1}^{n_M} M\big(x_{i_1}^1 \dots x_{i_M}^M\big) \Big(\omega^{u'} \otimes L^u\Big) \end{aligned} \tag{5.47}$$

Similarly, the sums in equation (5.47) can also be split up into terms that are connected to u and those to u' as follows:

$$\int \mathscr{M}(X_u) dx_{u'} \approx \sum_{i_1=1}^{n_1} \dots \sum_{i_k=1}^{n_k} \Big(\underbrace{\sum_{i_{k+1}=1}^{n_{k+1}} \dots \sum_{i_M=1}^{n_M} \mathscr{M}\big(x_{i_1}^1 \dots x_{i_M}^M\big)\big(\omega^{u'}\big)}_{M_{(u')}(x_{i_1}^1 \dots x_{i_k}^k)} \Big) L^u \tag{5.48}$$

Since the model $M(.)$ is evaluated at all the collocation points and given that the weights $\omega^{u'}$ are computed according to the quadrature rule, the quantity $M_{(u')}$ is known and can be easily computed. Therefore, for the same cost of evaluation of the mean and variance, the Sobol' indices are computed based on different combinations of the already evaluated model at the collocation points.

The expression $\mathbb{E}\Big[\mathbb{E}\big[\mathscr{M}_u(X_u)\big]^2\Big]$ in equation (5.44) can thus be expressed as follows:

$$\mathbb{E}\Big[\mathbb{E}\big[\mathscr{M}_u(X_u)\big]^2\Big] = \sum_{i_1=1}^{n_1} \dots \sum_{i_k=1}^{n_k} M_{(u')}(x_{i_1}^1 \dots x_{i_k}^k)^2 \omega^u \tag{5.49}$$

The partial variance V_u in equation (5.44) is thus obtained by replacing the integral term with the equation (5.49), as follows:

$$V_u = \sum_{i_1=1}^{n_1} \dots \sum_{i_k=1}^{n_k} M_{(u')}(x_{i_1}^1 \dots x_{i_k}^k)^2 \omega^u - \sum_{w \subset u} V_w \tag{5.50}$$

The main and total Sobol' sensitivity indices are consequently retrieved according to their definition

$$S_u = \frac{V_u}{V} \tag{5.51}$$

$$S_{T,u} = \sum_{u \subseteq v \subseteq \mathscr{U}} \frac{V_v}{V} \tag{5.52}$$

Application for 3 RVs

For illustration purposes, we consider the model $\mathscr{M}(x_1, x_2, x_3)$ of $m = 3$ RVs. The latter is evaluated for each RV of the set $u \subseteq \{1,2,3\}$, following their associated collocation points n_u. Consequently, the model $\mathscr{M}$ is evaluated for all the possible combinations of the RVs. The partial variance V_u defined in equation (5.50), is updated for $m = 3$ RVs, through a specific re-arrangement of the evaluations of the $\mathscr{M}(x_1, x_2, x_3)$, such as

- for the RV X_1: $\{u\} = \{1\}$ and $\{u'\} = \{2,3\}$, the partial variance V_1 reads

$$V_1 = \sum_{i_1=1}^{n_1} M_{(2,3)}(x_{i_1}^1)^2 \omega^1 - \sum_{w \subset u} V_w \tag{5.53}$$

  where $M_{(2,3)} = \sum_{i_2=1}^{n_2} \sum_{i_3=1}^{n_3} M(x_{i_1}^1, x_{i_2}^2, x_{i_2}^3) \omega^2 \omega^3$.

- for the RV X_2: $\{u\} = \{2\}$ and $\{u'\} = \{1,3\}$, the partial variance V_2 reads

$$V_2 = \sum_{i_2=1}^{n_2} M_{(1,3)}(x_{i_2}^2)^2 \omega^2 - \sum_{w \subset u} V_w \tag{5.54}$$

  where $M_{(1,3)} = \sum_{i_1=1}^{n_1} \sum_{i_3=1}^{n_3} M(x_{i_1}^1, x_{i_2}^2, x_{i_2}^3) \omega^1 \omega^3$.

- for the RV X_3: $\{u\} = \{3\}$ and $\{u'\} = \{1,2\}$, the partial variance V_2 reads

$$V_3 = \sum_{i_3=1}^{n_3} M_{(1,2)}(x_{i_3}^3)^2 \omega^3 - \sum_{w \subset u} V_w \tag{5.55}$$

  where $M_{(1,2)} = \sum_{i_1=1}^{n_1} \sum_{i_2=1}^{n_2} M(x_{i_1}^1, x_{i_2}^2, x_{i_2}^3) \omega^1 \omega^2$.

Sobol' indices of first-order S_1, S_2 and S_3, are thus deduced by dividing the associated partial variance $V_{i,\ i \in \{1,2,3\}}$ by the total variance, following their definition in equation (5.51).

The Sobol' indices are known to be good descriptors of the sensitivity of the model response to its input parameters. In contrast to Morris indices (qualitative analysis) [117], allowing hierarchization of the input parameters according to their impact on the output, Sobol' indices quantify not only the impact of each RV on the output but all the interactions between the M input quantities.

5.2 Domain Decomposition method for stochastic analysis

The **deterministic** DD method, as presented in section (2.1.1), is based on the evaluation of the impulse responses of the sub-systems. The solution of the global system is built afterward through a linear combination of these partial solutions, evaluated only once and referred to as **deterministic**. For the stochastic case, the variations around the nominal values of the RVs in a sub-system require a re-evaluation of the impulse responses characterizing it. Without loss of generality, we base our stochastic analysis on the SC method. While retaining the core of the DD method, its formulation will be adapted for the stochastic scenario in the following section.

Based on the theoretical foundations of the stochastic collocation method outlined in section (5.1.1), and the DD's general principle presented in section (2.1.1), the evaluation of the global **stochastic** solution V_j^k of the linear system G, defined in section (2.1.1), consists mainly on projecting the general DD's formula (2.5) on Lagrange polynomial basis of a given order.

Let's consider the model $\mathscr{M}$ of M input variables $(x_1,...,x_M)$, whose polynomial approximation on the Lagrange polynomial basis of orders $(n_1,...,n_M)$, is given by equation (5.13). We suppose that the model $\mathscr{M}(x_1,..,x_M)$ for a given system is represented by the voltage $V_j^k(x_1,..,x_M)$ of the sub-system k as follows:

$$V_j^k(x_1,...,x_M) = \sum_{\{i\}} h_{ij}^k\big(x_1,...,x_M\big) * V_{si}^k\big(x_1,...,x_M\big) + \sum_{\{l\}} h_{lj}^k\big(x_1,...,x_M\big) * V_{\sim l}^k\big(x_1,...,x_M\big) \quad (5.56)$$

We recall that the first term of the right-hand member of equation (5.56) reflects the contributions of the real sources V_{si}^k, while its second term gives the contributions of the equivalent sources $V_{\sim l}^k$ at the interface(s) level to the output V_j^k, through the corresponding impulse responses h_{ij}^k and $h_{\sim l}^k$. Both these responses depend on the input set $(x_1,...,x_M)$ and need to be

re-evaluated if one or more inputs vary. Similarly, the equivalent sources $V^k_{\sim l}$ also depend on the M input variables. They translate the contributions of the dispersed sources in the neighboring sub-systems and implicitly feature other impulse responses evaluated for the set of M input parameters. The detailed description of the equation as well as the sub-indices $\{i\}$ and $\{l\}$ are given in section (2.1.1). To lighten the upcoming equations, we introduce the following notation

$$C^k_{Rs}(x_1,...,x_M) = \sum_{\{i\}} h^k_{ij}(x_1,...,x_M) * V^k_{si}(x_1,...,x_M) \tag{5.57}$$

$$C^k_{\sim s}(x_1,...,x_M) = \sum_{\{l\}} h^k_{lj}(x_1,...,x_M) * V^k_{\sim l}(x_1,...,x_M) \tag{5.58}$$

where $C^k_{Rs}(x_1,...,x_M)$, respectively $C^k_{\sim s}(x_1,...,x_M)$, refers to the contribution of the real sources, respectively the equivalent sources.

The **stochastic** DD method's formulation is thus retrieved by projecting its deterministic formula (5.56) on the Lagrange polynomial basis, following the equation (5.13), such as

$$\begin{aligned} V^k_j(x_1,...,x_M) &\approx \sum_{t_1=0}^{n_1} ... \sum_{t_M=0}^{n_M} V^k_j\left(x_1{}^{(t_1)},...,x_M{}^{(t_M)}\right)\left(L^1_{t_1}\otimes ...\otimes L^M_{t_M}\right) \\ &\approx \sum_{t_1=0}^{n_1} ... \sum_{t_M=0}^{n_M} \left[C^k_{Rs}\left(x_1{}^{(t_1)},...,x_M{}^{(t_M)}\right) + C^k_{\sim s}\left(x_1{}^{(t_1)},...,x_M{}^{(t_M)}\right)\right]\left(L^1_{t_1}\otimes ...\otimes L^M_{t_M}\right) \end{aligned} \tag{5.59}$$

5.2.1 Uncertainty quantification based on stochastic DD method

Due to the Lagrange polynomials property (Kronecker symbol) and based on quadrature rules, the mean and variance of the M-dimensionnal output V^k_j are respectively deducted from equations (5.11) and (5.12). The expectation of the output V^k_j reads

$$\begin{aligned} \mathbb{E}\left[V^k_j(X_1,...,X_M)\right] &\approx \sum_{t_1=0}^{n_1} ... \sum_{t_M=0}^{n_M} \omega_{t_1}...\omega_{t_M} V^k_j\left(x_1^{(t_1)},...,x_M^{(t_M)}\right) \\ &\approx \sum_{t_1=0}^{n_1} ... \sum_{t_M=0}^{n_M} \omega_{t_1}...\omega_{t_M}\left[C^k_{Rs}\left(x_1{}^{(t_1)},...,x_M{}^{(t_M)}\right) + C^k_{\sim s}\left(x_1{}^{(t_1)},...,x_M{}^{(t_M)}\right)\right] \\ &\approx \sum_{t_1=0}^{n_1} ... \sum_{t_M=0}^{n_M} \left[C^{k'}_{Rs}\left(x_1{}^{(t_1)},...,x_M{}^{(t_M)}\right) + C^{k'}_{\sim s}\left(x_1{}^{(t_1)},...,x_M{}^{(t_M)}\right)\right] \end{aligned} \tag{5.60}$$

where

$$C_{Rs}^{k'}\left({x_1}^{(t_1)},...,{x_M}^{(t_M)}\right) = \omega_{t_1}...\omega_{t_M} C_{Rs}^{k}\left({x_1}^{(t_1)},...,{x_M}^{(t_M)}\right) \tag{5.61}$$

$$C_{\sim s}^{k'}\left({x_1}^{(t_1)},...,{x_M}^{(t_M)}\right) = \omega_{t_1}...\omega_{t_M} C_{\sim s}^{k}\left({x_1}^{(t_1)},...,{x_M}^{(t_M)}\right) \tag{5.62}$$

Similarly, the variance is expressed as follows:

$$\begin{aligned} Var\left[V_j^k(X_1,...,X_M)\right] &= \sum_{t_1=0}^{n_1}...\sum_{t_M=0}^{n_M} \omega_{t_1}...\omega_{t_M} V_j^k\left(x_1^{(t_1)},...,x_M^{(t_M)}\right)^2 - \mathbb{E}\left[V_j^k(X_1,...,X_M)\right]^2 \\ &= \sum_{t_1=0}^{n_1}...\sum_{t_M=0}^{n_M}\left[C_{Rs}^{k"}\left({x_1}^{(t_1)},...,{x_M}^{(t_M)}\right)^2 + C_{\sim s}^{k"}\left({x_1}^{(t_1)},...,{x_M}^{(t_M)}\right)^2\right] \\ &\quad - \mathbb{E}\left[V_j^k(X_1,...,X_M)\right]^2 \end{aligned} \tag{5.63}$$

where

$$C_{Rs}^{k"}\left({x_1}^{(t_1)},...,{x_M}^{(t_M)}\right)^2 \approx \omega_{t_1}...\omega_{t_M} C_{Rs}^{k}\left({x_1}^{(t_1)},...,{x_M}^{(t_M)}\right)^2 \tag{5.64}$$

$$C_{\sim s}^{k"}\left({x_1}^{(t_1)},...,{x_M}^{(t_M)}\right)^2 \approx \omega_{t_1}...\omega_{t_M} C_{\sim s}^{k}\left({x_1}^{(t_1)},...,{x_M}^{(t_M)}\right)^2 \tag{5.65}$$

5.2.2 Sensitivity analysis based on stochastic DD method

The Sobol' indices, as presented in section (5.1.2), are written in terms of partial variances. Their evaluation using the SC-DD association consists of deducing the partial variance of the stochastic output V_j^k.

By identification to the equation (5.50), the partial variance related to the RV X_u evaluated using the DD method is written as follows:

$$V_u = \sum_{i_1=1}^{n_1}...\sum_{i_k=1}^{n_k} \left(V_j^k\right)_{u'}(x_{i_1}^1...x_{i_k}^k)^2\omega^u - \sum_{w\subset u} V_w \tag{5.66}$$

The new output $\left(V_j^k\right)_{u'}$ refers to the model evaluated for the complementary set u'. Its expression depends on the new terms $\left(C_{Rs}^k\right)_{u'}$ and $\left(C_{\sim s}^k\right)_{u'}$ translating respectively the contribution of real and equivalent sources in the sub-system k for the complementary set u'. Their respective expressions are given by

$$\left(C_{Rs}^k\right)_{u'}\left(x_1,...,x_k\right) = \sum_{\{i\}}\left(h_{ij}^k\right)_{u'}\left(x_1,...,x_k\right) * \left(V_{si}^k\right)_{u'}\left(x_1,...,x_k\right) \tag{5.67}$$

$$\left(C_{\sim s}^k\right)_{u'}\left(x_1,...,x_k\right) = \sum_{\{l\}}\left(h_{lj}^k\right)_{u'}\left(x_1,...,x_k\right) * \left(V_{\sim l}^k\right)_{u'}\left(x_1,...,x_k\right) \tag{5.68}$$

The partial variance V_u can be deducted from the square values of the weighted terms $(C^k_{Rs})_{u'}$ and $(C^k_{\sim s})_{u'}$, and the Sobol' indices can thus be retrieved following their definition in section (5.1.2).

In synthesis, the Stochastic Collocation Domain Decomposition (SC-DD) association assesses the **stochastic** response (mean and variance) as well as Sobol' indices of the global system based on **deterministic** partial solutions. In other words, this offline-online strategy evaluates the model V^k_j, through the deterministic terms C^k_{Rs} and $C^k_{\sim s}$, n' number of times[4] in the offline level first. Then, the stochastic response is yielded through the online phase that combines the interactions between the RV(s) of each sub-system. Depending on the studied system and the decomposition, a given sub-system can feature one or several input variables. It is also possible that a sub-system doesn't feature any of the M inputs or features them all, for which the equation (5.59) can be further simplified. With the intrinsic advantages of each method, SC and DD, their association allows easy formulation for both UQ and SA.

5.3 Stochastic DD method for uncertainty quantification and sensitivity analysis

With the theoretical foundations of the new stochastic DD method in place, different numerical applications will be presented in this section. For different configurations, the aim is to validate the SC-DD association while demonstrating its main advantages.

5.3.1 Propagation of uncertainties within sub-systems

We begin by demonstrating the DD method's ability to propagate uncertainties within the systems, through two applications of transmission line networks featuring uncertainty in their input parameters. The uncertainty quantification will be assessed based on the theoretical expressions of mean and variance of the stochastic outcome V^k_j, established earlier.

5.3.1.1 First case study: field-to-wire coupling

Resolution of the global system

In EMC real-world problems, field-to-wire coupling is a significant concern as it can result

[4]This number depends on the number of RVs in the sub-system and the collocation points. For instance, for the same number of collocation points, $n = 3$ for instance, n' equals 3, respectively, 9 for 1, respectively, 2 RVs.

in electromagnetic interference (EMI), and may potentially disrupt the proper functioning of electronic devices and/or systems. With uncertainties arising in these systems, it is crucial to examine whether the variations in the input parameters cause defective functioning. Within this framework, we study the transmission line network in Figure (5.1), where a part of the shielded transmission lines go inside a closed electromagnetic cavity (see Figure (5.2a)). Due to imperfect shielding connection or aging of the electrical wires, the shielding efficiency is deficient at the localized point P of the line L_3. Consequently, a field-to-wire coupling occurs at this point, and the network is prone to interferences caused by the coupling of the electric field measured in the cavity. The electric field, measured at the receptor point R in Figure (5.2a), is

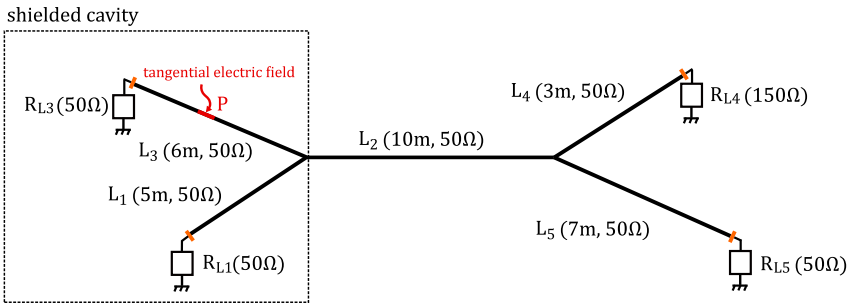

Figure 5.1: *Schematic of the global transmission line network with the coupling electric field at the point P.*

the response of the cavity to a Gaussian excitation at the emitter E, defined by equation (2.38) for $A = 100V$, $\sigma = 1.26ns$ and $t_c = 12ns$. Its tangential component, evaluated in the time domain (see the curve in blue in Figure (5.2b)), falls back to 0 due to losses introduced in the electromagnetic cavity according to the approach described in the thesis by Raphaël Vernet [144]. The modeling of both the electromagnetic cavity and the transmission line network is carried out using the FDTD numerical method.

The coupling of this field to the line L_3 at the point P creates an induced voltage source denoted $V_{P,3}$. At the level of the load resistance R_{L3}, its propagation in the network is recorded with different magnitudes due to the mismatch at the junction (see Figure (5.3a)). The frequency spectrum of the voltage V_3 is, on the other hand, the image of the coupled field spectrum with different magnitude levels (see Figure (5.3b)).
We suppose that uncertainties are associated with both the characteristic impedance Z_{c4} of the line L_4, and the load resistance R_{L5} of the line L_5, they are thus modeled as RVs, following a uniform distribution law on $[-1,1]$. Their respective intensities α is equal 5% and 15%. The electric coupled field E_p at the punctual point P of the line L_3 is considered an RV as well

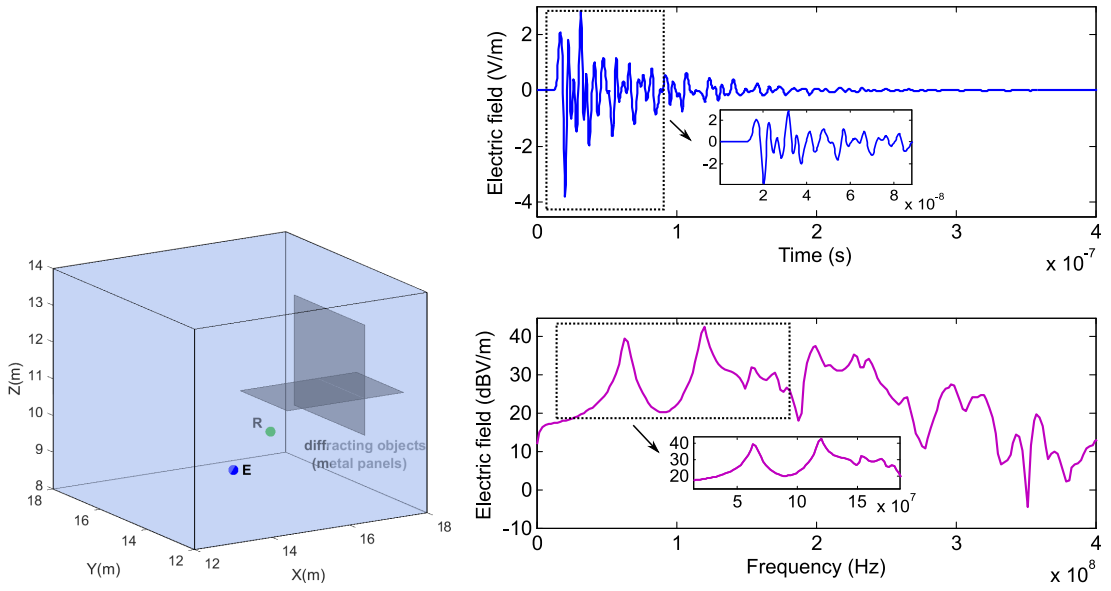

(a) (b)

Figure 5.2: *Schematic 3D representation of the electromagnetic cavity (a), tangential electric field measured at the receptor point R in both time and frequency domains (b).*

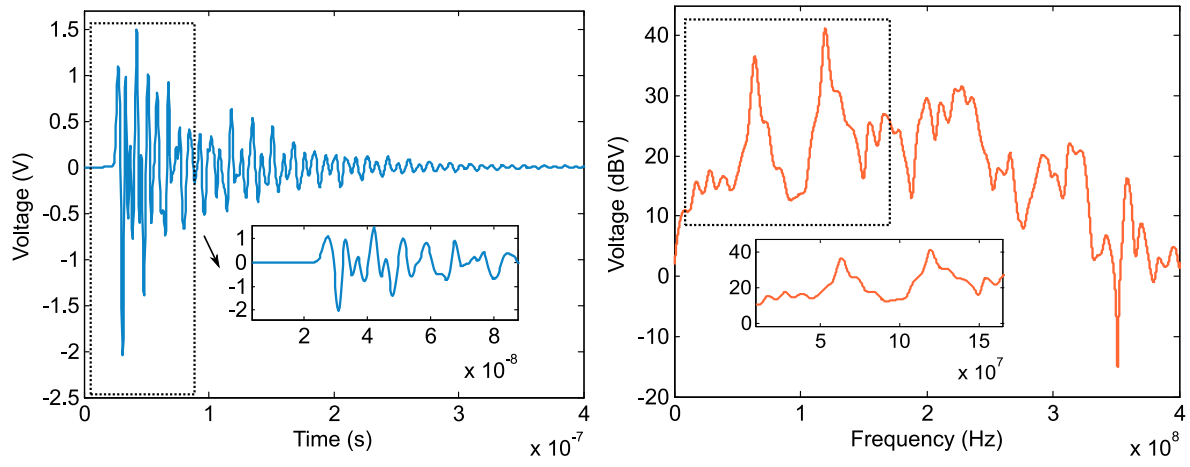

(a) (b)

Figure 5.3: *Voltage V_3 across the load resistance R_{L3} evaluated in both time (a) and frequency (a) domains.*

due to uncertainties introduced in the shielded electromagnetic cavity related to the excitation source at the emitter point E. We suppose that the width of mid-height σ of the Gaussian pulse is uncertain with an intensity of $\alpha = 25\%$ following a uniform law on $[-1, 1]$. The induced voltage source $V_{P,3}$ at the coupling point P is consequently considered a random variable too.

To simplify notation in the following, the RVs $V_{P,3}$, Z_{c4} and R_{L5} will be referred to as R_1, R_2 and R_3 in the same order. Each of these input parameters $R_{i\in\{1,2,3\}}$ can be defined as follows:

$$R_i = R_i^0(1+\alpha X) \tag{5.69}$$

where R_i^0 and α stand respectively for the initial value and the intensity of the RV, and X follows a certain distribution law.
First, we evaluate the voltage V_3 for three cases:

- case 1: refers to the nominal configuration for which each RV equals its initial value R_i^0,
- case 2: refers to the values obtained by considering the lower bound of the interval, such as $R_i = R_i^0(1-\alpha)$,
- case 3: refers to the values obtained by considering the upper bound of the interval, such as $R_i = R_i^0(1+\alpha)$.

From the results in Figure (5.4a), small variations around the initial (nominal) values of the RVs yield different outputs of the voltage V_3. We observe differences in signal magnitudes with the appearance of new reflections depending on the reflection coefficients at the junction and the load end of line L_5, due respectively to the effect of the characteristic impedance Z_{c4}, and the load resistance R_{L5}. The effect of the variation of the induced voltage source $V_{P,3}$ on the other hand, is better observed in the frequency domain. From the results in Figure (5.4b), the magnitude levels are different for the three cases. The variation of the electric field, and subsequently the voltage $V_{P,3}$, has a strong influence on the output V_3. These results demonstrate the impact of variations of the inputs on the voltage V_3 and highlight the interest in conducting a stochastic analysis to account for the uncertainties in the input parameters.
Based on the equations (5.15) and (5.16), mean and variance values of the QoI, i.e. the voltage V_3, are evaluated to gain insight into its expected value and dispersion.
To begin with, we represent in Figure (5.5) the voltage V_3 obtained for the 10 000 realizations of the considered RVs, i.e. $V_{P,3}$, Z_{c4} and R_{L5}.
The multiple outputs, evaluated for N draws, form a distribution that showcases the full range of variation of the QoI. By overlaying the mean value of these N evaluations within the distribution, a first overview of the central tendency of the output is observed.
To better quantify the dispersion of the values around their mean, we evaluate the standard deviation, as reported in Figure (5.6).
From the obtained results, the standard deviation varies over the considered time interval. The dispersion of values around their mean is better observed in the frequency domain in Figure (5.6b). The small variation of the standard deviation suggests that the values are relatively

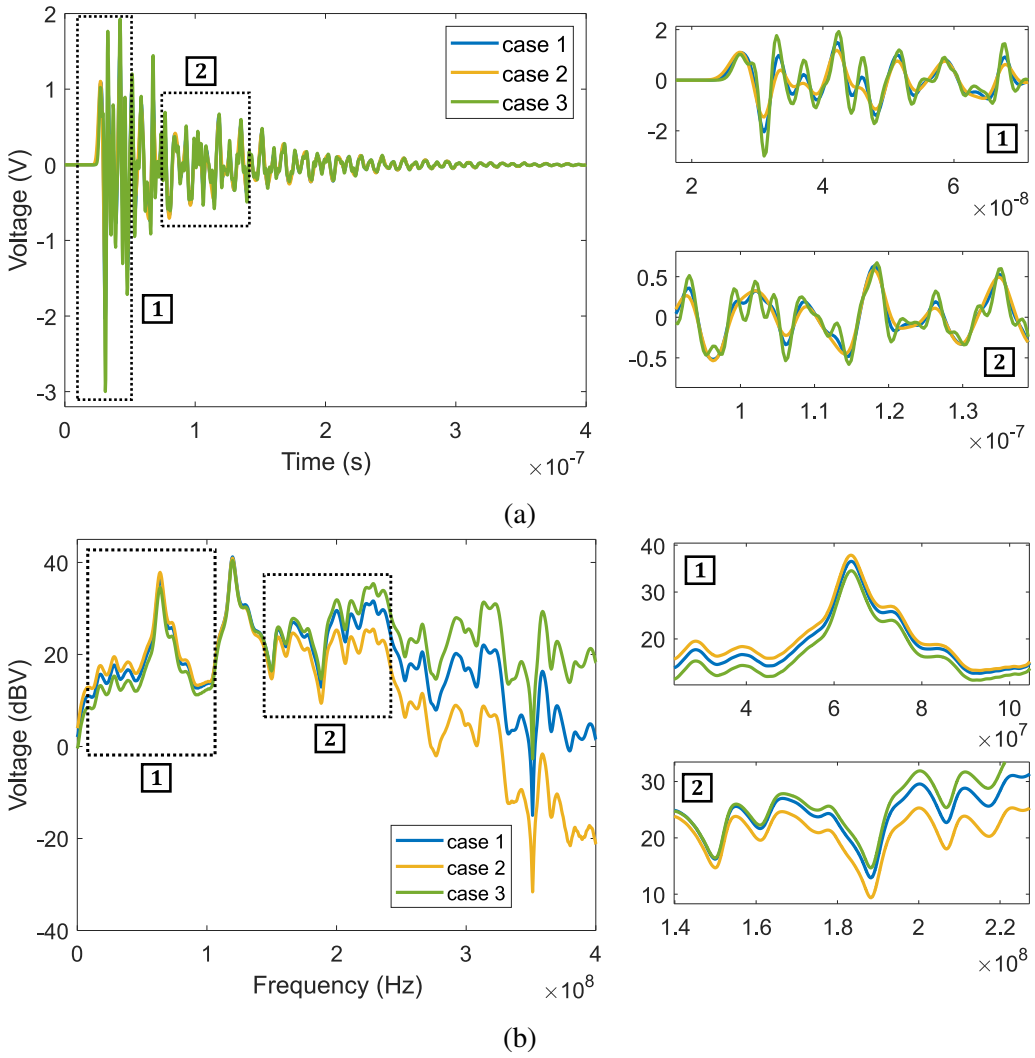

Figure 5.4: *Voltage V_3 across the load resistance R_{L3} for the three cases of parametric study evaluated in both time (a) and frequency (b) domains.*

consistent and don't deviate significantly from the average value, whereas at some frequencies its higher values indicate an important variability of the output.

Although the MC method provides accurate results, it is computationally expensive and time-consuming as it requires a high number of realizations. Note that as part of this study, the simulations carried out with the software CST Cable® were automated by driving the software via Matlab®. The tool enables to carry the simulation of each RV and export the corresponding result. This automation eases the use of the MC method, however, powerful machines are still required, along with considerable computer storage capacity. Alternatively, the stochastic

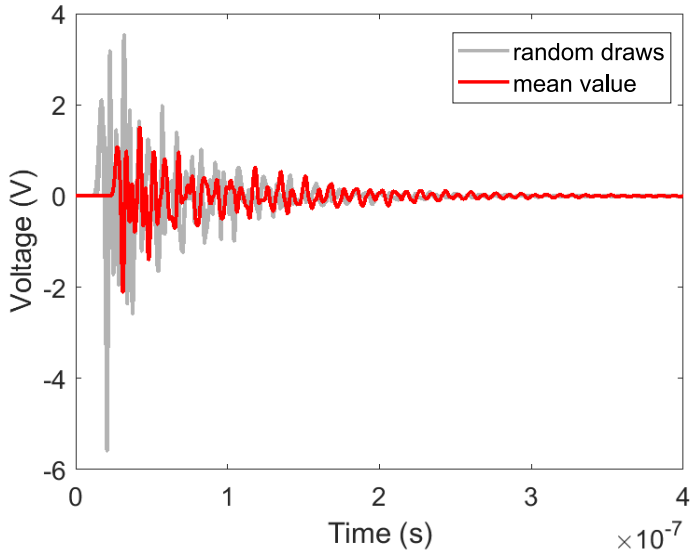

Figure 5.5: *Random draws of the output using the MC method (in grey), mean value of the output (in red), for* $N = 10\,000$.

analysis will be held using the SC method. First, both mean and standard deviation values are evaluated for 5, 7 and 9 collocation points. In Figure (5.7), the output approaches a stable pattern as the number of points increases. The convergence will be assumed reached with 7 collocation points, as the corresponding result is very close to the one obtained with 9 points.

To ensure that the obtained results with the SC are reliable, we compare the moving average[5] at the instant $t = 0.14\mu s$ using the MC for 10 000 random draws, and the SC method for 5, 7 and 9 points.

Based on Figure (5.8a), the blue curve shows important fluctuation, suggesting significant variation in the underlying data. As the number of draws increases, the moving average seems to converge towards a more stable result. This convergence was reached with a very large number of draws, compared to the SC method for which 7 points allowed leaning towards the convergence. These first results emphasize the main advantage of the SC technique: its high convergence rate. However, the method lacks a criterion for convergence and is assumed to be reached with 7 points because of the closeness of the obtained results with 9 points. This issue is addressed by evaluating the Leave-One-Out (LOO) error [145]. The LOO is based on the evaluation of the model when one data is "left out" from the dataset. The model is then performed using the remaining data points, and the outcome is assessed based on how well

[5]The moving average is used to analyze most frequently time series by creating a series of averages of different selections of the full data set.

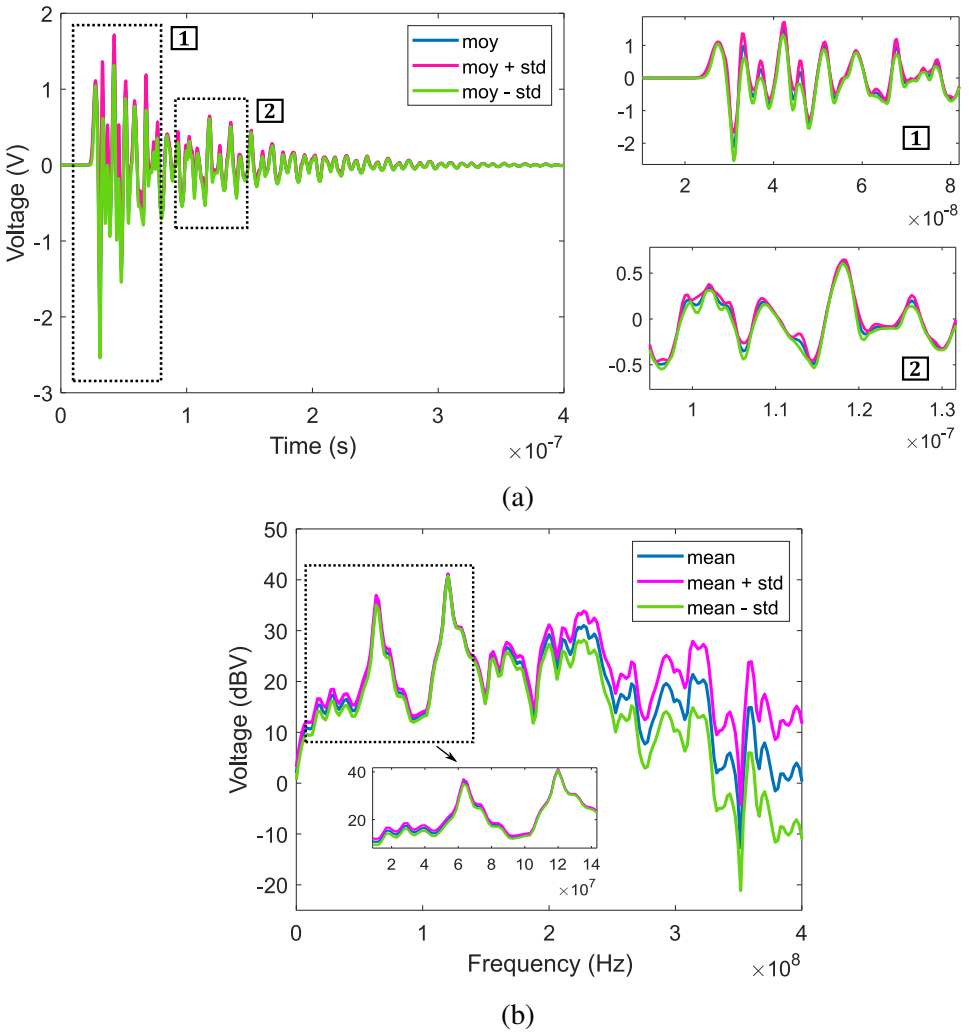

(a)

(b)

Figure 5.6: *Mean and standard deviation values of the voltage V_3 using the MC method in both time (a) and frequency (b) domains.*

the model predicts the left-out data point. If the LOO is close to 1, the metamodel is highly modified. It is expressed on the basis of the mean-square error between the original model $\mathscr{M}$ and the surrogate model $\hat{\mathscr{M}}$ (evaluated with the new dataset) as follows:

$$LOO = \frac{1}{n}\sum_{i}^{n}\left(\frac{\hat{\mathscr{M}}_{/i}(X_i) - \mathscr{M}_i}{\mathscr{M}_i}\right) \tag{5.70}$$

In our case, the surrogate model corresponds to the Lagrange polynomials approximation of the output V_3. The LOO decreases with the increasing of the number of collocation points used to build the model as reported in Figure (5.8b). The close values obtained for 7 ($1.4464e-8$), respectively 9 collocation points ($7.9316e-9$), confirm that the convergence is reached with 7

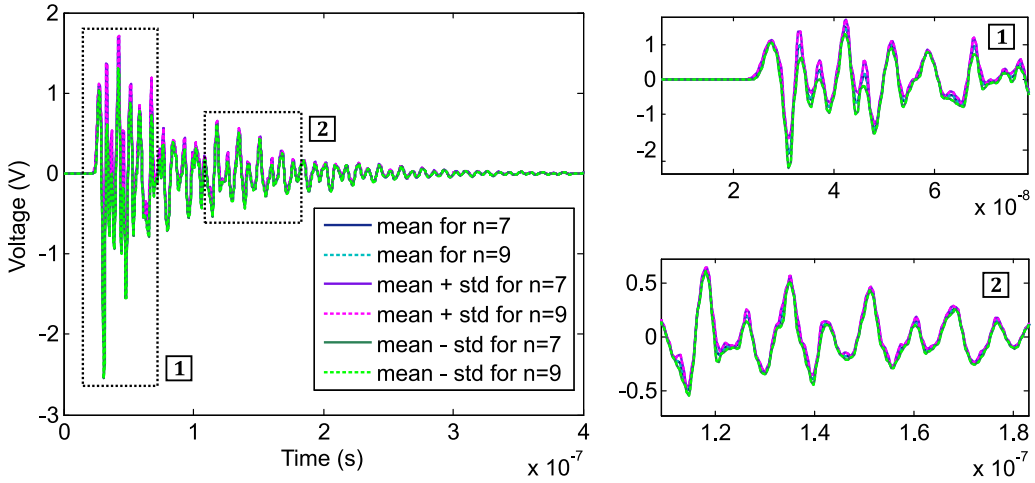

Figure 5.7: *Mean and standard deviation values of the voltage V_3 of the global network evaluated for 7 and 9 collocation points using the SC technique.*

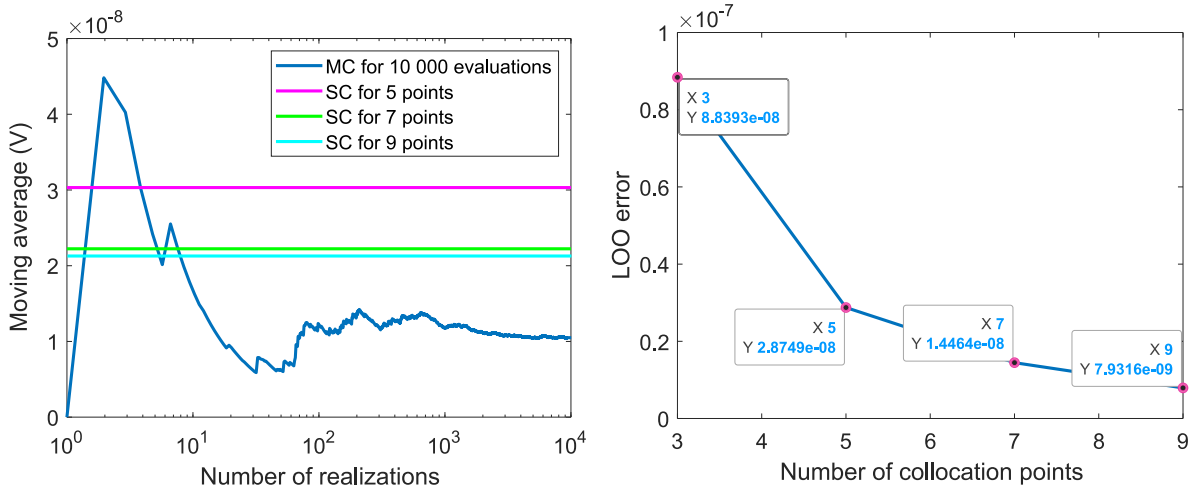

(a) (b)

Figure 5.8: *Analysis of the SC method's convergence according to the collocation points: moving average of the voltage V_3 evaluated for a specific instant using the MC and SC methods (a), LOO error evaluated for 3, 5, 7 and 9 collocation points (b).*

points.

These results offer valuable insights into the variability of the output, i.e. the voltage V_3, caused by the uncertainties related to the inputs (RVs). Due to the randomness of the electric field, the network is prone to interferences that may exceed threshold values defined either for standard norms or system validation. In real-world situations, two different operators can study this system. The first considers the transmission line network alone, while the second is interested

in the electromagnetic cavity and its coupling with a segment of a line of the network. From this standpoint, the DD method fits perfectly as it allows each operator to model its sub-system independently. Our focus is therefore placed now towards the evaluation of the stochastic response V_3^1 using the DD technique.

Resolution for the split system using the DD technique

We supposed that the global problem in Figure (5.1) is split at the middle of the line L_2 into two sub-networks as represented in Figure (5.9a).

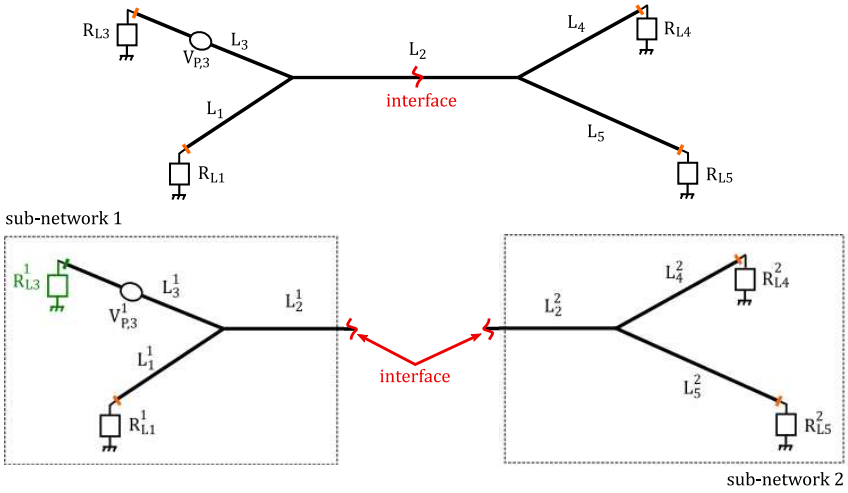

(a)

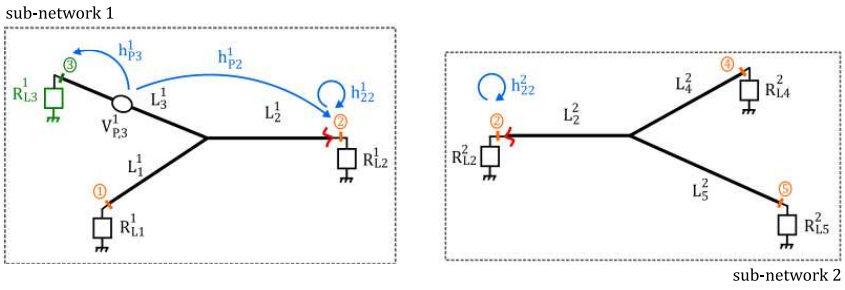

(b)

Figure 5.9: *Decomposition of the global network into two sub-networks at the middle of the line L_2 (a), Schematic representation of the impulse responses of each sub-network (b).*

The voltage V_3^1 is located in the sub-network 1, consequently, the deterministic DD method is applied based on equation (2.5) for $k = 1$ as follows:

$$\begin{aligned} V_3^1 &= h_{P3}^1 * V_{P,3}^1 + h_{23}^1 * V_{\sim 2}^1 \\ &= h_{P3}^1 * V_{P,3}^1 + h_{23}^1 * \left(h_{22}^2 * (h_{P2}^1 * V_{P,3}^1)\right) \end{aligned} \tag{5.71}$$

The first term $(h^1_{P3} * V^1_{P,3})$ gives the direct propagation of the induced voltage source $V_{P,3}$ to the output. The term $\left(h^2_{22} * (h^1_{P2} * V^1_{P,3})\right)$ on the other hand, translates the contribution of the sub-network 2 to the incoming voltage $(h^1_{P2} * V^1_{P,3})$ from the sub-network 1 to the interface level. Its product with the impulse response h^1_{23} gives the contribution of the equivalent source at the interface to the output.

Now that we have estimated the voltage V^1_3 using the DD method, we move on to the implementation of the stochastic DD technique for the stochastic analysis. In our case, the random response V^1_3 depends on three random variables, consequently, the two first moments are deducted from the general equations (5.60) and (5.63) for $M = 3$. As they both depend on the terms $C^{1'}_{Rs}$ and $C^{1'}_{\sim s}$, we start by adapting their expression based on the voltage V^1_3.
Following the decomposition, the RV R_1 is located in the sub-network 1, while both RVs R_2 and R_3 are located in the sub-network 2. The terms C^1_{Rs} and $C^1_{\sim s}$ can be simplified further by considering only the variables on which they depend. More specifically, the term C_{Rs} translates the contribution of the source $V_{P,3}$ to the output. As this latter is considered an RV (as an image of the electric field), the term C^1_{Rs} depends only on the RV R_1. The term $C^1_{\sim s}$ on the other hand, gives the contribution of both sub-networks to the interface, it thus depends on the three RVs. By identification of each of these contributions in equations (5.67) and (5.68), we obtain the explicit expressions of both terms C^1_{Rs} and $C^1_{\sim s}$.

$$C^1_{Rs}(r_1) = h^1_{P3} * V^1_{P,3}(r_1) \tag{5.72}$$

$$C^1_{\sim s}(r_1, r_2, r_3) = h^1_{23} * \left(h^2_{22}(r_2, r_3) * \left(h^1_{P2} * V^1_{P,3}(r_1)\right)\right) \tag{5.73}$$

Consequently, the terms $C^{1'}_{Rs}$ and $C^{1'}_{\sim s}$ are deducted from the weighted products:

$$C^{1'}_{Rs}\left(r_1{}^{(t_1)}\right) = \omega_{t_1} C^1_{Rs}\left(r_1{}^{(t_1)}\right) \tag{5.74}$$

$$C^{1'}_{\sim s}\left(r_1{}^{(t_1)}, r_2{}^{(t_2)}, r_3{}^{(t_3)}\right) = \omega_{t_1}\omega_{t_2}\omega_{t_3} C^1_{\sim s}\left(r_1{}^{(t_1)}, r_2{}^{(t_2)}, r_3{}^{(t_3)}\right) \tag{5.75}$$

To simplify the analysis, we assume the same order n of Lagrange polynomials for the projection of the voltage V^1_3. We start first by evaluating the expectation (mean) of the voltage V^1_3, its expression is given by

$$\begin{aligned}\mathbb{E}\left[V^1_3(R_1, R_2, R_3)\right] = &\sum_{t_1=0}^{n} \omega_{t_1}\left(h^1_{P3} * V^1_{P,3}\left(r_1{}^{(t_1)}\right)\right) \\ &+ \sum_{t_1=0}^{n}\sum_{t_2=0}^{n}\sum_{t_3=0}^{n} \omega_{t_1}\omega_{t_2}\omega_{t_3} * \left(h^1_{23} * \left(h^2_{22}(r_2{}^{(t_2)}, r_3{}^{(t_3)}) * \left(h^1_{P2} * V^1_{P,3}(r_1{}^{(t_1)})\right)\right)\right)\end{aligned} \tag{5.76}$$

Similarly, the variance is expressed as follows:

$$
\begin{aligned}
Var\left[V_3^1(R_1,R_2,R_3)\right] = & \sum_{t_1=0}^{n} \omega_{t_1} \left(h_{P3}^1 * V_{P,3}^1\left(r_1{}^{(t_1)}\right)\right)^2 \\
& + \sum_{t_1=0}^{n}\sum_{t_2=0}^{n}\sum_{t_3=0}^{n} \omega_{t_1}\omega_{t_2}\omega_{t_3} * \left(h_{23}^1 * \left(h_{22}^2(r_2{}^{(t_2)}, r_3{}^{(t_3)}) * \left(h_{P2}^1 * V_{P,3}^1(r_1{}^{(t_1)})\right)\right)\right)^2 \\
& - \mathbb{E}\left[V_3^1(r_1,r_2,r_3)\right]^2
\end{aligned}
\tag{5.77}
$$

For both mean and variance, the impulse responses $h_{\cdot\cdot}^1$ in sub-network 1 are only evaluated once since no parameter of the sub-network itself is modified. Its stochastic response however is given through the n evaluations of the source V_{P3} associated with the RV R_1. Whereas, the impulse response h_{22}^2 of the sub-network 2 is evaluated n^2 times as the latter features two RVs R_2 and R_3. This aspect represents a major advantage for the computational cost that will be discussed later in this chapter.

We first start by computing the equation (5.76) to evaluate the mean of the voltage V_3^1, and obtain the results reported in Figure (5.10).

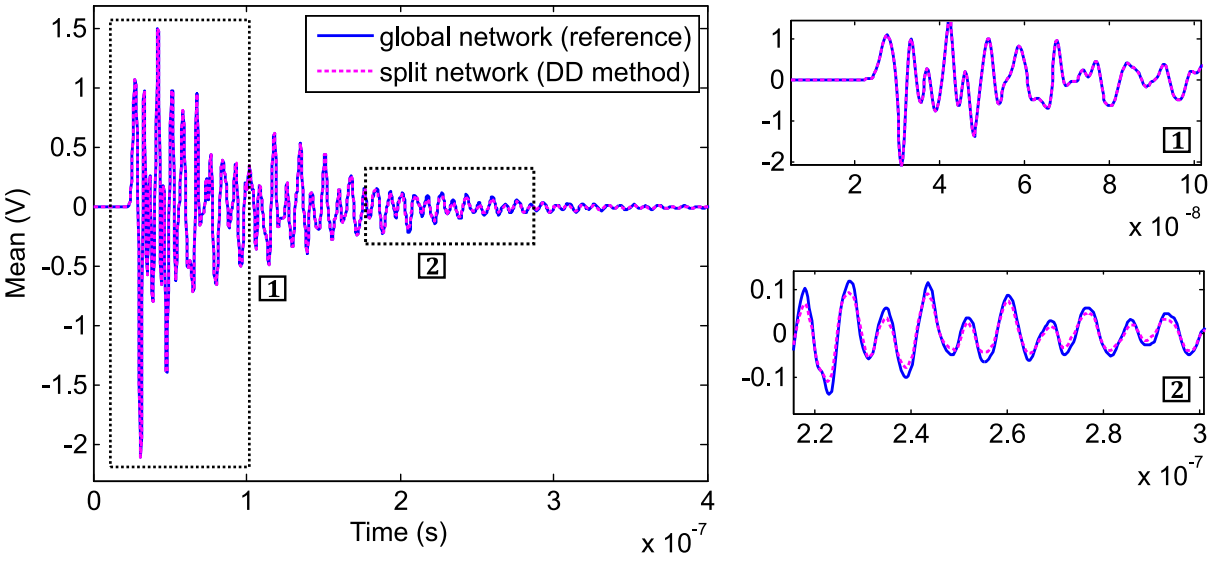

Figure 5.10: *Comparision of the mean value of the voltage V_3 for both the global (reference) and split (DD method) networks.*

The mean value evaluated with the stochastic DD method seems to approach the expected result in the first instants. Whereas from time $t = 0.82\mu s$ onwards, the obtained result doesn't follow the reference anymore. In fact, these differences are due to the "incomplete" formulation of

the voltage V_3^1, since the orders retrieving the multiple reflection of the induced voltage source $V_{P,3}$ are not considered. As we have demonstrated earlier in section (2.1.1), the retro-actions of each sub-network to the other are yielded through an additional term evaluated to a given order q. In this case, the differences are not very significant, especially since the reflections are rather negligible due to signal attenuation. However, in general, this aspect is particularly crucial in stochastic analysis since the assessment of mean and variance is based on weighted sums of the outcome V_j^k. Depending on the studied configuration, if the latter is not evaluated properly (missing reflections), the information contained in the two stochastic moments is therefore not exploratory.

Given that a similar decomposition configuration was previously studied, we refer the reader to section (3.2) for further details on the formulation. We give the new formulation of the voltage V_3^1 for which the multiple round trips of the induced voltage $V_{P,3}$ up to the order q are retrieved:

$$V_3^1 = h_{P3}^1 * V_{P,3}^1 + h_{23}^1 * V_{\sim 2,1}^1 + \sum_{i=2}^{q} h_{23}^1 * \left(h_{22}^2 * (h_{11}^2 * V_{\sim 2,i}^1)\right) \tag{5.78}$$

where $V_{\sim 2,i}^1$ is defined as the i-th order of the equivalent source at the interface level and is given by

$$V_{\sim 2,i}^1 = h_{22}^2 * (h_{22}^1 * V_{\sim 2,i-1}^1) \tag{5.79}$$

The voltage $V_{\sim 2}^1$ is denoted $V_{\sim 2,1}^1$ in the equation (5.78) as reference to the first order.

By evaluating the equation (5.78) to the order $q = 4$, the mean and variance of the voltage V_3^1 superimposes perfectly the reference given by the global network's simulation, as reported in Figure (5.11).

As a synthesis, the DD method proves its efficiency in propagating the uncertainty between the two sub-networks when higher orders are considered in the formulation, whether the uncertainties are linked to the excitation source itself or to network parameters. The implementation of the DD method is more interesting when both operators are different and do not depend on each other in time or space. Introducing uncertainties into the system represents a challenge, as the global system would have to be re-evaluated for the different possible combinations of the RVs' values. The SC-DD association overcomes this constraint, by modeling only the modified subsystems (featuring the uncertainties). This aspect allows consideration of different sources for the study of EMI in the system. It also allows significant time savings and important evaluation cost reduction.

5.3.1.2 Second case study: threshold analysis

Within the framework of reliability analysis, the threshold analysis may be considered to

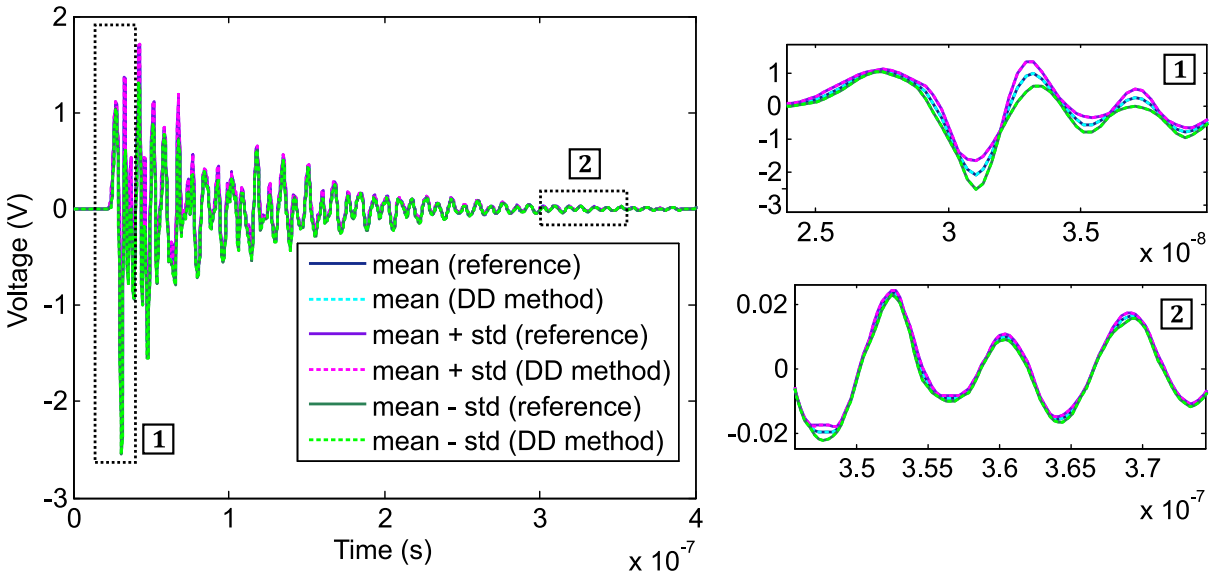

Figure 5.11: *Comparison of the mean and standard deviation values of the voltage V_3 for both the global (reference) and split (DD method for $q = 4$) networks.*

assess the highest potential risks of malfunctioning of a system. The most critical consequence of the uncertainties in the input parameters may concern the overvoltage and overcurrent values of the system's output. This latter may cause serious damage to sensitive electrical and electronic equipment, resulting in system failure.

In this context, we study the transmission line network in Figure (5.12) consisting of 6 RG-58 coaxial cables and 2 junctions and modeled using the commercial software CST Cable Studio®. The voltage V_{s1} injected at the entrance of line L_1 is the Gaussian pulse represented

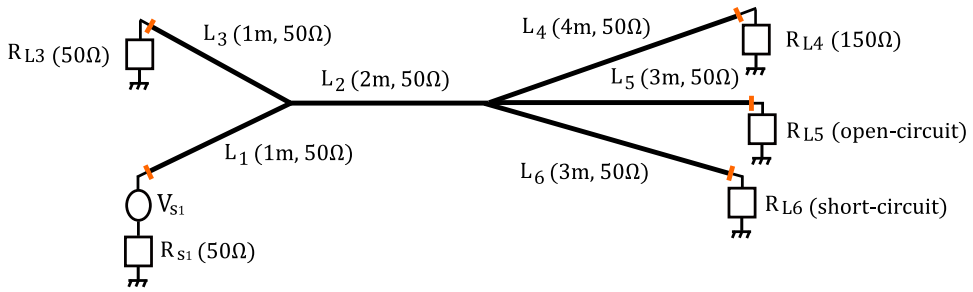

Figure 5.12: *Charastictic of the studied global network.*

in Figure (5.13). The parameters of the transient simulation performed with the commercial software are summarized in Table (5.1).

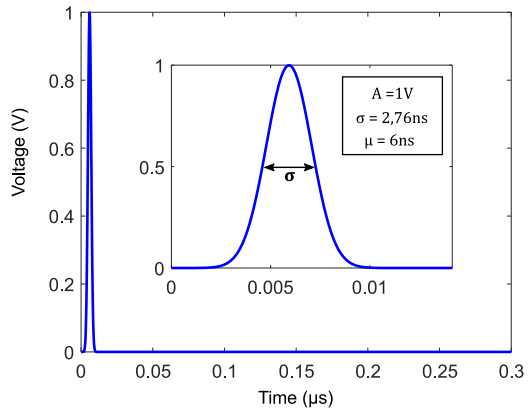

Figure 5.13: *The excitation source V_{s1}.*

Simulation task	"Transient"
Simulation duration	$0.3\mu s$
Maximum frequency	$300MHz$

Table 5.1: *Simulation parameters.*

Based on the SC method, we evaluate the stochastic response (mean and variance) of the QoI given by the voltage V_4 across the load resistance R_{L4}, when each of L_3, L_5 and L_6 as considered as RVs and defined by (5.69). To simplify notation in the following, the RVs L_3, L_5 and L_6 will be referred to as R_1, R_2 and R_3 in the same order. Their respective initial value R_i^0, intensity α and the law of distribution are summarized in Table (5.2).

	P^0	α (%)	Distribution law
L_3	0,9	20	$\sim \mathcal{N}(0,1)$
L_5	2,9	10	
L_6	2,9	10	

Table 5.2: *Mean values, intensities and distribution laws of the RVs.*

Based on the results in Figure (5.14), we assume that the convergence of both mean and standard deviation is reached with 7 collocation points given their closeness with the results obtained with 9 points.

We observe that the first peak of the Gaussian pulse, propagated within lines L_1, L_2 and L_4, is recorded with the same magnitude with no temporal shift since no uncertainties are associated with these lines. As time progresses, the stronger impact of the RVs in some instances is recorded. If we suppose that our generic system represented by the network in Figure (5.12), is compliant (e.g. for transmission or emission) for only one authorized absolute voltage value over $0.2V$, this condition may no longer be verified due to uncertainties in the input parameters. This information however isn't recovered from the mean and standard deviation, as they alone do not give the complete spectrum for a thorough stochastic analysis. To capture the full range

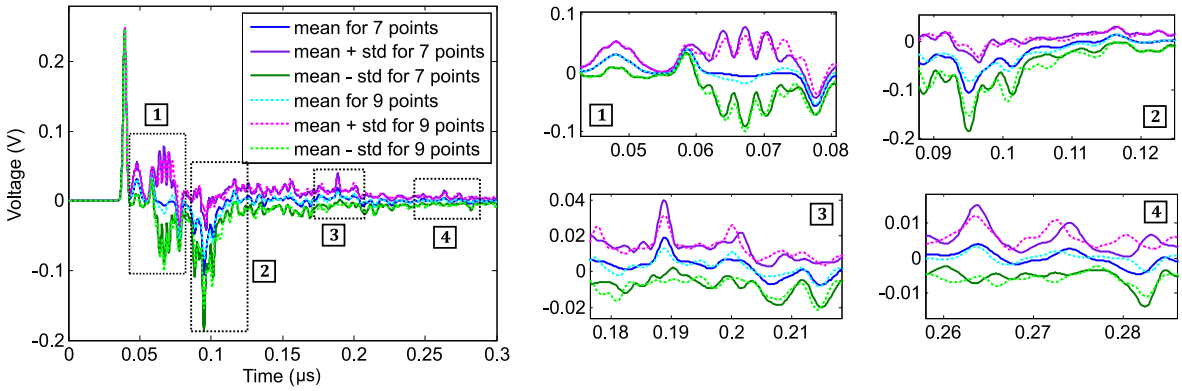

Figure 5.14: *Mean and standard deviation values of the voltage V_4 of the global network evaluated for 7 and 9 collocation points.*

of values that could accurately represent the underlying parameters, we define the confidence interval (CI). The latter acknowledges the variability in data by providing a range of values within which the output values are likely to reside. This interval takes into account the sampling variability and provides a better assessment of the output's possible values. We represent the upper and lower boundary of the confidence interval $]mean-3std, mean+3std[$, defined for a level of confidence equal to 95%. Based on random draws of the voltage V_4 as represented in Figure (5.15b), some RVs combinations result in voltage values that exceed the absolute threshold value $0.2V$ at some instants. The condition defined previously is no longer verified in this case, consequently, uncertainties in the input may cause malfunction or damage to the system.

We assume that this problem is now solved by the DD method, such that the network is split at the middle of the line L_2 into two sub-networks as shown in Figure (5.16). Following the principle of the DD technique in section (2.1.1), the voltage V_4^2, located at the sub-network $k=2$, is expressed as follows:

$$V_4^2 = h_{24}^2 * V_{\sim 2}^2 + h_{24}^2 * \underbrace{\left(h_{22}^2 * (h_{22}^1 * V_{\sim 2}^2)\right)}_{V_{\sim 2,1}^2} + \sum_{i=2}^{q} h_{24}^2 * \left(h_{22}^2 * (h_{22}^1 * V_{\sim 2,i}^2)\right) \tag{5.80}$$

where $V_{\sim 2}^2$ is the equivalent voltage at the exchange interface given by the product $(h_{12}^1 * V_{s1}^1)$, and $V_{\sim 2,i}$ is defined as its i-th order and expressed as follows:

$$V_{\sim 2,i}^2 = h_{22}^2 * (h_{22}^1 * V_{\sim 2,i-1}^2) \tag{5.81}$$

In this case, no physical voltage source is injected in the sub-network $k=2$, consequently, the only contribution to the measurand is retrieved through the direct propagation of the voltage

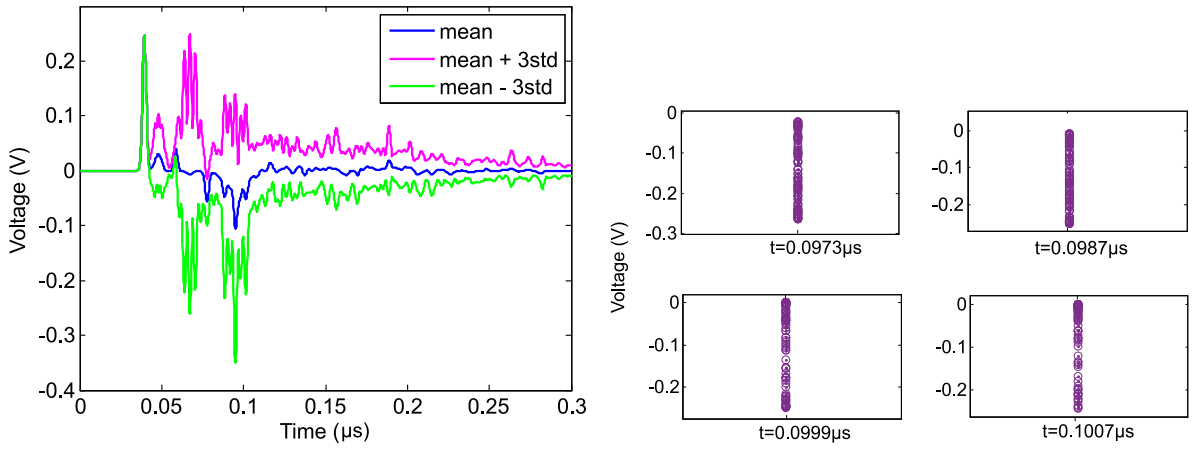

(a) (b)

Figure 5.15: *Mean and standard deviation values of the voltage V_4 using the SC method for 7 collocation points (a), random draws of the voltage V_4 at specific instants using the MC approach (b).*

source V_{s1}^1 given by the product $(h_{24}^2 * V_{\sim 2}^2)$, and its multiple round trips between the two sub-networks to the order q expressed by the additional term in equation (5.80).
As a result of the decomposition, the RV R_1 represented by the length L_3 is located in the sub-network 1, whereas the two RVs R_2 and R_3 are isolated in the sub-network 2. The stochastic term translating the contribution of the equivalent source to the output $C_{\sim s}^2$ in equation (5.68) is explicitly expressed by

$$C_{\sim s}^2(r_1, r_2, r_3) = h_{24}^2(r_2, r_3) * \left(h_{12}^1(r_1) * V_{s1}^1\right) \tag{5.82}$$

By assuming the same order n of Lagrange polynomials for the projection of the voltage V_4^2, the mean and standard deviation values of the stochastic voltage V_4^2 are respectively given by

$$\begin{aligned}
\mathbb{E}\left[V_4^2(R_1,R_2,R_3)\right] &= \sum_{t_1=0}^{n}\sum_{t_2=0}^{n}\sum_{t_3=0}^{n} \omega_{t_1}\omega_{t_2}\omega_{t_3} * \left(h_{42}^2(r_2^{(t_2)}, r_3^{(t_3)}) * \left(h_{12}^1(r_1^{(t_1)}) * V_{s1}^1\right)\right) \\
Var\left[V_4^2(R_1,R_2,R_3)\right] &= \sum_{t_1=0}^{n}\sum_{t_2=0}^{n}\sum_{t_3=0}^{n} \omega_{t_1}\omega_{t_2}\omega_{t_3} * \left(h_{42}^2(r_2^{(t_2)}, r_3^{(t_3)}) * \left(h_{12}^1(r_1^{(t_1)}) * V_{s1}^1\right)\right)^2 \\
&\quad - \mathbb{E}\left[V_4^2(r_1,r_2,r_3)\right]^2
\end{aligned} \tag{5.83}$$

In contrast to the previous case, the impulse responses $h_{\cdot\cdot}^1$ of sub-network 1 are evaluated n times, as the latter features the RV R_1.

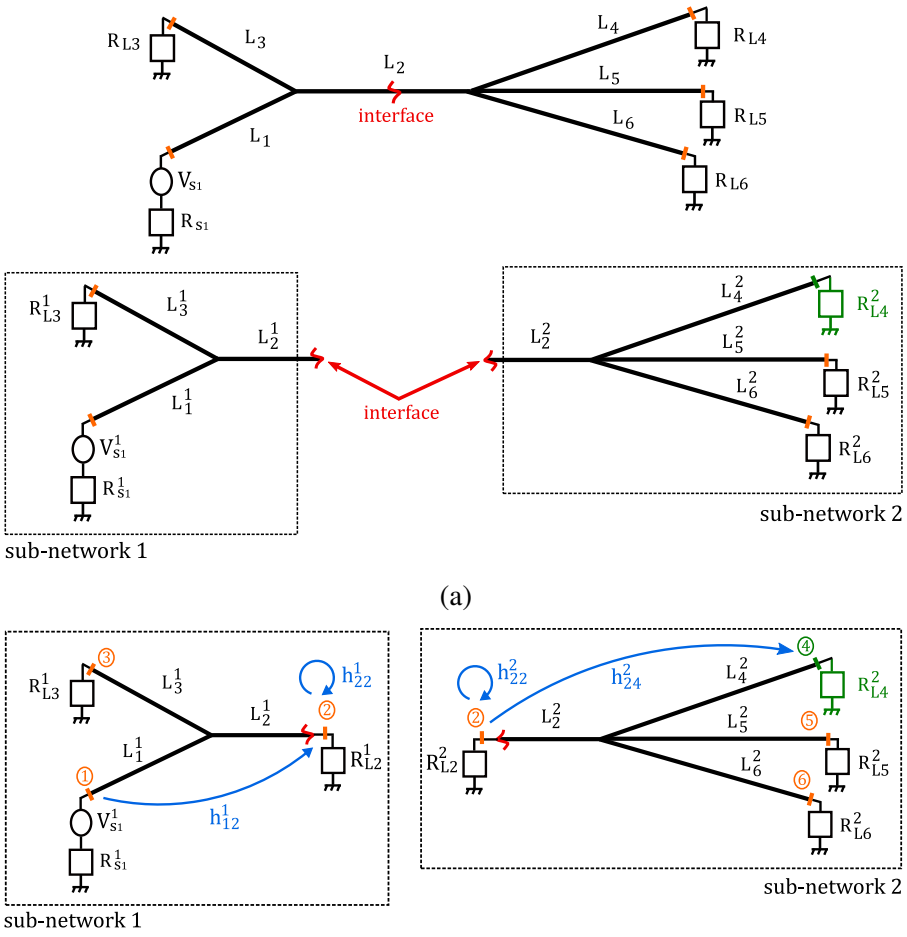

Figure 5.16: *Decomposition of the global network into two sub-networks at the middle of the line L_2 (a), Schematic representation of the impulse responses of each sub-network (b).*

Note that these equations only consider the propagation of the equivalent source $V^2_{\sim 2}$ to the output for demonstration purposes. The assessment of mean and variance of the voltage V^2_4 given by equation (5.80) can be easily deduced by considering the stochastic expression of the term $C^2_{\sim s}(r_1, r_2, r_3)$.

By computing the voltage V^2_4 to the order $q = 4$, the mean and standard deviation values are in very good agreement with the reference given by the global network's simulation. The DD technique proves, once again, its ability to propagate uncertainties within sub-network when both their parameters have been modified.

The stochastic study showed that some RV combinations exceed the defined threshold value in some instances, and may damage the system. The asynchronous nature of the DD technique offers a great advantage for RA studies as different combinations of RVs can be studied

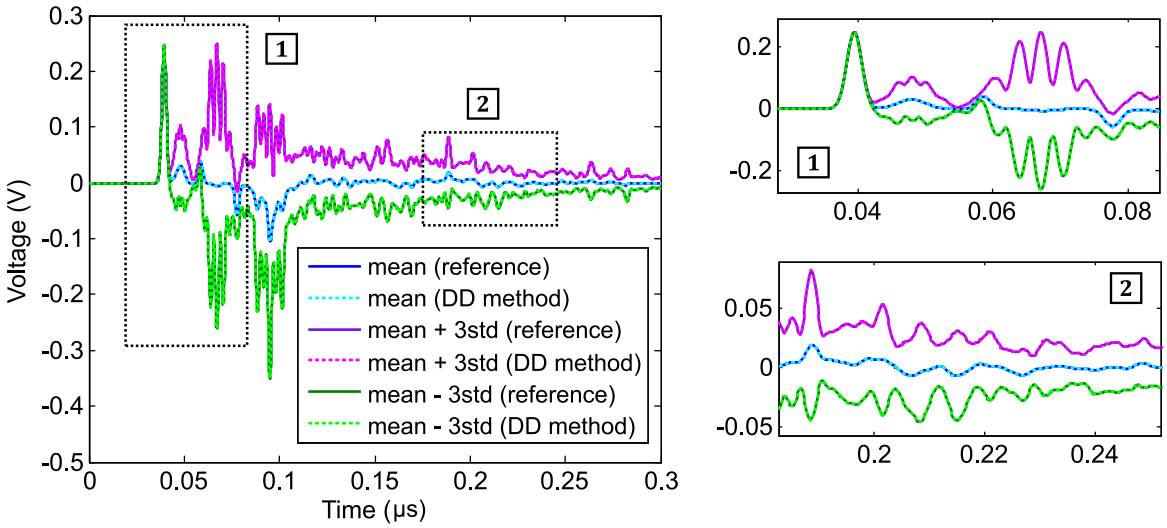

Figure 5.17: *Comparision of the mean and standard deviation values of the voltage V_3 for both the global (reference) and split (DD method for $q = 4$) networks.*

without re-evaluating the global system. In this configuration, although both sub-networks are re-evaluated through their impulse responses, the SC-DD association enables solving less complex systems with a lower stochastic dimension.

5.3.2 DD method for stochastic-parametric analysis

To go further with the stochastic analysis, different initial values, intensities or distribution laws of the RVs can be studied to investigate their respective impact on the variability of the output. In this section, we propose to study different stochastic configurations to highlight the additional advantage of the DD technique for stochastic parametric studies.

We consider the network of transmission lines of Figure (5.18), composed of 5 multi-conductor lines and 2 nodes, and modeled using the commercial software CST Cable®, whereas each bundle associated to the multi-transmission line $MTL_i, i \in \{1,2,...,5\}$ is composed of a group of single cables (LIFY_0qmm05, 0_AWG and 4_AWG) loaded from the software library, to which a screen is added serving as a ground plane. The excitation source is a Gaussian pulse of amplitude $1V$ injected at the input of conductor 1 of the MTL_1. We suppose that all conductors in each MTL$_i$ are of the same lengths, and all their load resistances equal 50Ω.

At the load resistance $R_{L3,2}$ of the second conductor of the MTL_3, we measure the crosstalk, reported in Figure (5.19a), caused by the proximity of conductors in the MTL.

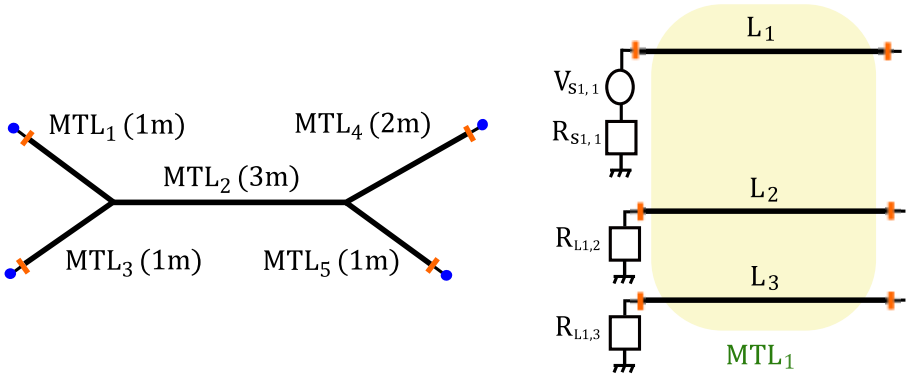

Figure 5.18: *Global transmission line network and schematic representation of the multiconductor* MTL_1.

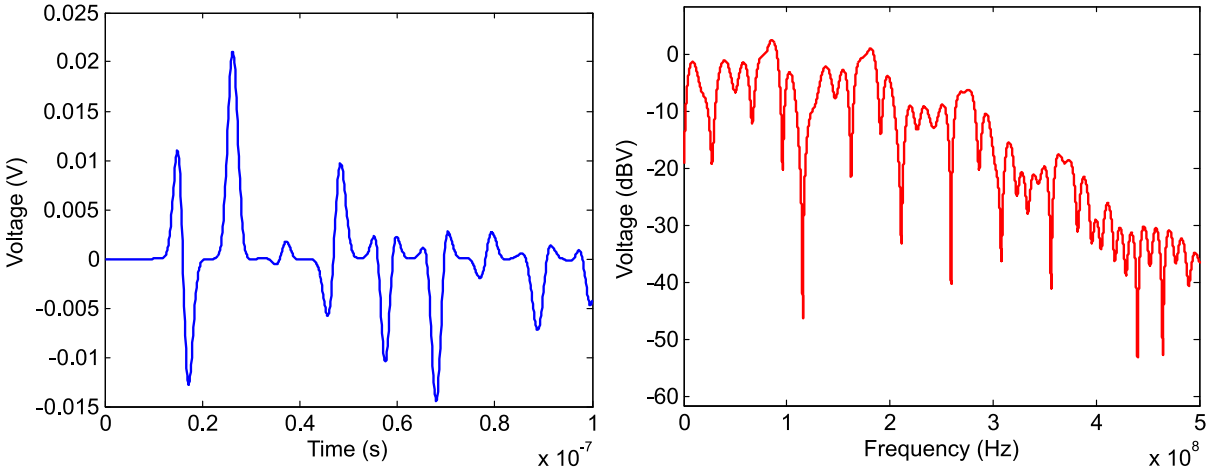

(a) (b)

Figure 5.19: *Voltage* $V_{3,2}$ *measured across the load resistance* $R_{L3,2}$ *of the second conductor* L_2 *of the* MTL_3 *in both time (a) and frequency (b) domains.*

We aim to quantify the impact of uncertainties, associated with the length in the multiconductor MTL_1 and the load resistance $R_{L3,2}$ of the line L_2 of the MTL_3, on the voltage $V_{3,2}$ measured across the load resistance $R_{L3,2}$ of the second conductor of the MTL_3.

Initially, the global network is studied considering several configurations of the distribution laws and uncertainty intensities for the two RVs. For the first configuration, the distribution law for both RVs varies while conserving the same intensities α. The second configuration, on the other hand, considers the same distribution law for each case and varies the intensities α. The details for both configurations A and B and their corresponding cases are summarized in

Table (5.3).

		L_1	$R_{L3,2}$
configuration A	case 1	$\alpha = 5\%$ uniform in [-1,1]	$\alpha = 20\%$ uniform in [-1,1]
	case 2	$\alpha = 5\%$ normal $\sim \mathcal{N}(0,1)$	$\alpha = 20\%$ uniform in [-1,1]
	case 3	$\alpha = 5\%$ uniform in [-1,1]	$\alpha = 20\%$ normal $\sim \mathcal{N}(0,1)$
configuration B	case 1	$\alpha = 3\%$ uniform in [-1,1]	$\alpha = 20\%$ uniform in [-1,1]
	case 2	$\alpha = 5\%$ uniform in [-1,1]	$\alpha = 1\%$ uniform in [-1,1]
	case 3	$\alpha = 10\%$ uniform in [-1,1]	$\alpha = 5\%$ uniform in [-1,1]

Table 5.3: *Multiple cases of the variation of either the distribution law (configuration A) or the uncertainty intensity α (configuration B) for the RVs.*

For all the studied cases, the standard deviation of the output is not constant over the considered time interval as shown in Figures (5.20) and (5.21). For configuration A, with uniform distribution laws for both RVs, the standard deviation is very low. For different laws for each RV, the mean value of the output is different and the standard variation is more important for case 3. For the second configuration B, the mean value of the output is different than the previous configuration. The variation of the output is noticeable for case 3 due to the important intensity (10%) of the random variable MTL_1. In summary, the variation of the output is more important if one of the two considered RVs follows a normal distribution law.
Based on these results, for different configurations of distribution laws and intensity of the RVs, the stochastic responses are different. For our study, the number of configurations, chosen for illustration purposes, remains reasonable. In practice, the possible combinations can be nearly infinite, and consequently hard if not impossible to achieve. At this level, the implementation of the stochastic DD offers important computational gains for stochastic-parametric studies. This particular aspect will be later detailed in the next section.

We focus now on the evaluation of the stochastic response of the voltage $V^1_{3,2}$ using the DD method when the global network is split at the middle of the MTL_2, as shown in Figure (5.22). The adopted notations are chosen in compliance with the established definition of the MTL

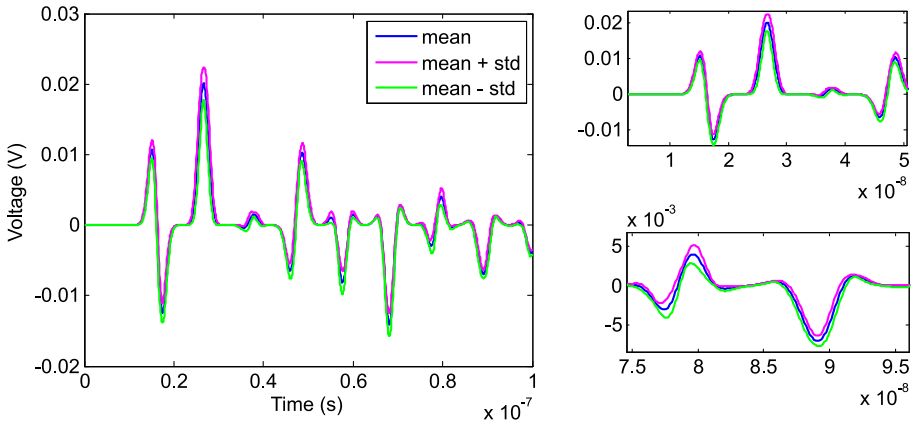

(a) *case 1*

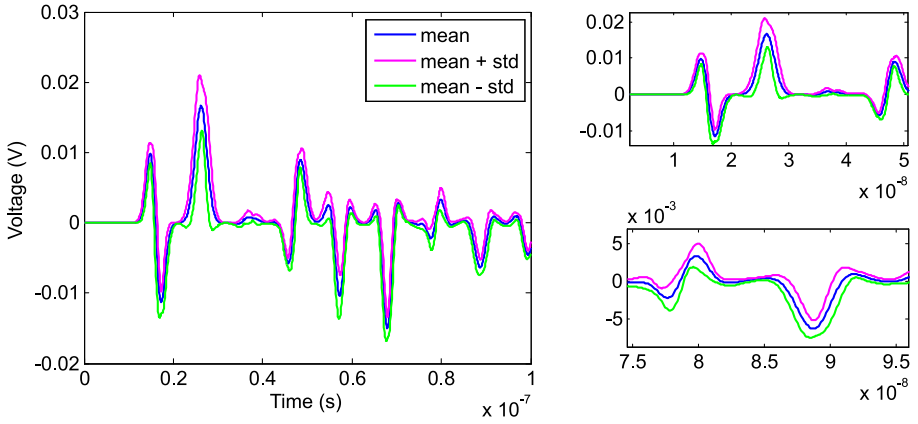

(b) *case 2*

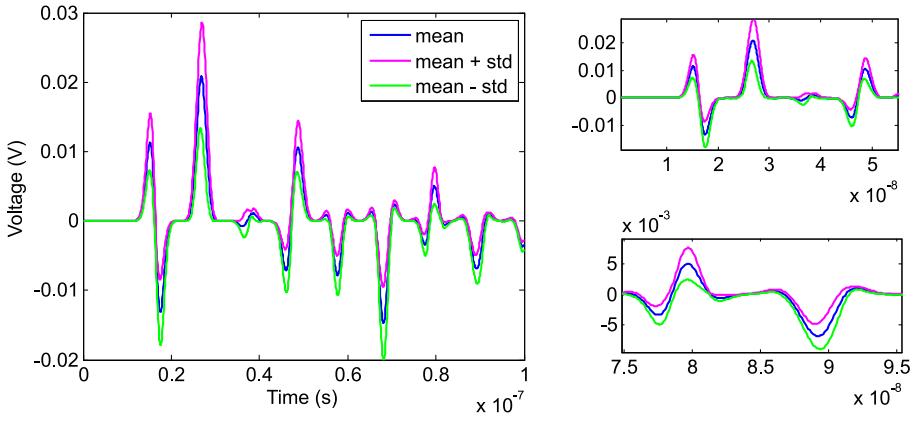

(c) *case 3*

Figure 5.20: *Mean and standard deviation of the voltage $V_{3,2}$ evaluated for 7 collocation points considering different distribution laws of the RVs for each case of configuration A.*

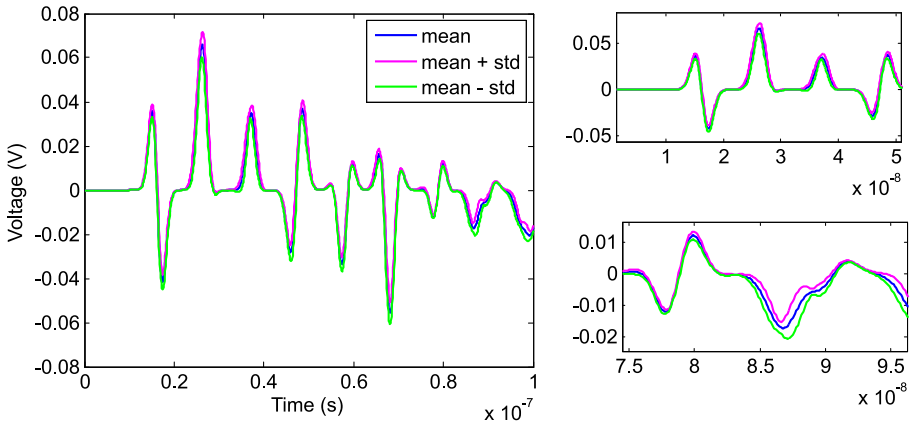

(a) *case 1*

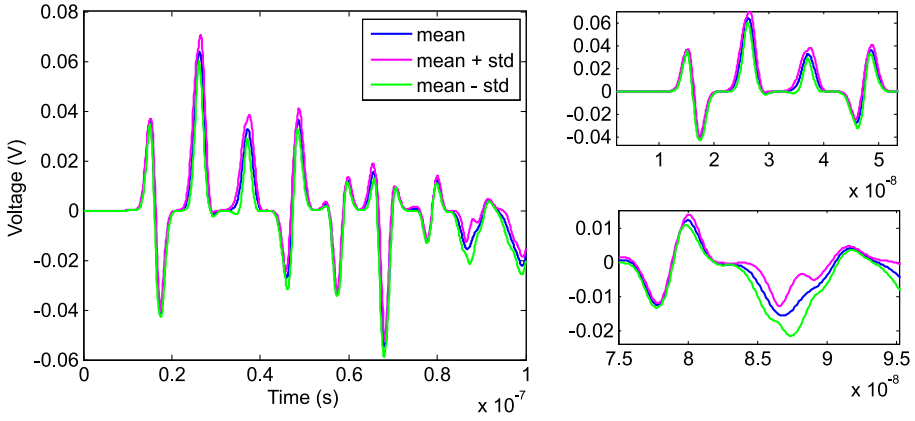

(b) *case 2*

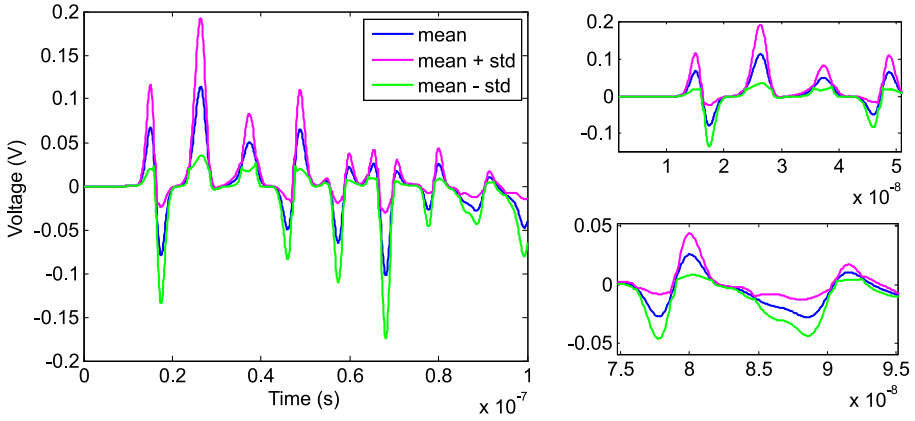

(c) *case 3*

Figure 5.21: *Mean and standard deviation of the voltage $V_{3,2}$ evaluated for 7 collocation points considering different uncertainty intensities of the RVs for each case of configuration B.*

network studied in section (3.4).

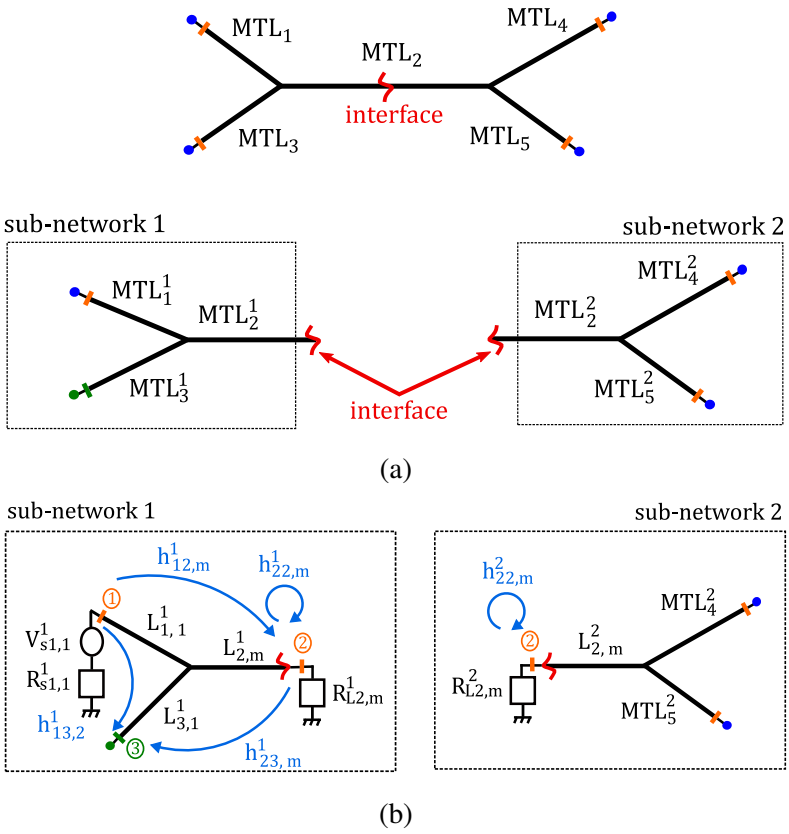

Figure 5.22: *Decomposition of the global network into two sub-networks at the middle of the line MTL_2 (a), Schematic representation of the impulse responses of each sub-network (b).*

In this configuration, the QoI is located in sub-network 1, featuring both real and equivalent sources. The evaluation of the voltage $V^1_{3,2}$ is similar to the studied case in section (3.2) adapted to three one-point interfaces. Given that the aim is to demonstrate the interest of the stochastic DD method, we won't dwell on the details of the formulation, and will give its expression directly:

$$V^1_{3,2} = h^1_{13,2} * V^1_{s1,1} + \sum_{m=1}^{3} h^1_{23,m} * \underbrace{\left(h^2_{22,m} * \left(h^1_{12,m} * V^1_{s1,1}\right)\right)}_{V^1_{\sim 2,m,1}} + \sum_{i=2}^{q} \left(\sum_{m=1}^{3} h^1_{23,m} * \left(h^2_{22,m} * \left(h^1_{22,m} * V^1_{\sim 2,m,i}\right)\right)\right) \tag{5.84}$$

with $V^1_{\sim 2,m,i}$ is defined as the i-th order of the equivalent source at the m interface level and is given by

$$V^1_{\sim 2,m,i} = h^2_{22,m} * (h^1_{22,m} * V^1_{\sim 2,m,i-1}) \tag{5.85}$$

Following this decomposition, each sub-network $k \in \{1,2\}$ features one RV R_i. By identification to the equations (5.67) and (5.68), the terms C^1_{Rs} and $C^1_{\sim s}$ can be written as follows:

$$\begin{aligned} C^1_{Rs}(r_1) &= h^1_{13,2}(r_1) * V^1_{s1,1} \\ C^1_{\sim s}(r_1,r_2) &= \sum_{m=1}^{3} h^1_{23,m}(r_1) * \Big(h^2_{22,m}(r_2) * \big(h^1_{12,m}(r1) * V^1_{s1,1} \big) \Big) \\ &\quad + \sum_{i=2}^{q} \Bigg(\sum_{m=1}^{3} h^1_{23,m}(r_1) * \Big(h^2_{22,m}(r_2) * \big(h^1_{22,m}(r_1) * V^1_{\sim 2,m,i}(r_1,r_2) \big) \Big) \Bigg) \end{aligned} \tag{5.86}$$

The mean of the voltage $V^1_{3,2}$ can thus be deducted from the general expression given by equation (5.60), as follows:

$$\begin{aligned} \mathbb{E}\Big[V^1_{3,2}(R_1,R_2)\Big] \approx & \sum_{t_1=0}^{n} \omega_{t_1} \Big(h^1_{13,2}\big(r_1{}^{(t_1)}\big) * V^1_{s1,1} \Big) \\ & + \sum_{t_1=0}^{n} \sum_{t_2=0}^{n} \omega_{t_1}\omega_{t_2} * \Bigg\{ \sum_{m=1}^{3} h^1_{23,m}\big(r_1{}^{(t_1)}\big) * \Big(V^1_{\sim 2,m,1}\big(r_1{}^{(t_1)}, r_2{}^{(t_2)}\big) \Big) \\ & + \sum_{m=1}^{3} \Bigg(\sum_{i=2}^{q} h^1_{23,m}\big(r_1{}^{(t_1)}\big) * \Big(h^2_{22,m}\big(r_2{}^{(t_2)}\big) * h^1_{22,m}\big(r_1{}^{(t_1)}\big) * V^1_{\sim 2,m,i}\big(r_1^{(t_1)}, r_2^{(t_2)}\big) \Big) \Bigg) \Bigg\} \end{aligned} \tag{5.87}$$

Similarly, the variance is deducted from the equation (5.63) and expressed as follows:

$$\begin{aligned} Var\Big[V^1_{3,2}(R_1,R_2)\Big] \approx & \sum_{t_1=0}^{n} \omega_{t_1} \Big(h^1_{13,2}\big(r_1{}^{(t_1)}\big) * V^1_{s1,1} \Big)^2 \\ & + \sum_{t_1=0}^{n} \sum_{t_2=0}^{n} \omega_{t_1}\omega_{t_2} * \Bigg\{ \sum_{m=1}^{3} h^1_{23,m}\big(r_1{}^{(t_1)}\big) * \Big(V^1_{\sim 2,m,1}\big(r_1{}^{(t_1)}, r_2{}^{(t_2)}\big) \Big) \\ & + \sum_{m=1}^{3} \Bigg(\sum_{i=2}^{q} h^1_{23,m}\big(r_1{}^{(t_1)}\big) * \Big(h^2_{22,m}\big(r_2{}^{(t_2)}\big) * h^1_{22,m}\big(r_1{}^{(t_1)}\big) * V^1_{\sim 2,m,i}\big(r_1^{(t_1)}, r_2^{(t_2)}\big) \Big) \Bigg) \Bigg\}^2 \\ & - \mathbb{E}\Big[V^1_{3,2}(R_1,R_2)\Big]^2 \end{aligned} \tag{5.88}$$

These expressions can be further simplified by introducing the weighted impulse response $(h^k_{\cdot\cdot})'$ as the product of the impulse response $h^k_{\cdot\cdot}(r_k)$ with the weight ω^k_{tk}, for the sub-network k.

	sub-network 1	sub-network 2	
inputs	outputs	outputs	inputs
RV	$(\omega_1^1 \times h_{..}^{1,1}) = (\mathrm{h}_{..}^{1,1})'$	$(h_{..}^{2,1})' = (\omega_2^1 \times h_{..}^{2,1})$	RV
distribution law	$(\omega_2^1 \times h_{..}^{1,2}) = (\mathrm{h}_{..}^{1,2})'$	$(h_{..}^{2,1})' = (\omega_2^2 \times h_{..}^{2,2})$	distribution law
intensity of the uncertainty	$\vdots$	$\vdots$	intensity of the uncertainty
n collocation points	$(\omega_n^1 \times h_{..}^{1,n}) = (\mathrm{h}_{..}^{1,n})'$	$(h_{..}^{2,n})' = (\omega_n^2 \times h_{..}^{2,n})$	n collocation points

Table 5.4: *Inputs and outputs of each sub-network $k \in \{1,2\}$, and the weighted impulse responses $(h^{k,n})'_{..}$ exchanged at the interface level.*

This new formulation allows to preserve not only the confidentiality of the numerical models but also the stochastic configuration. By exchanging the n weighted impulse responses of each sub-network at the exchange interface, evaluated for n collocation points, the mean and variance of the output are retrieved based on the weighted impulse response $(h_{..}^{k,n})'$ of each sub-network. The expression of the expectation of the output $V_{3,2}^1$ with this new notation is given by

$$\begin{aligned}\mathbb{E}\left[V_{3,2}^1(R_1,R_2)\right] \approx & \sum_{t_1=0}^{n}\left((h_{13,2}^{1,t_1})'\left(r_1{}^{(t_1)}\right) * V_{s1,1}^1\right) \\ & + \sum_{t_1=0}^{n}\sum_{t_2=0}^{n}\sum_{m=1}^{3}\left((h_{23,m}^{1,t_1})'\left(r_1{}^{(t_1)}\right) * V_{\sim 2,m,1}^1(r_1,r_2)\right) \\ & + \sum_{t_1=0}^{n}\sum_{t_2=0}^{n}\sum_{m=1}^{3}\sum_{i=2}^{q}(h_{23,m}^{1,t_1})'\left(r_1{}^{(t_1)}\right) * \left((h_{22,m}^{2,t_2})'\left(r_2{}^{(t_2)}\right) * (h_{22,m}^{1,t_1})'\left(r_1{}^{(t_1)}\right)\right. \\ & \left. * V_{\sim 2,m,i}^1(r_1^{(t_1)}, r_2^{(t_2)})\right)\end{aligned} \tag{5.89}$$

Let's assume that each sub-network $k \in \{1,2\}$ is treated by an operator k. The n exchanged weighted impulse responses $(h_{..}^{k})'$ from both sub-networks, can either refer to the actual evaluations of an RV evaluated for n collocation points, or the number of possible combinations evaluated for more than one RV. For instance, for 9 weighted impulse responses exchanged from one sub-network to the interface level, it can either represent their evaluation for 9 collocation points of one RV or the 9 possible combinations for 2 RVs evaluated at 3 collocation points (n^2). This additional advantage of the SC-DD association is very valuable in the industrial context, where uncertainties are not revealed as they may reflect system limitations or weaknesses.

5.3.3 Stochastic DD method for sensitivity analysis

In the continuity of the previous stochastic study, we carry a variance-based approach for

global sensitivity analysis. The aim is to identify the inherent impact of each input variable, and their combined effects on the output, through the first and second-order Sobol' indices and total indices.

We base our global sensitivity analysis on the SC technique and PC expansion approach. For the latter, the evaluation of Sobol' indices depends on the coefficients $\hat{y}_\alpha$, also used to calculate the variance of the output. We first start by comparing the standard deviation values using the PC method and SC technique for case 1 of configuration B in section (5.3.2).

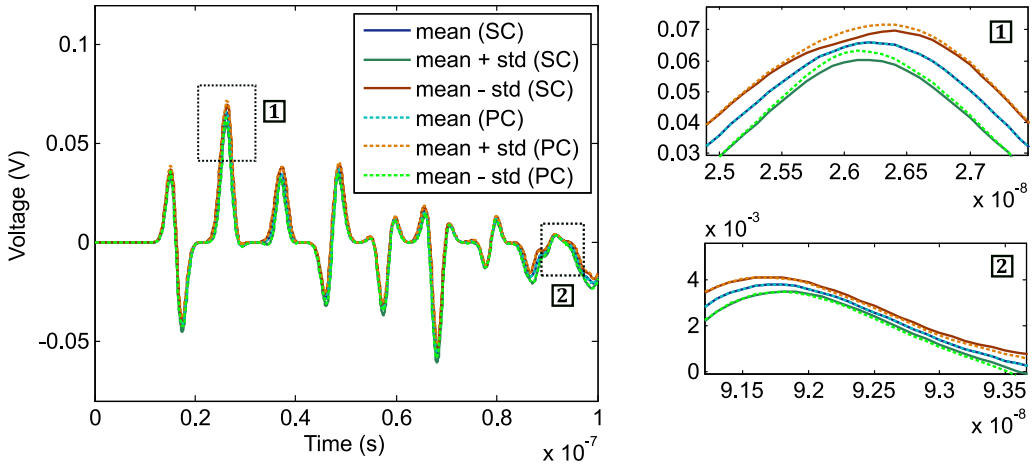

Figure 5.23: *Comparison of the standard deviation values of the voltage $V_{3,2}$ evaluated for 7 collocation points with the SC method and PC technique.*

Given that both RVs follow a uniform distribution law, the chaos basis is built using the Gauss-Legendre polynomials up to a chosen degree $q = 3$. Both results in Figure (5.23) follow the same pattern for the standard deviation, meanwhile, the results for the mean of the output are equivalent, due to their similar formulation for both techniques.

We now proceed to evaluate Sobol' indices using the SC and PC methods for the three cases of configuration B. The QoI of this application, represented by the voltage $V_{3,2}$, is evaluated for each discrete time step of the interval $[0, 0.1\mu s]$. For discussion purposes, we evaluate the first and second orders of Sobol' indices for different time instants. Both SC and PC techniques give close results for the first and second order of Sobol' indices as reported in Figures (5.24), (5.25) and (5.26). For the same case, first and second-order indices are different for each instant. For the three cases, the influence of the length of the MTL_1 is the most dominant overall. This result was expected, given the sensitivity of the crosstalk to the length of the conductors. The impact of the second RV ($R_{L3,2}$) is important for the first case only, due to its higher intensity $\alpha = 20\%$.

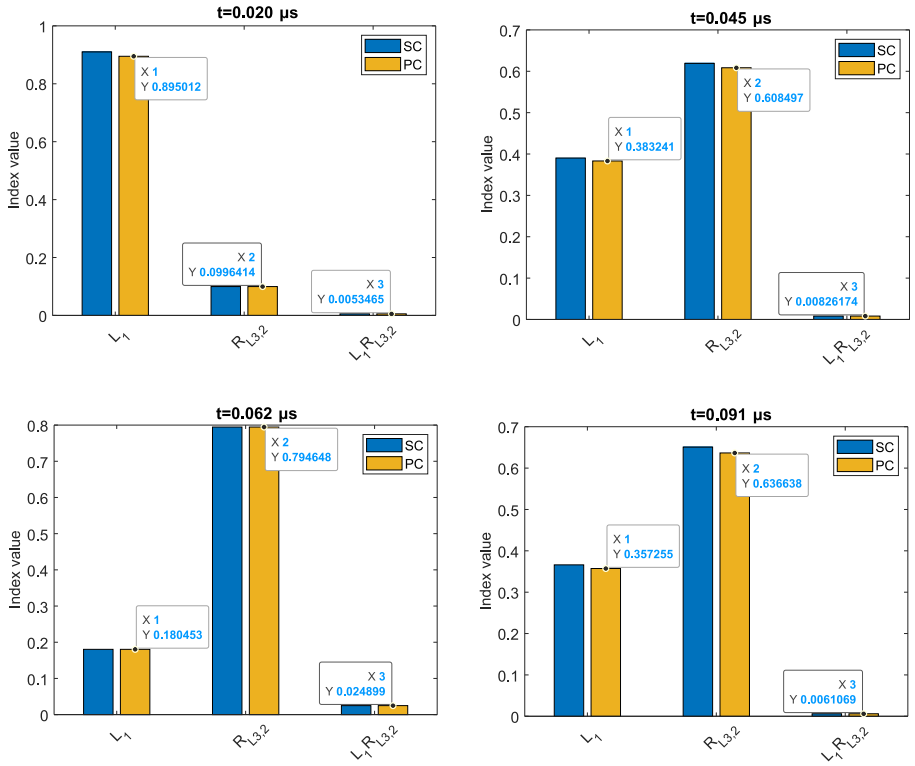

Figure 5.24: *Comparison of the first (L_1 and $R_{L3,2}$) and second orders ($L_1R_{L3,2}$) of Sobol' indices using SC and PC method for case 1 of configuration B.*

Its individual and joint effect is practically non-existent for low intensities $\alpha = 5$ and 10% for cases 2 and 3. From these results we conclude that for different intensities, the proper impact of the RVs as well as their joint influence vary. Given that the distribution law also impacts the output's variability, we compare case 1 of configuration B to case 2 of configuration A, for which both the distribution law and intensity of the first RV are modified.

From the results in Figure (5.27), the impact of the RV MTL_1 is once again demonstrated for both cases. The second RV however has no effect for both configurations at the time instant $t = 0.0949\mu s$.

Depending on the purpose for which the SA is being evaluated, it may be required to evaluate different configurations of distribution laws and/or intensities variations. The DD method achieves this goal with no additional evaluations of the output. Its asynchronous feature can be employed to use two different stochastic techniques to evaluate the Sobol' indices. For instance, sub-network 1 can be modeled using the SC technique, whereas sub-network 2 can be evaluated with the PC expansion. Given that both methods use quadrature rules to evaluate the collocation points, they are similar for both sub-networks. For 7 collocation points, based on the evaluated weighted impulse responses, Sobol' indices computed with the stochastic

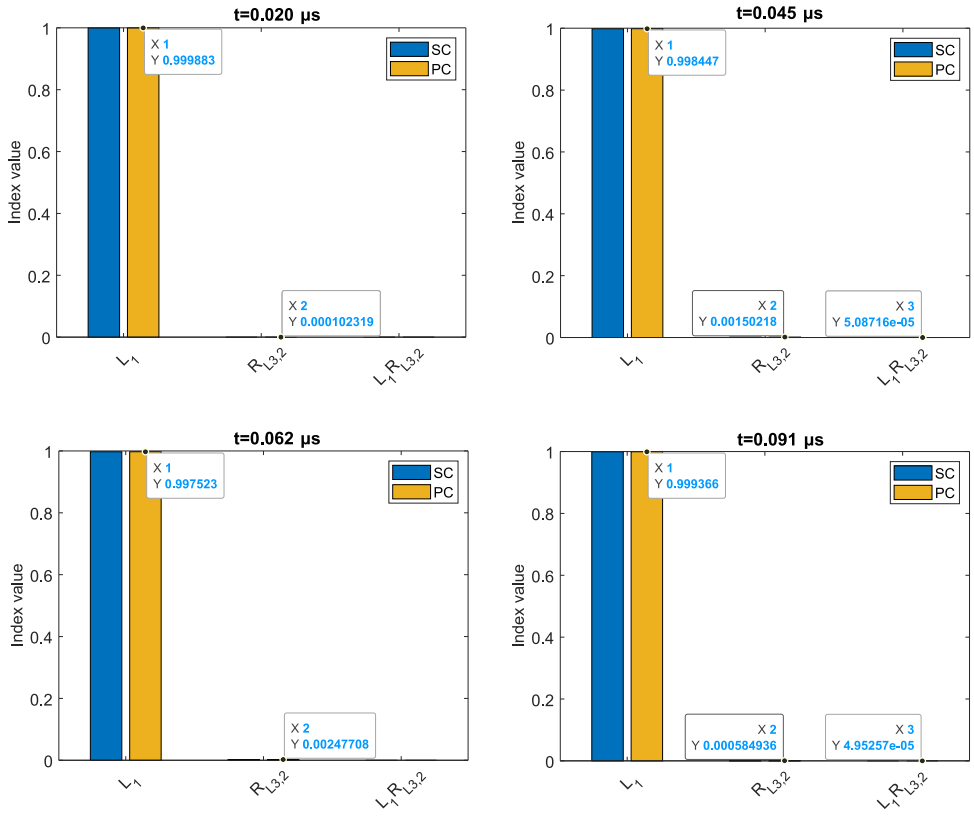

Figure 5.25: *Comparison of the first (L_1 and $R_{L3,2}$) and second orders ($L_1R_{L3,2}$) of Sobol' indices using SC and PC method for case 2 of configuration B.*

DD method are retrieved. The total Sobol' index of the RV $MLTL_1$, measured at the instant $t = 0.0575\mu s$, for case 1 of configuration B equals 0.8754214 with the proposed stochastic DD method. The yielded result is very close to both references given respectively by 0.882445 and 0.8678451 for SC, respectively PC techniques.

In synthesis, the SC-DD association comes with additional advantages for the global SA analysis based on Sobol' indices. The latter are computed through new linear combinations of the already evaluated model serving for UQ assessment (mean and variance). The variable separation in the SC-DD' formulation takes our stochastic analysis a step further with different stochastic scenarios (different RVS, laws, intensities or initial values) with a local re-evaluation of the modified sub-systems. The model's evaluation cost gain is important and will be discussed further. In addition, the choice of the stochastic method is irrelevant to the SC-DD association thanks to the asynchronous feature of the DD technique itself. This aspect is very interesting in an industrial context where the partners don't necessarily dispose of the same

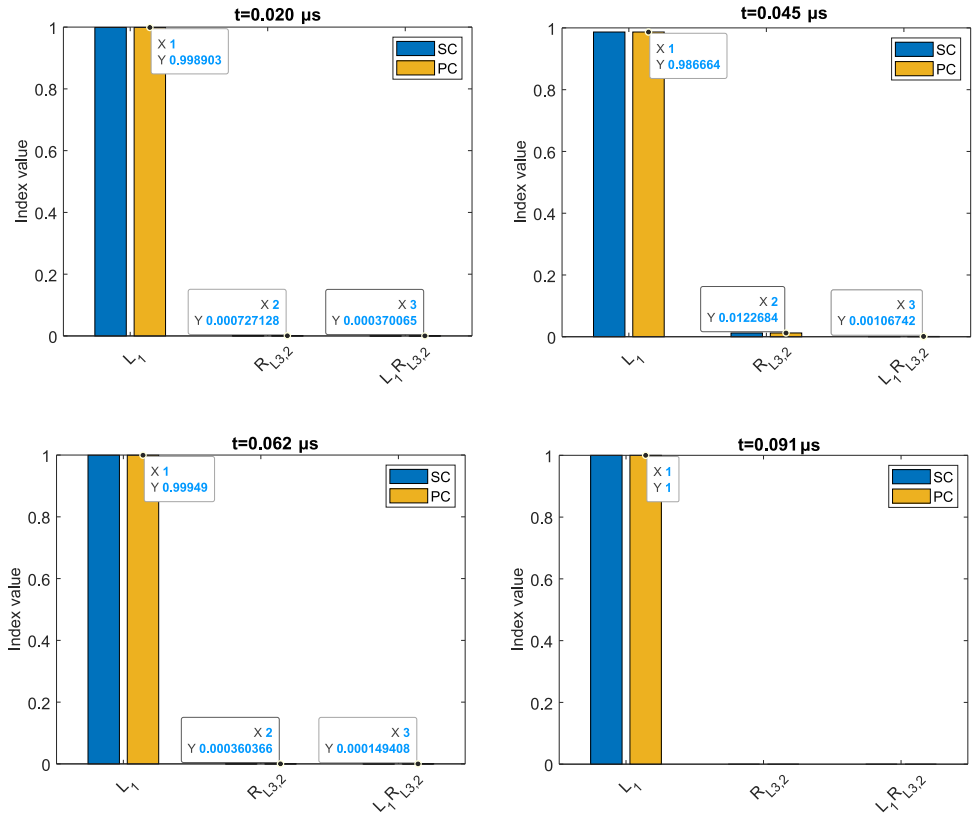

Figure 5.26: *Comparison of the first (L_1 and $R_{L3,2}$) and second orders ($L_1R_{L3,2}$) of Sobol' indices using SC and PC method for case 3 of configuration B.*

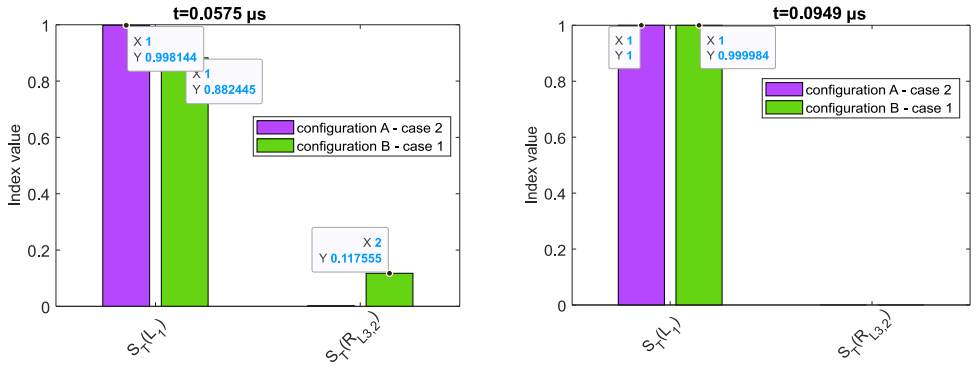

Figure 5.27: *Comparison of the total Sobol' indices using SC and PC method for case 2 of configuration A and case 1 of configuration B.*

stochastic tools.

5.4 Alleviating the Curse of dimensionality

In computational electromagnetic applications, the computational cost is a real challenge, especially for multi-scale, multi-system and multi-physics problems. This complexity increases with the uncertainty dimension, for which the deterministic model $\mathscr{M}$ is evaluated a specific number of times. The MC method, known as the reference, requires a high number of evaluations, resulting in a slow convergence rate. Alternatively, new methods known as *accelerating* techniques have been proposed [146–148] including the support vector methods, surrogate-model and sparse-grid techniques. In our work, we have based our stochastic analysis mainly on the SC method, chosen for its non-intrusive nature and ease of use. Although, in the case of a few RVs, the SC technique as well as other methods (Kriging and polynomial chaos) ensure high computational efficiency for evaluating the statistical moments of the model's response, the question of the dimension still arises for a large number of RVs. For n collocation points and m RVs, the evaluation cost n^m increases exponentially with higher values of RVs. Beyond about 5 RVs, the SC method entails significant computational cost almost the same size as the MC method (10 000 evaluations typically), as shown in Figure (5.28).

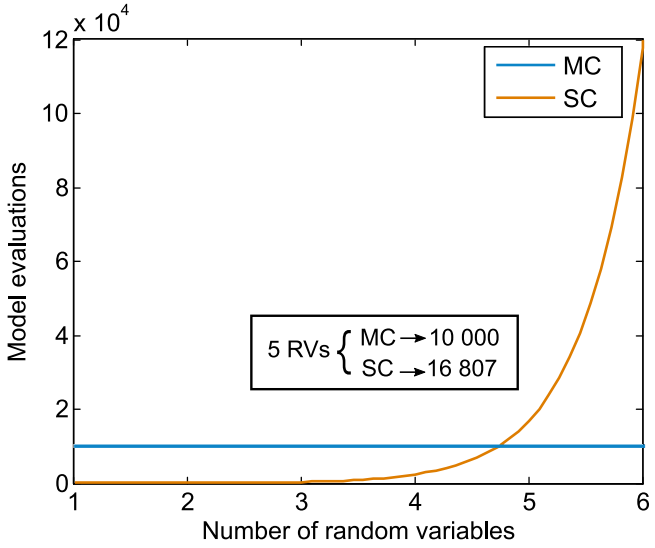

Figure 5.28: *Comparison of the typical costs between MC and SC method (evaluated for 7 collocation points).*

This phenomenon is called "the curse of dimensionality" and refers to the extraordinarily rapid growth in the difficulty of problems as the number of variables increases. This term was first introduced by Richard E. Bellman [149], to describe the explosive nature of increasing data dimensions for dynamic programming problems. Today, this phenomenon is more and more

observed in other fields, more specifically, electromagnetic problems [150, 151].

In this thesis, we propose an easy-to-implement solution based on the online-offline SC-DD strategy motivated by the asynchronous intrinsic nature of the DD method. As a result of the decomposition, the RVs are isolated in distinct sub-domains, modeled independently from each other. However, the unavoidable interactions between the RVs are considered in a second step to obtain the global response of the system under study. The expected interest of the proposed approach is highlighted as the evaluation cost of the model $\mathscr{M}$ is dramatically reduced as shown in Figure (5.29).

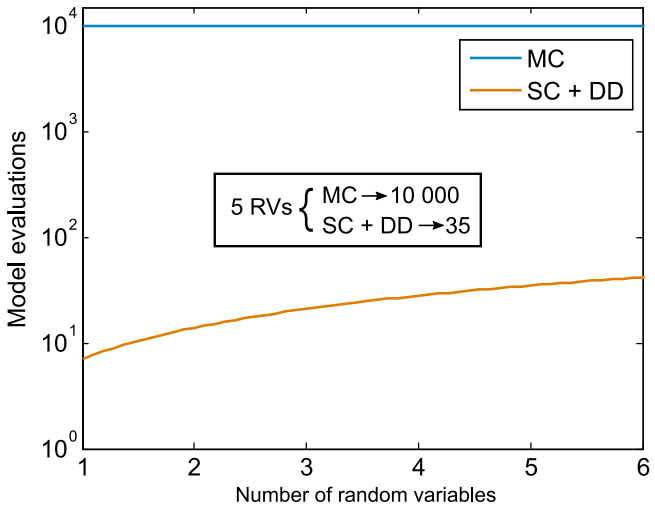

Figure 5.29: *Comparison of the typical costs between MC and the association of SC and DD methods (evaluated for 7 collocation points).*

In the literature, few works based on the use of classical DD methods to alleviate the curse of dimensionality have been proposed in other engineering fields [152, 153]. The approach within the EMC context is relatively novel. Our contribution in this particular field of research is translated mainly by the DD method itself and the resolution in the time domain.
This section aims to highlight the advantages of the association of the SC with the DD method. We begin by defining what we intend by computational cost and distinguish it from the cost of model evaluations, for the configurations under study. An optimal case configuration for evaluation cost reduction will be later discussed.

5.4.1 Computational cost for SC-DD association

In section (2.1.2), we have defined the computational complexity and distinguished it from

the evaluation cost of the model itself. In this section, we establish the latter for deterministic and stochastic analyses for both global and split systems.

Let's consider the model $\mathscr{M}$ in equation (5.1), translating the relationship between the inputs and outputs of a system. The latter is only evaluated once for a deterministic study. In this case, no additional cost is added to compute the model's response Y. For the deterministic scenario, the computational cost is thus equivalent to the evaluation cost of the model itself as previously mentioned in section (2.1.2). On the other hand, the non-intrusive SC method requires n^m times evaluations of the model $\mathscr{M}$ in the stochastic configuration, where n is the number of collocation points and m is the number of RVs, as schematized in Figure (5.30).

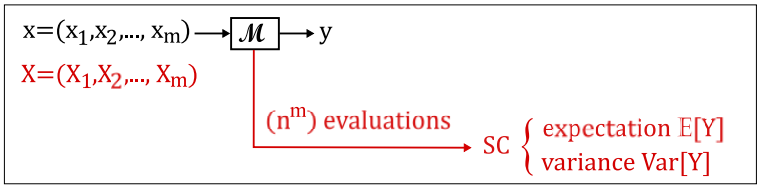

Figure 5.30: *Diagram of the global model's output for both deterministic estimation (in black) and stochastic estimation for n collocation points (in red).*

With the DD technique, the decomposition is managed to isolate at best one RV R_i only in a specific sub-system $s_{i,\ i\in\{1,\dots,m\}}$, thanks to its asynchronous feature allowing parallel modeling. The process of the SC-DD association, as defined in section (5.3), starts at an offline level where each RV is evaluated n times independently of other inputs. Then, an online level will assemble all these combinations through (5.56), (5.60), and (5.63).
The assessment of mean and variance, based on weighted sums evaluated according to the collocation points, comes at an additional cost. The computational cost for the stochastic analysis is thus given by the summation of the evaluation cost of the deterministic model and the cost of computing the stochastic moments, which can be deduced from the complexity cost previously established in section (2.1.2). The latter is not given in detail as our main focus is to compare the evaluation cost of the global model and the sub-models with our DD method. For both deterministic and stochastic analysis, these computational costs are summarized in Table (5.5). This (SC-DD) approach allows going from n^m evaluations of the global complex model $\mathscr{M}$, to $(n \times \tau \times m)$ evaluations of smaller and less complex sub-models s_i[6], as schematized in Figure (5.31). All the combinations of the RVs are however still considered in the offline phase for n^m applications of equation (2.5). Given that the main time-consuming task is the

[6]We recall that the parameter τ_i refers to the number of impulse responses to be evaluated for a given syb-system s_i, defined in section (2.1.2).

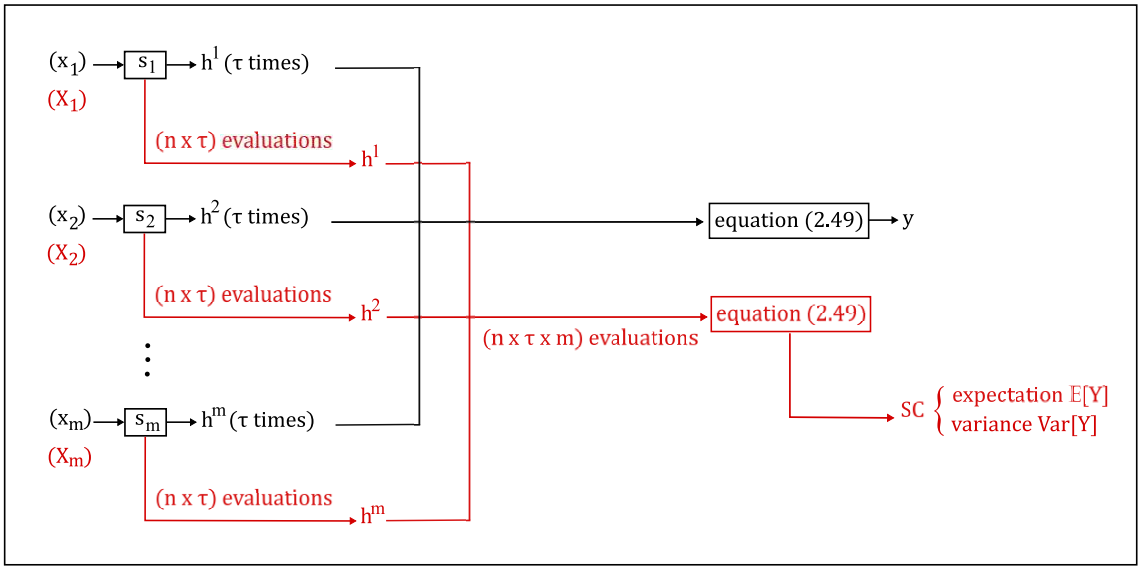

Figure 5.31: *Diagram of the split model's output for both deterministic estimation (in black) and stochastic estimation for n collocation points (in red).*

		Computational cost
GLOBAL	Deterministic	unique evaluation ($\mathscr{M}$)
	Stochastic	n^m **evaluations** ($\mathscr{M}$) + equations (5.60) and (5.63)
DD	Deterministic	$(\tau \times m)$ evaluations $(s_1, ..., s_m)$ + equations (5.56)
	Stochastic	$(n \times \tau \times m)$ **evaluations** $(s_1, ..., s_m)$ + (n^m times) eq (5.56) + equations (5.60) and (5.63)

Table 5.5: *Computational costs for global and split models for both deterministic and stochastic analysis.*

evaluation of the model $\mathscr{M}$, the SC-DD method has a real potential to highly alleviate the exponential growth arising from the "curse of dimensionality".

Following up on our stochastic analysis, we recall that the choice of a global SA, based on variance decomposition, is mainly focused on the evaluation of the variance for UQ assessment. The computation gain of the Sobol' indices is already significant, and more emphasized with our SC-DD method as no additional model evaluations are required. Although additional computational complexity is added for the Sobol' indices calculation, it is negligible compared with the cost of evaluation of the partial variances[7].

[7]The SC-DD allows evaluation gain for the partial variances as well, thanks to the asynchronous feature of the

5.4.2 Optimal configuration of the SC-DD association

The asynchronous feature of the DD method allows independent modeling of each sub-system $s_{i,\ i\in\{1,\dots,m\}}$. Following the topology of the system (terminations, distributions of the α inputs and β outputs and the observable), the number of impulse responses to be evaluated for each sub-system s_i, given by τ_i, is independent of the number of RVs n. Consequently, we propose an optimal configuration for which the reduction of the evaluation cost of the model is further emphasized. For this ideal case, two hypotheses must be verified: 1) each sub-system isolates only one RV, 2) for a set of m sub-systems, the excitation source, respectively, the observation point (variable of interest), are in sub-system 1, respectively, m. Figure (5.32) illustrates this optimal configuration for $m = 3$ sub-systems.

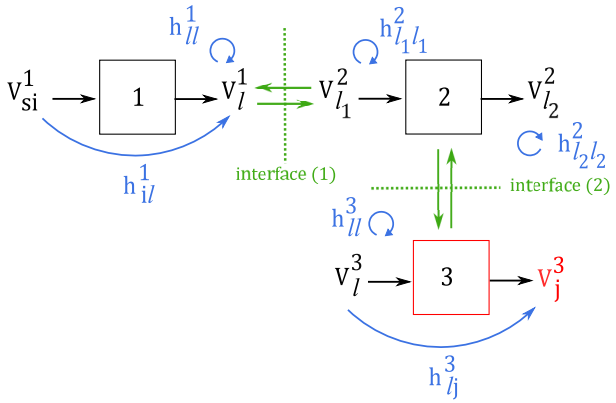

Figure 5.32: *Schematic representation of $m = 3$ sub-systems split at one point exchange interfaces and their corresponding impulse responses.*

In this case, each sub-network m, characterized by $\tau = 2$ impulse responses, is evaluated only $(2 \times n)$ times. We can then define a maximum theoretical gain relative to the evaluation of the model $\mathscr{M}$, represented by the output V_j^k in equation (2.5) for $k = m$ in our case, as follows:

$$Gain = \frac{n^m}{2 \times n \times m} = \frac{n^{(m-1)}}{2 \times m}. \tag{5.90}$$

Table (5.6) shows this gain for different configurations. For a given number of RVs, the proposed SC-DD method leads to a significant gain when the number of collocation points increases. On the other hand, increasing the number of R.V.s for the same number of collocation points increases the gain as well.

As previously illustrated in Figure (5.28), the dimensionality challenge arises around 5 R.V.s and 7 collocation points with 16 807 simulations vs 10 000 for the MC. One must be aware

DD technique allowing variable-separation

		Global	Split	Gain
k=4	n=5	625	40	15,625
	n=7	2 401	56	42,875
	n=9	6 561	72	91,125
	MC	10 000	$4 \times 10\,000$	
k=5	n=5	3 125	50	62,5
	n=7	16 807	70	240,1
	n=9	59 049	90	656,1
	MC	10 000	$5 \times 10\,000$	
k=6	n=5	15 625	60	260,41
	n=7	117 649	84	1 400,58
	n=9	531 441	108	4 290,75
	MC	10 000	$6 \times 10\,000$	

Table 5.6: *Number of model evaluations for both the global and split network using the SC-DD method (for m RVs and n collocation points), and using the MC method.*

that the total computational cost for the SC-DD method includes an extra computational cost (Table 5.5). Yet, once again the main challenge relies on the evaluation of the model $\mathscr{M}$. Our approach considerably reduces this cost, especially since the models to be evaluated are smaller and these operations can be done in parallel. In practice, the total gain will depend on the problem and the topology of its subdivision. But from 5 RVs, we can already expect a significant gain compared to MC and in all cases, the "curse of dimensionality" is greatly alleviated.

In synthesis, through the SC-DD association, the proposed domain decomposition method proved its efficiency in propagating uncertainty between the sub-systems. The second objective of this thesis is thus fulfilled as the stochastic response of the global system is recovered from partial deterministic partial solutions. The requirements of the ANR *ECOCES* project are also met:

1. The stochastic configuration is not revealed: the RVs, their number, distribution law, intensities, and initial values are not exchanged. The confidentiality of the stochastic models is thus preserved,

2. The offline-online stochastic DD approach enables fully asynchronous modeling of the

sub-systems.

An additional advantage of this association arises with the asynchronous feature of the DD method, that is the evaluation cost reduction. This particular aspect is very promising for challenging high-dimensional stochastic EMC applications.

Conclusion

In this chapter, the DD was extended for stochastic linear EMC applications. The new formulation of the stochastic DD method, for both UQ and global SA assessment is established. The association of both techniques is based on an offline–online strategy, motivated by the asynchronous nature of the DD technique and the non-intrusive feature of the SC method. Through different configurations of stochastic studies, the various advantages of this association were highlighted. The DD technique has proved to be efficient in propagating uncertainties within sub-systems, as long as the q order is considered in the formulation of the output. In addition to preserving the confidentiality of the numerical models themselves, their stochastic configuration is also preserved by exchanging weighted impulse responses only. The re-evaluation of the modified sub-systems only is a major advantage for parametric-stochastic studies and offers the possibility of extending stochastic analysis to multiple configurations. With this advantage, the SC-DD alleviates the curse of dimensionality arising with high-dimensional stochastic problems, thanks to its asynchronous feature allowing RV separation. Although the stochastic DD method was illustrated with the SC technique, the approach is general and can be applied with different stochastic techniques including PC expansion. The hybridization of different stochastic methods adds to the benefits of this original association. It has great potential for industrial applications since it preserves the confidentiality of each sub-model employed as well as its uncertainty features.

General Conclusion and Perspectives

THIS thesis work is mainly oriented towards the development of a domain decomposition approach for EMC analysis of complex linear systems. The assessment of the system's response is guaranteed through the partial solutions of the sub-systems, modeled each independently. The need to develop such methods is mainly motivated by the shortcomings of the existing approaches, hybridization of numerical temporal tools for instance, to 1) allow fully independent simulations of the sub-systems, 2) preserve the confidentiality of the models, and 3) overpass their interface adaptation complexity (for time and/or space discretization) to adapt for general applications regarding the geometry and/or material properties of the studied systems.

Our contribution, regarding the ANR *ECOCES* project specifications, overcomes these technical and industrial constraints established in the context section. The proposed DD method is an easy-to-implement technique, based on an offline-online strategy characterizing less complex sub-systems through their impulse responses only, from which the global solution is yielded based on a linear combination. The detailed formulation of the method and its practical implementation were presented in Chapter 2, from which we deduce three valuable advantages that offers our methodology:

- the decomposition is **general**, it is case-independent, and can be automated for any linear application,
- the formulation is **asynchronous**, meaning that the sub-systems are modeled independently at the offline level. Their responses are combined in the online phase, to take into account the physical properties of the initial problem and the existing couplings between the sub-systems,
- the **confidentiality** of the models is **preserved**, as no proprietary information and/or result is exchanged.

These advantages were demonstrated through numerical applications for different configurations of wiring networks in Chapter 3. The method has been generalized for several interfaces (multiple decomposition levels) paving the way for more complex ramified network line applications or other linear applications. Its application with different parameters (time step) or modeling tools demonstrates its robustness and overcomes the *multi-models* constraint. The

adjustment of the DD technique to several one-point interfaces is promising for 3D applications, for which the adaptation of the method is necessary but its essence remains unchanged.

As part of our study, the proposed DD method was experimentally applied in Chapter 4, with the aim of testing its efficiency in a noisy environment. Its application was carried out for different wire network configurations, after adapting its theoretical formulation to match experimental constraints. The asynchronous feature of the DD methods shines through with the experimental applications, especially for different measurement equipment for each sub-system. The configuration not only provides a practical demonstration of the true meaning of asynchronous decomposition, based on independent characterization (both temporal and spatial) using different instruments, but also approaches real-world situations implying suppliers and assemblers, in the automotive context. Given that experiments tend to be costly (in terms of time and human resources), the DD method enables significant cost gains for parametric studies.

This additional advantage has considerable potential for more costly applications: stochastic analysis. But first, the association of the SC method and the DD technique, in Chapter 5 was studied. The obtained results demonstrated the ability of the domain decomposition approach to propagate uncertainties within the sub-systems. Through different stochastic scenarios, the DD technique's main advantage (asynchronous and independent modeling) preserves the confidentiality of stochastic models. The *multi-uncertainties* constraint with traditional methods is bypassed. Moreover, the stochastic DD method alleviates the curse of dimensionality challenge arising from high stochastic dimension problems, as it reduces significantly the number of evaluations of the model, which are mostly very expensive to evaluate. This feature is very promising and maintains the efficiency of techniques such as SC and PC without compromising on the computational cost.

The results of this work have been presented at several conferences, both national [154] and international [155–157]. In addition, a publication derived from the stochastic analysis was published at the *IEEE-Transactions on Electromagnetic journal*, allowing to share our findings with a wider audience and actively contribute to the research field [158].

Perspectives

We proposed through the presented work in this thesis a non-overlapping domain decompo-

sition approach to solve EMC linear applications. The technique gave efficient and significant results for both deterministic and stochastic applications. In the continuity of this thesis, we propose some perspectives for future works, regarding:

1. *the numerical aspect*:

   - from a computing point of view: the DD technique can be integrated into a simulation platform involving several partners. Each partner models a sub-system m, and exchanges two pieces of information only: 1) the impulse response of their system at the interface level $h^m_{\cdot\cdot}$, and 2) the incoming wave voltage from the physical sources V_{si_m} in this system to the interface level denoted $V^m_{i_m l}$. In practice, each submodel is able to exchange the first information, contrary to the second one which may not be available (if no physical sources are featured within this sub-system). The formula can still be generalized by assuming that all subnetworks exchange both elements, simply by associating a flag (0 or 1) with the source $V^m_{i_m l}$, depending on its availability.
   - for an applicative extension: the DD technique can be applied to radiated EMC problems, as well as the electromagnetic/electrical coupling for special cases (electromagnetic cavities with openings).

2. *the experimental aspect*: the DD method can be fully experimental, starting with the evaluation of impulse responses, taking into account higher orders, and ending with the evaluation of the final formulation. This new vision calls for the implementation of a more complex set-up bench, and the development of a control system for the various generation and acquisition tools to automate the measurement process.

3. *the uncertainty dimension*: the uncertainty aspect can be pushed further by combining the DD method with different stochastic methods, other than SC and PCE, where the challenge arises with different samples on either side of the interface. The method will therefore need to be adapted to overcome this constraint, but its core idea and principle remain the same.

   From an industrial application point of view, the proposed DD method can be applied to the modeling of cable networks for reflectometry analysis [159]. This discipline enables fault detection while guaranteeing system reliability and proactive intervention to mitigate potential risks. Integrating our DD method into these industrial practices promises to minimize measurement resources and time, thanks to its asynchronous feature. Its

implementation offers parametric studies with a significant gain of cost for multiple configurations and thus allows comprehensive insights into the behavior, performance, and underlying mechanisms of the studied wiring systems.

Bibliography

[1] H. A. Schwarz, *Ueber einen Grenzübergang durch alternirendes Verfahren*. Zürcher u. Furrer, 1870.

[2] A. Quarteroni and A. Valli, *Domain decomposition methods for partial differential equations*. Oxford, UK: Oxford University Press, 1999.

[3] P.-L. Lions, "On the Schwarz alternating method. I," in *First international symposium on domain decomposition methods for partial differential equations*, vol. 1, pp. 1–42, SIAM Philadelphia, 1988.

[4] P.-L. Lions, "On the Schwarz alternating method. III: A variant for nonoverlapping subdomains," in *Third International Symposium on Domain Decomposition Methods for Partial Differential Equations*, vol. 6, pp. 202–223, SIAM Philadelphia, 1990.

[5] K. Gustafson, "Domain decomposition, operator trigonometry, Robin condition," *Contemporary Mathematics*, vol. 218, pp. 432–437, 1998.

[6] E. Haynsworth, "On the Schur complement: Basel mathematical notes," *University of Basel, BMN*, vol. 20, 1968.

[7] J. S. Przemieniecki, "Matrix structural analysis of substructures," *AIAA Journal*, vol. 1, pp. 138–147, 1963.

[8] L. C. Cowsar, J. Mandel, and M. F. Wheeler, "Balancing domain decomposition for mixed finite elements," *Mathematics of Computation*, vol. 64, no. 211, pp. 989–1015, 1995.

[9] C. Farhat and F.-X. Roux, "A method of finite element tearing and interconnecting and its parallel solution algorithm," *International Journal for Numerical Methods in Engineering*, vol. 32, no. 6, pp. 1205–1227, 1991.

[10] K. Zhao, V. Rawat, and J.-F. Lee, "A domain decomposition method for electromagnetic radiation and scattering analysis of multi-target problems," *IEEE Transactions on Antennas and Propagation*, vol. 56, no. 8, pp. 2211–2221, 2008.

[11] Z.-Q. Lu, X. An, and W. Hong, "A fast domain decomposition method for solving three-dimensional large-scale electromagnetic problems," *IEEE Transactions on Antennas and Propagation*, vol. 56, no. 8, pp. 2200–2210, 2008.

[12] J. Lu, Y. Chen, D. Li, and J.-F. Lee, "An embedded domain decomposition method for electromagnetic modeling and design," *IEEE Transactions on Antennas and Propagation*, vol. 67, no. 1, pp. 309–323, 2019.

[13] D. M. Solís, V. F. Martín, M. G. Araújo, D. Larios, F. Obelleiro, and J. M. Taboada, "Accurate EMC engineering on realistic platforms using an integral equation domain decomposition approach," *IEEE Transactions on Antennas and Propagation*, vol. 68, no. 4, pp. 3002–3015, 2019.

[14] X. Wang, Z. Peng, K.-H. Lim, and J.-F. Lee, "Multisolver domain decomposition method for modeling EMC effects of multiple antennas on a large air platform," *IEEE Transactions on Electromagnetic Compatibility*, vol. 54, no. 2, pp. 375–388, 2011.

[15] A. Takei, S.-I. Sugimoto, M. Ogino, S. Yoshimura, and H. Kanayama, "Full wave analyses of electromagnetic fields with an iterative domain decomposition method," *IEEE Transactions on Magnetics*, vol. 46, no. 8, pp. 2860–2863, 2010.

[16] T. Wan, B. Tang, and M. Li, "An iteration-free domain decomposition method for the fast finite element analysis of electromagnetic problems," *IEEE Transactions on Antennas and Propagation*, vol. 68, no. 1, pp. 400–410, 2020.

[17] W.-J. Wang, R. Xu, H.-Y. Li, Y. Liu, X.-Y. Guo, Y. Xu, H.-L. Li, H.-J. Zhou, and W.-Y. Yin, "Massively parallel simulation of large-scale electromagnetic problems using one high-performance computing scheme and domain decomposition method," *IEEE Transactions on Electromagnetic Compatibility*, vol. 59, no. 5, pp. 1523–1531, 2017.

[18] H. E. Abd-El-Raouf, R. Mittra, and J.-F. Ma, "A new domain decomposition finite-difference time domain for solving large electromagnetic problems," *Microwave and Optical Technology Letters*, vol. 48, no. 12, pp. 2399–2405, 2006.

[19] Z. Lou and J.-M. Jin, "A novel dual-field time-domain finite-element domain-decomposition method for computational electromagnetics," *IEEE Transactions on Antennas and Propagation*, vol. 54, no. 6, pp. 1850–1862, 2006.

[20] P. Bonnet, *Résolution des équations de Maxwell instationnaires et harmoniques par une technique de volumes finis. Application à des problemes de comptabilité électromagnétique*. Ph.D. dissertation, Blaise Pascal University, Clermont-Ferrand, France, 1998.

[21] S. Gaucher, C. Guiffaut, A. Reineix, O. Cessenat, and G. Maze-Merceur, "Wideband simulations of periodic structures by the hybrid spectral FDTD/TD-VFz method," *IEEE Antennas and Wireless Propagation Letters*, vol. 21, no. 5, pp. 933–937, 2022.

[22] Q. Sun, Q. Ren, Q. Zhan, and Q. H. Liu, "3-D domain decomposition based hybrid finite-difference time-domain/finite-element time-domain method with nonconformal meshes," *IEEE Transactions on Microwave Theory and Techniques*, vol. 65, no. 10, pp. 3682–3688, 2017.

[23] V. Vahrenholt, H.-D. Brüns, and H. Singer, "Fast EMC analysis of systems consisting of PCBs and metallic antenna structures by a hybridization of PEEC and MoM," *IEEE Transactions on Electromagnetic Compatibility*, vol. 52, no. 4, pp. 962–973, 2010.

[24] C.-Y. Tian, Y. Shi, and C. H. Chan, "An improved vector wave equation-based discontinuous Galerkin time domain method and its hybridization with Maxwell's equation-based discontinuous Galerkin time domain method," *IEEE Transactions on Antennas and Propagation*, vol. 66, no. 11, pp. 6170–6178, 2018.

[25] L. Zhang, L. Zhang, B. Wang, S. Liu, and C. Papavassiliou, "Hybrid prediction method for the electromagnetic interference characteristics of printed circuit boards based on the equivalent dipole model and the finite-difference time domain method," *IEEE Access*, vol. 6, pp. 6520–6529, 2018.

[26] A. Monorchio, A. Bretones, R. Mittra, G. Manara, and R. Martin, "A hybrid time-domain technique that combines the finite element, finite difference and method of moment techniques to solve complex electromagnetic problems," *IEEE Transactions on Antennas and Propagation*, vol. 52, no. 10, pp. 2666–2674, 2004.

[27] M. Cryan, I. Craddock, R. Penty, C. Railton, and I. White, "Electromagnetic compatibility analysis of multilayer PCBs using a hybrid finite difference time domain (FDTD) - partial element equivalent circuit (PEEC) method," in *2001 31st European Microwave Conference*, pp. 1–4, 2001.

[28] K. S. Yee, "Numerical solution of initial boundary value problems involving Maxwell's equations in isotropic media," *IEEE Transactions on Antennas and Propagation*, vol. 14, pp. 302–307, 1966.

[29] S.-M. Sadrpour, V. Nayyeri, M. Moradi, M. Soleimani, and O. M. Ramahi, "A 3-D hybrid implicit explicit single-field finite-difference time-domain method," *IEEE Transactions on Electromagnetic Compatibility*, vol. 61, no. 3, pp. 945–953, 2019.

[30] P. Bonnet, R. Vernet, and F. Paladian, "Coupling different numerical methods to solve an EMC problem," in *2003 IEEE International Symposium on Electromagnetic Compatibility*, vol. 2, pp. 1070–1073 Vol.2, 2003.

[31] Y. Z. Z. L. He, K. Huang and C. H. Liang, "A new local time-step scheme for hybrid finite difference/finite volume method," *Journal of Electromagnetic Waves and Applications*, vol. 26, no. 5-6, pp. 641–652, 2012.

[32] D. Jiao, M. Lu, E. Michielssen, and J.-M. Jin, "A fast time-domain finite element-boundary integral method for electromagnetic analysis," *IEEE Transactions on Antennas and Propagation*, vol. 49, no. 10, pp. 1453–1461, 2001.

[33] A. B. Diallo, *Co-simulation pour la Modélisation des Phénomènes de Compatibilité Électromagnétique des Systèmes Électriques Complexes*. Ph.D. dissertation, École Centrale de Lyon, France, 2023.

[34] G. Kron, "Generalized theory of electrical machinery," *Transactions of the American Institute of Electrical Engineers*, vol. 49, no. 2, pp. 666–683, 1930.

[35] O. Maurice, "Modified Kron's method for electromagnetic compatibility -MKME- an abstract," 2007.

[36] O. Maurice, "Adaptation of Kron's Tensorial Analysis of Network for the EMC Design and Analysis of Systems." 2016.

[37] O. Maurice, "Caractères remarquables de la méthode de kron," 2016.

[38] S. Leman, A. Reineix, F. Hoeppe, Y. Poiré, M. Mahmoudi, B. Démoulin, F. Üstüner, and V. P. Rodriguez, "Kron's method applied to the study of electromagnetic interference occurring in aerospace systems," in *2012 ESA Workshop on Aerospace EMC*, pp. 1–6, 2012.

[39] S. Op't Land, R. Perdriau, M. Ramdani, O. Maurice, and M. Drissi, "Kron simulation of field-to-line coupling using a meshed and a modified Taylor cell," in *2013 9th International Workshop on Electromagnetic Compatibility of Integrated Circuits (EMC Compo)*, pp. 15–20, IEEE, 2013.

[40] M. Stojanovic, F. Lafon, P. Fernandez-Lopez, S. Op't Land, and R. Perdriau, "Modified Kron's method (MKME) for EMC optimization, applied to an EMC filter," in *2016 Asia-Pacific International Symposium on Electromagnetic Compatibility (APEMC)*, vol. 1, pp. 782–784, IEEE, 2016.

[41] M. Stojanovic, F. Lafon, R. Perdriau, and M. Ramdani, "Accurate analytical prediction of EMI filter attenuation by considering intercomponent coupling phenomena," *IEEE Transactions on Electromagnetic Compatibility*, vol. 61, no. 4, pp. 1042–1051, 2019.

[42] G. Kron, *Diakoptics: Piecewise Solution of Large-scale Systems*. General Electric, 1957.

[43] H. Happ, "Diakoptics - The solution of system problems by tearing," *Proceedings of the IEEE*, vol. 62, no. 7, pp. 930–940, 1974.

[44] P. Aitchison, "Diakoptics as a general approach in engineering," *Journal of Engineering Mathematics*, vol. 21, no. 1, pp. 47–58, 1987.

[45] F. Uriarte, "On Kron's Diakoptics," *Electric Power Systems Research*, vol. 88, p. 146–150, 2012.

[46] A. Klos, "What is Diakoptics?," *International Journal of Electrical Power Energy Systems*, vol. 4, no. 3, pp. 192–195, 1982.

[47] V. Fusco, L. Merugu, and S. McDowall, "An efficient Diakoptics based algorithm for electromagnetic field mapping," in *1991 International Conference on Computation in Electromagnetics*, pp. 51–54, 1991.

[48] L. Merugu and V. F. Fusco, "Concurrent network Diakoptics for electromagnetic field problems," *IEEE Transactions on Microwave Theory and Techniques*, vol. 41, no. 4, pp. 708–716, 1993.

[49] M. Righi, W. J. Hoefer, M. Mongiardo, and R. Sorrentino, "Efficient TLM Diakoptics for separable structures," *IEEE Transactions on Microwave Theory and Techniques*, vol. 43, no. 4, pp. 854–859, 1995.

[50] K. Guillouard, M. Wong, V. F. Hanna, and J. Citerne, "Diakoptics using finite element analysis," in *1996 IEEE MTT-S International Microwave Symposium Digest*, vol. 1, pp. 363–366, 1996.

[51] M. Howykowycz and P. Stakhiv, "Application of Diakoptics approach to analysis of electromagnetic field by means of finite-difference method," *Computational Problems of Electrical Engineering*, vol. 5, no. 2, pp. 79–82, 2015.

[52] E. Chobanyan, D. Olcan, M. Ilic, and B. Notaros, "Volume integral equation-based diakoptic method for electromagnetic modeling," *IEEE Transactions on Microwave Theory and Techniques*, vol. 64, pp. 1–11, 2016.

[53] T. P. Stefański and T. Dziubak, "FDTD simulations on disjoint domains with the use of discrete Green's function Diakoptics," in *2016 21st International Conference on Microwave, Radar and Wireless Communications (MIKON)*, pp. 1–4, 2016.

[54] C.-H. Lai, "Diakoptics, domain decomposition and parallel computing," *The Computer Journal*, vol. 37, no. 10, pp. 840–846, 1994.

[55] C. E. Baum, "The theory of electromagnetic interference control," in *IN: Modern radio science 1990 (A92-17351 05-31). Oxford*, pp. 87–101, 1990.

[56] J. P. Parmantier, "Approche topologique pour l'étude des couplages électromagnétiques," 1991.

[57] P. Besnier, "Etude des couplages électromagnétiques sur des réseaux de lignes de transmission non-uniformes à l'aide d'une approche topologique," 1993.

[58] I. Junqua, J.-P. Parmantier, and W. Quenum, "Couplages électromagnétiques haute fréquence dans des bâtiments – Application des concepts de topologie électromagnétique et Power Balance," in *CEM 2016 : 18ème Colloque international et Exposition sur la Compatibilité Electromagnétique, Rennes, France*, 2016.

[59] C. Kasmi, M. Hélier, M. Darces, and E. Prouff, "High-frequency impedance measurement of electronic devices using a de-embedding technique," in *Ultra-Wideband, Short-Pulse Electromagnetics 10*, pp. 393–401, Springer, 2014.

[60] K. Yong, Y. Li-Ping, Z. Xiang, Z. Hai-Jing, L. Qiang, and H. Ka-Ma, "Electromagnetic topology based fast algorithm for shielding effectiveness estimation of multiple enclosures with apertures," *Acta Physica Sinica -Chinese Edition-*, vol. 65, no. 3, 2016.

[61] S. Zhou, W. Li, and Q. Li, "Level-set based topology optimization for electromagnetic dipole antenna design," *Journal of Computational Physics*, vol. 229, no. 19, pp. 6915–6930, 2010.

[62] E. Genender, H. Garbe, and F. Sabath, "Probabilistic risk analysis technique of intentional electromagnetic interference at system level," *IEEE Transactions on Electromagnetic Compatibility*, vol. 56, no. 1, pp. 200–207, 2013.

[63] M. Olivas, J. Genoulaz, and L. Incarbone, "Modelling multi-conductor transmission lines using BLT equation for wire diagnosis," in *SAE Technical Paper*, vol. 7, 2013.

[64] E. de Rocquigny, "La maîtrise des incertitudes dans un contexte industriel. 1ère partie : une approche méthodologique globale basée sur des exemples," *Journal de la Société française de statistique*, vol. 147, no. 3, pp. 33–71, 2006.

[65] B. Sudret, *Uncertainty propagation and sensitivity analysis in mechanical models – Contributions to structural reliability and stochastic spectral methods*. HDR dissertation, Blaise Pascal University, Clermont-Ferrand, France, 2007.

[66] M. N. O. Sadiku, *Monte Carlo Methods for Electromagnetics*. Hoboken, NJ: CRC Press, 2009.

[67] L. Musso, V. Berat, F. Canavero, B. Demoulin, *et al.*, "A plane wave Monte Carlo simulation method for reverberation chambers," in *EMC Europe 2002, International Symposium on Electromagnetic Compatibility*, vol. 1, pp. 45–50, 2002.

[68] A. Litvinenko, A. C. Yucel, H. Bagci, J. Oppelstrup, E. Michielssen, and R. Tempone, "Computation of electromagnetic fields scattered from objects with uncertain shapes using multilevel Monte Carlo method," *IEEE Journal on Multiscale and Multiphysics Computational Techniques*, vol. 4, pp. 37–50, 2019.

[69] E. Genender, H. Garbe, and F. Sabath, "Probabilistic risk analysis technique of intentional electromagnetic interference at system level," *IEEE Transactions on Electromagnetic Compatibility*, vol. 56, no. 1, pp. 200–207, 2014.

[70] S. Lalléchère, S. Girard, P. Bonnet, and F. Paladian, "Stochastic approaches for ElectroMagnetic Compatibility: A paradigm from complex reverberating enclosures," in *2013 International Conference on Electromagnetics in Advanced Applications (ICEAA)*, pp. 374–377, 2013.

[71] Y. Li, X. Zhao, L. Yan, K. Huang, and H. Zhou, "Probabilistic-statistical model based on mode expansion of the EM field of a reverberation chamber and its Monte Carlo simulation," in *2016 Asia-Pacific International Symposium on Electromagnetic Compatibility (APEMC)*, vol. 01, pp. 779–781, 2016.

[72] G. P. Veropoulos, P. J. Papakanellos, and C. Vlachos, "A probabilistic approach for the susceptibility assessment of a straight PCB trace excited by random plane-wave fields," *IEEE Transactions on Electromagnetic Compatibility*, vol. 60, no. 1, pp. 258–265, 2018.

[73] S. R. Rengarajan, M. S. Zawadzki, and R. E. Hodges, "Waveguide-slot array antenna designs for low-average-sidelobe specifications," *IEEE Antennas and Propagation Magazine*, vol. 52, no. 6, pp. 89–98, 2010.

[74] Y. Zhao, X. Zhao, L. Yan, C. Liu, K. Huang, Q. Liu, and H. Zhou, "Analysis of field-to-transmission line coupling inside a reverberation chamber based on mode expansion method," in *2018 IEEE International Symposium on Electromagnetic Compatibility and 2018 IEEE Asia-Pacific Symposium on Electromagnetic Compatibility (EMC/APEMC)*, pp. 84–87, 2018.

[75] H. Niederreiter, *Random Number Generation and Quasi-Monte Carlo Methods*. Society for Industrial and Applied Mathematics, 1992.

[76] T. Simpson, T. Mauery, J. Korte, and F. Mistree, "Comparison of response surface and Kriging models for multidisciplinary design optimization," in *7th AIAA/USAF/NASA/ISSMO Symposium on Multidisciplinary Analysis and Optimization*, 1998.

[77] V. Rannou, F. Brouaye, M. Hélier, and W. Tabbara, "Kriging the quantile: application to a simple transmission line model," *Inverse Problems*, vol. 18, no. 1, pp. 1–37, 2002.

[78] T. Houret, P. Besnier, S. Vauchamp, and P. Pouliguen, "Controlled stratification based on Kriging surrogate model: An algorithm for determining extreme quantiles in Electromagnetic Compatibility risk analysis," *IEEE Access*, vol. 8, pp. 3837–3847, 2020.

[79] T. Bdour, C. Guiffaut, and A. Reineix, "Use of adaptive Kriging metamodeling in reliability analysis of radiated susceptibility in coaxial shielded cables," *IEEE Transactions on Electromagnetic Compatibility*, vol. 58, no. 1, pp. 95–102, 2016.

[80] C. Chauviere, J. S. Hesthaven, and L. C. Wilcox, "Efficient computation of RCS from scatterers of uncertain shapes," *IEEE Transactions on Antennas and Propagation*, vol. 55, no. 5, pp. 1437–1448, 2007.

[81] C. Kasmi, S. Lalléchère, J. L. Esteves, S. Girard, P. Bonnet, F. Paladian, and E. Prouff, "Stochastic EMC/EMI experiments optimization using resampling techniques," *IEEE Transactions on Electromagnetic Compatibility*, vol. 58, no. 4, pp. 1143–1150, 2016.

[82] F. Diouf, F. Paladian, M. Fogli, C. Chauvière, and P. Bonnet, "Emission in reverberation chamber: numerical evaluation of the total power radiated by a wire with a stochastic

collocation method," *2007 18th International Zurich Symposium on Electromagnetic Compatibility*, pp. 99–102, 2007.

[83] S. Lalléchère, P. Bonnet, and F. Paladian, "Electrical stochastic modeling of cell for bioelectromagnetic compatibility applications," *Annales des télécommunications*, vol. 69, pp. 295–308, 2014.

[84] F. Paladian, P. Bonnet, and S. Lalléchère, "Modeling complex systems for EMC applications by considering uncertainties," in *2011 XXXth URSI General Assembly and Scientific Symposium*, pp. 1–4, 2011.

[85] N. Wiener, "The homogeneous chaos," *American Journal of Mathematics*, vol. 60, no. 4, pp. 897–936, 1938.

[86] R. Ghanem and P. Spanos, *Stochastic Finite Elements: A Spectral Approach*. Dover Publications, 1991.

[87] P. Manfredi and F. G. Canavero, "Polynomial chaos representation of transmission-line response to random plane waves," *International Symposium on Electromagnetic Compatibility - EMC EUROPE*, pp. 1–6, 2012.

[88] P. Manfredi and F. G. Canavero, "General decoupled method for statistical interconnect simulation via polynomial chaos," in *2014 IEEE 23rd Conference on Electrical Performance of Electronic Packaging and Systems*, pp. 25–28, 2014.

[89] P. Manfredi and F. G. Canavero, "Numerical calculation of polynomial chaos coefficients for stochastic per-unit-length parameters of circular conductors," *IEEE Transactions on Magnetics*, vol. 50, no. 3, pp. 74–82, 2014.

[90] P. Manfredi, D. Vande Ginste, D. De Zutter, and F. G. Canavero, "Generalized decoupled polynomial chaos for nonlinear circuits with many random parameters," *IEEE Microwave and Wireless Components Letters*, vol. 25, no. 8, pp. 505–507, 2015.

[91] I. S. Stievano, P. Manfredi, and F. G. Canavero, "Parameters variability effects on multiconductor interconnects via Hermite polynomial chaos," *IEEE Transactions on Components, Packaging and Manufacturing Technology*, vol. 1, no. 8, pp. 1234–1239, 2011.

[92] P. Manfredi, "A hierarchical approach to dimensionality reduction and nonparametric problems in the polynomial chaos simulation of transmission lines," *IEEE Transactions on Electromagnetic Compatibility*, vol. 62, no. 3, pp. 736–745, 2020.

[93] G. J. K. Tomy and K. J. Vinoy, "A fast polynomial chaos expansion for uncertainty quantification in stochastic electromagnetic problems," *IEEE Antennas and Wireless Propagation Letters*, vol. 18, no. 10, pp. 2120–2124, 2019.

[94] T. Bdour and A. Reineix, "Global sensitivity analysis and uncertainty quantification of radiated susceptibility in PCB using nonintrusive polynomial chaos expansions," *IEEE Transactions on Electromagnetic Compatibility*, vol. 58, no. 3, pp. 939–942, 2016.

[95] A. Kouassi, J.-M. Bourinet, S. Lalléchère, P. Bonnet, and M. Fogli, "Reliability and sensitivity analysis of transmission lines in a probabilistic EMC context," *IEEE Transactions on Electromagnetic Compatibility*, vol. 58, no. 2, pp. 561–572, 2016.

[96] E. Genender, H. Garbe, and F. Sabath, "Probabilistic risk analysis technique of intentional electromagnetic interference at system level," *IEEE Transactions on Electromagnetic Compatibility*, vol. 56, no. 1, pp. 200–207, 2014.

[97] A. R. Ruddle a and A. J. Martin, "The need for a risk-based systems engineering approach in automotive EMC engineering," in *2018 International Symposium on Electromagnetic Compatibility (EMC EUROPE)*, pp. 293–298, 2018.

[98] E. Garcia, "Electromagnetic compatibility uncertainty, risk, and margin management," *IEEE Transactions on Electromagnetic Compatibility*, vol. 52, no. 1, pp. 3–10, 2010.

[99] IEC TR 61000-1-6:2012, "Electromagnetic compatibility (EMC) - part 1-6: General - Guide to the assessment of measurement uncertainty,"

[100] CISPR TR 16-4-1:2009, "Specification for radio disturbance and immunity measuring apparatus and methods - Part 4-1: Uncertainties, statistics and limit modelling - Uncertainties in standardized EMC tests,"

[101] T. Houret, P. Besnier, S. Vauchamp, and P. Pouliguen, "Controlled stratification based on Kriging surrogate model: An algorithm for determining extreme quantiles in electromagnetic compatibility risk analysis," *IEEE Access*, vol. 8, pp. 3837–3847, 2020.

[102] T. Houret, P. Besnier, S. Vauchamp, and P. Pouliguen, "Combining Kriging and controlled stratification to identify extreme levels of electromagnetic interference," in *2019 International Symposium on Electromagnetic Compatibility - EMC EUROPE*, pp. 404–409, 2019.

[103] C. Kasmi, S. Lalléchère, J. L. Esteves, S. Girard, P. Bonnet, F. Paladian, and E. Prouff, "Stochastic EMC/EMI experiments optimization using resampling techniques," *IEEE Transactions on Electromagnetic Compatibility*, vol. 58, no. 4, pp. 1143–1150, 2016.

[104] B. Iooss and P. Lemaître, "A review on global sensitivity analysis methods," *Operations Research/ Computer Science Interfaces Series*, vol. 59, 2014.

[105] D. Cacuci, *Sensitivity & Uncertainty Analysis, Volume 1: Theory*, vol. 1. CRC Press, 2003.

[106] I. M. Sobol, "Sensitivity estimates for nonlinear mathematical models," in *Mathematical Modelling and Computational Experiments*, vol. 4, pp. 407–414, 1993.

[107] T. Homma and A. Saltelli, "Importance measures in global sensitivity analysis of nonlinear models," *Reliability Engineering System Safety*, vol. 52, no. 1, pp. 1–17, 1996.

[108] A. Saltelli, S. Tarantola, and K. P.-S. Chan, "A quantitative model-independent method for global sensitivity analysis of model output," *Technometrics*, vol. 41, no. 1, pp. 39–56, 1999.

[109] S. Andrea, C. K, and S. E. Marian, *Sensitivity Analysis*, vol. 134. J. Wiley Sons, 2000.

[110] A. Saltelli and I. M. Sobol', "About the use of rank transformation in sensitivity analysis of model output," *Reliability Engineering System Safety*, vol. 50, no. 3, pp. 225–239, 1995.

[111] B. Efron and C. Stein, "The Jackknife Estimate of Variance," *The Annals of Statistics*, vol. 9, no. 3, pp. 586 – 596, 1981.

[112] R. Cukier, H. Levine, and K. Shuler, "Nonlinear sensitivity analysis of multiparameter model systems," *Journal of Computational Physics*, vol. 26, no. 1, pp. 1–42, 1978.

[113] A. Saltelli, S. Tarantola, and K. P.-S. Chan, "A quantitative model-independent method for global sensitivity analysis of model output," *Technometrics*, vol. 41, no. 1, pp. 39–56, 1999.

[114] R. I. Cukier, J. H. Schaibly, and K. E. Shuler, "Study of the sensitivity of coupled reaction systems to uncertainties in rate coefficients. III. Analysis of the approximations," *The Journal of Chemical Physics*, vol. 63, no. 3, pp. 1140–1149, 2008.

[115] A. Saltelli and R. Bolado, "An alternative way to compute fourier amplitude sensitivity test (FAST)," *Computational Statistics Data Analysis*, vol. 26, no. 4, pp. 445–460, 1998.

[116] G. E. B. Archer, A. Saltelli, and I. M. Sobol, "Sensitivity measures, ANOVA-like techniques and the use of bootstrap," *Journal of Statistical Computation and Simulation*, vol. 58, no. 2, pp. 99–120, 1997.

[117] M. D. Morris, "Factorial sampling plans for preliminary computational experiments," *Quality Engineering*, vol. 37, pp. 307–310, 1991.

[118] M. Larbi, P. Besnier, and B. Pecqueux, "Probability of EMC failure and sensitivity analysis with regard to uncertain variables by reliability methods," *IEEE Transactions on Electromagnetic Compatibility*, vol. 57, no. 2, pp. 274–282, 2015.

[119] H. Acikgoz and R. Mittra, "Statistical analysis of electromagnetic structures and antennas using the polynomial chaos expansion method," in *2017 11th European Conference on Antennas and Propagation (EUCAP)*, pp. 798–800, 2017.

[120] A. Kouassi, N. Nguyen-Trong, T. Kaufmann, S. Lalléchère, P. Bonnet, and C. Fumeaux, "Reliability-aware optimization of a wideband antenna," *IEEE Transactions on Antennas and Propagation*, vol. 64, no. 2, pp. 450–460, 2016.

[121] F. Yildiz, H.-D. Brüns, and C. Schuster, "Variance-based iterative model order reduction of equivalent circuits for EMC analysis," *IEEE Transactions on Electromagnetic Compatibility*, vol. 61, pp. 128–139, 2019.

[122] T. Bdour, C. Guiffaut, and A. Reineix, "Use of adaptive Kriging metamodeling in reliability analysis of radiated susceptibility in coaxial shielded cables," *IEEE Transactions on Electromagnetic Compatibility*, vol. 58, no. 1, pp. 95–102, 2016.

[123] M. Cvetković, S. Lalléchère, K. Drissi, P. Bonnet, and D. Poljak, "Stochastic sensitivity in homogeneous electromagnetic-thermal dosimetry model of human brain," *Applied Computational Electromagnetics Society Journal*, vol. 31, pp. 644–652, 2016.

[124] C. S. Burrus and T. Parks, "Convolution algorithms," *Citeseer: New York, NY, USA*, vol. 6, p. 15, 1985.

[125] P. Bachmann, *Die Analytische Zahlentheorie / Dargestellt Von Paul Bachmann.* MPublishing, 2006.

[126] C. Caloz and T. Itoh, *Electromagnetic metamaterials: Transmission line theory and microwave applications*. John Wiley & Sons, 2005.

[127] K. Yee, "Numerical solution of initial boundary value problems involving Maxwell's equations in isotropic media," *IEEE Transactions on Antennas and Propagation*, vol. 14, no. 3, pp. 302–307, 1966.

[128] A. Al Ibrahim, *Linear and Nonlinear Numerical Methods for Real-World Inverse Problems of Time-Domain Electromagnetic Active Shaping - From Theory to Experiment*. Ph.D. dissertation, Clermont Auvergne University, Clermont-Ferrand, France, Jan. 2021.

[129] A. N. Tikhonov, "Solution of incorrectly formulated problems and the regularization method," *Sov Dok*, vol. 4, pp. 1035–1038, 1963.

[130] K. Kunz and R. Luebbers, *The Finite Difference Time Domain Method for Electromagnetics*. CRC Press, 2018.

[131] J. Jin, *The Finite Element Method in Electromagnetics*. IEEE Press, Wiley, 2015.

[132] R. Rubinstein and D. Kroese, *Simulation and the Monte Carlo Method*, vol. 707. 2008.

[133] P. Bonnet, F. Diouf, C. Chauvière, S. Lalléchère, M. Fogli, and F. Paladian, "Numerical simulation of a reverberation chamber with a stochastic collocation method," *Comptes Rendus Physique*, vol. 10, no. 1, pp. 54–64, 2009.

[134] D. Xiu, *Numerical Methods for Stochastic Computations: A Spectral Method Approach*. Princeton University Press, 2010.

[135] G. Blatman and B. Sudret, "Adaptive sparse polynomial chaos expansion based on least angle regression," *Journal of Computational Physics*, vol. 230, no. 6, pp. 2345–2367, 2011.

[136] Y. Shin and D. Xiu, "Nonadaptive quasi-optimal points selection for least squares linear regression," *SIAM Journal on Scientific Computing*, vol. 38, pp. A385–A411, 2016.

[137] G. E. Andrews and R. Askey, "Classical orthogonal polynomials," in *Polynômes Orthogonaux et Applications*, pp. 36–62, Springer Berlin Heidelberg, 1985.

[138] O. P. Le Maıtre, M. T. Reagan, H. N. Najm, R. G. Ghanem, and O. M. Knio, "A stochastic projection method for fluid flow: II. Random process," *Journal of Computational Physics*, vol. 181, no. 1, pp. 9–44, 2002.

[139] W. Hoeffding, "A Class of Statistics with Asymptotically Normal Distribution," *The Annals of Mathematical Statistics*, vol. 19, no. 3, pp. 293 – 325, 1948.

[140] I. M. Sobol, "Global sensitivity indices for nonlinear mathematical models and their Monte Carlo estimates," *Mathematics and Computers in Simulation*, vol. 55, no. 1, pp. 271–280, 2001.

[141] B. Sudret, "Global sensitivity analysis using polynomial chaos expansion," *Reliability Engineering System Safety*, vol. 93, pp. 964–979, 2008.

[142] P. Bonnet, C. Chauvière, and S. Lalléchère, "Analyse de sensibilité globale par une méthode non intrusive de collocation stochastique," in *19ème Colloque International & Exposition sur la Compatibilité Electromagnétique, Paris, France*, 2018.

[143] G. Tang, G. Iaccarino, and M. Eldred, *Global Sensitivity Analysis for Stochastic Collocation*. 2010.

[144] R. Vernet, *Approche mixte théorie / expérimentation pour la modélisation numérique de chambres réverbérantes à brassage de modes*. Ph.D. dissertation, Clermont-Ferrand 2 University, Clermont-Ferrand, France, June 2006.

[145] J. F. Trevor Hastie, Robert Tibshirani, *The Elements of Statistical Learning*. Springer New York, NY, 2009.

[146] M. Awad and R. Khanna, *Support Vector Regression*, pp. 67–80. Apress, 2015.

[147] B. Sudret, S. Marelli, and J. Wiart, "Surrogate models for uncertainty quantification: An overview," in *2017 11th European Conference on Antennas and Propagation (EUCAP)*, pp. 793–797, 2017.

[148] T. Gerstner and M. Griebel, "Numerical integration using sparse grids," *Numerical Algorithms*, vol. 18, pp. 209–232, 2004.

[149] R. Bellman, "Dynamic programming," *Science*, vol. 153, no. 3731, pp. 34–37, 1966.

[150] S. Clénet, "Approximation methods to solve stochastic problems in computational electromagnetics," in *Scientific Computing in Electrical Engineering*, pp. 199–214, Springer International Publishing, 2016.

[151] R. Y. Rubinstein and P. W. Glynn, "How to deal with the curse of dimensionality of likelihood ratios in Monte Carlo simulation," *Stochastic Models*, vol. 25, no. 4, pp. 547–568, 2009.

[152] L. Chen, Y. Chen, and Q. Li, "Stochastic domain decomposition based on variable-separation method," *arXiv preprint arXiv:2304.05708*, 2023.

[153] J. F. Reis, O. P. Le Maître, P. M. Congedo, and P. Mycek, "Stochastic preconditioning of domain decomposition methods for elliptic equations with random coefficients," *Computer Methods in Applied Mechanics and Engineering*, vol. 381, p. 113845, 2021.

[154] I. Massaoudi and P. Bonnet, "Mise en œuvre expérimentale d'une méthode de co-simulation temporelle totalement asynchrone pour un réseau de lignes de transmission," in *21ème Colloque International et Exposition sur la Compatibilité Electromagnétique (CEM FRANCE), Toulouse, France*, 2023.

[155] I. Massaoudi and P. Bonnet, "A non-overlapping time domain decomposition method," in *2023 International Conference on Electromagnetics in Advanced Applications (ICEAA), Venise, Italy*, pp. 612–612, IEEE, 2023.

[156] I. Massaoudi and P. Bonnet, "Uncertainty propagation with an asynchronous temporal co-simulation method applied to a transmission line network," in *2022 International Symposium on Electromagnetic Compatibility (EMC EUROPE), Gothenburg, Sweden*, pp. 305–310, IEEE, 2022.

[157] I. Massaoudi and P. Bonnet, "An asynchronous co-simulation method for time-dependent simulations: Application to a transmission line network," in *2022 International Conference on Antennas and Electromagnetic Systems (AES), Marrakesh, Morocco*, pp. 367–368, 2020.

[158] I. Massaoudi and P. Bonnet, "A domain decomposition approach for cost effective transmission lines time domain stochastic simulations," *IEEE Transactions on Electromagnetic Compatibility*, vol. 66, no. 1, pp. 180–188, 2024.

[159] O. Osman, S. Sallem, L. Sommervogel, M. Olivas Carrion, P. Bonnet, and F. Paladian, "Distributed reflectometry for soft fault identification in wired networks using neural network and genetic algorithm," *IEEE Sensors Journal*, vol. PP, pp. 1–1, 2020.

List of Personal Publications

Journal Paper:

I. Massaoudi and P. Bonnet, "A Domain Decomposition Approach for Cost Effective Transmission Lines Time Domain Stochastic Simulations", *IEEE Transactions on Electromagnetic Compatibility*, vol. 66, no. 1, pp. 180-188, Feb. 2024, doi: 10.1109/TEMC.2023.3342275. [**Available here**]

Conference Papers:

- **I. Massaoudi** and P. Bonnet, "An Asynchronous Co-Simulation Method for Time-Dependent Simulations: Application to a Transmission Line Network", *8th International Conference on Antennas and Electromagnetic Systems AES*, Marrakech, Morocco, 2022, pp. 367-383. [**Available here**]
- **I. Massaoudi** and P. Bonnet, "Uncertainty Propagation with an Asynchronous Temporal Co-simulation Method Applied to a Transmission Line Network," *2022 International Symposium on Electromagnetic Compatibility – EMC Europe*, Gothenburg, Sweden, 2022, pp. 305-310. [**Available here**]
- **I. Massaoudi** and P. Bonnet, "Mise en œuvre Expérimentale d'une Méthode de Co- Simulation Temporelle Totalement Asynchrone pour un Réseau de Lignes de Transmission", *21ème Colloque International et Exposition sur la Compatibilité Electromagnétique*, 6 pages, Toulouse, France, 2023.
- **I. Massaoudi** and P. Bonnet, "A Non-Overlapping Time Domain Decomposition Method", *International Conference on Electromagnetics in Advanced Applications ICEAA*, Venice, Italy, 2023.

APPENDIX : 1D FDTD Modeling of the Transmission Line Equations

In this appendix, we provide additional elements for a better understanding of the discretization of the telegrapher's equations (2.7) and (2.8), defined in section (2.2.1) of Chapter 2, using the Finite-Difference-Time-Domain (FDTD) method. The discretized equations of the voltage (2.28) and current (2.29) have been succinctly given in section (2.2.3), as they serve primarily to model the propagation phenomenon in transmission lines numerically. We propose through this appendix to add further details with a complete demonstration of these equations in the first section. For the first and last meshes of the transmission lines, new boundary conditions are introduced, the voltage (or current) should be therefore updated. The demonstration of equations (2.30) and (2.31) respectively referring to the voltage at the first and last meshes of the transmission line will be detailed in the second section. The voltage and current obtained at the junction level for a Y-branched transmission lines network, given by equations (2.32) and (2.33) will be detailed in the third section.

A.1 Transmission lines theory

A.1.1 Background and history

The foundations of modern electromagnetic theory were laid by James Clerk Maxwell in 1873, who proved mathematically with four equations the propagation of the electromagnetic wave and the idea that light is a form of electromagnetic energy. Maxwell's equations describe the coupling between electric and magnetic fields. They also show how electromagnetic waves interact with the surrounding medium. Oliver Heaviside (1880-1887) was the first to study the guided propagation of electrical signals through pairs of straight, parallel wires of finite conductivity. Using Maxwell's electromagnetic theory, Heaviside developed the theory of transmission lines as we know it today and eliminated many of the mathematical complexities of Maxwell's theory. The theory of transmissions establishes the link between Maxwell's theory of electromagnetics and G. Kirchhoff's theory of circuits by G. Kirchhoff, so this method is of significant importance in the analysis of microwave circuits and microwave devices. Heaviside obtained his model from a formulation based directly on a quasi-transverse propagation

approximation transverse propagation (quasi-TEM) using Maxwell field theory. The proposed model is based on the following assumptions following assumptions:

- The quasi-parallel interconnection wires are metals, whose electrical behavior is governed by Ohm's law.
- The structure of the electromagnetic fields surrounding the wires is of the quasi-TEM type.
- The total current flowing through each cross-section is zero.

A.1.2 'RLCG' Transmission lines' model

Transmission lines guide the propagation of electromagnetic energy from a source terminal to a load terminal. Transmission lines can take on many physical forms, including a twisted pair line used for telephony or internet connections, coaxial cables, or any of a number of multi-conductor wave guiding systems. Transmission line modeling is typically a one-dimensional approximation of the physical model, representing line voltages and currents as a function of the transmission line axis. A transmission line of elementary length dx is represented schematically as a two-wire line (since transmission lines always have at least two wires) is shown in Figure (A.1.1).

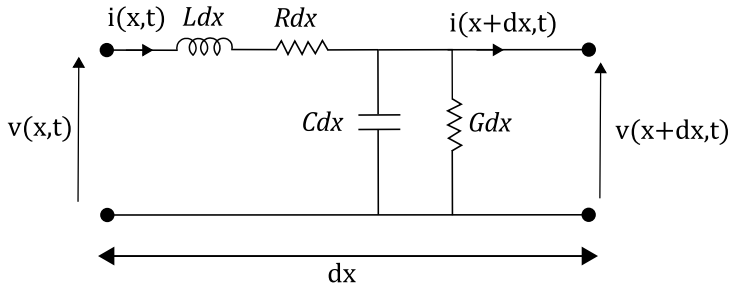

Figure A.1.1: *Schematic representation of the elementary component of a transmission line (RLCG model).*

The series inductance L $(H.m^{-1})$ represents the self-inductance of the two conductors, and the capacitance C $(F.m^{-1})$ is due to the proximity between the two conductors. R $(\Omega.m^{-1})$ represents the resistance due to the conductivity of the conductors, and conductance G $(S.m^{-1})$ is due to dielectric losses in the material separating the conductors. R and G therefore represent losses. A finite length of a transmission line can be viewed as a cascade of sections of the form shown in Figure (A.1.1).

The voltage and current in a transmission line are functions of two variables, position x and time t. Based on Figure (A.1.1), Kirchhoff's laws give the voltage and current equations given by

$$v(x+dx,t)-v(x,t)=-Rdxi(x,t)-Ldx\frac{\partial i(x,t)}{\partial t} \tag{A.1.1}$$

$$i(x+dx,t)-i(x,t)=-Gdxv(x+dx,t)-Cdx\frac{\partial v(x+dx,t)}{\partial t} \tag{A.1.2}$$

Dividing both equations (A.1.1) and (A.1.2) by dx, where $dx \to 0$, gives the following transmission line equations also known as the telegrapher's equations of Heaviside 1880, as follows:

$$\frac{\partial v(x,t)}{\partial x}=-Ri(x,t)-L\frac{\partial i(x,t)}{\partial t} \tag{A.1.3}$$

$$\frac{\partial i(x,t)}{\partial x}=-Gv(x,t)-C\frac{\partial v(x,t)}{\partial t} \tag{A.1.4}$$

where $v(x,t)$ is the line voltage at position x along the transmission line axis at time t and $i(x,t)$ is the line current.

The two equations can be combined into the familiar wave equation governing the line's voltage and current, such as

$$\frac{\partial^2 v(x,t)}{\partial^2 x}=LC\frac{\partial^2 v(x,t)}{\partial t}+(RC+LG)\frac{\partial v(x,t)}{\partial t}+RGv(x,t) \tag{A.1.5}$$

$$\frac{\partial^2 i(x,t)}{\partial^2 x}=LC\frac{\partial^2 i(x,t)}{\partial t}+(RC+LG)\frac{\partial i(x,t)}{\partial t}+RGi(x,t) \tag{A.1.6}$$

These equations has a well-known solution expressed as a superposition of forward and backward traveling waves, given by

$$V(x,t)=V^{(+)}f(x-\frac{t}{\sqrt{LC}})+V^{(-)}f(x+\frac{t}{\sqrt{LC}}) \tag{A.1.7}$$

$$I(x,\omega)=I^{(+)}f(x-\frac{t}{\sqrt{LC}})+I^{(-)}f(x+\frac{t}{\sqrt{LC}}) \tag{A.1.8}$$

where $f(.)$ is a general function representing the wave, and $V^{+/(-)}$ (and $I^{+/(-)}$) is the amplitude of the forward and the backward traveling waves, respectively. The actual values of $f(.)$ and $V^{(+)/(-)}$ (and $I^{+/(-)}$) are determined by the appropriate initial conditions and boundary conditions at the terminating ends of the transmission line.

A.2 Numercial modeling of the transmission lines

A.2.1 Finite Difference Approximations

To study the numerical solution to the coupled first-order transmission line equations expressed by equations (A.1.3) and (A.1.4), the first-order space and time derivatives will be approximated via "Finite-Difference" approximations. If the function $f(.)$ is continuous, a Taylor series expansion of f about the points $x \pm \frac{\Delta x}{2}$ can be performed

$$f(x \pm \frac{\Delta x}{2}) = f(x) \pm \frac{\partial f(x)}{\partial x}\frac{\Delta x}{2}\frac{1}{1!} + \frac{\partial^2 f(x)}{\partial x^2}(\frac{\Delta x}{2})^2\frac{1}{2!} + \frac{\partial^3 f(x)}{\partial x^3}(\frac{\Delta x}{2})^3\frac{1}{3!} + ... \tag{A.2.1}$$

where Δx is assumed to be small. We then subtract the two expansions and normalize the result by Δx, leading to

$$\frac{f(x+\frac{\Delta x}{2}) - f(x-\frac{\Delta x}{2})}{\Delta x} = \frac{\partial f(x)}{\partial x} + \Delta x^2 \frac{\partial^3 f(x)}{\partial x^3}\frac{1}{24} + ... \tag{A.2.2}$$

Note that the terms with even-order derivatives cancel. Rearranging terms, the first-order derivative with respect to x can be expressed as

$$\frac{\partial f(x)}{\partial x} \approx \frac{f(x+\frac{\Delta x}{2}) - f(x-\frac{\Delta x}{2})}{\Delta x} + \mathcal{O}(\Delta x^2) \tag{A.2.3}$$

This is known as the "central difference" approximation of the first-order derivative. The trailing term on the right-hand side represents the leading order error in the approximation. The error will decay as Δx^2 with decreasing Δx. The approximation is thus said to be "second-order accurate."

A.2.2 Explicit time update solution of the Telegraph' equations

It would appear that the transmission line equations can be approximated to second-order accuracy using central differences. To this end, the transmission line equations (A.1.3) and (A.1.4) are expressed as

$$\frac{v(x+\frac{\Delta x}{2},t) - v(x-\frac{\Delta x}{2},t)}{\Delta x} \approx -Ri(x,t) - L\frac{i(x+\frac{\Delta x}{2},t) - i(x-\frac{\Delta x}{2},t)}{\Delta t} \tag{A.2.4}$$

$$\frac{i(x+\frac{\Delta x}{2},t) - i(x-\frac{\Delta x}{2},t)}{\Delta x} \approx -Gv(x,t) - C\frac{v(x+\frac{\Delta x}{2},t) - v(x-\frac{\Delta x}{2},t)}{\Delta t} \tag{A.2.5}$$

where Δx is the spacing between discrete spatial samples, and Δt is the spacing between discrete time samples. Both of these equations are second-order accurate at (x,t) in space and time. These approximate equations can be mapped to a discrete space by sampling V and I at discrete locations in space and time at uniformly spaced intervals of Δx and Δt, respectively. However, it is observed from equations (A.2.4) and (A.2.4) that the discrete samples of v and i cannot be co-located in space or time if these two equations are to be consistent. In fact, the discrete samples of v and i are separated in both space and time by Δx and Δt, respectively, as shown in the spatial-time grid of Figure (A.2.1).

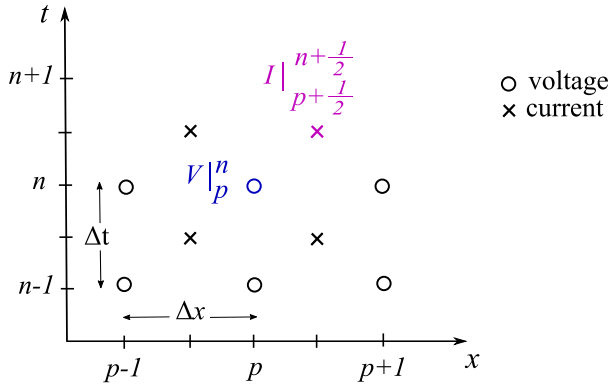

Figure A.2.1: *Staggered grid sampling of the voltage V (circle) and the current I (cross) in space x and time t.*

Following this schematic representation, the discrete representation for a uniform, staggered time and space sampling of the voltage and current of equations (A.1.3) and (A.1.4) are defined by

$$V|_p^n = v(p\Delta x, n\Delta t) \tag{A.2.6}$$

$$I|_p^n = i(p\Delta x, n\Delta t) \tag{A.2.7}$$

where p and n are integers. With this sampling, the discrete transmission line equations (A.2.4) and (A.2.4) are expressed as follows:

$$\frac{V|_{p+1}^n - V|_p^n}{\Delta x} \approx -RI|_{p+\frac{1}{2}}^n - L\frac{I|_{p+\frac{1}{2}}^{n+\frac{1}{2}} - I|_{p+\frac{1}{2}}^{n-\frac{1}{2}}}{\Delta t} \tag{A.2.8}$$

$$\frac{I|_{p+\frac{1}{2}}^{n+\frac{1}{2}} - I|_{p-\frac{1}{2}}^{n+\frac{1}{2}}}{\Delta x} \approx -GV|_p^{n+\frac{1}{2}} - C\frac{V|_p^{n+1} - V|_p^n}{\Delta t} \tag{A.2.9}$$

By approximating the terms $I|_{p+\frac{1}{2}}^{n}$ of equation (A.2.8), respectively $V|_{p}^{n+\frac{1}{2}}$ of equation (A.2.9), with the following equations

$$I|_{p+\frac{1}{2}}^{n} = \frac{I|_{p+\frac{1}{2}}^{n+\frac{1}{2}} + I|_{p+\frac{1}{2}}^{n-\frac{1}{2}}}{2} \tag{A.2.10}$$

$$V|_{p}^{n+\frac{1}{2}} = \frac{V|_{p}^{n+1} + V|_{p}^{n}}{2} \tag{A.2.11}$$

We obtain the discrete equation of voltage and current

$$\frac{V|_{p+1}^{n} - V|_{p}^{n}}{\Delta x} \approx -R\Big(\frac{I|_{p+\frac{1}{2}}^{n+\frac{1}{2}} + I|_{p+\frac{1}{2}}^{n-\frac{1}{2}}}{2}\Big) - L\Big(\frac{I|_{p+\frac{1}{2}}^{n+\frac{1}{2}} - I|_{p+\frac{1}{2}}^{n-\frac{1}{2}}}{\Delta t}\Big) \tag{A.2.12}$$

$$\frac{I|_{p+\frac{1}{2}}^{n+\frac{1}{2}} - I|_{p-\frac{1}{2}}^{n+\frac{1}{2}}}{\Delta x} \approx -G\Big(\frac{V|_{p}^{n+1} + V|_{p}^{n}}{2}\Big) - C\Big(\frac{V|_{p}^{n+1} - V|_{p}^{n}}{\Delta t}\Big) \tag{A.2.13}$$

We strat by expanding the equation (A.2.12) as follows:

$$\begin{aligned}
\frac{V|_{p+1}^{n} - V|_{p}^{n}}{\Delta x} &\approx -\frac{R}{2} I|_{p+\frac{1}{2}}^{n+\frac{1}{2}} - \frac{R}{2} I|_{p+\frac{1}{2}}^{n-\frac{1}{2}} - \frac{L}{\Delta t} I|_{p+\frac{1}{2}}^{n+\frac{1}{2}} + \frac{L}{\Delta t} I|_{p+\frac{1}{2}}^{n-\frac{1}{2}} \\
&\approx I|_{p+\frac{1}{2}}^{n+\frac{1}{2}}\Big(-\frac{R}{2} - \frac{L}{\Delta t}\Big) + I|_{p+\frac{1}{2}}^{n-\frac{1}{2}}\Big(-\frac{R}{2} + \frac{L}{\Delta t}\Big) \\
&\approx I|_{p+\frac{1}{2}}^{n+\frac{1}{2}}\Big(\frac{-2\Delta t - 2L}{2\Delta t}\Big) + I|_{p+\frac{1}{2}}^{n-\frac{1}{2}}\Big(\frac{-R\Delta t + 2L}{2\Delta t}\Big)
\end{aligned} \tag{A.2.14}$$

We then extract the current $I|_{p+\frac{1}{2}}^{n+\frac{1}{2}}$ as follows:

$$\begin{aligned}
I|_{p+\frac{1}{2}}^{n+\frac{1}{2}} &\approx \frac{-2\Delta t}{R\Delta t + 2L}\Big(\frac{V|_{p+1}^{n} - V|_{p}^{n}}{\Delta x}\Big) - \frac{2\Delta t}{R\Delta t + 2L} \times \frac{-R\Delta t + 2L}{2\Delta t} I|_{p+\frac{1}{2}}^{n-\frac{1}{2}} \\
&\approx \frac{-2\Delta t}{(R\Delta t + 2L)\Delta x}\Big(V|_{p+1}^{n} - V|_{p}^{n}\Big) - \frac{R\Delta t - 2L}{R\Delta t + 2L} I|_{p+\frac{1}{2}}^{n-\frac{1}{2}}
\end{aligned} \tag{A.2.15}$$

We thus retrieve the discretization of the current $I|_{p+\frac{1}{2}}^{n+\frac{1}{2}}$ using the 1D scheme of the FDTD method, expressed concisely in Chapter 2 by equation (2.29).

We move our attention to the equation (A.2.13), by expanding it as follows:

$$\begin{aligned}\frac{I|_{p+\frac{1}{2}}^{n+\frac{1}{2}} - I|_{p-\frac{1}{2}}^{n+\frac{1}{2}}}{\Delta x} &\approx -\frac{G}{2}V|_p^{n+1} + \frac{G}{2}V|_p^n - \frac{C}{2\Delta t}V|_p^{n+1} + \frac{C}{\Delta t}V|_p^n \\ &\approx V|_p^{n+1}\Big(-\frac{G}{2} - \frac{C}{\Delta t}\Big) + V|_p^n\Big(-\frac{G}{2} + \frac{C}{\Delta t}\Big) \\ &\approx V|_p^{n+1}\Big(\frac{-G\Delta t - 2C}{2\Delta t}\Big) + V|_p^n\Big(\frac{-G\Delta t + 2C}{2\Delta t}\Big)\end{aligned} \tag{A.2.16}$$

We deduce the expression of the voltage $V|_p^{n+1}$ such as

$$\begin{aligned}V|_p^{n+1} &\approx -\frac{2\Delta t}{G\Delta t + 2C}\Big(\frac{I|_{p+\frac{1}{2}}^{n+\frac{1}{2}} - I|_{p-\frac{1}{2}}^{n+\frac{1}{2}}}{\Delta x}\Big) - \frac{2\Delta t}{G\Delta t + 2C} \times \frac{-G\Delta t + 2C}{2\Delta t}V|_p^n \\ &\approx -\frac{2\Delta t}{(G\Delta t + 2C)\Delta x}\Big(\frac{I|_{p+\frac{1}{2}}^{n+\frac{1}{2}} - I|_{p-\frac{1}{2}}^{n+\frac{1}{2}}}{\Delta x}\Big) - \frac{G\Delta t - 2C}{G\Delta t + 2C}V|_p^n\end{aligned} \tag{A.2.17}$$

The obtained expression gives the discretization of the voltage $V|_p^{n+1}$ using the 1D scheme of the FDTD method, expressed concisely in Chapter 2 by equation (2.28).

The equations (A.2.17) and (A.2.15) are valid for all the segments x of the line except for the first $x = 1$ and last $x = ndx + 1$ ones corresponding respectively to the source and load levels. The 1D-FDTD discretization of the voltage at these levels will be detailed in the next section.

A.3 Discretization of the voltage at the source and load levels of a transmission line

At the terminal conditions, the discretized voltages and currents at each end of the line are not collocated in space or time. Whereas the terminal conditions relate the voltage and current at the same position and at the same time. We define I_s the current at the first mesh of the transmission line ($x = 0$) at the source level, and I_L the current at the first mesh of the transmission line ($x = L$) at the source level.

First we evaluate the equation (A.1.4), considering the instant $t = (n + \frac{1}{2})\Delta t$ and the position in space $x = p\Delta x$, as follows:

$$\frac{I|_p^{n+\frac{1}{2}} - I|_{p-1}^{n+\frac{1}{2}}}{\Delta x} = -GV|_p^{n+\frac{1}{2}} - C\frac{V|_p^{n+1} - V|_p^n}{\Delta t} \tag{A.3.1}$$

Then, we write the previous equation for $p = 1$ corresponding to the first mesh ($x = 0$)

$$\frac{I|_1^{n+\frac{1}{2}} - I|_0^{n+\frac{1}{2}}}{\frac{\Delta x}{2}} = -GV|_1^{n+\frac{1}{2}} - C\frac{V|_1^{n+1} - V|_1^n}{\Delta t} \tag{A.3.2}$$

The current $I|_0^{n+\frac{1}{2}}$ is not defined and consequently will be approached by averaging the source $I|_s$ to obtain a value located in time as the same time point $I|_1^{n+\frac{1}{2}}$. Whereas the voltage $V|_1^{n+\frac{1}{2}}$ is deduced from equation (A.2.11). Equation (A.3.2) is now written as follows:

$$\frac{I|_1^{n+\frac{1}{2}} - \frac{I|_s^{n+1} + I|_s^n}{2}}{\frac{\Delta x}{2}} = -G\frac{V|_1^n + V|_1^{n+1}}{2} - C\frac{V|_1^{n+1} - V|_1^n}{\Delta t} \tag{A.3.3}$$

We extract the voltage $V|_1^{n+1}$ from the previous equation

$$V|_1^{n+1} = \frac{2C - G\Delta t}{2C + G\Delta t}V|_1^n - \frac{4\Delta t}{\Delta x(2C + G\Delta t)}I|_1^{n+\frac{1}{2}} + \frac{2\Delta t}{\Delta x(2C + G\Delta t)}(I|_s^{n+1} + I|_s^n) \tag{A.3.4}$$

In the case of resistive terminations, the terminal characterizations are written in terms of generalized Thevenin's equation as $V_1 = V_s - R_s I_s$, where R_s is the source resistance. By replacing the current I_s in equation (A.3.4) by $I|_s = -G_s V_1 + G_s V_s$, where $G_s = \frac{1}{R_s}$, the voltage $V|_1^{n+1}$ is given by

$$V|_1^{n+1} = \frac{2C - G\Delta t}{2C + G\Delta t}V|_1^n - \frac{4\Delta t}{\Delta x(2C + G\Delta t)}I|_1^{n+\frac{1}{2}} \tag{A.3.5}$$

$$+ \frac{2\Delta t}{\Delta x(2C + G\Delta t)}(-G_s V|_1^{n+1} + G_s V|_s^{n+1} - G_s V|_1^n + G_s V|_s^n) \tag{A.3.6}$$

$$\tag{A.3.7}$$

We rearrange the previous equation to group terms depending on the voltage $V|_1^{n+1}$ as follows:

$$V|_1^{n+1}\Big(1 + \frac{2G_s\Delta t}{\Delta x(2C + G\Delta t)}\Big) = V|_1^n\Big(\frac{2C - G\Delta t}{2C + G\Delta t} - \frac{G_s 2\Delta t}{\Delta x(2C + G\Delta t)}\Big) - \frac{4\Delta t}{\Delta x(2C + G\Delta t)}I|_1^{n+\frac{1}{2}} \tag{A.3.8}$$

$$+ \frac{2\Delta t G_s}{\Delta x(2C + G\Delta t)}(V|_s^{n+1} + V|_s^n) \tag{A.3.9}$$

After some simplification, we extract the final expression of the voltage $V|_1^{n+1}$

$$
\begin{aligned}
V|_1^{n+1} &= \Big(1+\frac{2G_s\Delta t}{\Delta x(2C+G\Delta t)}\Big)^{-1}\Bigg(V|_1^n\Big(\frac{(2C-G\Delta t)\Delta x-2G_s\Delta t}{\Delta x(2C+G\Delta t)}\Big)-\frac{4\Delta t}{\Delta x(2C+G\Delta t)}I|_1^{n+\frac{1}{2}} \\
&+\frac{2G_s\Delta t}{\Delta x(2C+G\Delta t)}(V|_s^{n+1}+V|_s^n)\Bigg) \\
&= \Big(1+\frac{2G_s\Delta t}{\Delta x(2C+G\Delta t)}\Big)^{-1}\Big(\frac{2G_s\Delta t}{\Delta x(2C+G\Delta t)}\Big)\Bigg(V|_1^n\Big(\frac{(2C-G\Delta t)\Delta x}{2G_s\Delta t}-1\Big)-\frac{4\Delta t}{2G_s\Delta t}I|_1^{n+\frac{1}{2}} \\
&+V|_s^{n+1}+V|_s^n\Bigg) \qquad \text{(A.3.10)}
\end{aligned}
$$

For the particular case where the transmission line is assumed to be lossless, the losses R and G are nul, the previous equation can be simplified as follows:

$$
\begin{aligned}
V|_1^{n+1} &= \Big(1+\frac{G_s\Delta t}{C\Delta x}\Big)^{-1}\Big(\frac{G_s\Delta t}{C\Delta x}\Big)\Bigg(V|_1^n\Big(\frac{C\Delta x}{G_s\Delta t}-1\Big)-\frac{2}{G_s}I|_1^{n+\frac{1}{2}}+V|_s^{n+1}+V|_s^n\Bigg) \\
&= \Big(1+\frac{\Delta x}{\Delta t}R_sC\Big)^{-1}\Bigg(\Big(\frac{\Delta x}{\Delta t}R_sc-1\Big)V|_1^n-2R_sI|_1^{n+\frac{1}{2}}+V|_s^{n+1}+V|_s^n\Bigg) \qquad \text{(A.3.11)}
\end{aligned}
$$

The obtained expression corresponds to the discretization of the voltage at the level source of a lossless transmission line, given directly by equation (2.30) in section (2.2.3) of Chapter 2.

Following the same principle for the evaluation of the voltage at the first mesh of the transmission line, we deduce the voltage at the load level by writing the equation (A.3.1) for $p = ndx$ corresponding to the last mesh $x = L$. In this configuration, the current $I|_p^{n+\frac{1}{2}}$ is is substituted by the average current I_L such that

$$
\frac{\frac{I|_L^{n+1}+I|_L^n}{2}-I|_{ndx}^{n+\frac{1}{2}}}{\frac{\Delta x}{2}} = -G\frac{V|_{ndx+1}^n+V|_{ndx+1}^{n+1}}{2}-C\frac{V|_{ndx+1}^{n+1}-V|_{ndx+1}^n}{\Delta t} \qquad \text{(A.3.12)}
$$

We then extract the voltage $V|_{ndx+1}^{n+1}$ from the previous equation

$$
V|_{ndx+1}^{n+1} = \frac{2C-G\Delta t}{2C+G\Delta t}V|_{ndx+1}^n+\frac{4\Delta t}{\Delta x(G\Delta t+2C)}I|_{ndx}^{n+\frac{1}{2}}-\frac{2\Delta t}{\Delta x(2C+G\Delta t)}(I|_L^{n+1}+I|_L^n) \qquad \text{(A.3.13)}
$$

Similarly, with the terminal characterizations at the load defined with Thevenin's equation as $V_{ndx+1} = V_L + R_LI_L$, where R_L is the load resistance. By replacing the current I_L in equation (A.3.13) by $I|_L = G_LV_{ndx+1} - G_LV_L$, where $G_L = \frac{1}{R_L}$, the voltage $V|_{ndx+1}^{n+1}$ is given by

$$V|_{ndx+1}^{n+1} = \frac{2C - G\Delta t}{2C + G\Delta t} V|_{ndx+1}^{n} + \frac{4\Delta t}{\Delta x(2C + G\Delta t)} I|_{ndx}^{n+\frac{1}{2}} \tag{A.3.14}$$

$$- \frac{2\Delta t}{\Delta x(2C + G\Delta t)} (G_L V|_{ndx+1}^{n+1} - G_L V|_{L}^{n+1} + G_L V|_{ndx+1}^{n} - G_L V|_{L}^{n}) \tag{A.3.15}$$

We rearrange the previous equation to group terms depending on the voltage $V|_{ndx+1}^{n+1}$ as follows:

$$V|_{ndx+1}^{n+1}\Big(1 + \frac{2G_L\Delta t}{\Delta x(2C + G\Delta t)}\Big) = V|_{ndx+1}^{n}\Big(\frac{2C - G\Delta t}{2C + G\Delta t} - \frac{G_L 2\Delta t}{\Delta x(2C + G\Delta t)}\Big) + \frac{4\Delta t}{\Delta x(2C + G\Delta t)} I|_{ndx}^{n+\frac{1}{2}}$$
$$+ \frac{2\Delta t G_L}{\Delta x(2C + G\Delta t)} (V|_{L}^{n+1} + V|_{L}^{n}) \tag{A.3.16}$$

After some simplification, we extract the final expression of the voltage $V|_{ndx+1}^{n+1}$

$$V|_{ndx+1}^{n+1} = \Big(1 + \frac{2G_L\Delta t}{\Delta x(2C + G\Delta t)}\Big)^{-1} \Bigg(V|_{ndx+1}^{n}\Big(\frac{(2C - G\Delta t)\Delta x - 2G_L\Delta t}{\Delta x(2C + G\Delta t)}\Big) + \frac{4\Delta t}{\Delta x(2C + G\Delta t)} I|_{ndx}^{n+\frac{1}{2}}$$
$$- \frac{2\Delta t G_L}{\Delta x(2C + G\Delta t)} (V|_{L}^{n+1} + V|_{L}^{n})\Bigg)$$
$$= \Big(1 + \frac{2G_L\Delta t}{\Delta x(2C + G\Delta t)}\Big)^{-1} \frac{2\Delta t G_L}{\Delta x(2C + G\Delta t)} \Bigg(V|_{ndx+1}^{n}\Big(\frac{(2C - G\Delta t)\Delta x}{2G_L\Delta t} - 1\Big) + \frac{4\Delta t}{2G_L\Delta t} I|_{ndx}^{n+\frac{1}{2}}$$
$$+ V|_{L}^{n+1} + V|_{L}^{n}\Bigg) \tag{A.3.17}$$

For the particular case where the transmission line is assumed to be lossless, the terms R and G are null, the previous equation can be simplified as follows:

$$V|_{ndx+1}^{n+1} = \Big(1 + \frac{G_L\Delta t}{C\Delta x}\Big)^{-1} \Big(\frac{G_L\Delta t}{C\Delta x}\Big) \Bigg(V|_{ndx+1}^{n}\Big(\frac{C\Delta x}{G_L\Delta t} - 1\Big) + \frac{2}{G_L} I|_{ndx}^{n+\frac{1}{2}} + V|_{L}^{n+1} + V|_{L}^{n}\Bigg) \tag{A.3.18}$$

$$= \Big(1 + \frac{\Delta x}{\Delta t} C R_L\Big)^{-1} \Bigg(\Big(\frac{\Delta x}{\Delta t} C R_s - 1\Big) V|_{ndx+1}^{n} + 2R_L I|_{ndx}^{n+\frac{1}{2}} + V|_{L}^{n+1} + V|_{L}^{n}\Bigg) \tag{A.3.19}$$

The obtained expression corresponds to the discretization of the voltage at the level source of a lossless transmission line, given directly by equation (2.31) in section (2.2.3) of Chapter 2.